# CITY UNIVERSITY LONDON

**EST 1894**

# INVESTIGATION OF ADVANCED EXPERIMENTAL AND COMPUTATIONAL TECHNIQUES FOR BEHAVIOURAL CHARACTERISATION OF PHASE CHANGE MATERIALS (PCMs)

A thesis submitted in partial fulfillment of the requirements
for the degree of Doctor of Philosophy

Stanislava B. Stanković, M. Sc.

School of Engineering and Mathematical Sciences
City University London

May 2014

*Мојој драгој мами Љиљани*
*и вољеној успомени мог тате Бранка.*

# Table of Contents

# List of Tables

# List of Figures

13

# ACKNOWLEDGEMENTS

# DECLARATION

This thesis and the encompassing work it describes are entirely of my own efforts. Any ideas, data, text, or images resulting from the work of other people (whether published or unpublished) are fully identified as such within the work and attributed to their creator in the text and bibliography. This thesis has not been submitted in whole or in partial for any other academic degree or professional qualification. Here, I grant powers of discretion to the University Librarian to allow the thesis to be copied in whole or in part without further reference to me as the author.

# ABSTRACT

The existing Phase Change Material (PCM) thermal investigation methods have significant drawbacks and limitations in terms of the correct determination of phase change temperature and enthalpy values. It results in the inaccuracy and sometimes absence of experimental data which are required for the implementation of PCM based Thermal Energy Storage (TES) systems. An advanced T-history method for PCM characterisation was developed to overcome some of the shortcomings of the existing PCM thermal investigation procedures. The advanced T-history setup and the instrumentation system coupled with the LabView virtual instrument, which allows the continuous acquisition of T-history signals, were carefully designed, developed and evaluated. The development process was performed by sequentially addressing all the issues relating to the control and sensing mechanisms of the T-history setup, measurement accuracy and precision, PCM data representation, hysteresis, and finally subcooling. The instrumentation system was iteratively redeveloped and validated in a series of studies until the $\pm 0.5\,°C$ accuracy in PCM related measurements was achieved. Once the desired temperature accuracy was reached the data evaluation technique was implemented in MATLAB to allow the determination of thermo-physical PCM properties from the measured T-history data. Furthermore, detailed studies of PCMs from the RT and PT organic series were performed. These comprehensive PCM investigations revealed various results including the details regarding the materials' behaviour upon both cooling and heating, the heat release/storage in given $0.5\,°C$ wide temperature intervals, the respective enthalpy-temperature curves, and the total heat released/stored with respect to mass and volume. The comparison of the RT results with the data provided by the manufacturer showed very good agreement in terms of temperature ($\pm 1\,°C$ margin) and heat release/storage content ($\pm 10\,\%$ margin) proving the validity of the advanced T-history method. A new

data evaluation technique considering subcooling was implemented in MATLAB to allow correct characterisation of inorganic PCMs and the obtained results were presented accordingly. Moreover, the PT PCM data were re-evaluated showing that subcooling in these materials can be neglected. Finally, pilot optical transmittance studies in a wide wavelength range (from 280 to 700 nm) at different temperatures were carried out and showed that the phase change temperature is one of the most determinative factors of material's applicability in PCM enhanced glazing units used in solar applications. The results from the PCM characterisation measurements confirmed that a better planned PCM experimental tests in terms of more accurate and precise sensing and control modalities provide more comprehensive and reliable results than those described in the literature so far and hence enable the development of more efficient PCM based TES systems.

# List of Abbreviations

ES          Energy Storage

TES         Thermal Energy Storage

PCM         Phase Change Material

RTD         Resistance Temperature Detector

PCS         Phase Change Slurry

PDE         Partial Differential Equation

1D          1-Dimensional

3D          3-Dimensional

SNR         Signal-to-Noise Ratio

DSC         Differential Scanning Calorimeter

T-history   Temperature-history

DTA         Differential Thermal Analysis

ASC         Adiabatic Scanning Calorimeter

PID         Proportional Integral Derivative

EMF         ElectroMotive Force

NTC         Negative Temperature Coefficient

PTC         Positive Temperature Coefficient

o/d         outer diameter

IC          Integrated Circuit

DC          Direct Current

AC          Alternating Current

DAQ         Data AcQusition

USB         Universal Serial Bus

PC          Personal Computer

RAM         Random Access Memory

VI          Virtual Instrument

| | |
|---|---|
| WB | Wheatstone Bridge |
| PSU | Power Supply Unit |
| SPR | Serial Parallel Resistor |
| VIS | VISible (part of the electromagnetic spectrum) |
| UV | Ultra-Violet (part of the electromagnetic spectrum) |
| UVA | Ultra-Violet A (part of the electromagnetic spectrum) |
| UVB | Ultra-Violet B (part of the electromagnetic spectrum) |

# Chapter 1

# INTRODUCTION

Due to the growing problem of global energy crisis and associated climate change the focus of energy research in the last decades has shifted towards the investigation of sustainable resources (Mehling and Cabeza, 2008). These resources are mainly of natural origin such as sunlight, wind, rain, waves, but they can also be a by-product of artificial processes (e.g. waste heat). In any case, the principal aim is the reduction/cessation of fossil fuel based energy production through enhanced utilisation of the aforementioned resources. The component of vital importance in alternative energy applications is the Energy Storage (ES). Energy storage enables storing of some form of energy so it can be drawn upon at a later time on demand (Gil et. al., 2008). There is a large variety of ES systems such as mechanical, chemical, biological, and magnetic energy storages. However, in many applications, the renewable energy manifests itself as thermal energy (Bailey, 2010). Therefore, Thermal Energy Storage (TES) is amongst the most important ES types. One of the most efficient means of TES implementation is through the use of Phase Change Materials (PCMs) (Zalba et. al., 2003; Mehling and Cabeza, 2008).

PCMs are able to absorb/release large amounts of heat (latent heat) during the phase change which takes place in almost isothermal conditions or in a very narrow temperature range (Mehling and Cabeza, 2008; Maldonado, 2011). The isothermal phase change process enables the usage of these materials for temperature control so the application areas of PCMs are numerous including transport and general storage and medical applications. Meanwhile, high latent heat content enables utilisation of PCMs for TES applications (predominantly in buildings).

The development of efficient PCM based TES system is a challenging task which includes several development stages: PCM characterisation i.e. determination of important material properties, design and modelling, and finally the implementation of

such system. Usually the design and modelling stage requires the solution of transient heat transfer problems involving phase change which is a relatively complicated task in itself. Nevertheless, according to Mehling and Cabeza (2008), one of the major limiting factors for both modelling and implementation of efficient PCM based TES systems is the inaccuracy/lack of the experimentally determined material data especially in terms of phase change temperature and enthalpy. This represents a serious problem since the accurate knowledge of thermo-physical material properties of PCMs is a prerequisite for more optimal and efficient design and implementation of PCM based TES units and the prediction of long-term behaviour of such systems. Moreover, more reliable determination of thermo-physical properties of existing PCMs should provide better understanding of the limitations of those materials and induce novel ideas to help the research activities regarding the development of new phase change materials.

The existing PCM thermal investigation methods have significant drawbacks primarily related to the limited size of the investigated PCM samples and the unreliable determination of the phase change temperature and the phase change enthalpy. The aim of this research is to overcome some of the shortcomings of the existing PCM thermal investigation procedures.

The main hypothesis underlying this project is that a better planned experimental tests in terms of more accurate and precise sensing and control modalities will be able to provide more comprehensive and reliable results than those described in the literature so far. This thesis describes various improvements developed for the implementation of the method originally developed for the exclusive investigation of PCM i.e. the T-history method (Zhang et al., 1999). The improvements are achieved by addressing the issues relating to the control and sensing mechanisms of the T-history setup, measurement accuracy and precision, effects of subcooling and hysteresis, and data representation. The details of the selected control and sensing modalities, developed measurement systems and mathematical data processing techniques required for the implementation of the advanced T-history method are discussed. Also, this thesis details the parametric studies performed on the well-known organic PCM which were carried out to discover which parameters affect the PCM characterisation mostly and to what extent. Additionally, the thesis illustrates the resulting accuracy of the

evaluation and characterisation studies of both organic and inorganic PCMs using the advanced T-history method. Finally, the potential of PCMs for solar heating applications and the preliminary optical tests of organic PCMs are also discussed.

A brief description of the subjects that are covered in the following chapters is presented below.

**Chapter 2** introduces the science behind the PCMs. The chapter covers comprehensively the thermo-physical, kinetic, and chemical properties of various PCM classes. Basic technical principles of the development and production processes of PCMs are also covered.

**Chapter 3** covers various applications of PCMs starting from the use of PCMs for transport and general storage, through medical applications towards the applications in buildings.

**Chapter 4** is entirely dedicated to an explanation of the heat transfer mechanisms of thermal energy storage. The basic thermodynamics of PCM based TES systems is discussed. As heat transfer theory is vital for the understanding of PCM working principles, hence different mathematical formulations of a phase change problems are given including the basic analytical solution given by Stefan in 1891. Moreover, the development and execution of a simple parametric test, performed in order to estimate the most influential PCM properties in phase change processes, is explained.

**Chapter 5** gives an overview of the current technologies and methods used for the characterisation of PCMs. This is probably the most important review chapter since it gives a clear and in-depth insight into the experimental investigations on PCMs. In addition, the limitations of the current methods are reviewed in this chapter.

**Chapter 6** describes the development of the design strategy and the experimental setup of the advanced T-history method. The development of the experimental setup is explained detailing the investigation and selection of the appropriate control and sensing modalities. The design and development of the testing containers is also described.

**Chapter 7** covers the iterative development of the instrumentation system of the advanced T-history method. The first PCM temperature measurements are presented and discussed.

**Chapter 8** presents the experimental studies of organic PCMs using the advanced T-history method which led to important conclusions regarding the influence of the certain parameters on the T-history data.

**Chapter 9** describes the experimental studies of inorganic PCMs using the advanced T-history method. It also details the mathematical improvements of the T-history data evaluation technique through the utilisation of the subcooling phenomenon and consequently the data re-evalution process for some organic materials.

**Chapter 10** covers the pilot optical investigation of organic PCMs. Spectrophotometric studies and transmittance spectra of tested PCMs are described in detail.

**Chapter 11** presents the conclusions and discussion along with the future work suggestions.

# Chapter 2

# FUNDAMENTAL PHYSICAL AND TECHNICAL PRINCIPLES OF PHASE CHANGE MATERIALS (PCMs)

Renewable energy resources and energy efficiency (improvements) are identified as the two main supporting technologies of the sustainable energy scheme (Mehling and Cabeza, 2008). The sources of renewable energy are various such as sunlight, wind, rain, ocean, and biomass. The common properties that the foregoing resources share are their natural origin and the possibility of timely replenishment (Amaya, 2009). Nevertheless, the sustainable energy concept can also be implemented by artificial means. In the context of sustainability, energy efficiency is represented by the efforts taken towards the reduction of energy requirements in the provision of different products and services (Dincer, 2000). This reduction can be achieved in different ways. Namely, the second law of thermodynamics tells us that a 100 % efficiency of energy conversion processes is not attainable, so a surplus of heat, usually designated as the waste heat, is produced as a by-product of those processes (Bailey, 2010). The generators of the excess thermal energy are abundant like household and industrial processes, electronic equipment, human body, and solar radiation (Zalba et al., 2003). However, the major barrier for overall energy efficiency improvement is both the spatial and the temporal gap between the waste heat production and energy requirements (Chiu, 2011; Maldonado, 2011). Adequate harvesting and storage of the excess thermal energy is the main mechanism to bridge this gap. This can be achieved through the utilisation of various thermal energy storage methodologies (Bailey, 2010).

# 2.1 Thermal Energy Storage (TES)

The concept of thermal energy storage is very old. Since ancient times, people had the practice of putting food in the snow and using ice as cold storage. According to the history records, the Romans were using ceramic tiles as heat storage media in under floor heating systems about 2 millennia ago. Nonetheless, for the greater part of our history, heat and cold energy storages did not have an important role in the course of human development. This direction changed with the arrival of steam engines, the increasing development of machine tools, and the overall transition to new manufacturing processes. That was the time of the great industrial revolution when the living standard and human comfort demand changed forever. Nowadays, different heat and cold technologies which store thermal energy using various storage reservoirs are employed on a daily basis (Dincer and Rosen, 2011). Thermal energy storage is used in both household and industrial processes and it serves to bridge the spatial and temporal gap between the supply and demand of energy. Moreover, it matches different powers on both supply and demand side (Mehling and Cabeza, 2008; Chiu, 2011; Maldonado, 2011).

TES systems can be classified according to the various criteria (Gil et. al., 2008). However, the classification, which is of the most interest for this study, is the classification according to the storage medium. According to that classification TES systems can be implemented through the physical or chemical means, depending on the type of the storage medium. TES systems implemented through the physical processes use two types of media, sensible and latent heat storage whereas systems implemented through the chemical processes rely on the heat of chemical reactions (Dincer and Rosen, 2011).

## 2.1.1 Sensible heat

In many applications like domestic hot water and various underground TES systems, to name a few, thermal energy is stored as sensible heat. In these applications energy is stored by changing the temperature of the storage medium and since this change can be detected by sensors or human senses the energy stored is called sensible heat (Whiffen

and Riffat, 2012). The usage of the term "heat" in this context could be interpreted as a misnomer since heat itself is not a physical quantity, but rather a process or a mode of energy transfer (Atkins, 2010). However, in the aforementioned context, the terms "heat" and "energy" are often interchanged and therefore will be used in that way throughout the text.

Evidently, the most distinctive feature of sensible heat storage medium is the accompanying increase of temperature (Figure 2.1). The heat stored $\Delta Q$ upon the temperature change $\Delta T$ can be measured and is expressed as the property called heat capacity $C_p$ of the storage medium. This relation is given in Equation 2.1:

$$C_p = \Delta Q / \Delta T, \qquad (2.1)$$

where the subscript $p$ is used to denote the fact that, in the TES context, processes usually imply constant pressure (Mehling and Cabeza, 2008).
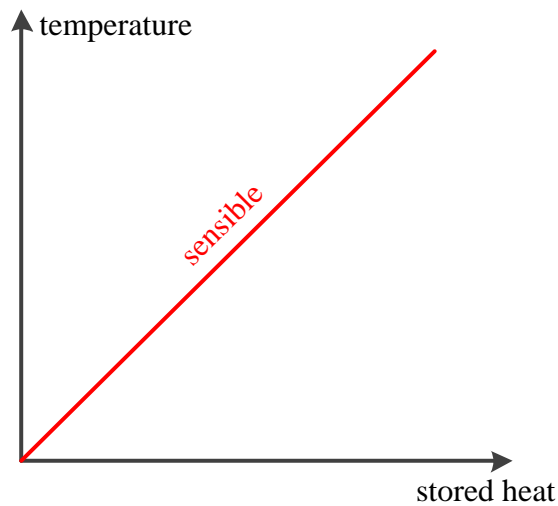


**Figure 2.1:** *Stored heat-temperature relation for ideal sensible storage media (amended from Mehling and Cabeza, 2008, p. 2).*

The heat capacity is an extensive property and thus dependent on the amount of material in use (Atkins, 2010). Therefore more practical, intensive properties which are independent on the amount of material present are used. These include: mass heat capacity, volumetric heat capacity, and molar heat capacity. The mass heat capacity is often simply called specific heat capacity or just specific heat. These quantities basically represent the heat capacity given with respect to the mass, the volume, and

the amount of substance. Certainly, the most important and often used property is the specific heat capacity $c_p$, calculated by using Equation 2.2:

$$c_p = C_p / m. \qquad\qquad (2.2)$$

Simplicity is the main advantage of sensible heat applications. However, the disadvantages are far-reaching. Namely, the usage of sensible TES systems requires large volumes of the storage media and the large driving temperature range for the storage/release of heat. To remedy these drawbacks another thermal energy storage technology in the form of latent heat storage media is used (Sharma et al., 2004; Mehling and Cabeza, 2008).

## 2.1.2 Latent heat

Latent heat is the heat released or absorbed by a chemical substance or a thermodynamic system during a change of phase (state of matter) that occurs without a change in temperature or in almost isothermal conditions (Mehling and Cabeza, 2008; Maldonado, 2011). The most common phase change processes are melting of ice and boiling of water. Given the almost isothermal conditions upon the change of phase the heat stored/released is hidden to human senses and therefore the term "latent" is used to describe such quantity (Mehling and Cabeza, 2008).

Latent heat can be stored/released in three different ways: solid-vapour, solid-solid, and solid-liquid phase transformation. Solid-vapour transition, although accompanied with the highest values of latent heat, undergo large changes of volume resulting in complex and impractical systems. Solid-solid transformations usually do not result in large latent heat values but are yet to be fully explored. In contrast to the possible limitations of solid-vapour and solid-solid transitions, solid-liquid transformations i.e. melting and solidification are characterised by a relatively large amount of latent heat (5-14 times greater than its sensible equivalent) and a small volume change (less than 10 %) making them economically attractive for the use in TES systems (Sharma et al., 2009). Therefore solid-liquid transformations are of the most interest in this study and from this point onwards the term "phase change" will only refer to the solid-liquid transitions.

As previously stated, solid-liquid phase change is characterised by a small volume change. Moreover, in the context of TES, such transitions usually occur without significant change of pressure. In this way melting and solidification of the storage material also proceed at a constant temperature or in a very narrow temperature range (Figure 2.2).
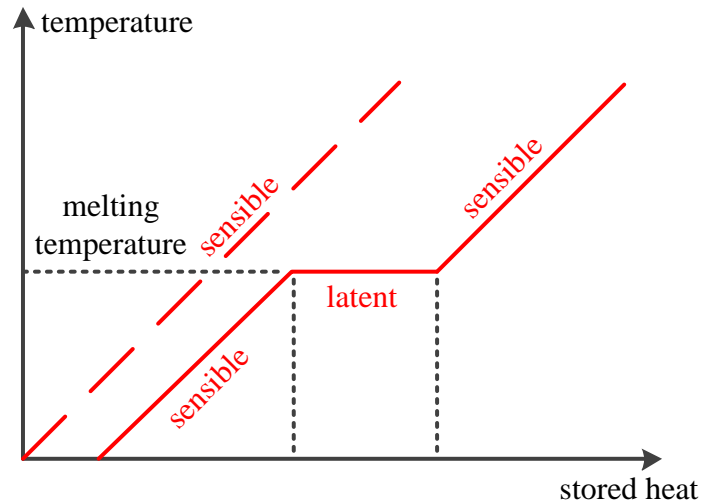


***Figure 2.2:*** *Stored heat-temperature relation for ideal sensible and latent storage media (amended from Mehling and Cabeza, 2008, p. 3).*

The temperature, upon melting/solidification, at which the heat is transferred/taken to/from the storage material, is called the melting/solidification temperature or temperature range depending on the direction of the heat flow during the process. In addition, the term "phase change" temperature or temperature range can be used (Mehling and Cabeza, 2008). After the completion of phase change further energy is stored in the form of sensible heat (Figure 2.2).

The latent heat *ΔQ* that is stored/released upon melting/solidification, due to the small volume change and the constant pressure, in the case of usual conditions, equals the enthalpy difference *ΔH* between the solid and the liquid phase as expressed by Equation 2.3:

$$\Delta Q = \Delta H. \tag{2.3}$$

This heat, in the case of solid-liquid transitions, is called heat of fusion or phase change enthalpy. It is an extensive property and therefore depends on the amount of material.

For this reason, an intensive property, specific enthalpy change $\Delta h$, is often used to describe the storage potential of solid-liquid transformations as in Equation 2.4:

$$\Delta h = \Delta H / m. \qquad\qquad (2.4)$$

Given the aforementioned descriptions and terminology, the materials which undergo solid-liquid transformation, with relatively large associated heats of fusion, to make them suitable for storage of heat or cold, are commonly denoted as latent heat storage materials or simply phase change materials i.e. PCMs (Mehling and Cabeza, 2008).

## 2.1.3 Heat of chemical reactions

Although of no interest for this study, the thermal energy storage by means of chemical reactions will be briefly discussed, for consistency purposes. Heat of reaction is the amount of heat that needs to be added/removed during a chemical reaction in order to keep all the present substances in thermal equilibrium. If the pressure in the reacting container is kept at a constant value, the measured heat of reaction will be equal to the difference between the enthalpy of the end products and the enthalpy of the reactants. If the reaction is endothermic, heat will be absorbed by the reaction substances in contrast to the exothermic reaction where heat is released. Any reversible chemical reaction with high heat of reaction can be used for thermal energy storage (Mehling and Cabeza, 2008).

## 2.2 Phase Change Materials (PCMs)

One of the most efficient means of thermal energy storage implementation is through the utilisation of phase change materials. Phase change material (PCM) refers to any substance able to undergo reversible solid-liquid transformation and store/release large values of energy at constant temperature or within a narrow temperature range during the transformation process. Here, the term "large" refers to the enhanced energy storage capacity (heat of fusion) in regard to the heat capacities of the conventional, usually sensible, TES media. The chemical bonds within the substance break upon the

transformation and as a result the material changes its molecular structure manifesting in change of phase from solid to liquid or vice versa (Baetens et al., 2010; Dincer and Rosen, 2011).

Although the usage of PCMs dates back into ancient days (water and ice storages) the elaborated investigation of these materials has commenced only in the past few decades. According to Agyenim et al. (2010) Telkes and Raymond reported on some pioneering studies in 1940s, but those results didn't receive much attention until later times and the emerging energy crisis of late 1970s and early 1980s. Zalba et al. (2003) emphasized that the first thorough PCM references were given by Abhat and Lane in 1983. In the last 20 years the research areas of PCMs have expanded considerably as witnessed in numerous reviews, starting by two of the firsts and most comprehensives given by Zalba et al. (2003) and concluding with the most recent ones (Zhu et. al., 2009; Agyenim et al., 2010; Baetens et al., 2010; Oro et al., 2012; Whiffen and Riffat, 2012; Zhou et al., 2012). Nowadays, information on PCMs is quantitatively enormous containing the results obtained from diverse fields of material studies. However, fundamental principles for the exploitation of PCMs remain unchanged until today. Two defining properties of phase change materials are:

     (i)     Constant or almost constant phase change temperature and

     (ii)     High heat of fusion.

In addition to these, few more material properties are essential for optimal and design of efficient TES systems based on PCMs and therefore will be explained in detail.

## 2.2.1 Material properties

Many materials have been investigated as potential PCMs. However, for a material to be useful some criteria must be met and those are best described in terms of material properties. The attractive properties of PCMs can be classified into four major categories: thermo-physical, kinetic, chemical, and economic properties (Sharma et al., 2004; Oro et al., 2012).

## *2.2.1.1 Thermo-physical properties*

Predominantly depending on the values of the thermo-physical properties, a PCM is determined to be better for a specific application than some other material (Oro et al., 2012). The most important thermo-physical properties of PCMs include:

      (i)      Phase change temperature (range),

      (ii)      Heat of fusion (i.e. latent heat or phase change enthalpy),

      (iii)      Specific heat (including molar and volumetric heat capacities),

      (iv)      Thermal conductivity,

      (v)      Cycling stability, and

      (vi)      Volume change.

Specifically, phase change temperature (range) needs to be known and determined with high accuracy in order to assure the storage and release of heat in the desired operating temperature range. This range is usually quite narrow, in the order of $\pm 10\,°C$ around the phase change temperature of the material or even $\pm 5\,°C$ (Günther et al., 2009). The phase change also takes place over a narrow temperature range and thus the design of thermal energy storage system within this range has to be founded on reliable and high resolution material data (Günther et al., 2006).

Additionally, PCMs need to have high heat of fusion. This results in higher storage densities than those provided by sensible heat storage media. Higher storage density leads to volume reduction of the storage containers and more compact TES systems (Dincer and Rosen, 2011).

High specific heat and consequently high molar and volumetric heat capacities are desirable to provide additional sensible heat storage which can be valuable in certain applications (Sharma et al., 2004).

Furthermore, high thermal conductivity in solid and liquid phases is also desirable to assure fast storage/release of energy in a given storage volume and thus assist the charging/discharging process of the storage media. Low thermal conductivity may prove to be one of the major problems of some otherwise high-quality PCMs; therefore PCMs are often combined with materials of high thermal conductivity like metals and graphite. The solution to low thermal conductivity problems is usually

addressed through the more optimal and efficient design strategies of the TES systems (Sharma et al., 2004; Dincer and Rosen, 2011).

Also, PCMs need to remain stable upon cycling in order to be used for the storage/release of heat as many times as required. The number of cycles varies depending on the application, Sometimes, only one cycle is necessary as when the PCM is used for heat protection from a fire. In other situations several thousand cycles are inevitable like in building applications. One of the main indications of unstable cycling is the phase separation. Namely, upon PCM cycling phases with different compositions can form. This happens within materials which are assembled of several components. Phase separation is a visible effect since the phases with different composition separate macroscopically. Generally the phase with the higher density sinks to the bottom and the phase with the lower density flows to the top. This effect is also called decomposition. The problem can cause the decrease of the heat storage capacity of the phase change material during repetitive cycling. There are several methods to solve this like artificial mixing of the material, gelling, and thickening (Mehling and Cabeza, 2008).

Small volume change is also desirable to reduce mechanical stability requirement of the PCM containers (Dincer and Rosen, 2011).

Clearly, phase change materials need to meet some requirements in terms of their thermo-physical properties in order to be used as effective thermal energy storage media. Evidently, the most important thermo-physical properties are the phase change temperature (range) and heat of fusion; therefore the proper determination of these properties with high accuracy is an integral part of any design, development, and implementation process of thermal storage system based on PCMs.

## *2.2.1.2 Kinetic properties*

Vital kinetic properties of phase change materials include:

(i)     Nucleation rate, and

(ii)    Rate of crystal growth.

PCMs need to have high nucleation rate to avoid excessive subcooling of the liquid phase (Sharma et al., 2004). This phenomenon is one of the most serious

problems in terms of phase change materials. Subcooling (also called supercooling) is the effect manifesting in the decrease of the material's temperature significantly below the expected phase change temperature before the material begins to solidify and release heat during the discharging process of the PCM. If that lower temperature (also called nucleation temperature) is not reached, the PCM will not solidify at all and thus will not release latent heat. Moreover, in the case of the new charging cycle and accompanying temperature increase it will store only sensible heat (Mehling and Cabeza, 2008).

Subcooling is an important aspect to observe since it can significantly diminish the usability of a PCM upon discharging. Namely, if the nucleation temperature is reached and solidification triggered, some sensible heat will be lost upon the temperature rise of the material from the nucleation to the phase change point. If that heat is larger than the heat released upon solidification or if the rate of heat loss to the ambient is greater than the rate of heat release during solidification the material will never reach its phase change point. The subcooling is usually expressed as the degree of subcooling represented by the difference between the phase change and nucleation temperatures. Considering the impact of the subcooling on the discharging processes of PCMs, profound investigations were taken towards the potential reduction of the subcooling effect. In these studies special additives (called nucleators) were investigated and developed to reduce subcooling. The additives often have similar crystal structure to the one of the solid PCM to allow the solid phase of the phase change material to grow. Nucleators also have higher melting temperatures than PCMs to avoid deactivation upon PCM melting. During solidification, the slow nucleation process is followed by the rapid crystal growth. The higher the rate of crystal growth the better the process of heat recovery from the storage system is (Günther et al., 2007; Oro et al., 2012).

The study of kinetic properties of PCMs is important. However, the performance of these materials is dominated by the phase change temperature and enthalpy; therefore the studies of these two thermo-physical properties are the most important in terms of PCM investigations.

## 2.2.1.3 Chemical properties

Important chemical properties of PCMs are:

(i)     Chemical stability,

(ii)    Compatibility with other materials,

(iii)   Flammability, and

(iv)    Toxicity.

Chemical stability of PCMs is desirable to assure long lifetime of the materials in the case of exposure to severe conditions in terms of elevated temperatures, radiation, gases, etc. Compatibility of PCMs with other materials is also important to assure long lifetime of the storage containers and of the surrounding materials in the case of leakage. One of the most important properties is corrosiveness. PCMs need to be non-corrosive in order to be used as thermal energy storage since metal is used as one of the most common container materials in TES systems. In the case of metal containers, preliminary corrosion tests need to be performed prior to any application of the unknown PCMs (Mehling and Cabeza, 2008).

Furthermore, the implementation of thermal energy storage can be restricted by laws imposing the use of non-flammable and non-toxic materials. Although other safety constraints can be applied these are the most common ones; therefore flammability and toxicity are emphasized as important chemical properties of PCMs (Sharma et al., 2004; Agyenim et al., 2010).

## 2.2.1.3 Economic properties

Even the best PCMs, in terms of their thermo-physical, kinetic, and chemical properties, will not be good for commercial or widespread use unless they meet the satisfying levels of some basic economic properties:

(i)     Cost,

(ii)    Availability, and

(iii)   Environmental performance.

Useful PCMs need to be low cost and easily available on the large scale. Apart from that, the materials need to be easily recyclable and show good overall environmental performance (Sharma et al., 2004; Oro et al., 2012).

## 2.2.2 Classes of materials

Through the years of research an abundant number of potential PCMs have been identified (Zalba et. al., 2003), but most of those can be categorised into four classes (Pasupathy et al., 2008; Zhou et al., 2012):

(i)    Organic (paraffin materials, fatty acids, and sugar alcohols),

(ii)   Inorganic (water, salt-hydrates, and metallics)

(iii)  Eutectics, and

(iv)   Miscellaneous materials (e.g. clathrates).

Since the two most important PCM properties i.e. the phase change temperature and the phase change enthalpy depend on molecular effects, it is not surprising that materials within the same class behave similarly. Now, each class of PCMs will be explained in more detail.

### *2.2.2.1 Organic PCMs*

Organic PCMs are one of the most common phase change materials for latent heat storage. The phase change temperatures of these materials range between -30 °C and 200 °C. At higher temperature the covalent bonds within these materials break causing instability. In addition, the density of organic PCMs is usually less than $10^3$ kgm$^{-3}$ making organics less dense than most inorganic materials like water and salt hydrates. This results in smaller phase change enthalpy per volume (volumetric phase change enthalpy) values (Mehling and Cabeza, 2008).

The most frequently used organic PCMs are paraffin materials. Paraffin is a technically used term for an alkane, but in the context of PCMs it is used to denote linear alkanes with the general formula $C_nH_{2n+2}$. With the rising number of *C* atoms and the expanding chain length the phase temperature of these materials increases (Mehling and Cabeza, 2008). Commercial paraffins are obtained from petroleum distillation and

they usually are not pure materials yet a combination of different hydrocarbons (Hiran et al., 1994). Moreover, these PCMs are easily available from different manufacturers but generally more expensive than the matching salt hydrates. The storage capacities of commercial paraffins vary from $120\,kJkg^{-1}$ to $210\,kJkg^{-1}$ (Baetens et al., 2010). Another advantage is the relatively low degree of subcooling so it is not necessary to introduce any type of nucleators into the phase change material. Paraffins are safe and non-reactive substances, compatible with most metal containers and therefore easily incorporated into TES systems. Conversely, special care needs to be taken when using plastic containers as paraffins tend to penetrate and soften some plastics. Another disadvantage of paraffin materials is their low thermal conductivity (around $0.2\,Wm^{-1}K^{-1}$), especially in the solid state. This can cause problems in the case of high heat transfer rate requirements during the charging/discharging processes. The solution of this problem is usually implemented through more optimal design of the TES systems by using finned containers and metallic fillers or by combining latent with the sensible storage media. Paraffins are flammable substances, but this can be easily controlled through the use of an inflammable containers. In contrast to inorganic salt hydrates, commercial paraffins usually do not have sharp well-defined melting/solidification temperatures since they are a mixture of materials and therefore not entirely pure substances. The lack of sharp phase change temperatures partially decreases the efficiency of the heat storage systems (Sharma et al., 2004; Mehling and Cabeza, 2008).

Fatty acids represent another subclass of organic PCMs, characterised by the chemical formula $CH_3\text{-}(CH_2)_{2n}\text{-}COOH$. These materials are very much similar to paraffins. Their advantage of sharper phase change temperatures is cancelled out by the fact of being about three times more expensive than paraffins. In addition, they are mildly corrosive. Their phase change enthalpy is matching to that of paraffin waxes, and accordingly their phase change temperature increases with the molecular length. Since they are composed of only one component fatty acids don't undergo phase separation and remain stable upon cycling. Similar to paraffins, fatty acids show small or no degree of subcooling and have a low thermal conductivity (Sharma et al., 2004; Mehling and Cabeza, 2008).

Sugar alcohols are essentially hydrogenated carbohydrates represented by the general chemical formula $HO-CH_2-[CH-(OH)]_n-CH_2-OH$. These are a rather newly investigated material class and therefore reliable information is limited. Their phase change temperatures range from 90 °C to 200 °C and their specific phase change enthalpies are generally high. Moreover, they have high densities resulting in high volumetric phase change enthalpies. Contrary to other organic materials, sugar alcohols show a certain degree of subcooling. In general, these are safe materials given that some like xylitol are proposed to replace sugar as sweetener (Mehling and Cabeza, 2008).

## 2.2.2.2 Inorganic PCMs

The second category of phase change materials are the inorganic PCMs. Apart from water which is by far the most known PCM, the main subcategory of inorganic phase change materials are the salt hydrates.

Salt hydrates are some of the most important heat storage PCMs. They consist of a salt and water mixed in a discrete ratio in the form of *salt·nH₂O*. The salt and water are combined in a crystalline matrix when the material solidifies. Salt hydrates are sometimes used alone or as a part of eutectic mixtures. Their phase change temperatures range from 15 °C to 117 °C. Principally, the low cost and easy availability makes them commercially attractive for TES applications. Two easily available and the least expensive salt hydrates are $CaCl_2 \cdot 6H_2O$ and $Na_2SO_4 \cdot 10H_2O$. One advantage of these materials which increases the overall efficiency of the heat storage system is their sharp phase change temperature. In addition, they show high thermal conductivity values in comparison to other PCMs. This is beneficial in terms of the increased heat transfer ratios upon charging/discharging of the TES systems. They have a high phase change enthalpy resulting in smaller storage units. Also, salt hydrates undergo a lower volume change than other PCMs upon melting/solidification. However, since they are composed of few substances they suffer from a segregation process (formation of other hydrates or dehydrated salts resulting in the reduction of the active volume available for heat storage) and accompanying phase separation problems. These problems can be partially eliminated through the use of gels or

thickening mixtures. However, that can diminish the heat storage capacity even further. Salt hydrates show larger degree of subcooling compared to organic PCMs. This can be reduced by using proper nucleating agents to initiate the crystal growth in the materials. Another disadvantage of salt hydrates is the predisposition to cause corrosion in metal containers that are often used in TES systems. For this reason, material compatibility check is necessary in the case of salt hydrates and container materials (Sharma et al., 2004; Zhang et al., 2007; Zhou et al., 2012).

## 2.2.2.3 Eutectics

Eutectic compositions are mixtures of two or more constituents, which melt/freeze congruently. The material is said to melt/freeze congruently in the case when the state before the phase change is of the same homogeneous composition throughout as the state after the phase change plus the same phase change enthalpy and temperature are observed at any place; therefore eutectic compositions usually do not show phase separation. In addition, eutectic mixtures usually have sharp phase change temperature. However, they tend to cause corrosion. These materials as potential PCMs are still in an early investigation stage and limited data are available on their thermo-physical properties, but three main subcategories have been identified: organic-organic, inorganic-organic, and inorganic-inorganic (Sharma et al., 2004; Mehling and Cabeza, 2008; Baetens et al., 2010; Oro et al., 2012).

## 2.2.2.4 Miscellaneous materials

PCMs that do not belong under the three main, aforementioned categories can simply be denoted as miscellaneous PCMs. An important subcategory of these phase change materials are clathrates. Clathrates are crystalline structures formed when molecules of one type get implanted in the crystal lattice of another. If the crystal lattice is that of water the clathrates are called clathrate hydrates. The phase change temperature range of clathrates is usually limited between 0 °C and 30 °C. The advantage of these materials is their high phase change enthalpy, but unfortunately their low thermal conductivity represents a problem (Mehling and Cabeza, 2008).

It becomes clear that none of the mentioned categories represents a perfect PCM due to variety of drawbacks. Some materials have high phase change enthalpy and are quite stable, but on the other hand they have low thermal conductivity or high degree of subcooling. Therefore different approaches are used in research to suppress undesired behaviour and enhance the inherent qualities of PCMs resulting in the creation of various PCM objects.

## 2.2.3 PCM objects

These objects are the results of the efforts being made in order to suppress undesired behaviour of PCMs and achieve best possible performance. In these processes various material properties are treated. Subcooling is usually suppressed through introduction of special additive materials in the form of nucleators into the PCMs. These nucleators serve to initiate crystal growth and the solidification itself. In the case of phase separation artificial mixing is often used. Apart from this, diffusion processes can be used to aid homogenisation. However, this is only effective if the separation distances are small which in turn can be assured through gelling using various substances. Another alternative method to reduce decomposition is by thickening the phase change material. This implies the use of additional material in order to increase the viscosity of the PCM and thus avoid far separation of phases. In addition, corrosion is usually suppressed by using appropriate PCM containers (Ravikumar and Srinivasan, 2005; Mehling and Cabeza, 2008).

Furthermore, increase in thermal conductivity is usually achieved through a composition with a highly conductive material. A composite material is a material that is developed by the composition of several different materials in order to improve the properties of the initial material. In the context of PCMs a composite can be formed by either embedding a new material into the PCM or embedding the PCM into the matrix of another material. The first combination is obtained through the introduction of metal or graphite (in the form of fibers, foam, or powder) into the phase change material. The second method is the infiltration of the phase change material into the graphite matrix. For PCMs which cannot be infiltrated into the matrix, a different approach is taken by mixing of PCMs and graphite in a compounding process. Compared to the matrix

infiltration, this method achieves somewhat lower values of thermal conductivities but the great advantage is that it allows the use of any and it can be moulded into any shape (Mehling and Cabeza, 2008).

All of the aforementioned methods aim to improve the thermal performance of PCMs, but certainly one of the best methods to achieve better operation is the encapsulation of PCMs. One of the reasons is to avoid contact between the phase change material and the environment. Another reason is to increase the heat transfer between the PCM and the capsule and moreover the overall heat transfers from the capsule to the environment since the capsule itself serves directly as a heat exchanger. Furthermore, encapsulation increases the mechanical stability of the material. Based on the capsule size, PCMs can be classified into: macroencapsulated (capsule size (i.e. relevant dimensions) varies from 1-1000 mm) and microencapsulated (capsule size varies from 2-1000 µm) PCMs (Khudhair and Farid, 2004; Mehling and Cabeza, 2008).

## *2.2.3.1 Macroencapsulated PCMs*

The relevant dimensions in macroencapsulated units vary from 1 to 1000 mm. Therefore, in this case, capsule shells can accommodate several ml up to few litres of PCMs. The capsules are usually in the form of metal or plastic containers or bags made in different shapes and sizes. Upon macroencapsulation, special care needs to be taken in terms of volume. Namely, the volume of the containers needs to be small enough to prevent merely edge solidification and poor heat transfer due to the low conductivity of PCMs (Khudhair and Farid, 2004; Mehling and Cabeza, 2008).

## *2.2.3.2 Microencapsulated PCMs*

Microencapsulation is the introduction of phase change material in liquid or solid form into capsules (shells) of the diameter between 2-1000 µm. Encapsulation entails many benefits from the enhanced heat transfer rates to the environment, due to the large surface to volume ratios of the capsules, to the improved mechanical stability. Apart from those, the problem of phase separation and cycling stability is also reduced due to

the reduction of molecular distances to the microscopic levels. In addition, it is possible to incorporate microencapsulated phase change material with other materials like solid blocks, bricks, concrete, and gypsum plates. The disadvantage of microencapsulation manifests in the potential occurrence of increased subcooling. Numerous microencapsulation products have been tested over the last decade. Some of those have even been commercialised. One of the leading manufacturers of microencapsulated paraffins is Basf chemical company (Basf SE, Ludwigshafen, Germany). The PCMs are available as fluid dispersion or as dried powder (Mehling and Cabeza, 2008; Zhou et al., 2012). Additionally, it is worth mentioning that the most recent investigations on microencapsulated PCMs aim towards the reduction of capsule sizes to nanoscale dimensions (Chen et al., 2012; Fuensanta et al., 2013; Seyf et al., 2013).

## 2.2.3.3 Phase Change Slurries (PCSs)

Special type of a PCM object is the Phase Change Slurry (PCS). They are widely used for active latent heat storage systems. Phase change slurry is a special type of PCM enabled to store/release latent heat through a phase change yet always remain in the liquid form. A very good PCS is the mixture of water with microencapsulated PCMs. In this case the phase change material stores/releases the latent heat while water works as a carrier fluid. This assures the slurry remains liquid even when the microencapsulated phase change material undergoes solidification. A PCS increases the storage density, increases the power of the TES system since more energy is transported per volume of fluid and finally improves the heat transfer coefficients. In a real application, PCSs are usually stored in a storage tank and pumped through the piping network resulting in improvement of heat transfer coefficients and thus smaller heat exchangers and less equipment. One of the problems of using slurries is the stratification resulting from difference of densities between the phase change materials and heat transfer fluids. The layers with higher content of PCMs and thus higher viscosity can form. In these cases, the pumps of greater power are required in order to circulate the slurry. Another form of PCS is the emulsion slurry. It is formed by a direct mixture of PCMs and the fluid, usually water. Sometimes different emulsifiers will be added to prevent time degradation of the initially homogeneous mixtures. Unlike

microencapsulated PCSs these slurries do not comprise shells which may decompose inside the system. Nevertheless, in comparison to the microencapsulated slurries the emulsions are less stable since the mixtures tend to separate over time. Current efforts in this field aim to overcome these problems (Mehling and Cabeza, 2008).

### *2.2.3.4 Shape stabilised PCMs*

Shape stabilised PCMs are stable composite materials formed through the dispersion of PCM into another phase of supporting material like polyethylene. Some of the first studies on shape stabilised PCMs were conducted by Inaba and Tu (1997), but recently these materials are getting more attention due to their attractive properties in terms of large apparent specific heat capacities, acceptable thermal conductivities, and the ability to preserve their shape during the phase change process. The utilisation of shape stabilised PCMs seems to greatly simplify the implementation of TES systems (Zhang et al., 2006a; Zhou et al., 2012)

## 2.3 Summary

The emerging energy sustainability concerns can largely be addressed by adequate harvesting and storage of the abundant thermal energy, produced from various processes. Thermal energy storage technologies offer an efficient solution for energy harvesting and storage. Currently, one of the most attractive TES techniques includes the application of phase change materials. Many materials are being investigated as potential PCMs. However, a good quality phase change material needs to meet some basic criteria in terms of its thermo-physical, kinetic, chemical and economic properties. Depending on these substantial parameters PCMs can be classified in few categories: organic, inorganic, eutectic, and miscellaneous PCMs. All of these have correlated advantages and disadvantages. The objectives of numerous research studies focus towards the suppression of the existing problems of PCMs resulting in the development of various PCM objects. The overall technology is not yet fully matured. Many studies are still being conducted in terms of the development and testing of new materials (Dimaano and Watanabe, 2002; Matsui et al., 2007; Li et al., 2013a),

reduction of subcooling effect and improvements of cycling stability and phase separation (Kumano et al., 2009), corrosion tests (Cabeza et al., 2001), and efforts towards the thermal conductivity enhancement (Fukai et al., 2003; Zhou et al., 2011, Xiao et al., 2013). Nevertheless, some materials have undergone commercialisation generating the currently available market products. Finally, it can be inferred that, independently of the material development stages, the working principles of PCMs are primarily based on the phase change temperature and enthalpy resulting in the differentiation of two major application fields of PCMs: temperature control and storage of heat or cold. Various applications within these fields are discussed in the next chapter.

# Chapter 3

# APPLICATIONS OF PCMs

Given the two defining properties of PCMs, the phase change temperature and phase change enthalpy, the temperature control and the energy storage naturally impose as the two leading application categories of these materials. However this classification is rather complex in terms of individual applications. Namely, the more comprehensible outline of PCM applications requires a mildly different approach based on the application area. Therefore the applications, reviewed in this chapter, are divided into three main groups: transport and general storage, medical, and building applications. Each group is briefly analysed and then illustrated with some examples.

## 3.1 Transport and general storage applications

Although the technology of PCMs is not yet fully matured, the applications of PCMs for transport and general storage facilities have been extensively commercialised, especially in the course of the last decade. In essence, all these applications fall under the temperature control area considering their common feature, the necessity to keep the potential products thermally stable. Namely, when it is imperative to keep the sensitive merchandise within a narrow temperature swing, PCMs offer an unmatched solution. Moreover, the use of PCMs for temperature control of various products is especially convenient in impervious places with the limited or non-existent power grid accessibility where conventional heating/cooling appliances cannot be used. Few different methods in terms of PCM placement are used. Sometimes the PCM units are placed in direct contact with the products that need to be preserved. Frequently, the PCM is used alongside the wall insulation material of the product containers. Furthermore, in the case of large volume containers, the PCM is placed apart from the container wall and convection is used to aid the temperature stability (Bailey, 2010).

The transport and general storage applications cover many diverse fields like the transport and storage of fresh or cooked food, cold or hot beverages, electronic circuits, and many others. However, for brevity purposes, only a few typical examples are discussed below.

Transport containers enhanced with PCMs are especially useful in catering services. In other words, these containers can be used when fresh or cooked food is prepared at one point and has to be transported to another location. One commercialised solution for the transportation of meals is the pizza-heater (Rubitherm GmbH, Berlin, Germany). It is essentially a plate impregnated with PCM. The pizza is usually placed on top of the plate and then the whole entity enclosed in the pizza delivery box. In this way, the pizza is held at 65 ℃ three times longer than in conventional boxes. Rubitherm (Rubitherm GmbH, Berlin, Germany) also offers separate aluminium or plastic elements filled with PCM that can be used for the transport of various food products. These are available in numerous shapes and forms (Figure 3.1). Apart from Rubitherm (Rubitherm GmbH, Berlin, Germany), Teap PCM (Teap PCM, Mumbai, India), Climator (Climator Sweden AB, Skövde, Sweden), and va-Q-tec (va-Q-tec AG, Wuerzburg, Germany) are the companies with the largest variety of PCM products for food transport.
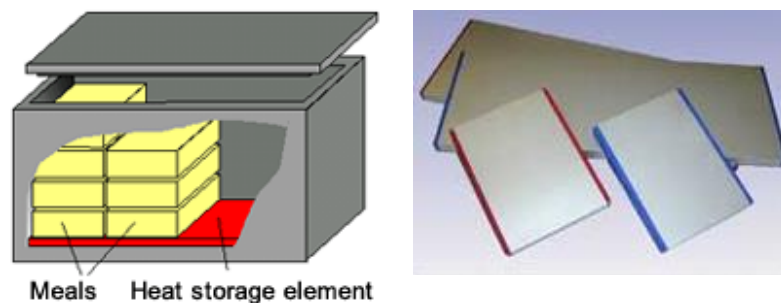


*Figure 3.1: PCM solutions for food transport (amended from Rubitherm GmbH, Berlin, Germany).*

Furthermore, the concept used for food can also be adapted for beverages. One of the well-known solutions is the ''isothermal bottle'' (Figure 3.2), developed by the company Sofrigam (Sofrigam, Rueil-Malmaison, France). The bottle has a double wall where the PCM fills the space between the walls.
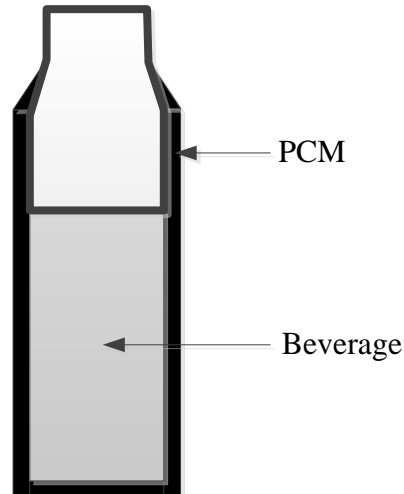
**Figure 3.2:** *The isothermal bottle concept (amended from Mehling and Cabeza, 2008, p. 200).*

The available volume of the bottle is about 0.5 l. Before the use, it needs to be cooled so the PCM can solidify. The performance is expressed in terms that the bottle can keep the beverage cold at about 13 °C for 3 h in the case of the ambient temperature of 25 °C (Mehling and Cabeza, 2008).

Apart from the specifically designed containers, multipurpose boxes or pads for transportation of products are sold by some companies like Sofrigam (Sofrigam, Rueil-Malmaison, France), PCM Products (PCM Products Limited, Yaxley, UK) (Figure 3.3), TCP Reliable (TCP Reliable, Edison, New Jersey), PCM Thermal Solutions (PCM Thermal Solutions, Chicago, Illinois), Air Container (Air Container, Åkersberga, Sweden), and Entropy Solutions (Entropy Solutions Inc., Plymouth, Minnesota).



**Figure 3.3:** *Multipurpose transport solutions (amended from Sofrigam, Rueil-Malmaison, France and PCM Products Limited, Yaxley, UK).*

In addition, general storage applications also include the storage facilities for electronic equipment. Generally, electronics is highly temperature sensitive and works

best within a certain temperature margins. However, sometimes certain electronic equipment is exposed to outdoor conditions with large temperature swings between -40 °C and +50 °C, especially in desert areas. This can result in equipment's failure or lifetime reduction. The application of PCMs, in junction with the electronic parts, leads to smaller temperature fluctuations and provides better performance of the equipment (Mehling and Cabeza, 2008). An illustrative study and some of the pioneering achievements for thermal management of batteries were reported by Khateeb et al. (2005).

Moreover, the PCMs are also used as part of household and industrial refrigeration systems as explained in various studies (Cheralathan et al., 2007; Azzouz et al., 2009; Gin and Farid, 2010; Liu et al., 2012).

A short summary of the transport and general storage applications of PCMs was given. From the PCMs' perspective these applications include miscellaneous medical examples as well, but given the specifics of the application area those are explained in a separate section.

# 3.2 Medical applications

Medical applications of PCMs can be divided into two major groups: transport and storage of medical products and applications for the human body.

# 3.2.1 Transport and storage of medical products

Usually, medical products are quite expensive and strongly dependent on the transport and storage temperature. Although the transportation vehicles are equipped with air-conditioning to the desired temperature, the problems emerge during the transport between the hospital or other supplier and the transportation vehicle and also between the vehicle and the final destination (Mehling and Cabeza, 2008). PCMs seem to provide a natural solution for these difficulties. Apart from transplantation organs, one of the most sensitive medical products is positively blood since it needs to be kept within a really narrow temperature margin. In order to meet the blood demand, many hospitals have to obtain the blood units from remote suppliers. Conventional

transportation systems used to keep the blood within the prescribed temperature range are highly complex and very expensive. Systems based on PCMs offer a simple and a relatively cheap solution. For instance, PCMs from Rubitherm (Rubitherm GmbH, Berlin, Germany) are used for the implementation of an innovative transport system, called "BLOOD IN MOTION" (Figure 3.4). This is an important, but certainly not a unique example of safe and efficient blood transport methods.



*Figure 3.4: BLOOD IN MOTION solution (amended from Rubitherm GmbH, Berlin, Germany).*

Furthermore, some companies are developing containers to ensure the safe transport of various pharmaceutical products like insulin, vaccines, and other medications. A representative example given here are the transportation boxes developed by Sofrigam (Sofrigam, Rueil-Malmaison, France) (Figure 3.5).
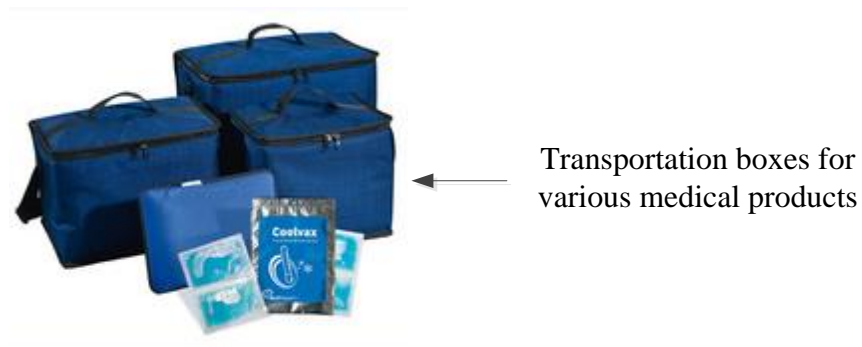


*Figure 3.5: Transportation boxes for medical products (amended from Sofrigam, Rueil-Malmaison, France).*

## 3.2.2 Application for the human body

Applications for the human body are quite similar to the applications for transport and general storage except that in the former there exists an additional internal heat source, the human body, and secondly, the insulation provided by clothes is usually not as effective as the insulation of transportation containers. However, the applications are equivalent in terms that they are both decentralised from the power sources. The main role of PCMs in this case is to provide thermal comfort for the human body. As with sensitive products, the human comfort temperature requirement range is very narrow and therefore PCMs appear as a promising solution. One approach to achieve thermal body comfort is to integrate PCMs into clothes either by utilisation of macroencapsulated materials (pouches filled with PCM), either by integration of microencapsulated PCMs directly into textiles (Mehling and Cabeza, 2008).

The number of companies developing and testing PCM textiles and fabrics seems ever-growing. One of the leading companies is Outlast Technologies (2012). This company incorporates PCMs into fibers spun to yarns used for further manufacturing of garments. In addition, Schoeller Textiles (Schoeller Textiles AG, Sevelen, Switzerland) is a Swiss company involved in the development of PCM based wool textiles which should be applied for the production of winter outfits. Also, they develop the kidney belts to be used by motor cyclists. These belts are based on the latent heat storage/release principle. Namely, when the body temperature or that of the environment increases, the microencapsulated PCM integrated into the belt absorbs and stores the excess heat and vice versa, when temperature falls the PCM releases the heat.

Furthermore, one of the best known applications of PCMs for the thermal body comfort is the pocket warmer. They are specific since in this case subcooling of the PCM is actually desirable since it allows the material to cool down to the ambient temperature without changing phase and releasing the latent heat. Only when heat is needed, a mechanical trigger integrated into the warmer is used to start the solidification process and release the latent heat. This is an example of the controlled phase change mechanism (Mehling and Cabeza, 2008).

In addition, various other thermal comfort PCM solutions are being developed like the cooling vests for people who need to endure hot environments (Climator

Sweden AB, Skövde, Sweden), the bedding products (Outlast Technologies LLC, Golden, Colorado), the shoe inlets (Colortex GmbH, Pirmasens, Germany) and numerous other products.

Heat and cold therapies are some of the most important medical applications. Cold therapy is useful for the reduction of body temperature in the case of fever as well as for the treatment of the inflamed body parts. On the other hand, heat therapy can be used for pain treatment, increase of blood flow, and muscle regeneration (Mehling and Cabeza, 2008). Some leading products in this are developed by Rubitherm (Rubitherm GmbH, Berlin, Germany) (Figure 3.6).



Rubitherm's hot products
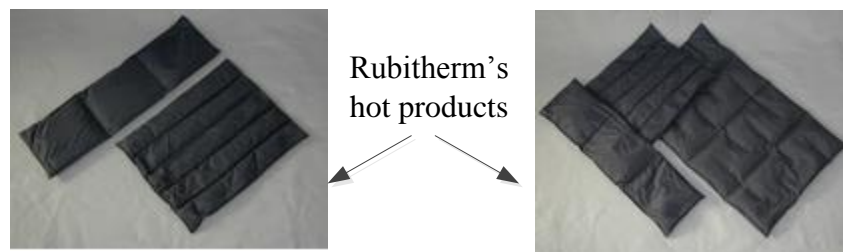
*Figure 3.6: Rubitherm's hot products for heat therapy (amended from Rubitherm GmbH, Berlin, Germany).*

These products are filled with fine grain PCM powder that stays soft at any temperature resulting in comfortable moulding of the products that fit the body contours at any time point. The used PCM is non-toxic and the products are completely safe and environmentally harmless.

# 3.3 Building applications

Recently, the energy demand for indoor human comfort has increased worldwide. Namely, apart from conventional heating demands, the use of electrical power for cooling and air-conditioning is rising fast resulting in increasing economical charges and an extending environmental impact (Bailey, 2010). During the course of the past decade, TES systems based on PCMs have been recognized as one of the leading technologies for the enhancement of energy efficiency and sustainability of buildings. Hence, building applications of PCMs are of the most interest for this study. The studies in this area are abundant and almost impossible to compile as indicated in

various review papers (Zhu et al., 2009; Agyenim et al., 2010; Baetens et al., 2010; Oro et al., 2012; Zhou et al., 2012). However, a modest attempt has been made here to briefly summarise these studies in terms of the most important spheres of interest.

## 3.3.1 Free-cooling applications

According to Zhu et al. (2009) the definition of free-cooling as the amount of cooling that can be acquired from existing, additional, or retrofitted components of the system during low ambient temperatures and used later on demand, given by De Saulles in 1996, stands even today. Usually two different approaches are used, water and air side free-cooling. It is worth noting that generally various mechanical tools are used to aid the heat transfer in these applications so technically speaking free-cooling is not indeed free. During the last few decades, various designs and solutions for free-cooling have been proposed, but only some will be mentioned at this point.

A testing system for free-cooling applications in buildings was designed by Zalba et al. (2004). Zhang et al. (2006b) and Butala and Stritih (2009) listed some ideal and candidate PCMs for free-cooling applications in terms of the available thermo-physical properties. Arkar et al. (2007) investigated the efficiency of free-cooling through the use of latent heat storage integrated into the ventilation system of a low energy building. Moreover, Medved and Arkar (2008) developed a correlation between the local climate conditions and the free-cooling potential of TES systems based on PCMs. In general, this and other studies showed that the capability of free-cooling primarily depends on the amplitudes of the outdoor temperature fluctuations.

## 3.3.2 Peak shifting applications

Diurnal weather conditions as well as the industrial and household activities dictate the electricity demand which varies significantly during the 24 h span. Many countries have a policy of higher peak utility rates imposing the need for the shift of peak energy demands towards the off-peak hours. TES systems using PCMs can use the cheap cool energy, stored through the PCM solidification during the nocturnal electricity rates, or an almost free one, coming from natural ambient conditions, to provide for the peak

cooling demand, later in the day. Moreover, the same latent heat storage/release principle can be used for shifting or reduction of peak heating loads in winter months (Zhu et al., 2009).

Hasnain (1998) presented an overview of the commercial TES technologies for off-peak air-conditioning mostly based on water, ice, and eutectic salt storage media. Over the following years both numerical and experimental studies were conducted. Yamaha and Misaki (2006) evaluated the PCM peak shaving methodology in air distribution systems. Later on, Halford and Boehm (2007) modelled the whole scenario of peak load shifting based on PCMs. The general conclusion of these studies was the same. Essentially, the price of the PCM is usually the most important parameter that needs to be taken into the account during the development of peak-shaving TES systems since it dictates the pay-back period and consequently the return on investment of these systems.

## 3.3.3 Active building systems

Active building systems are implemented through the integration of PCM solutions and mechanical heating/cooling equipment like heat pumps, floor and ceiling heating systems, heat recovery systems, and others. Few examples of these systems are presented to illustrate the general concept. Kaygusuz and Ayhan (1999) reported the experimental and theoretical investigations on PCM-aided solar heat pump system for residential buildings. In 2005, Saman et al. (2005) investigated the performance of PCM thermal storage unit for a roof integrated solar heating system. Following, Hammou and Lacroix (2006) developed a hybrid TES system for simultaneous management of solar and electric energy. Zeng et al. (2009) and Wang and Niu (2009) investigated the potential of microencapsulated phase change materials slurries in active TES systems. Moreover, Lin et al. (2005) and again Lin et al. (2007) studied the integration of shape stabilised PCM products and electric heating systems reporting satisfying results regarding the indoor temperature control. Many active TES systems remain only in the domain of numerical investigation, but many studies undergo an experimental validation too (Delgado et al., 2012; Dolado et al., 2012). In general, the

usability of the active TES systems highly depends on the heating/cooling loads of buildings and the associated costs of such systems.

## 3.3.4 Passive building systems

In the passive systems various forms of PCMs are directly integrated into building envelopes like walls, roofs, and floors to increase the thermal mass of buildings (Zhu et al., 2009). This can be achieved in various ways through the PCM enhanced wallboard, concrete (thermocrete), or other building insulation materials. Numerous passive systems are being tested in the laboratories as well as in the real world. Some of the studies report on the PCM enhanced wallboards since the wallboard is cheap and widely used as building material (Neeper, 2000; Chen et al., 2008; Kuznik et al., 2008; De Gracia et al., 2011). Other studies are involved with PCM enhanced concrete which is also called thermocrete (Bentz and Turpin, 2007; Cabeza et al., 2007; Pomianowski et al., 2012). Generally, the techniques used to impregnate the construction materials with PCMs are numerous and yet increasing. However, these are not an important subject of this study and therefore not discussed in detail.

## 3.3.5 Solar applications

Special and yet a challenging type of TES applications are the solar applications where PCMs are usually integrated with the glazing systems or used as window curtains in order to reduce the solar gain in buildings. These systems can be either passive or active. Some of the pioneering works in this field were reported by Ismail and Henriquez (2001) and Weinläder et al. (2005). Moreover, the company Greenlite Glass Systems (Greenlite Glass Systems, Port Coquitlam, British Columbia) commercialised the PCM enhanced glass façade system, called GLASS X. However, thorough information on the real-time performance of PCMs used in these solutions is still lacking.

# 3.4 Summary

Applications of PCMs are genuinely diverse. Transport and general storage as well as medical applications are being widely commercialised. Nonetheless, the area of building applications where PCMs seem to exhibit the greatest potential in terms of energy sustainability, large scale employment, and conceivable economic revenues, is still research in progress. Numerous achievements have been published, yet the technology is not mature enough. Various studies are intensely being conducted in terms of both development of new phase change materials and testing of whole laboratory/real world scale TES systems. Regardless of the type of studies, the essential research principle requires the precise knowledge of the heat transfer mechanisms underlying the phase change process. For this reason, the thermodynamics and heat transfer analysis of phase change processes are discussed in the next chapter.

# Chapter 4

# THE THERMODYNAMICS AND HEAT TRANSFER ANALYSIS OF PHASE CHANGE PROCESSES

Temperature control and storage/release of heat/cold are the two principal application areas of PCMs. The underlying mechanism that allows the control of temperature and the storage of energy is the transfer of heat. From the scientific point of view, the terms "heat" and "heat transfer" are equivalent (Atkins, 2010). Nevertheless, given the aforementioned perspective of TES and PCMs (discussed in chapter 2), the term "heat" is interchanged with the term "energy" and used as such in this thesis. There are three modes of heat transfer: conduction, convection, and thermal radiation. Some authors point out the phase change as one of the heat transfer modes. However, the change of phase is a very complex process that usually includes all three modes of heat transfer (Mehling and Cabeza, 2008).

The transient heat transfer problems combined with the melting/solidification are commonly denoted as "phase change" or "moving boundary" problems. Their mathematical formulation is governed by parabolic partial differential equation (PDE). These problems are nonlinear. The analytical solution of these problems is very difficult. Namely, the location of the moving solid-liquid interface is not known *apriori* and forms a part of the solution resulting in the nonlinearity of the phase change problems. A limited number of exact analytical solutions is available and only for few simplified cases (Dutil et al., 2011). Nonetheless, numerous numerical solutions have been published. Different approaches like finite differences, finite elements, or control volumes are used in these solutions. Additionally, the numerical studies can be classified into few categories depending on the underlying methods. These include: fixed grid methods, variable grid methods, front fixing method, adaptive grid

generation method, and enthalpy method (Verma et al., 2008). In literature, each category is supported by a number of studies (Hu and Argyropoulos, 1996; Verma et al., 2008), yet those specifics are not essential for this study; therefore only the basics of heat transfer in PCMs are discussed in this chapter, starting with the general formulation of the phase change problem.

# 4.1 Mathematical formulation of the phase change problem

For the simplicity purposes, the mathematical formulation of the phase change problem will be illustrated on an example given by Ozisik (1994): 1-Dimensional (1D) solidification/melting of a semi-infinite PCM layer. An important restriction used in this example assumes that there is no fluid motion so the heat transfer in solid and liquid parts proceeds by conduction only. Although this example is 1D, once it is formulated it is fairly easy to perform its generalisation for multidimensional space.

For the solidification process, a liquid semi-infinite PCM layer at initial temperature $T_i$ (higher than the phase change temperature $T_{pc}$) is confined within a region $0<x<\infty$. At time $t=0$ the temperature at the boundary surface $x=0$ is changed to $T_0$ which is lower than $T_{pc}$. At this moment the solidification of the PCM starts from the boundary $x=0$ and progresses in the positive $x$ direction as indicated by the location of the solid-liquid interface $s(t)$ (Figure 4.1).

The conduction processes within the solid and liquid parts of the PCM during phase change can be easily described mathematically by parabolic transient heat conduction Equations 4.1 and 4.2:

$$\frac{\partial T_s}{\partial x^2} = \frac{1}{\alpha_s} \frac{\partial T_s}{\partial t} \tag{4.1}$$

$$\frac{\partial T_l}{\partial x^2} = \frac{1}{\alpha_l} \frac{\partial T_l}{\partial t}, \tag{4.2}$$

where the $T_s\ (x,\ t)$ and $T_l\ (x,\ t)$ are the temperatures in the solid and liquid part of the PCM while the $\alpha_s$ and $\alpha_l$ are the corresponding thermal diffusivities of the material.
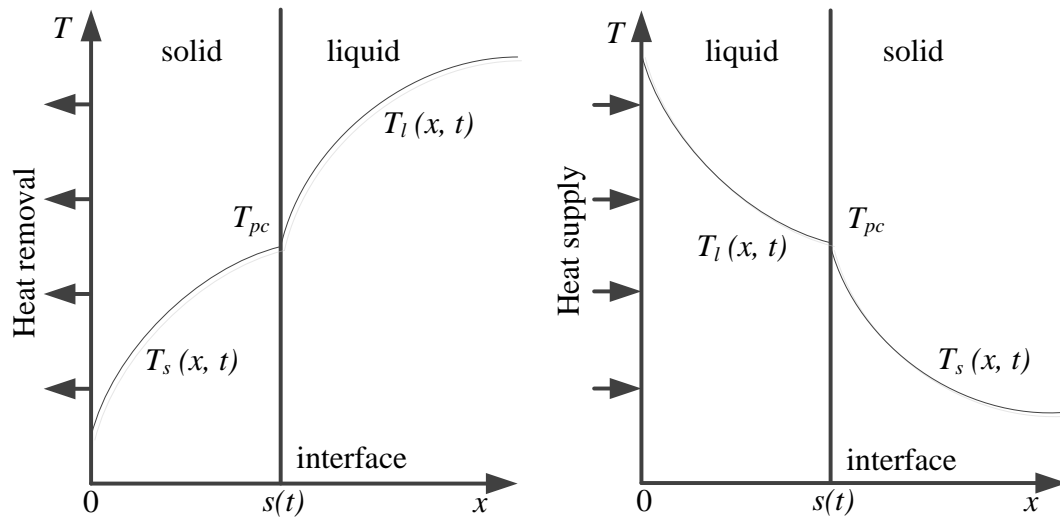
**Figure 4.1:** *1D solidification (left) and melting (right) of semi-infinite PCM layer (amended from Ozisik, 1994, p. 277).*

However, the situation at the solid-liquid interface at *x=s(t)* is rather different and needs to be described by the general energy balance equation (Figure 4.2).



**Figure 4.2:** *General energy balance equation at the solid-liquid interface during 1D solidification (amended from Ozisik, 1994, p. 277).*

This general equation can be expressed through the mathematical means in order to derive the first boundary condition for the solid-liquid interface. This condition represents one of the essential parts in phase change problem formulation and can be formally expressed as:

$$k_s \frac{\partial T_s}{\partial x} = k_l \frac{\partial T_l}{\partial x} + \rho_s L \frac{\partial s(t)}{\partial t}. \tag{4.3}$$

The $k_s$ and $k_l$ in the Equation 4.3 denote the thermal conductivities of the solid and liquid phases, $\rho_s$ represents the density of the solid phase and $L$ is the latent heat of

solidification/melting per unit mass (which usually equals the specific enthalpy change $\Delta_{pc}h$ or $\Delta h$ introduced in chapter 2).

Furthermore, the densities in solid and liquid phases are different, but when the solid density is used in the Equation 4.3 the convective effects due to the difference in densities cancel out (Ozisik, 1994).

Additionally, only one more equation (Equation 4.4) is necessary for the full formulation of the 1D solidification and that is the expression that describes the second boundary condition at the solid-liquid interface which essentially states that the temperature of the solid and liquid phases at the interface $x=s(t)$ are equal to the phase change temperature of the PCM.

$$T_s(s(t),t) = T_l(s(t),t) = T_{pc} \qquad (4.4)$$

The set of equations (Equations 4.1-4.4) fully defines the 1D solidification of the semi-infinite PCM layer. Moreover, the same equations can be applied for the melting process as well. The solid-liquid interface progresses in the positive $x$ direction even upon melting (Ozisik, 1994).

The presented solidification/melting problem is simple in terms of the complexities that can arise in real phase change applications, but is a very good example for the understanding of the underlying physics of the phase change processes. Since the location of the solid-liquid interface forms part of the solution the more complex phase change problems are very difficult to solve analytically giving into the expansion of numerical solutions.

According to Verma et al. (2008) and Dutil et al. (2011) various methods have been developed for phase change problem solving. The most important of the developed techniques and one of the most widely used is certainly the enthalpy method. Therefore, this method is explained in detail in the section 4.2.

# 4.2 Enthalpy method

In the mathematical phase change problem formulation, given previously, the solid-liquid interface location forms part of the solution and needs to be tracked in order to accurately solve the problem. Additionally, a constant phase change temperature was assumed in the previous mathematical schemes. However, in the real world problems phase change usually takes place in a narrow temperature range, but range nonetheless. In such situation, the presented phase change formulation is not applicable. The enthalpy method was developed to solve the problems in those situations. This formulation uses the temperature dependent *H(T)* function which represents the total heat content of the material (Ozisik, 1994).

The enthalpy formulation of the phase change problem is expressed in Equation 4.5:

$$\rho \frac{\partial H(T)}{\partial t} = \nabla(k\nabla T) + g(T), \qquad\qquad (4.5)$$

where *k* and *ρ* represent the thermal conductivity and density functions of the PCM and can be taken as constants or functions of the material temperature *T* depending on the specifics of the problem at hand. Moreover, the energy generation term *g(T)* can be used or overlooked depending on the presence of the internal energy generator in the investigated problem. Regardless, the enthalpy method reduces the phase change problem formulation to a single equation (Equation 4.5) to be solved in terms of enthalpy (Verma et al., 2008).

The enthalpy-temperature dependency, in the form of *H(T)* function, is defined for both PCMs with the constant phase change temperature and the PCMs with the solidification/melting range (Figure 4.3).

For the substances with the constant phase change temperature the *H(T)* function shows a discontinuity at the $T_{pc}$ resulting in an infinite derivative value of *∂H/∂T* in Equation 4.5. Nevertheless, according to Ozisik (1994), it was proved that the integral form of the Equation 4.5 without the *g(T)* term matches the classical formulation of the phase change problem. Consequently, the enthalpy method can be

used for the solution of phase change problems occurring either at constant temperature or within a narrow range.
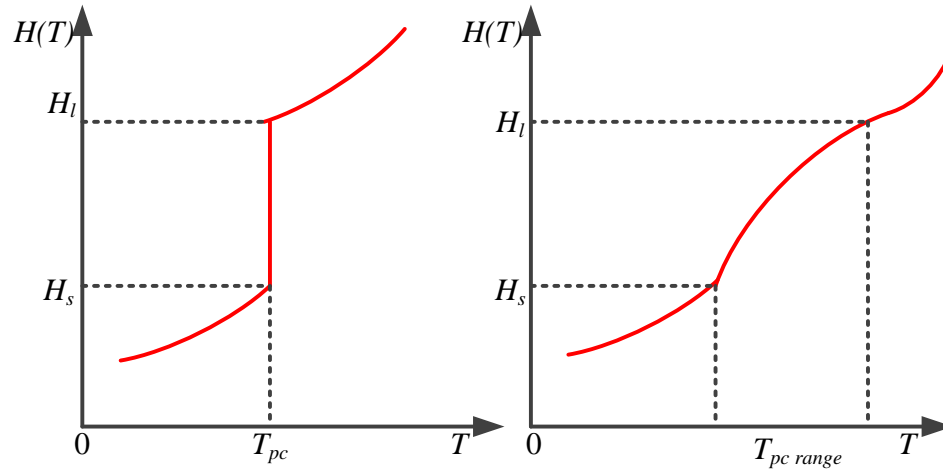


**Figure 4.3:** *Illustrative enthalpy-temperature relation for PCMs with constant phase change temperature (left) and for PCMs with phase change range (right) (amended from Ozisik, 1994, p. 297).*

For the problems with constant temperature $H(T)$ function needs to be defined in terms of sensible heat capacity $C_p$ and latent heat of solidification/melting $L$ as in Equation 4.6:

$$H(T) = \begin{cases} C_p(T - T_{pc}), T \leq T_{pc} \\ C_p(T - T_{pc}) + L, T > T_{pc}. \end{cases} \quad (4.6)$$

In addition, the numerical solutions founded on the enthalpy and classical phase change problem formulations are numerous, yet not of essential interest for this study. On the other hand, a solution, given by Stefan in 1890 as confirmed by Ozisik (1994), for the 1D solidification of semi-infinite PCM layer is very important for better understanding of the general thermodynamic mechanism and the main heat transfer parameters of the phase change processes.

## 4.3 Stefan solution

In 1891, Stefan generated an analytical solution for the solidification problem of the 1D semi-infinite PCM layer (Figure 4.4 and Figure 4.5) using some serious restrictions in terms of both, geometry and thermal effects (Mehling and Cabeza, 2008). The

geometry restrictions include 1D space, the semi-infinite PCM layer, and the assumption on constant volume during phase change. In addition, the thermal restrictions are following: the heat is stored only as latent heat because the sensible heat stored is negligible compared to the phase change enthalpy, the heat transfer is proceeding by conduction only in order to obtain linear temperature profiles, at the initial time point $t=0$ the PCM is liquid (upon solidification) and at the phase change temperature $T_{pc}$ throughout (or solid at $T_{pc}$ throughout upon heating), the temperature at the boundary $x=0$ is changed to $T_0$ at $t=0$ and further kept constant. This simple heat transfer model is called "Stefan problem" and its solution is very straightforward considering all the restrictions applied (Mehling and Cabeza, 2008).
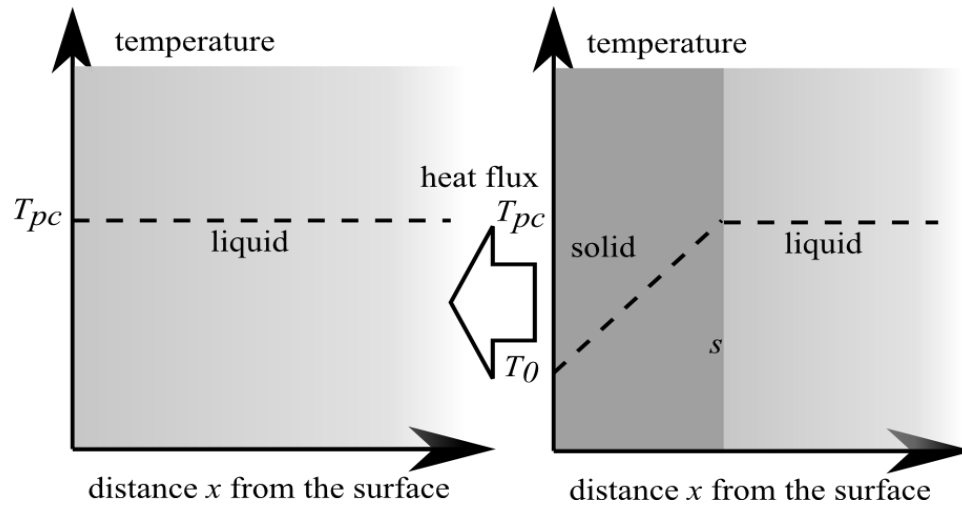


**Figure 4.4:** *Cooling of a 1D semi-infinite PCM layer at t=0 (left) and at later time (right) (amended from Mehling and Cabeza, 2008, p. 106).*

The amount of heat released $dQ$ when the solid-liquid interface moves the distance $ds$ is given in Equation 4.7:

$$dQ(t) = \Delta_{pc}hAds(t). \qquad (4.7)$$

The heat released when the interface is moving equals the heat that leaves at the surface at $x=0$ since no heat is stored in between (sensible heat is neglected).
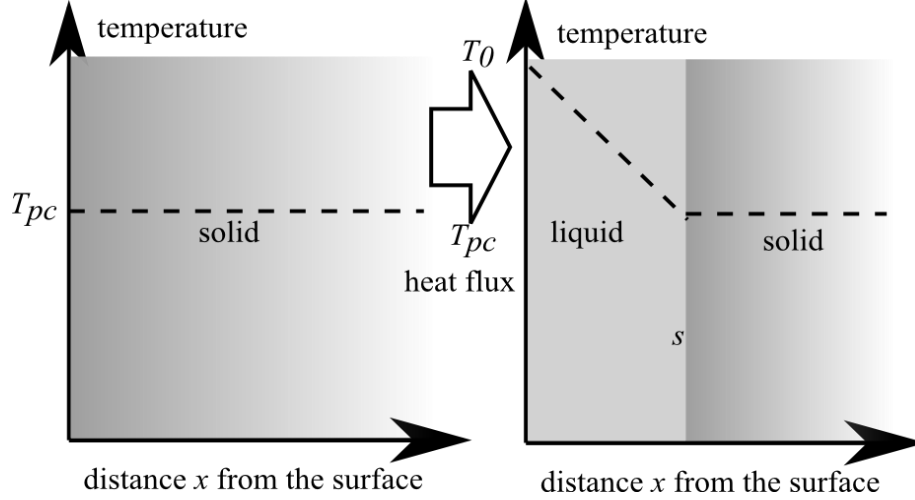
**Figure 4.5:** *Heating of a 1D semi-infinite PCM layer at t=0 (left) and at later time (right) (amended from Mehling and Cabeza, 2008, p. 107).*

The heat flux density (heat flux per area) at the surface is calculated as given in Equation 4.8:

$$\frac{dq(t)}{dt} = \Delta_{pc} h \frac{ds(t)}{dt}. \tag{4.8}$$

Since the heat transfer is by conduction only and sensible heat is negligible, temperature change from the location of the solid-liquid interface $s$ to the surface at $x=0$ is linear; therefore the heat flux density at the surface is calculated as given in Equation 4.9:

$$\frac{dq(s)}{dt} = k \frac{T_{pc} - T_0}{s}. \tag{4.9}$$

After the separation of the variables for the location $s$ and time $t$ and integration from Equations 4.8 and Equation 4.9 follows the expression given by Equation 4.10:

$$\frac{k(T_{pc} - T_0)}{\Delta_{pc} h} t = \frac{1}{2} s(t)^2. \tag{4.10}$$

From the above, the time for the solid-liquid interface to reach the location $s$ from the surface is given by Equation 4.11:

$$t = \frac{1}{2} \frac{\Delta_{pc} h}{k(T_{pc} - T_0)} s(t)^2. \tag{4.11}$$

Moreover, the location of the solid-liquid interface (phase front) $s$ as a function of time is expressed as given in Equation 4.12:

$$s = \sqrt{2 \frac{k(T_{pc} - T_0)}{\Delta_{pc} h} t}. \qquad (4.12)$$

Finally, the equations 4.11 and 4.12 form a solution of the Stefan phase change problem in terms of the time progress of the solid-liquid interface which is one of the most significant performance indicators of the TES systems based on PCMs (Mehling and Cabeza, 2008).

Additionally, the heat flux density as a function of time can be expressed as given in Equation 4.13:

$$\frac{dq(t)}{dt} = \sqrt{\frac{k(T_{pc} - T_0)\Delta_{pc} h}{2t} t}. \qquad (4.13)$$

The Equations 4.11-4.13 can be used to estimate the influence of various PCM parameters like the phase change temperature $T_{pc}$, the phase change enthalpy $\Delta_{pc} h$, and the thermal conductivity $k$, on the heat flux density and the movement of the solid-liquid interface of the 1D semi-infinite PCM layer. However, considering the fundamental principles behind the Stefan model, these assessments could certainly provide useful information on the behaviour of more complex PCM systems. For these reasons, a simple parametric test was implemented and executed, as explained in the following subchapter.

## 4.4 Parametric test

The real world phase change problems are rather complex. Nevertheless, considering the thermodynamic principles of the phase change process, the general conception of the behaviour of real TES systems can be obtained from the understanding of the simple phase change problem like Stefan's. Hence a simple parametric test was designed and implemented at this point, prior to any further research, to determine the most influential PCM properties in phase change processes. The general idea was that the influence of certain PCM parameters should reflect in similar manner in both

simple solutions like Stefan's and the highly complex ones, employed in real-time applications.

The parametric test was implemented using the Stefan solution given in the Equations 4.11 and 4.12. A MATLAB based program was developed and used to assess the influence of the most important PCM properties (phase change temperature, phase change enthalpy and thermal conductivity) on the time progression of the solid-liquid interface in 1D semi-infinite PCM case.

The parametric study was performed for the solidification process of an imaginary PCM with such properties to reflect the behaviour of common organic PCMs. The standard thermo-physical properties of this material were adopted as following: the phase change temperature was taken to be 21 °C, the phase change enthalpy was 140 kJkg$^{-1}$K$^{-1}$, and the thermal conductivity was 0.2 Wm$^{-1}$K$^{-1}$. Additionally, the driving temperature for the phase change was 18 °C. The available time for the phase change was evaluated in the range from 0 to 2 h.

Given the above parameters, the evolution of the solid-liquid interface was investigated depending on the 10 % marginal fluctuations of the following parameters: the phase change temperature $T_{pc}$, the phase change enthalpy $\Delta_{pc}h$, and the thermal conductivity $k$. Firstly, the phase change temperature was varied within the 21 °C±10 % range (Figure 4.6). Following, the phase change enthalpy was varied within the 140 kJkg$^{-1}$K$^{-1}$±10 % range (Figure 4.7). Finally, the thermal conductivity was varied within the 0.2 Wm$^{-1}$K$^{-1}$ ±10 % range (Figure 4.8).

In all three cases (Figure 4.6-4.8) the $y$ and $z$ axes were constant, representing the two most important parameters in Stefan's solution, the time of the phase change process and the location of the solid-liquid interface. The variable parameter, being the phase change temperature in the first case (Figure 4.6), the phase change enthalpy in the second (Figure 4.7), and the thermal conductivity in the third one (Figure 4.8), was represented on the $x$ axis. Evidently, given the same ranges of values for phase change temperature and the location of the solid-liquid interface in all three graphs (Figure 4.6-4.8), even upon a simple visual investigation of the 3-Dimensional (3D) plots, it can be concluded that the phase change temperature is the most influential parameter in the Stefan's solution.
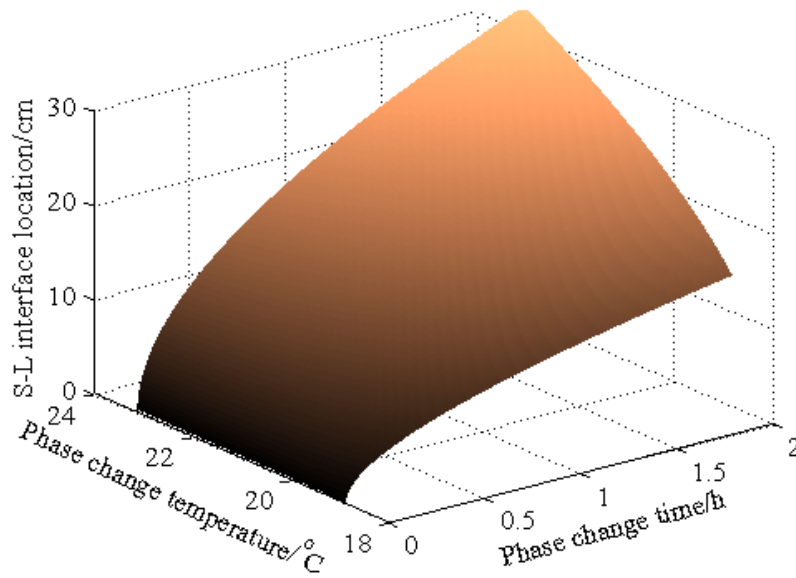
*Figure 4.6:* *The dependency of the solid-liquid interface location on the time available for the phase change process and the phase change temperature variation of the imaginary PCM reflecting the behaviour of common organic PCMs.*
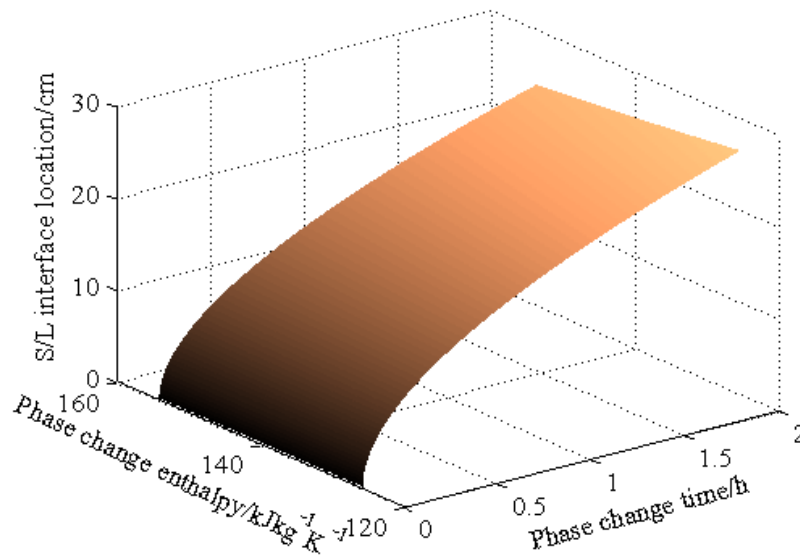


*Figure 4.7:* *The dependency of the solid-liquid interface location on the time available for the phase change process and the phase change enthalpy variation of the imaginary PCM reflecting the behaviour of common organic PCMs.*
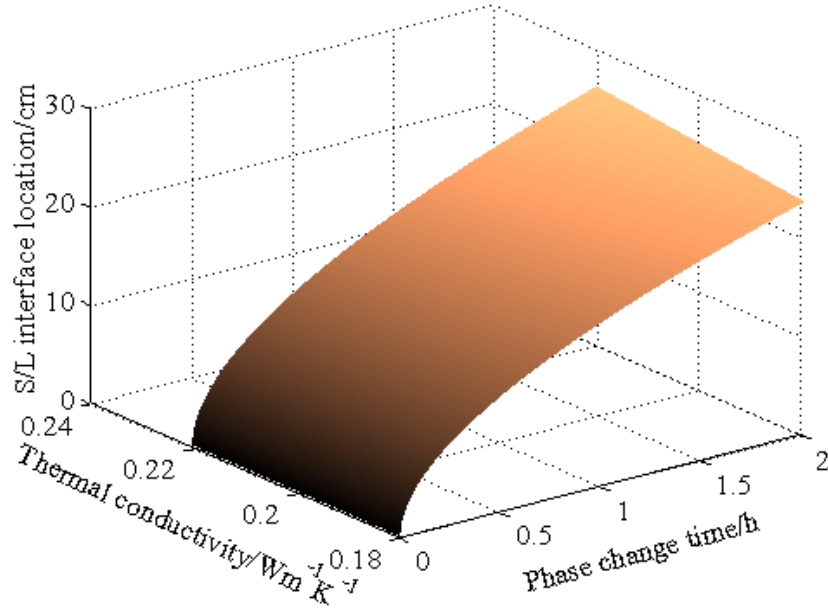
***Figure 4.8:*** *The dependency of the solid-liquid interface location on the time available for the phase change process and the thermal conductivity variation of the imaginary PCM reflecting the behaviour of common organic PCMs.*

Namely, the intersection of *yz* planes when *x=const.*, especially for higher values of *x,* with the plotted 3D surfaces results in the steepest and least linear curves in the first scenario (Figure 4.6) clearly indicating that the phase change temperature is the most significant parameter influencing the propagation of the solid-liquid interface during phase change process. The same curves are not as steep and nonlinear in the second case (Figure 4.7) as in the first one (Figure 4.6), but steeper and less linear than in the third case (Figure 4.8). This indicates that the influence of the phase change enthalpy in the Stefan's solution is greater than that of the thermal conductivity. Given the notion that the influence of certain PCM parameters should reflect in similar manner in both simple solutions like Stefan's and the highly complex ones the observed behaviour leads to the conclusion that the phase change temperature and the phase change enthalpy are indeed the most important properties of PCMs.

## 4.5 Summary

The design, implementation, and optimisation of any large scale TES system requires the solution of basic heat transfer problems regarding the components the system is based on. Considering the nonlinear nature of the phase change problems, analytical solutions appear unattainable. For this reason, the reported numerical solutions based on various implementation methods are numerous. However, all the solutions are founded on the mathematical description of the problems at hand. The mathematical equations rely on the physical quantities and their associated relations. Hence, it becomes clear that the essential part of any solution and the key for accurate prediction of the latent heat TES systems' performances is the precise knowledge of PCM properties. The thermo-physical properties, especially in terms of phase change temperature and enthalpy are the most important as evidently indicated in the parametric study explained in this chapter, therefore the current technologies for behavioural characterisation of phase change materials are discussed in detail in the next chapter.

# Chapter 5

# CURRENT TECHNOLOGIES FOR BEHAVIOURAL CHARACTERISATION OF PCMs

Currently, the overall technology of PCMs is ever-growing. The new developments in both research and commercial sectors evolve in two main directions, towards the development of latent heat TES systems in terms of small or large scale products and towards the development of new materials. Regardless of these directions the underlying heat transfer problems involving the change of phase need to be defined and solved. Due to the nonlinearity of the phase change process and the specific nature of PCMs the numerical solutions are preferred over the exact analytical solutions. The numerical solutions and predictions directly dictate the development of any new latent heat TES products or materials. In addition, these solutions predominantly depend on the physical quantities of materials under investigation. Hence, accurate and precise determination and knowledge of PCM properties is imperative for the design, development, and optimisation of any latent heat TES systems. One of the major limiting factors for both modelling and implementation of efficient PCM based TES systems is the inaccuracy/lack of the experimentally determined material data especially in terms of basic and the most deterministic thermo-physical properties, the phase change temperature and enthalpy (Mehling and Cabeza, 2008). Therefore, the current technologies and methods for the determination of these properties are discussed in this chapter. Due to the very specific nature of PCMs many problems with measurement procedures arise. These problems along with the necessary measurement premises are summarised in the first section of this chapter.

# 5.1 Basic measurement premises

Accurate knowledge of basic thermo-physical properties of PCMs primarily refers to the knowledge of the phase change temperature (range) and the energy stored/released. As briefly stated in the second chapter one of the most important principles which is used for characterisation of solid-liquid PCMs can be described by the following equation (Equation 5.1):

$$dH = dQ + Vdp,$$
(5.1)

which summarises the relations between enthalpy H, heat stored/released $Q$, volume $V$, and pressure $p$. This relation is a direct consequence of the first law of thermodynamics and the definition of enthalpy. Furthermore, since solids and liquids are incompressible under usual operational conditions the term $Vdp$ can be neglected resulting in the simpler relation given by Equation 5.2:

$$dH = dQ,$$
(5.2)

which represents the basis of calorimetric measurements (*measurements to determine the change of heat*) of solids and liquids. Namely, this equation enables the energy i.e. heat stored/released between two temperature levels to be calculated using the difference of the respective enthalpy values (Mehling and Cabeza, 2008). However, due to the specific nature of PCMs, which can have a very high heat storage/release density in a narrow temperature range, the common calorimetric standards can lead to significant errors in behavioural characterisation. For this reason an initiative was launched in 2005 by few companies (Fraunhofer ISE, Freiburg, Germany; ZAE Bayern, Garching, Germany) towards the standardisation of material testing and quality control for PCMs (Mehling et al., 2006; RAL, 2010).

Performing measurements on PCMs requires three general criteria to be taken into account:

(i)     The sample needs to be representative,

(ii)     Correct determination of the sample's temperature and heat stored/released needs to be provided, and

(iii)    Thermodynamic equilibrium in the sample needs to be assured (Mehling and Cabeza, 2008).

The first criterion requires the sample to be larger than typical in-homogeneities of the investigated material. To satisfy the second criterion the determination of the sample's temperature and heat stored/released needs to be subjected to corresponding calibration procedures. The third criterion requires the investigated sample to be isothermal and in reaction equilibrium. The "isothermal" part can be achieved through slow measurements or investigation of small samples. Unfortunately, the utilisation of small samples contradicts the first general criterion of representative samples. This contradiction evidently shows the importance of optimisations and balancing between different parameters in PCM measurements. The thermodynamic equilibrium can also be achieved by slow measurement i.e. small heating/cooling rates. This, however, can result in small Signal-to-Noise Ratios (SNRs) in certain measurement methods, emphasising once more the conflicts that can arise in PCM characterisation procedures. Additionally, the reaction equilibrium can be violated by various factors predominantly by very slow reactions and subcooling. The subcooling is related to the first criterion as well. Namely, the degree of subcooling can be dependent on the sample size requiring the sample used in characterisation methods to be the same or approximate size as in future PCM application (Mehling and Cabeza, 2008).

Furthermore, it is common to achieve different results upon heating and cooling measurement of PCMs. This effect is called *hysteresis*. It can be a real property of the material or sometimes the consequence of the measurement conditions. In the latter case it is known as an *apparent hysteresis*. For this reason, it is essential to perform both heating and cooling measurement of the PCM samples. Again, to determine the existence of real or apparent hysteresis the isothermal conditions in the sample need to be obtained. Given the possible conflicts that can arise regarding the small samples and low heating/cooling rates, it is suggested to balance between the mentioned parameters in order to keep the sample close to equilibrium conditions as much as possible (Mehling et al., 2006; Mehling and Cabeza, 2008).

To demonstrate the specifics of PCMs it is important to note that the thermal behaviour of the material in the temperature range where it does not undergo a phase

change can be characterised only by its (specific) heat capacity which is usually almost constant within a temperature interval of 10 °C. To describe the behaviour of the material when it undergoes a phase change, more parameters are necessary, usually at least four: phase change temperature (range), phase change enthalpy, (specific) heat capacity in the solid state and (specific) heat capacity in the liquid state. Few PCMs are pure materials with constant phase change temperature. Generally PCMs are not pure substances resulting in the existence of the phase change temperature range instead of the sharp temperature of transformation. Furthermore, this prevents the separation of sensible and latent heat values in measured/calculated data. Taking the onset or peak temperature of the melting/solidification measurement curves as the phase change temperature leads to significant errors in the design of a TES system and serious deviations between a planned system and an implemented one (Mehling and Cabeza, 2008).

Additionally, Arkar and Medved (2005) showed that even the shape of the apparent heat capacity curves, usually derived by using the four aforementioned parameters, influences the model predictions regarding the thermal responses of latent heat systems. The solution could be the results' representation in the form of heat stored/released as a function of temperature in given temperature intervals (Mehling et al., 2006; Mehling and Cabeza, 2008). In this way the definition of a single phase change temperature is avoided as well as the need to report a constant (specific) heat capacity in liquid and solid states. Moreover, the separation between sensible and latent heat is also avoided since ultimately it is not necessary. Usually the calculated heat stored/released is given as the heat stored/released per mass. It should also be given in the form of the heat stored/released per volume by multiplication of the heat stored/released per mass with the minimum density in the operating temperature range of application. Also, due to subcooling and hysteresis effects the heat stored/released should be given as a function of temperature in given temperature intervals for both, heating and cooling experiments. Subcooling should be eliminated from the stored/released heat data and given separately with reference to the sample mass and other conditions that influence it (Mehling and Cabeza, 2008; RAL, 2010). The

procedure for the elimination of subcooling effect was suggested by Mehling and Cabeza (2008) (see Figure 5.1).
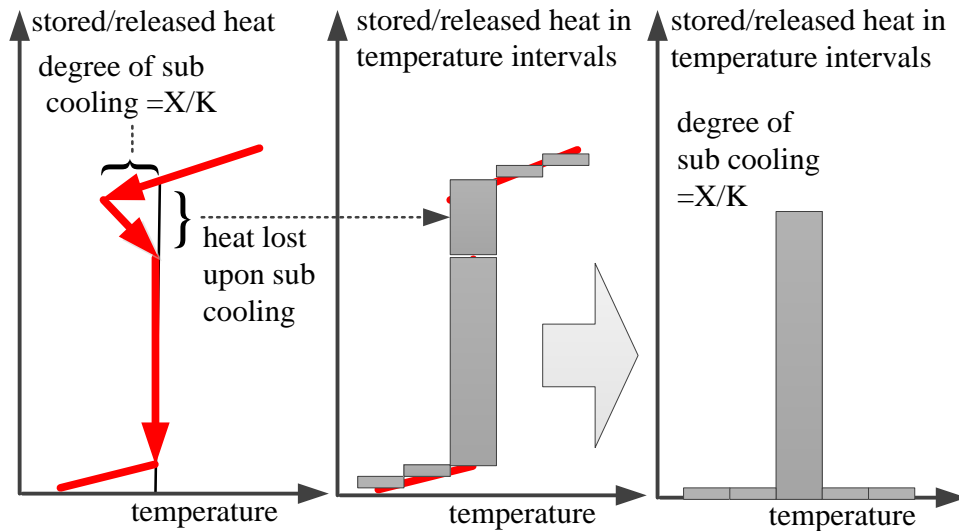


***Figure 5.1:*** *Determination of the stored/released heat as a function of temperature in given temperature intervals plus degree of subcooling (amended from Mehling and Cabeza, 2008, p. 68).*

Namely, according to Mehling and Cabeza (2008) the effect of subcooling should be eliminated from the heat stored/released graphs and given separately as the degree of subcooling while the heat lost upon subcooling should be attributed to the solidification temperature.

Based on the investigation of different materials and characterisation methodologies of PCMs, the initiative launched in 2005 resulted in the definition of few additional criteria that need to be satisfied between different measurements of the same PCM, apart from three, previously mentioned, general ones:

(i)     Change in total enthalpy (heat stored/released) not greater than 10 %,

(ii)    Change in heat stored/released-temperature profiles not greater than ±1 °C, and

(iii)   Change in mass not greater than 3 % (testing is imperative for encapsulated materials, but not for others) (RAL, 2010).

These represent the so called "damage" criteria to be used to assess if the investigated material has become defective after prolonged cycling. Moreover, the

desired accuracy levels for temperature and enthalpy measurements of PCMs are ±0.5 °C and ±10 %, respectively (Mehling et al., 2006).

The RAL quality standard (RAL, 2010) represents the set of general rules and criteria that need to be taken into the account in measurements and characterisation methods of PCMs. However, the practical implementation of these rules is not easy or straightforward, but dependent on the characterisation methodology. Therefore the main principles and limitations of the current characterisation methodologies of PCMs are discussed in the next subchapters with a special emphasis on the two most important methods, Differential Scanning Calorimeter (DSC) and Temperature-history (T-history) method.

## 5.2 Differential Scanning Calorimeter (DSC)

Differential scanning calorimeter is one of the most common calorimetric methods used for behavioural characterisation of different materials including PCMs. The technology is based on the detection of differences in the thermal responses between a sample substance and a reference material which are simultaneously subjected to the controlled heating/cooling environment (Günther et al., 2006). Two types of DSC systems are used, the Differential Thermal Analysis (DTA) (also called power-compensating DSC) and the heat-flux DSC (also called heat exchanging DSC). In DTA the sample and the reference are placed in identical, separate furnaces and kept at the same temperatures throughout the measurements by varying the power input of electrical heaters of the furnaces. This method unlike the heat-flux DSC is not commonly used. In opposition, the heat-flux DSC is frequently used for PCM characterisation. In this method, the sample (PCM in this case) and reference are enclosed inside the same furnace and linked by the heat-conducting support. A typical heat-flux DSC setup is represented in Figure 5.2. In heat-flux DSC the same amount of heat is supplied to or extracted from the sample and reference using the electrically heated furnace for heating and compression cooler or liquid nitrogen for cooling experiments. Given the same amount of heat supplied/extracted, the different thermal response of the sample and reference is reflected in their respective temperature

difference. This difference represents the useful signal recorded in heat-flux DSC measurements. The temperature difference between the symmetrically placed sample and reference crucibles is observed and recorded. (Mehling and Cabeza, 2008; Mehling et al., 2012).
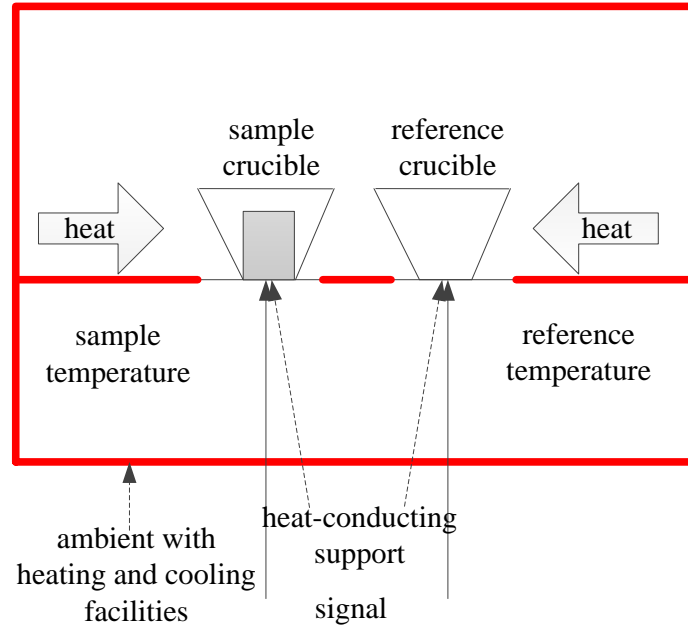


**Figure 5.2:** *Typical heat-flux DSC setup (amended from Mehling and Cabeza, 2008, p. 70).*

The heat-flux DSC measurements can be performed in two different modes, the dynamic and the isothermal steps mode. In the dynamic mode the ambient is subjected to the constant heating/cooling rates and the corresponding temperature difference between the sample and reference is measured. The basic equation for quantitative evaluation of measurements in dynamic DSC method is given by Equation 5.3:

$$\Delta T = R_{th}\beta(C_s - C_r),\qquad(5.3)$$

where $\varDelta T$ represents the measured signal, $R_{th}$ represents the thermal resistance of the heat-conducting path (as well as the sensitivity of the instrument) given in $KW^{-1}$, $\beta$ given in $Kmin^{-1}$ is the heating/cooling rate, and $C_s$ and $C_r$ are the heat capacities in $JK^{-1}$ of the sample and reference. The specific heat capacity $c_p(T)$ and the enthalpy $h(T)$ of the sample are calculated by using the given formula (Equation 5.3) and the measured signal $\varDelta T$ which can be the temperature difference given in K or a thermocouple

voltage expressed in µV (Mehling et al., 2012). Additionally, the proportionality constant $R_{th}\beta$ in the Equation 5.3 establishes the dependency between the signal-to-noise ratios in the heat capacity data and the heating/cooling rates in dynamic DSC measurements (Mehling and Cabeza, 2008).

Furthermore, to evaluate the desired thermal properties of the investigated PCM samples the necessary calibration procedures of the DSC instrument need to be performed. The calibration of the temperature sensors used in measurements is usually done through comparison of the recorded phase change temperatures of standard materials with the data available in literature. Moreover, in most cases the temperature calibration is directly applied to the measured data and included in the signal output of the DSC instrument (Mehling et al., 2012).

To determine the heat capacity and enthalpy values the instrument calibration needs to be done by using the materials with the well-known properties. The calibration procedures commonly used are the heat capacity and enthalpy calibration depending on the type of the property used. In heat capacity calibration three measurements need to be performed: measurement with an empty sample and reference crucibles to obtain the so called empty line, then measurement with a standard material inside the sample crucible and an empty reference crucible to get the standard line, and finally measurement with the sample inside the sample crucible and an empty reference crucible to determine the sample line (Figure 5.3).

Contrary to the situation displayed in Figure 5.3 the DSC software commonly makes the adjustments in such manner to represent the endothermic effect of the PCM upon heating with an upward peak of the raw signal since the endothermic effect is also manifested as an upward peak in heat capacity data (Mehling and Cabeza, 2008).

After the measurements of the empty, standard, and sample lines the specific heat capacity of the sample $c_{p,sample}$ can be evaluated at any point in time using Equation 5.4:

$$c_{p,sample} = c_{p,s\tan dard} \frac{m_{sample}}{m_{s\tan dard}} \frac{U_{sample} - U_{empty}}{U_{s\tan dard} - U_{empty}}, \qquad (5.4)$$

where $c_{p,standard}$ represents the specific heat of the standard, well-known material, terms

$m_{sample}$ and $m_{standard}$ represent the masses of the sample and standard material, and the $U$ values represent the corresponding measured signals (either temperature differences or the thermocouple voltages). The conversion between time and temperature for the specific heat capacity function of the sample can be done using the recorded temperature ramp. In this conversion the ambient or reference temperatures are commonly used (Mehling et al., 2012).
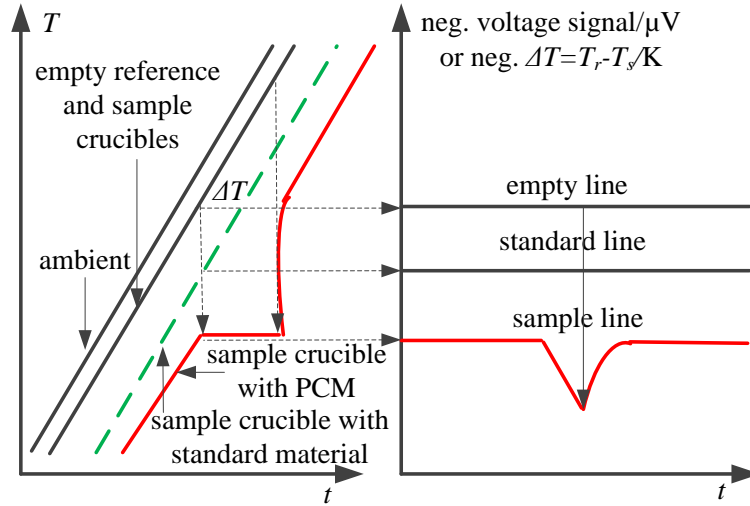


***Figure 5.3:*** *Temperatures (T) and measured signals (T differences) in dynamic DSC mode upon heating (amended from Mehling and Cabeza, 2008, p. 72).*

Another type of calibration is the enthalpy calibration. In this procedure the materials with the well-known phase change enthalpies are used. The calibration requires a set of measurements to be repeated every other month. The sensitivity of the instrument is determined for a particular standard material and attributed to the phase change temperature of that material. This is repeated for several standard materials to determine the instrument's sensitivity at different temperatures (Figure 5.4). Namely, based on the Equation 5.3, the integral of the peak area of the measured signal obtained from the standard material can be directly related to the phase change enthalpy $\Delta_{pc}H$ of the material where the proportionality constant is the sensitivity of the DSC instrument (Equation 5.5).

$$\int_{peakwidth} \Delta T dt = \int_{peakwidth} R_{th}\beta(C_s - C_r)dt = R_{th}\int_{peakwidth} \frac{dT}{dt}(C_s - C_r)dt = R_{th}\Delta_{pc}H \qquad (5.5)$$
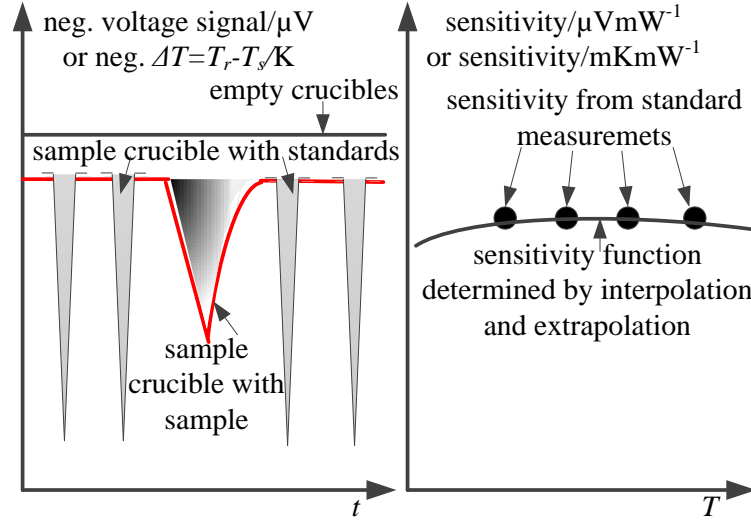


***Figure 5.4:*** *Measurement evaluation principles of the enthalpy calibration in heat-flux DSC method (amended from Mehling and Cabeza, 2008, p. 76).*

Equation 5.5 enables the evaluation of the instrument's sensitivity at various temperatures corresponding to the phase change temperatures of the standard materials. Since the peaks of these materials are narrow the sensitivity can be taken as constant within the particular temperature range. The sensitivity function of the instrument is determined by interpolation/extrapolation of the recorded sensitivity points. Once the sensitivity curve $R_{th}(T)$ is known the sample material can be evaluated and its enthalpy determined using Equation 5.6 (Mehling and Cabeza, 2008; Mehling et al., 2012):

$$\Delta_{pc}H = \int_{peakwidth} \frac{\Delta T}{R_{th}(T)} dt. \qquad (5.6)$$

Mehling et al. (2012) reported on the new calibration procedure for heat-flux DSC measurement which is optimised for PCMs. In this procedure the empty line is not measured as in the heat capacity calibration but constructed by connecting the signals measured in isothermal states when the ambient temperature is constant. It is assumed that the empty line is linear under both constant and dynamic ambient conditions.

Furthermore, heat-flux DSC can be used in isothermal steps mode. In this mode a stepwise change of the ambient in a given temperature intervals is applied (see Figure 5.5).
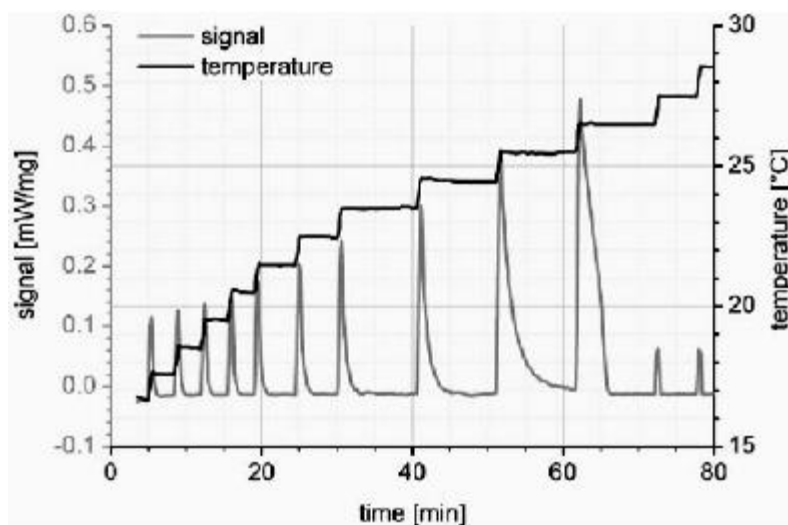


***Figure 5.5:*** *Typical heating ramp and signal in DSC measurement with isothermal steps mode (amended from Mehling and Cabeza, 2008, p. 78).*

The length of the steps is determined by the time that sample needs to come into thermal equilibrium with the ambient i.e. the time necessary for the signal to drop back to zero. At that moment the sample becomes isothermal. Consequently, the area below the corresponding peak is proportional to the heat stored by the sample in the heating experiment. The quantitative heat value can be estimated using the sensitivity curve obtained from the enthalpy calibration. The associated temperature uncertainty in this case equals the height of the corresponding step (Mehling and Cabeza, 2008).

Apart from the advancements in the calibration procedures and DSC modes some authors also reported on the improvements of the DSC instruments. André et al. (2012) described the so called MicroDSC detector that uses Peltier element based heat exchangers to provide proper ambient conditions in both heating and cooling measurements plus Peltier element based sensors to measure the DSC signals. This detector enables the measurement of relatively larger samples than the ones scanned in standard DSC units.

# 5.3 Temperature-history (T-history) method

In 1999 a new method, named Temperature-history or simply T-history, was specifically designed and developed for the thermal investigation of PCMs (Zhang et al., 1999). The typical experimental rig used in this methodology is represented in Figure 5.6.
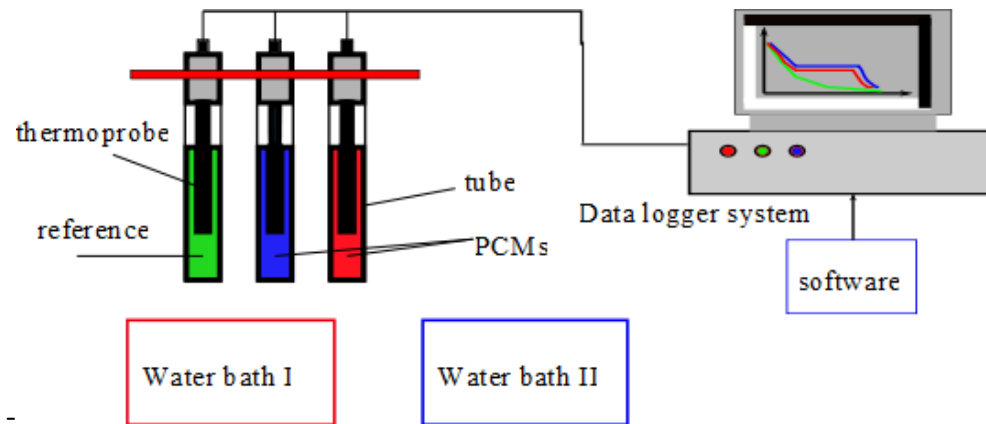


**Figure 5.6:** *A schematic diagram of the typical experimental rig for the T-history method (amended from Zhang et al., 1999, p. 204).*

Namely according to Zhang et al. (1999), the sample and reference (with well-known heat capacity usually distilled water) in the test tubes of a defined geometry (cylindrical) and at the same initial temperature $T_0$ ($T_0>T_{pc}=T_m$) are subjected to the ambient temperature $T_{\infty,a}(t)$ or simply $T_a$ ($T_a<T_{pc}$). Their temperature history is recorded upon cooling (inside the water bath) from the initial temperature until both samples reach equilibrium with the ambient. Consequently, comparisons of the recorded curves (see Figure 5.7), assuming the same heat transfer coefficient between sample and ambient as well as between reference and ambient, enable the determination of the heat released by the sample (Mehling and Cabeza, 2008).

Zhang et al. (1999) have developed the original T-history method using the Newton's law of cooling which relates the rate of heat exchange to object's temperature change with respect to the ambient. This law can be represented by equation in which the heat transfer coefficient between the ambient fluid and the object's surface is denoted as *h* and the surface itself is represented as *A* (Equation 5.7):

$$\frac{dQ(t)}{dt} = hA(T(t) - T_a). \tag{5.7}$$
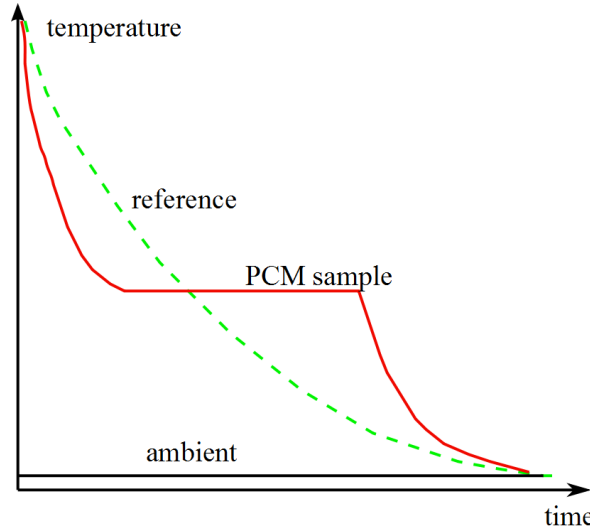


*Figure 5.7: Idealised T-history curves (amended from Mehling and Cabeza, 2008, p. 81).*

Another important parameter in T-history definition is the dimensionless Biot number ($B_i$) which represents the ratio of the heat transfer resistances inside and at the surface of an object i.e. the ratio between the convective and conductive heat transfer coefficients ($Bi=hL_C/k$ where $L_C$ is the characteristic length i.e. the ratio of the object's volume and surface, $k$ its thermal conductivity, and $h$ the convective heat transfer coefficient). Biot number describes the spatial temperature distribution inside an object. If the value of this number is below 0.1 a uniform temperature distribution within the object can be assumed (Zhang et al., 1999). Consequently, the object can be treated as a lumped capacitance heat reservoir allowing the application of the lumped capacitance model as in Equation 5.8:

$$C\frac{dT(t)}{dt} = -hA(T(t) - T_a), \tag{5.8}$$

where $C$ represents the heat capacity of the lumped object (sample or reference within the corresponding test tubes in T-history measurements).

Furthermore, Equation 5.8 is used to derive the final equations used in the original definition of the T-history method (Equation 5.9-5.11).

84

$$c_{p,s} = \frac{m_w c_{p,w} + m_t c_{p,t}}{m_p} \frac{A_3}{A'_2} - \frac{m_t}{m_p} c_{p,t} \qquad (5.9)$$

$$c_{p,l} = \frac{m_w c_{p,w} + m_t c_{p,t}}{m_p} \frac{A_1}{A'_1} - \frac{m_t}{m_p} c_{p,t} \qquad (5.10)$$

$$H_m = \frac{m_w c_{p,w} + m_t c_{p,t}}{m_p} \frac{A_2}{A'_1} (T_0 - T_s) - \frac{m_t}{m_p} c_{p,t} \qquad (5.11)$$

In these equations (Equations 5.9-5.11) $c_{p,s}$ and $c_{p,l}$ represent the mean specific heats of the solid and the liquid PCM; $H_m$ is the heat of fusion of the PCM or alternatively denoted as the enthalpy change $\Delta_{pc}H$ in the phase change range; $m_p$ or simply $m$, $m_w$ and, $m_t$ are the masses of the PCM sample, the reference and the test tube, respectively; $c_{p,w}$ or $c_{p,r}$ and $c_{p,t}$ are the mean specific heats of the reference and the tube material; the difference $\Delta T_m = T_m - T_S$ is the degree of subcooling also denoted as $\Delta_{sc}T = T_{pc} - T_N$ where $T_N$ represents the nucleation temperature; and $A_1$, $A_2$, $A_3$, $A'_1$, and $A'_2$ are the values of the corresponding integration areas obtained by integration of T-history curves (Figure 5.8 and Figure 5.9).
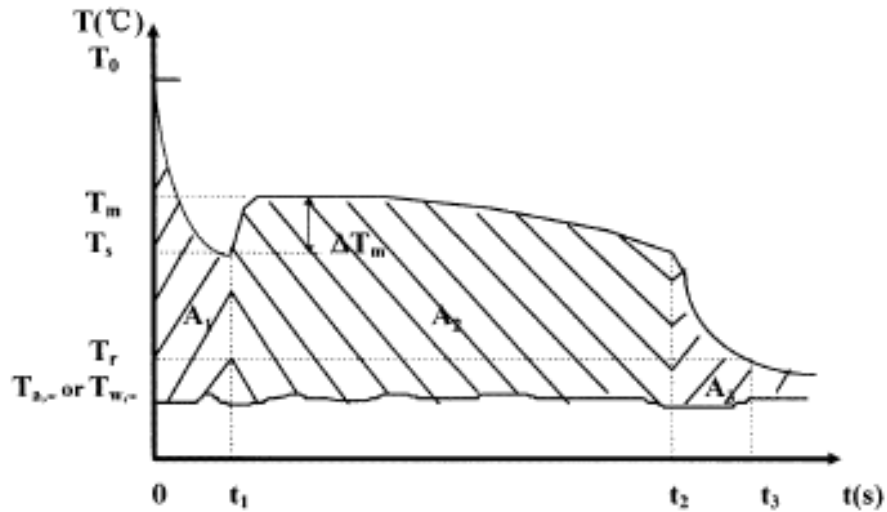


**Figure 5.8:** *A typical T-history curve of a PCM during cooling process with subcooling effect (amended from Zhang et al., 1999, p. 202).*
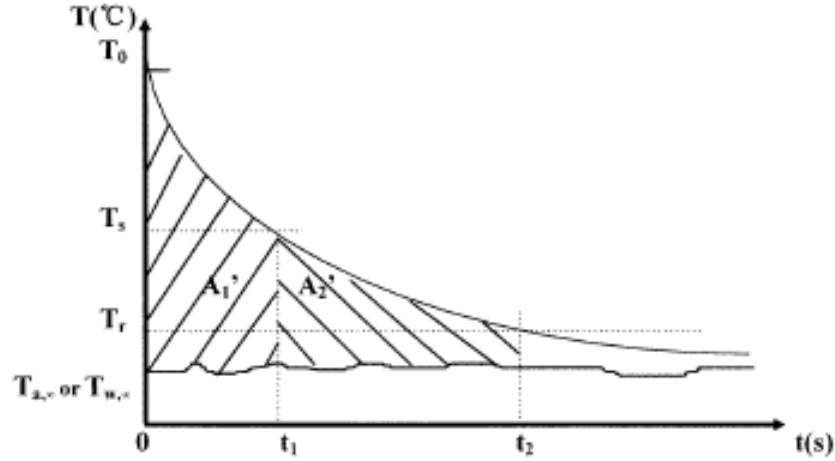
***Figure 5.9:*** *A typical T-history curve of a reference material during a cooling process (amended from Zhang et al., 1999, p. 202).*

For PCM without subcooling effect (Figure 5.10) where the temperature range of the phase change is between $T_{m,1}$ and $T_{m,2}$ the expression for $c_{p,s}$ and $c_{p,l}$ are the same as in Equations 5.9 and 5.10, but the heat of fusion $H_m$ is different (Equation 5.12):

$$H_m = \frac{m_w c_{p,w} + m_t c_{p,t}}{m_p} \frac{A_2}{A'_1} (T_0 - T_{m,1}) - \frac{m_t}{m_p} c_{p,t} (T_{m,1} - T_{m,2}) \cdot (5.12)$$
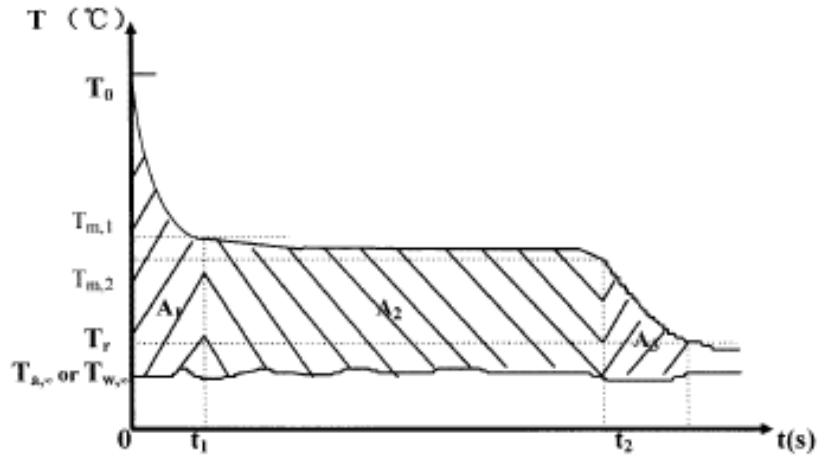


***Figure 5.10:*** *A typical T-history curve of a PCM during cooling process without subcooling effect (amended from Zhang et al., 1999, p. 202).*

T-history method has sustained several improvements since its definition; therefore the evolution of this method throughout the past decade is discussed in the next subsection.

## 5.3.1 Evolution of the T-history method

At the beginning of the last decade, Marin et al. (2001) performed several experiments using the T-history method and proposed the use of air instead of water in the heating/cooling experiments.

One of the major improvements of the original method was implemented by Marin et al. (2003). They emphasised that the original T-history method does not clearly define the determination of the boundary between the solid, phase change, and liquid states; therefore they developed an improved mathematical technique for the evaluation of the T-history data, the so called time delay technique. This technique is based on the concept of enthalpy-temperature functions $H(T)$ i.e. $H_p(T)$ and $h_p(T)$ (enthalpy and specific enthalpy functions of the PCM sample) instead on the simple concept of temperature variation with time. The authors observed the temperature variation of the sample and reference over very small temperature intervals $\Delta T_i$ corresponding to time intervals $\Delta t_i = t_{i+1} - t_i$ and $\Delta t'_i = t'_{i+1} - t'_i$ for PCM and reference respectively. Namely, they examined the time delay between the moments when sample and reference reach the specified temperature evaluation point. The temperature interval $\Delta T_i$ represents the interval between the two consecutive temperature evaluation points. Furthermore, using the theoretical basis of the T-history method (Equation 5.8) they calculated enthalpy changes $\Delta h_p(T_i)$ of the PCM in the corresponding temperature intervals $\Delta T_i$. Given the $\Delta h_p(T_i)$ values the calculation of the specific enthalpy function $h_p(T)$ is straightforward as given in Equation 5.13:

$$h_p(T) = \sum_{i=1}^{N} \Delta h_p(T_i) + h_p(T_0), \qquad (5.13)$$

where $h_p(T_0)$ represents the reference value of specific enthalpy. The temperature $T_0$ can be arbitrarily selected depending on the temperature range of investigation. Moreover, the specific heat capacity of the PCM $c_p(T)$ (also called apparent heat capacity function) can be determined from the enthalpy function. (Equation 5.14):

$$c_p(T) = \frac{\partial h_p(T)}{\partial T}. \qquad (5.14)$$

The authors also improved the original setup by putting the samples in a cool down chamber upon cooling instead of using a temperature bath.

Another group of authors Hong et al. (2004) also observed that the original method does not clearly define the solid, phase change, and liquid boundaries and therefore proposed the use of an inflection point to mark the boundary between phase change and solid-state periods. This is the point where the first derivative of T-history curve for PCM becomes minimal. The approach is justified by the fact that the temperature is constant or decreases gradually during the phase change, but decreases exponentially in cooling process where only sensible heat is present.

In 2005, a new installation of T-history was proposed (Marin et al., 2005). The improvements of this installation were based on better instrumentation and horizontal disposition of the tubes in the air enclosure in order to minimise the gravitational movements.

In 2006, Günther et al. (2006) gave a thorough comparison of the DSC and the T-history methods as the major tools used for determination of the heat storage/release capacity of PCMs and PCM objects. They also constructed a custom built test chamber with the heat exchanger connected to a thermostat to control the ambient temperature. In addition, a fan was used to enforce the convection inside the chamber. Moreover, they developed a special setup for the characterisation of PCM-objects. Additionally in 2006, Lazaro et al. (2006) gave a proper methodology for the verification of the correct instrument operation and data evaluation used in T-history installation. The methodology includes the sensor calibration and verification of the correct measurement of temperature and correct evaluation of enthalpy.

In 2009, another detailed comparison of the DSC and T-history results was presented (Günther et al., 2009). The comparative methodology in this study is based on the required measurement precision and accuracy.

In 2010, Rady at al. (2010) adapted the original T-history method and the corresponding data evaluation technique for the specific characterisation case of granular phase change composites. Also, a significant modification of the original T-history method was published in 2010 (Kravvaritis et al., 2010). The improvements refer to the experimental arrangement in the form of fully controlled indoor environment, the way of measurement processing, as well as the presentation format of the results. The proposed measurement processing technique is based on the use of the

thermal delay (i.e. temperature difference) between PCM (at temperature $T_{m,i}$) and a reference (at temperature $T_{r,i}$) at any specified time $t_i$ and not on the use of their time delay at any specified temperature as suggested by Marin et al. (2003). The effective thermal capacity function $c_{p,eff}$ as a final result is proved to be more useful than the results of the original T-history method. The year 2010 brought yet another significant improvement regarding the T-history data processing techniques Moreno-Alvarez et al. (2010) developed the differential formulation of the T-history method (the dT-history method). This method aims to include the important experimental effect of the speed of the thermal process i.e. the cooling/heating rates of the samples in calorimetric calculations. Starting from Equation 5.8 the authors evaluated the specific heat capacity of the PCM $c_p(T)$ using Equation 5.15:

$$c_p(T) = \frac{\left(\dfrac{dT}{dt}\right)^{-1} (T - T_a)}{\left(\dfrac{dT_r}{dt}\right)^{-1} (T_r - T_a)} \frac{m_r c_{p,r} + m_t c_{p,t}}{m} - \frac{m_t c_{p,t}}{m}. \qquad (5.15)$$

In 2011, Kravvaritis et al. (2011) reported the results from the characterisation experiments of various PCMs using the previously reported thermal delay method.

Important study was reported in 2012 by Rathgeber et al. (2012). The authors developed a T-history calorimeter for the characterisation of phase change materials in the temperature range from 50 °C to 200 °C. Air as the heat transfer fluid in a closed cycle was used for the construction of the instrument. Fast switching times of cooling sessions inside the instrument were implemented by short opening of the cycle to the ambient (indoor) air.

In 2013, Li et al. (2013) developed an analytical temperature model for the evaluation of the T-history curves. Apart from the lumped capacitance model, they assumed the rectangular shape of the effective specific heat capacity function and proposed the criteria for the selection of the start and end temperature of the phase change. The model was validated based on the evaluation of inorganic high temperature phase change materials.

# 5.4 Unconventional methods

Apart from DSC and T-history other, less conventional characterisation studies of PCMs have been reported in literature. These include the adiabatic scanning calorimeter (ASC) method and macroscale PCM investigations including studies of PCM composites.

In 2011, Losada-Perez et al. (2011) reported the heat capacity and enthalpy measurements of PCMs using the adiabatic scanning calorimeter (ASC) in constant power mode. The main equation describing the underlying operational principles of the ASC is given by Equation 5.16:

$$C_p = \frac{dQ}{dT} = \frac{dQ/dt}{dT/dt} = \frac{P}{dT/dt} = \frac{P^e}{dT/dt} = \frac{dH/dt}{dT/dt}. \qquad (5.16)$$

Generally, ASC can be run in four different modes by keeping $P$ or $dT/dt$ constant, while cooling or heating the sample. However, given the large values of latent heats, the constant power mode is usually used for PCM characterisation. The constant power ($P$ or $P^e$) upon heating is maintained using an electrical source. Adiabatic conditions are met by keeping the leakage power $P^l$ at its minimum value. Since the heating rate is proportional to the heat capacity the rise of sensible heat decreases the rates facilitating thermal equilibrium in the sample and the control of adiabatic conditions. During the phase change interval $\varDelta t$ the temperature change rate is close to zero resulting in Equation 5.17:

$$\Delta t = \frac{L}{P^e}, \qquad (5.17)$$

where $L$ represents the latent heat of transformation. Moreover, using Equation 5.16 ASC allows the direct evaluation of the enthalpy-temperature function (Equation 5.17):

$$H(T) = H(T_0) + P^e (t - t_0). \qquad (5.17)$$

Here, $t_0$ represents the starting time of the sample scan with the corresponding temperature of the sample $T_0$.

Implementation of the cooling ASC experiment is not as straightforward as in heating case. It is usually implemented by keeping the constant temperature difference between the sample and its isothermal environment and including a lot of calibration

measurements. Moreover, the typical heating/cooling rates in ASC are three orders of magnitude slower than in DSC resulting in the enthalpy dependency of equilibrium temperature and potential elimination or reduction of the subcooling in cooling measurements (Losada-Perez et al., 2011).

Additionally, some researchers develop the setups for macroscale evaluation of PCMs. Zalba et al. (2005) developed the experimental setup for the evaluation of PCM based TES using the design of experiments procedure. Le Du et al. (2012) reported on the development of the device for characterisation of a composite phase change material. In 2013, Barreneche et al. (2013) developed the device for the macroscale evaluation of thermal conductivity of real PCM samples as well as the device for registering the temperature-time response curves produced by such samples (Figure 5.11).
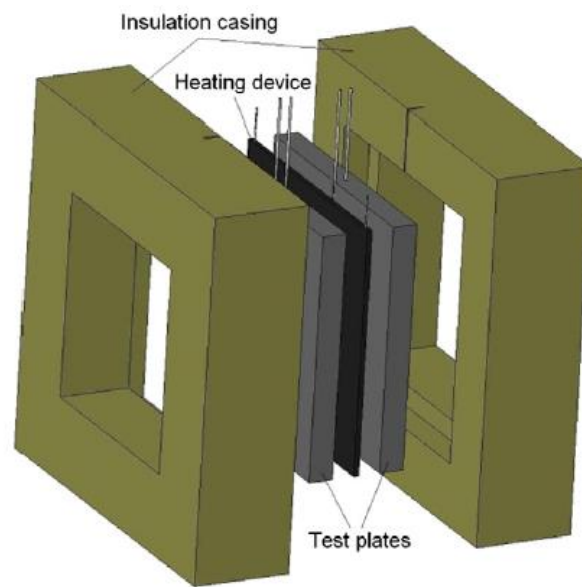


*Figure 5.11: Temperature-time curves device scheme (amended from Barreneche et al., 2013, p. 3).*

Although useful, the macroscale devices for characterisation of real-scale PCM sample are not particularly feasible since those devices are usually custom built for the investigation of specific PCM samples. Furthermore, these devices are sometimes closely coupled with the numerical models. This could result in significant errors upon PCM macro-evaluation in the case of unreliable material data underlying the operation of numerical models in question.

# 5.5 Limitations of the current technologies

Although the DSC and T-history related studies of PCMs are numerous, these two widespread methodologies still have limitations in terms of the measurement premises regarding the characterisation of PCMs.

The typical sample size in DSC experiments is in the range from 1 to 25 mg resulting in the violation of the first general criteria regarding PCM investigations. Namely, the thermo-physical properties of small samples determined in DSC experiments are usually non-representative and different from those of the bulk materials used in practical TES systems. Small DSC samples can also result in higher degree of subcooling and lower degree of phase segregation (Zhang at al., 1999; Günther et al., 2006). Moreover, the accuracy of the dynamic heat-flux DSC measurement is dependent on the heating/cooling rate (typically in the range from 0.5 to 1 $Kmin^{-1}$) and sample size. Standard DSC heating/cooling rates cannot be used for PCM investigations since those would result in low resolution data. During the change of phase in DSC measurements, the sample is not close to thermal equilibrium. Due to the typically low thermal conductivity a significant temperature gradient is created inside the PCM sample. This can result in deviations of several degrees of the determined heat storage capacity with respect to temperature. This deviation predominantly depends on the utilised sample size and heating/cooling rate. It is also dependent on the heat storage capacity and the thermal conductivity of the sample, but since these properties are usually unknown the deviation cannot be reduced through mathematical means. Experimentally, it is possible to reduce the temperature gradient and the imposed deviations by using smaller samples or heating/cooling rates. The differences in the $c_p(T)$ curves obtained from the measurements that were performed on the same material but with different sample masses and heating/cooling rates can be observed in Figure 5.12 (Günther et al., 2006).
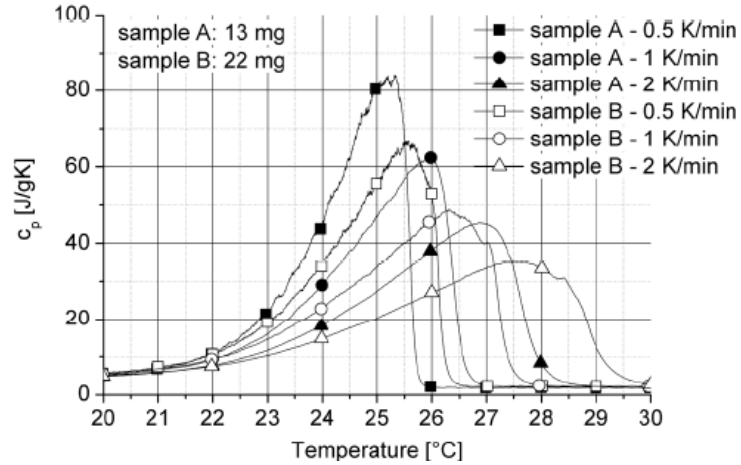
***Figure 5.12:*** *Effect of sample mass and heating/cooling rate variation in dynamic heat-flux DSC measurements on $c_p(T)$ curves (amended from Günther et al., 2006, p. 2).*

The end of the phase transformation peak is shifted from 26 °C (sample A-0.5 Kmin[-1] in Figure 5.12) to about 30 °C (sample B-2 Kmin[-1] in Figure 5.12). However, a reduction of the deviation is achieved at the expense of a weaker SNR (Günther et al., 2006). The increasing noise can be clearly observed in the measurements (sample A-0.5 K/min and sample B-0.5 K/min curves in Figure 5.12). The observed deviations in heat capacity curves were reported based on the measurements performed using a single DSC instrument by varying the mass of the sample and heating/cooling rates. Evidently, as reported by Lazaro et al. (2012) the DSC investigations of a single PCM can result in much larger deviations when multiple DSC instruments are used (Figure 5.13). Lazaro et al. (2012) concluded that the results of DSC investigations of PCMs highly depend on the DSC instrument, sample preparation, sample crucibles, heating/cooling rates, and data evaluation procedures.

The DSC measurement performed in isothermal steps mode provides better accuracy given both, heating and cooling curves. Moreover, the temperature uncertainty is confined to the step size and therefore precisely known. However, this mode is much more complex in terms of programming and data evaluation. Additionally, it requires much longer measurement time (Mehling and Cabeza, 2008).

93
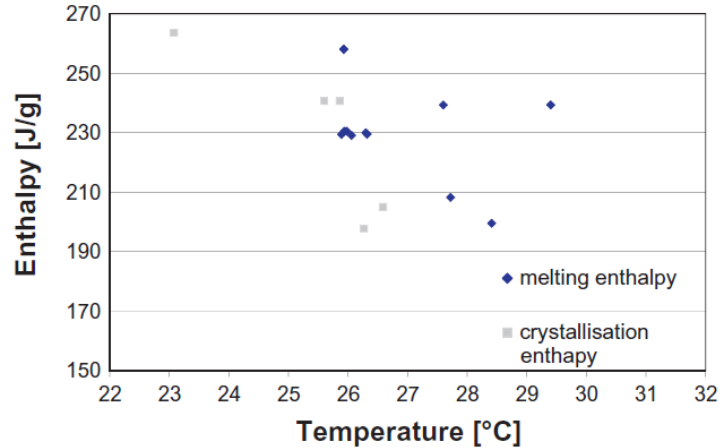
***Figure 5.13:*** *Comparison of DSC measurements of a single PCM from different laboratories (amended from Lazaro et al., 2012, p. 3).*

It is evident the DSC method has significant drawbacks in terms of PCM characterisation. In order to obtain more accurate results some of these drawbacks can be eliminated through the development of better data evaluation techniques and more precise measurement protocols (Lazaro et al., 2012; Mehling et al., 2012). However, the selection of optimal values for the sample size and heating/cooling rates in DSC measurements is a compromise between accuracy in temperature, accuracy in enthalpy and representation of the material (Castellon et al., 2008); therefore it still remains a challenging task.

In comparison to DSC, the T-history has few advantages, the sample size being one of the most important. Namely, the PCM samples used in T-history method are around 1000 times larger than those in DSC (Mehling and Cabeza, 2008). This allows more reliable investigation of PCMs. The original T-history method, defined in 1999, had serious drawbacks which were promptly addressed in the following years by various T-history improvement studies. Majority of these investigations were addressing the data evaluation issues in T-history measurements resulting in the development of different mathematical procedures for the evaluation of T-history data (Marin et al., 2003; Kravvaritis et al., 2010; Rady et al., 2010; Moreno-Alvarez et al., 2010, Li et al., 2013). However, very few of them addressed the issues regarding the control and sensing mechanisms of the T-history setup, accuracy and precision improvements, and problems of subcooling and hysteresis.

The original T-history experimental setup has gone through a number of improvements as indicated in the section 5.3.1 of this chapter and in the review article reported by Sole et al. (2013). Nevertheless, during the past decade researchers were developing their own custom built setups assembled from laboratory components without precise specification of the temperature control mechanisms in the T-history rigs. Moreover, only few authors gave some details regarding the sensor modalities used in their measurements (Zhang et al., 1999; Marin et al., 2003, Marin et al., 2005). They, however, did not highlight either the accuracy of the applied sensors or any other relevant sensor selection criteria.

Lazaro et al. (2006) discussed the importance of measurement precision and accuracy for determination of temperature and enthalpy values in T-history installations. The authors suggested and implemented a verification methodology for T-history measurements. In the latter studies, apart from the discussion about the tolerable uncertainties of data used in the design of PCM systems (Günther et al., 2009), majority of the authors didn't emphasise either the importance of sensor precision and accuracy in T-history measurements or the tolerable uncertainties in temperature and enthalpy data. Moreover, the T-history reports usually lack the information regarding very important properties of PCMs like subcooling and hysteresis as well as the results obtained in heating experiments.

Additionally, in order to avoid the possible ambiguities in PCM data, Mehling et al. (2006) suggested the standard format for the data representation which was further elaborated by Mehling et al. (2010). However, the recent T-history data are not reported in this form.

## 5.6 Summary

The inaccuracy/lack of reliable experimentally determined PCM data (especially in terms of phase change temperature and enthalpy) is one of the major limitations in the design and development processes of the efficient latent heat TES systems. For this reason, behavioural characterisation of PCMs is very important. Current technologies for the determination of thermo-physical properties of PCMs were presented in this

chapter with the emphasis on the two most important, DSC and T-history method. Both of them have significant drawbacks in terms of the basic premises that need to be satisfied during any measurement performed on PCMs. Namely, due to the very specific nature of PCMs many problems with measurement procedures arise limiting both methodologies.

Currently, DSC has an insurmountable drawback regarding the limited sample size resulting in the PCM data that do not reflect the thermo-physical properties of the bulk materials used in practical systems. In terms of the sample size the T-history method performs much better since the PCM samples used in this method are around 1000 times larger than those in DSC However, despite the many improvements reported during the last decade, T-history method has not yet been commercialised. Namely, the current method still has obvious limitations in terms of the correct determination of the phase change temperature and enthalpy of the investigated materials. This represents a serious problem since the accurate knowledge of these thermo-physical properties is a prerequisite for more optimal and efficient design and implementation of latent heat TES systems. Good prediction of the long-term behaviour of such systems also depends on the accurate characterisation of PCMs. Moreover, more reliable determination of thermo-physical properties of existing PCMs should enable better understanding of the limitations of current materials and focus the research of new materials towards the right direction. Therefore, there is an evident need to solve the present T-history related problems.

In an attempt to overcome the limitations of the current T-history implementations an advanced T-history methodology was designed, developed and evaluated. In this process the issues relating to the control and sensing mechanisms of the current T-history setups, accuracy and precision improvements, problems of subcooling and hysteresis, and data representation were taken into consideration and addressed sequentially.

As indicated at the beginning of the thesis the main hypothesis underlying this project is that better planned experimental tests in terms of more accurate and precise sensing and control modalities will be able to provide more comprehensive and reliable results than those described in the literature so far. To validate this hypothesis, the

design strategy and the experimental setup of the advanced T-history method were carefully developed as described in detail in the next chapter.

# Chapter 6

# DEVELOPMENT
# OF THE DESIGN STRATEGY AND
# THE EXPERIMENTAL SETUP OF
# THE ADVANCED T-HISTORY METHOD

Despite the recent improvements the T-history method has significant limitations, especially in terms of the correct determination of the phase change temperature and enthalpy of PCMs. To overcome these limitations an advanced T-history methodology was designed and developed. Given the specific nature of PCMs to store/release large amounts of energy in narrow temperature intervals, special care had to be taken to ensure the correct thermal characterisation of the investigated materials. During the development process of the advanced T-history the basic measurement premises and requirements, as described in the previous chapter, were taken into consideration. The aim in this process was to follow the rules and criteria established by the RAL quality standard (RAL, 2010) as close as possible. Due to the necessity to balance between different parameters like sample size and heating/cooling rates in PCM measurements, as explained in the previous chapter, the implementation of the given rules in the new T-history setup was not straightforward. Therefore a proper strategy to attack the specific aspects of the T-history method had to be developed. The issues that were addressed primarily include the control and sensing mechanisms of the T-history setup with the emphasis on the measurement accuracy and precision. Namely, the main hypothesis underlying this project was that a better planned experimental tests in terms of more accurate and precise sensing and control modalities will be able to provide more comprehensive and reliable results than those described in the literature so far. Furthermore, the subcooling and hysteresis problems as well as the data evaluation and

representation techniques also had to be analysed. The details of the development of the design strategy and the experimental setup of the advanced T-history method are the subject of this chapter.

# 6.1 Design strategy

The design strategy for the implementation of the advanced T-history method was developed in the form of a flowchart diagram (Figure 6.1). The first component of this diagram, the *Design rules*, represents a set of input parameters that had to be taken into consideration prior to any developments of the advanced T-history setup. These parameters are predominantly defined by the basic measurement premises given in the previous chapter. Namely, the general criteria in terms of the sample's size, correct determination of its temperature and heat stored/released, and the thermal equilibrium maintained within the sample were taken into the account and defined as the first set of the design rules. In this way, the development of the entire T-history setup was continuously bound by the main criteria that need to be satisfied in any PCM measurement. Additionally, as explained in the previous chapter, the T-history method is based on the lumped capacitance model (Zhang et al., 1999). This model governs the exchange of heat between the body and its environment. Therefore, to correctly determine the thermal parameters of the PCM bodies i.e. test tubes filled with PCM samples in T-history measurements an additional requirement had to be considered. This requirement which enables the application of the lumped capacitance model is defined by the upper boundary imposed on the value of the Biot number. Hence, an additional design rule to keep the Biot number below 0.1 was adopted enabling uniform temperature distribution within the T-history samples and consequently the application of the lumped capacitance model.

The next strategic action in the implementation of the advanced T-history method was identified as the development of the *Experimental setup*. This process mostly refers to the investigation and selection of the control and sensing mechanisms of the setup. However, it contains several sub processes which will be explained in detail in the separate section of this chapter.
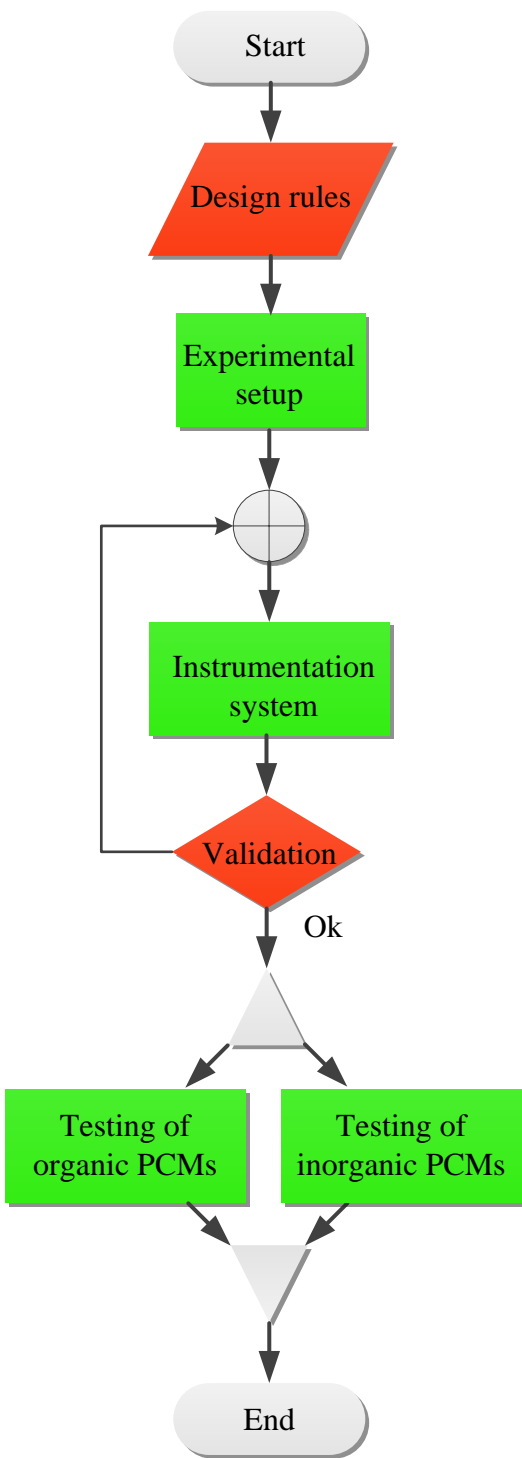
**Figure 6.1:** *Design strategy of the advanced T-history method.*

Another important stage, the development of the *Instrumentation system*, was predefined in the implementation of the advanced T-history setup. A proper measurement system had to be developed in order to enable the correct temperature

measurements of the investigated samples. This stage is also closely linked with the *Validation* point of the developed flowchart (Figure 6.1). Namely, as indicated in the previous chapter, a desired technical goal for the temperature accuracy in the PCM related measurements is $\pm0.5\,°C$ (Mehling et al., 2006). This value was selected as the validity factor for the instrumentation system. It was presumed that any instrumentation system will be evaluated in the appropriate temperature measurement and also redesigned in the case the desired accuracy target of $\pm0.5\,°C$ is not achieved. The design was made so the achievement of the desired accuracy level would stop the evaluation process.

Once the evaluation of the instrumentation system would be identified as successful the T-history setup would be used for testing of PCMs. Given the distinguishable properties of the organic and inorganic materials it was planned to carry out two different processes, *Testing of organic PCMs* and *Testing of inorganic PCMs*. Finally, the design was made to use the output of the two set of studies to evaluate the advanced T-history method and draw appropriate conclusions.

Given its direct relation with the set of the design rules discussed here the development of the experimental setup will be explained in detail in this chapter. Adversely, the details of the three other processes identified in the design strategy (Figure 6.1) will be given in the following chapters.

## 6.2 Experimental setup

The development of the experimental setup included several sub processes: investigation and selection of the control modality, investigation and selection of the sensing modalities, and the design and development of testing containers (Figure 6.2). These sub processes will be explained in detail in separate subsections.
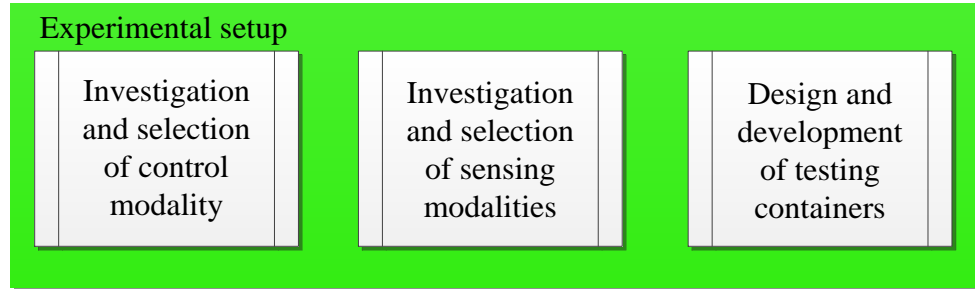
*Figure 6.2:* *Development of the experimental setup of the advanced T-history method.*

## 6.2.1 Investigation and selection of control modality

The usage of hot and cold temperature baths was suggested to maintain the temperature control in the original T-history method (Zhang et al., 1999). The authors however reported only the results obtained in the cooling setup. Nevertheless, the original T-history method has gone through a number of improvements as explained in the previous chapter. Marin et al. (2003) performed the cooling T-history measurements in a cool down chamber. Marin et al. (2005) were among the first to report the results obtained from the heating experiments. They concluded that those results don't show good agreement with the data obtained by other methods and suggested that this happens due to the internal temperature gradients in the air enclosure which was used as a control setup. The solution of the problems, suggested by the authors, was to disperse the heat source inside the air enclosure and add a Proportional Integral Derivative (PID) controller. This solution was adopted by Lazaro et al. (2006) and Günther et al. (2009) for the analysis of PCMs in a wide temperature range from -20 °C to 65 °C. Kravvaritis et al. (2010) used the same principle to transform a deep freezer into an automated, insulated test chamber in which temperatures from -30 °C to 120 °C could be obtained. This chamber was designed to accommodate both cooling and heating measurements. However, in the reported T-history studies the temperature control chambers were custom built using different laboratory components making an absolute precision of the controlled environment questionable. Moreover, the detailed specifications of the temperature control facilities used in the reported studies were not given. The utilisation of the non-precise control mechanism could lead to potential uncertainties in the T-history temperature measurements and consequently to erroneous

PCM data. Therefore, one of the aims of this study was to develop a T-history setup with the precisely specified details of its temperature control mechanism.

Given the aforementioned design rules and the general T-history concept the important parameters for the implementation of the control mechanism of the advanced T-history method were identified. These parameters include:

    (i)      Temperature range,

    (ii)     Temperature accuracy,

    (iii)    Heating/Cooling rate, and

    (iv)    Dimensions.

The materials of most interest in this study were PCMs used for building applications. The typical phase change temperature range is in the human comfort zone between 18 °C and 28 °C. A comprehensive study of a PCM requires the characterisation in a temperature range wider than its phase change range. This characterisation range was defined by RAL procedure as shown in Figure 6.3 (RAL, 2010).
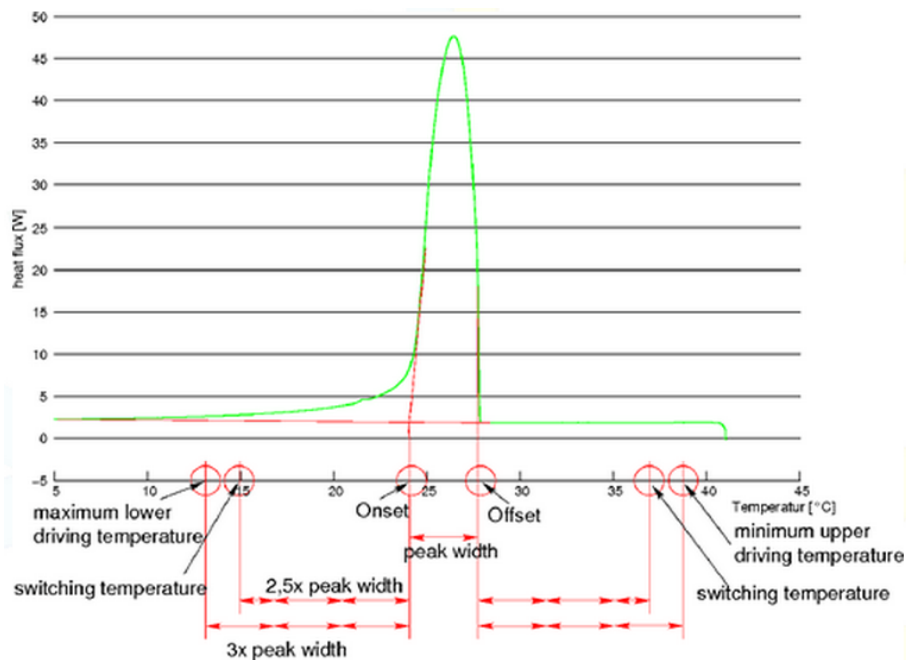


***Figure 6.3:*** *Definition of the characterisation temperature range for PCMs (amended from RAL, 2010).*

Namely, the onset characterisation temperature should be minimally three times the width of phase change range below the onset of phase change and the end

characterisation temperature should be three times the phase change width above the phase change end temperature (Figure 6.3). Given the definition of the characterisation temperature for PCMs, the typical phase change range of PCMs used in building applications, and the assumption that the phase change range of a single, good quality PCM should be below 3 °C it was concluded that the control facility of the advanced T-history method should provide the temperature control at least between 9 °C and 37 °C. As explained in the previous chapters, the desired accuracy level for temperature measurements of PCMs is ±0.5 °C. To obtain such accuracy the sensor calibration in T-history studies should be regularly performed. Lazaro et al. (2006) suggested that the calibration of sensors used in T-history could be performed in a thermostatic bath using a pre calibrated sensor as a reference and checked later by comparing the values of different sensors when the entire T-history setup is in temperature equilibrium. In this case the temperature accuracy of the T-history would depend on several parameters: the accuracy of the temperature bath, the accuracy of the pre calibrated sensor, the accuracy of the T-history setup, the nominal accuracy of the T-history sensors, and the accuracy of the T-history temperature measurement system. Every parameter adds a certain level of uncertainty. It was concluded that the best accuracy level can be achieved if the number of the aforementioned parameters is minimised. One way to achieve this was to implement the control mechanism of the T-history setup in such way that it could also be used for the calibration of the T-history sensors. In that case the number of uncertainty parameters would be reduced from the initial five to three: the accuracy of the T-history control setup, the nominal accuracy of the T-history sensors, and the accuracy of the T-history temperature measurement system. Given the desired accuracy level for temperature measurements of PCMs it was decided that the accuracy of the T-history control facility should be equal or below ±0.5 °C.

In addition, the recommended value for heating/cooling rates in T-history measurements is 1 Kmin$^{-1}$(±0.1 Kmin$^{-1}$) as suggested in RAL (2010). Accordingly, this value was adopted as the desired heating/cooling rate of the T-history control facility. Furthermore, one of the objectives of this project was to investigate the dependence of the T-history data on the size of PCM samples. Given the T-history restrictions regarding the value of the Biot number the PCM samples need to be placed in narrow

long cylinders. Since the diameter of the test tubes needs to be small their volume is highly dependent on their height. Consequently, the size of the investigated samples is also dominated by the height of the test tubes. Therefore it was determined that the height was the most critical dimension of the T-history control facility. Zhang et al. (1999) used 180.06 mm long cylinders. Marin et al. (2005) reported that the height of their cylinders was 130 mm. Since the objective was to investigate the dependence of the T-history data on the size of PCM samples it was decided that at least some test tubes need to be longer than 180.06 mm. Consequently, it was assumed that the height of the control facility should be above 300 mm.

The desired specifications of the T-history control modality are summarised in Table 6.1.

| Parameter | Desired value |
|---|---|
| Temperature range | Between 9 °C and 37 °C |
| Temperature accuracy | Below ±0.5 °C |
| Heating/Cooling rate | Recommended 1 Kmin$^{-1}$(±0.1 Kmin$^{-1}$) |
| Dimensions | Height above 300 mm |

**Table 6.1:** *Desired specifications of the T-history control modality.*

Given the discussion about the specification parameters for the T-history control mechanism it was concluded that such specifications can be guaranteed through the usage of a commercial temperature control chamber. Accordingly, an adequate environmental chamber was purchased. The selected model was BINDER KMF 115 (Binder GmbH, Tuttlingen, Germany) shown in Figure 6.4.

The specifications of the environmental chamber are given in Table 6.2.

Evidently, the chamber provides the temperature control between -10 °C and 100 °C which is much wider than the desired range from 9 °C to 37 °C. The control inside the selected chamber is assured with high accuracy of ±0.2 °C, again well below the earlier specified value of ±0.5 °C. The mean heating rate of the chamber is 1.3 Kmin$^{-1}$ and in relatively good agreement with the recommended value of 1 Kmin$^{-1}$ (±0.1 Kmin$^{-1}$). Before the purchase of the environmental chamber, an assumption was made that in the case of erroneous PCM data the excess in heating rate could be compensated through other means (e. g. insulation of test tubes). The cooling rate is not as the recommended value; however it is lower and therefore should provide reduced

temperature gradients inside the investigated samples as required in PCM measurements. The interior dimensions of the chamber are in a very good agreement with the previously imposed height restriction. In addition, the chamber enables precise humidity control between 10 %RH and 90 %RH. As previously explained, the selection of the BINDER KMF 115 environmental chamber was based on various factors. However, the most important criterion was the temperature accuracy since ±0.2 °C is the value well below the desired accuracy of ±0.5 °C for PCM data.



**Figure 6.4:** *Binder KMF 115 environmental chamber (amended from Binder GmbH, Tuttlingen, Germany).*

| Parameter | Value at 25 °C ambient |
|---|---|
| Temperature range | Between -10 °C and 100 °C |
| Temperature accuracy | ±0.2 °C |
| Mean heating rate | 1.3 Kmin$^{-1}$ |
| Mean cooling rate | 0.5 Kmin$^{-1}$ |
| Interior dimensions (*W x H x D*) | 600 mm *x* 483 mm *x* 351 mm |
| Exterior dimensions(*W x H x D*) | 885 mm *x* 1050 mm *x* 730 mm |
| Humidity range | Between 10 %RH and 90 %RH |

**Table 6.2:** *Specifications of the BINDER KMF 115 environmental chamber.*

## 6.2.2 Investigation and selection of sensing modalities

As explained in the previous chapter, only a few authors gave some details regarding the sensor modalities used in their T-history measurements. Zhang et al. (1999) used thermocouples and concluded that the errors in heat capacity data mainly originate from temperature measurement errors. Marin et al. (2003) also used thermocouples (type T). Marin et al. (2005) used Pt-100 due to its higher precision of ±0.05 °C. The authors, however, did not give details regarding the sensor calibration and achieved accuracy. Moreover, the other relevant sensor selection criteria were not discussed either. Lazaro et al. (2006) discussed the importance of sensor calibration and measurement precision for determination of temperature and enthalpy values of PCMs. They used type K thermocouples calibrated with the Pt-100 sensor. Günther et al. (2009) reported that the typical operational temperature ranges of PCM applications are in the order of ±10 °C around the phase change temperature. Moreover, this range in practice is often reduced to ±5 °C or less (e.g. in free-cooling applications). This implies that the maximum decrease in the temperature uncertainty in PCM measurements is very important since it should enable a more optimal utilisation of these materials. The decrease in temperature uncertainty can be achieved through the usage of properly calibrated and accurate temperature sensors. Mehling et al. (2006) stated that the desired accuracy level in temperature measurements of PCMs should be equal or below ±0.5 °C. In addition to accuracy, the size of the temperature sensor is another important parameter since the sensor should be small. Namely, even the smallest sensor inside the PCM sample can act as a nucleating agent and thereby change the natural course of the phase change process. This can further result in incorrect determination of PCM properties (e.g. the degree of subcooling). For this reason it is important to use temperature sensors as small as possible.

Taking into an account the specifics of the T-history method and the identified parameters in terms of accuracy and size few types of temperature sensors have been investigated and their characteristics highlighted.

## 6.2.2.1 Thermocouples

Essentially, thermocouples consist of two wires made of different but homogeneous metals or alloys and joined at one end (measuring or hot junction). The free ends of the two wires connect to the measuring instrument to form a closed path i.e. the thermoelectric circuit in which current can flow (Claggett and Worrall, 1982). After the thermocouple wires connect to the measuring instrument, the junction made inside the device is identified as reference or cold junction (Figure 6.5).
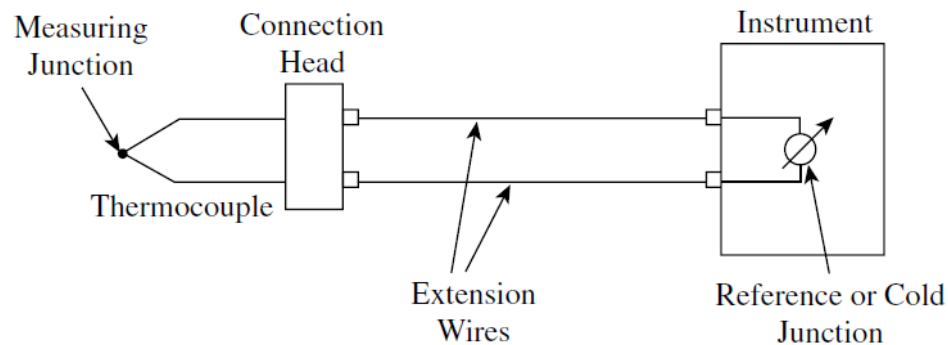


*Figure 6.5: Thermocouple terminology (amended from Claggett and Worrall, 1982, p. 675).*

Temperature changes at the measuring junction induce a change in ElectroMotive Force (EMF) between the other ends (reference junction) since the current flows in the closed thermoelectric circuit (Figure 6.5). This effect was discovered by Thomas Seebeck in 1821. As temperature goes up the output EMF i.e. the Seebeck voltage of the thermocouple rises. If the reference temperature is known, the unknown temperature at the measuring junction can be calculated using Equation 6.1:

$$unknown\ temperature = (measured\ EMF/Seebeck\ coefficient) + reference\ temperature. \quad (6.1)$$

The rise of the measured EMF is not necessarily linear nor the Seebeck coefficient (the amount of voltage generated in μV by a one degree temperature change) is constant (Claggett and Worrall, 1982). The value of the Seeback coefficient is temperature dependent and different for various thermocouple types. Another problem regarding the Seebeck coefficient is its low value (sometimes around

10 $\mu V°C^{-1}$) resulting in weak signals. Namely, the typical industrial transmitters have a minimum absolute error of about 0.01 mV i.e 10 $\mu V$. Hence it is difficult to obtain a measurement using industrial transmitter and some thermocouples, which would have less than a 1 °C error. This value is acceptable for higher temperature measurements but is not acceptable for measuring low temperatures. Additionally, the Seebeck voltage cannot be directly measured since direct connection of e.g. voltmeter with copper wires introduces a new thermoelectric circuit in the form of two additional metallic junctions. The technique which is used to eliminate the effect of additional junctions is called the cold junction compensation and it needs to be implemented in all thermocouple measurements (Claggett and Worrall, 1982).

The advantages of thermocouples compared to other temperature sensors are: ability of utilisation in a wide temperature range, robustness, small price, and easy availability. The main disadvantages are low accuracy and low nonlinear output resulting in weak signals. However, given their advantages and the history of usage in previous T-history studies (Marin et al., 2003; Lazaro et al., 2006) it was decided that these sensors will be used as the sensing modality in the advanced T-history method, at least for comparison purposes. The details about the selected thermocouples and the appropriate instrumentation are given in the next chapter.

## *6.2.2.2 Thermistors*

Thermistors belong into the group of resistance temperature devices. They are based on the resistance change in a ceramic semiconductor and have either a Negative (NTC) or Positive (PTC) resistance Temperature Coefficient. More usual thermistor types are NTC thermistors where their resistance drops nonlinearly with temperature rise. The PTCs are more linear, but less sensitive than NTCs (Claggett et al., 2003). The resistance-temperature relation can be expressed in the table form with the number of resistances associated with different temperatures or in the form of Steinhart-Hart equation (Equation 6.2):

$$\frac{1}{T} = a + b\ln(R) + c\ln^3(R), \qquad (6.2)$$

where $T$ represents the absolute temperature expressed in Kelvins and $R$ the thermistor's resistance at temperature $T$. Thermistors are usually designated according to their nominal resistances at 25 °C. The most common of these ratings are 2.252 kΩ, 5 kΩ, and 10 kΩ.

The $R(T)$ relation of a thermistor is negative and highly nonlinear which is one of their major drawbacks. Thermistor's nonlinearity poses a serious problem for engineers who need to design their own circuitry. Figure 6.6 illustrates the nonlinearity aspects of various temperature sensors clearly showing the main thermistors' disadvantage.
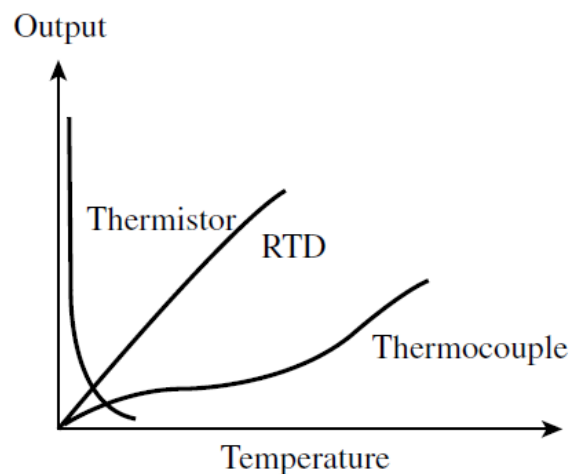


*Figure 6.6:* *Nonlinearity aspects of various temperature sensors (amended from Claggett et al., 2003, p. 668).*

However, the difficulty regarding the nonlinearity can be eased by using different hardware or software approaches and linearisation techniques depending on the application. Additionally, a potential problem that needs to be controlled in a thermistor circuit is self-heating. Namely, the electric conditioning circuits associated with a thermistor originate a current flow in the sensor. If the current flow is large, the heat generated within the thermistor will gradually begin to raise its temperature above that of its environment. This will in turn lower its resistance and consequently enable more current to flow. The self-heating problem can also be resolved by appropriately limiting the current through the thermistor (Claggett et al., 2003). Despite the high nonlinearity, thermistors have great advantages in terms of high sensitivity and accuracy making them particularly responsive to changes in temperature. Additional

advantages are accessibility of small probes and short response time (Claggett at al., 2003).

Given their advantages especially in terms of high precision and accuracy these sensors were selected as the principal sensing modalities in the implementation of the advanced T-history method. The details about the particular sensors and the corresponding instrumentation are explained in the next chapter.

### *6.2.2.3 Resistance temperature detectors (RTDs)*

RTDs as the second type of resistance temperature devices were investigated as well. These devices exploit the highly predictable change in the electrical resistance of a metallic material due to its temperature changes. As their name indicates, RTDs rely on resistance change in a metal. Their resistance rises more or less linearly with temperature. The main advantages of these sensors are the wide temperature range of utilisation, high accuracy and fairly good linearity. However, due to the disadvantages in terms of low sensitivity, relatively long response time, limited availability of small temperature probes, and due to their metallic non PCM compatible material properties RTDs (including Pt-100) were discarded as the possible sensing modalities for the advanced T-history implementation.

## 6.2.3 Design and development of testing containers

As explained in the previous chapter, T-history assumes the limitation on the Biot number value ($Bi=hL_C/k < 0.1$). Namely, since the parameters like heat transfer coefficient ($h \sim 5\text{-}15\ \mathrm{Wm^{-2}K^{-1}}$ – typical values for free convection) and thermal conductivity ($k \sim 0.2\ \mathrm{Wm^{-1}K^{-1}}$ – typical value for PCMs) are relatively fixed the Biot number predominately depends on the characteristic length $L_C$ of the investigated bodies. Since the characteristic length represents the volume to surface ratio the Biot limitation directly defines the specific geometry of the test containers for the PCM sample and reference material test tubes need to be very narrow and long cylinders. Zhang et al. (1999) used 180.06 mm long cylinders with the diameter of 10.4 mm. Marin et al. (2005) reported that the height of their cylinders was 130 mm and the

diameter 10 mm. Given these values, the internal height of the environmental chamber (483 mm), the earlier established objective to investigate larger samples in this study as well as the discussed Biot restriction it was decided that the test tubes with two different heights of 300 mm and 430 mm will be used. Another restriction for the test tubes was their transparency. This was necessary to assure the correct placement of sensors in advanced T-history measurements. The transparency could be achieved by using glass test tubes. Additional requirement was to avoid the use of any sample holders to minimise the direct contact between the investigated samples and the environment. To achieve this special design of the test tubes had to be made (Figure 6.7).
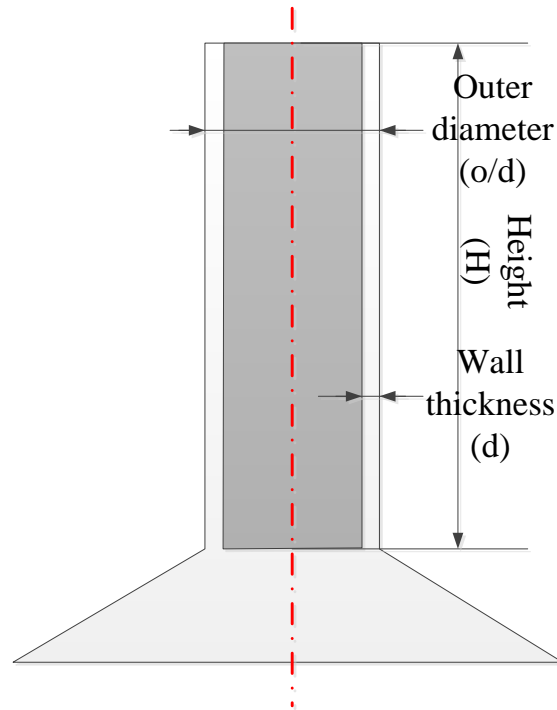


***Figure 6.7:*** *Cross section of the designed test tubes.*

The tubes were designed in the form of long narrow cylinders with the appropriate base to enable self-accommodation within the environmental chamber. The desired outer diameter (o/d) and wall thickness (d) were set to be as small as possible. Once the design was finished the test tubes had to be custom made. The design was sent to the well-known glass making company Dixon Glass Limited (Dixon Glass Limited, Kent, UK). Given the design scheme and the desired height of the test tubes the outer diameter and wall thickness parameters were determined by taking into an

account the limitations of the manufacturing process. The outer diameter values were 12 mm and 15 mm for the corresponding heights of 300 mm and 430 mm (see Figure 6.8). On the other hand, the corresponding wall thicknesses were set to 1 mm and 1.2 mm, respectively. The SIMAX glass with the thermal conductivity of 1.2 $Wm^{-1}K^{-1}$ was used as the test tube material.
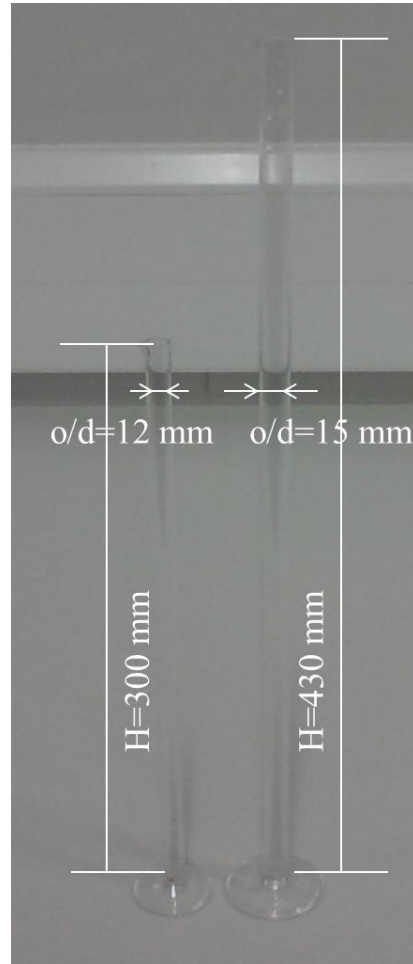


*Figure 6.8: Custom made test tubes.*

The specifications of the test tubes are summarised in Table 6.3.

| Test tube ID | Height | Outer diameter (o/d) | Wall thickness (d) | Material |
|---|---|---|---|---|
| 1 | 300 mm | 12 mm | 1 mm | Simax glass |
| 2 | 430 mm | 15 mm | 1.2 mm | Simax glass |

*Table 6.3: Specifications of the test tubes.*

# 6.3 Summary

This chapter described the development of the design strategy and the experimental setup of the advanced T-history method.

The design strategy was explained in terms of the most important actions that need to be taken in order to implement the advanced T-history setup. The special emphasis was put on the set of design rules that need to be considered prior to any developments. These rules were identified using basic PCM measurement premises and the restriction imposed by the T-history definition in terms of the Biot number value.

The majority of the steps that need to be performed for the successful development of the advanced T-history method were briefly discussed, while the development of the experimental setup of the method was presented in detail. The investigation and selection of control and sensing mechanisms were explained in depth as well as the design and development of testing containers. All the important restrictions imposed on these processes were discussed in detail. The thermocouples and thermistors were identified as the types of sensors to be used in the advanced T-history implementation based on their respective advantages and disadvantages. The selection of the particular sensor models as well as the development of the corresponding instrumentation systems are the main subject of the next chapter.

# Chapter 7

# DEVELOPMENT OF THE INSTRUMENTATION SYSTEM OF THE ADVANCED T-HISTORY METHOD

The development of the instrumentation system was identified as the second constructive process in the implementation of the advanced T-history setup. One of the main parts of the T-history method is to record the temperature history of the reference and the PCM under investigation. Therefore, a proper measurement system had to be developed to enable the correct temperature measurements of the investigated samples. The development of the instrumentation is closely linked with the validation point in the design strategy flowchart (Figure 7.1). As indicated in the previous chapters, the value of ±0.5 °C was set as the desired technical goal for the temperature accuracy in the PCM related measurements (Mehling et al., 2006). Consequently, this value was selected as the validation criterion in the instrumentation development. Moreover, a requirement to evaluate any developed instrumentation system in the appropriate temperature measurement and redesign it should the desired accuracy target of ±0.5 °C is not achieved was adopted. In this way the development of the proper instrumentation system was performed in an iterative procedure until the validation criterion was met (Figure 7.1). Given the selection of thermocouples and thermistors as the temperature sensing modalities in the advanced T-history measurements, as explained in the previous chapter, and the temperature accuracy requirement (±0.5 °C) three different instrumentation systems had to be developed and validated. The details of the development and validation procedures of these systems are discussed in the following subsections.
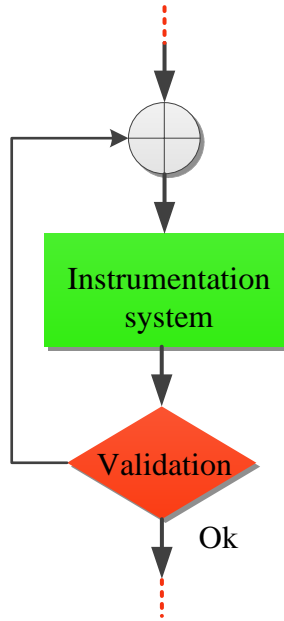
***Figure 7.1:*** *Constructive steps of the instrumentation development in the design strategy flowchart.*

# 7.1 Instrumentation system 1

Given the history of thermocouple usage in previous T-history studies (Marin et al., 2003; Lazaro et al., 2006) it was decided that these sensors will be used as one of the sensing modalities in the advanced T-history method. Thermocouples are nonlinear temperature devices. For this reason a proper instrumentation system had to be developed in order to perform temperature measurements. This instrumentation system was named instrumentation system 1. The development process of the instrumentation system 1 was split into several sub-processes (Figure 7.2). The first of those was the selection of the specific sensor device. The reason this sub-process is included in the development process is its close relation with the next two stages: linearisation and signal conditioning and data acquisition. The second sub-process, linearisation and signal conditioning, was one of the most important since it was developed to convert the nonlinear and weak thermocouple signal into the signal suitable for acquisition. The final stage, the development of the data acquisition system, enabled continuous temperature measurements. The details of these sub-processes as well as of the validation process will be explained in detail in the following subsections.
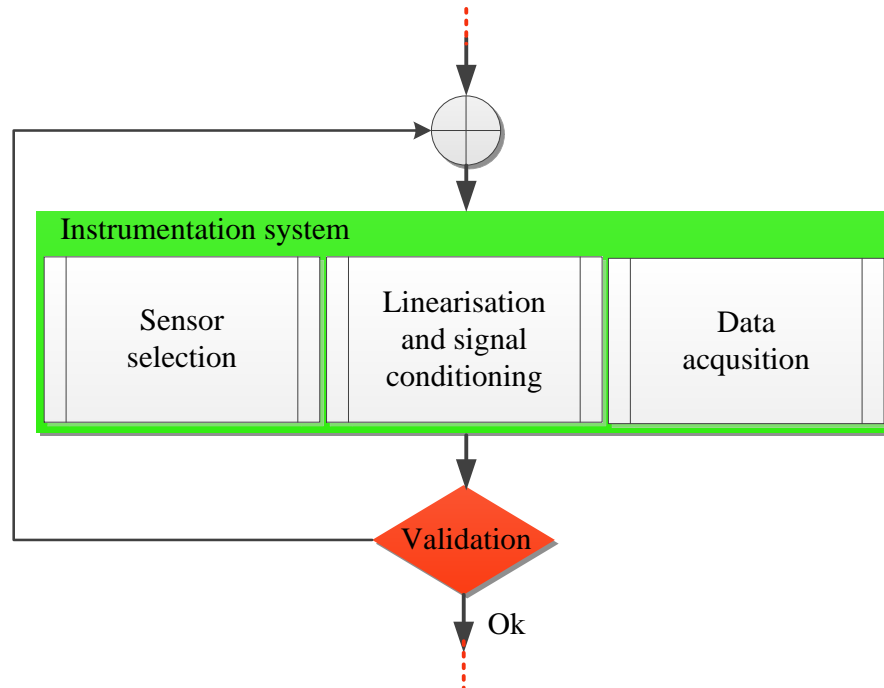
**Figure 7.2:** *A detailed view of the constructive steps of the instrumentation development in the design strategy flowchart.*

## 7.1.1 Sensor selection

As mentioned in the previous chapter, Marin et al. (2003) and Lazaro et al. (2006) used thermocouples in their studies. Marin et al. (2003) used type T thermocouples while Lazaro et al. (2006) used type K thermocouples. One of the aims of this project was to verify the suitability of thermocouples for T-history temperature measurements. Given this aim and the advantages of type K thermocouples in terms of easy availability, small size and low price this thermocouple type was selected for the measurements in this study. As noted earlier, T-history assumes the limitation on the Biot number value ($Bi < 0.1$), which implies the utilisation of specifically long and narrow cylindrical test containers. This therefore requires the usage of small temperature probes. Small and thin temperature probes are a prerequisite in this type of measurements also due to the nature of PCMs. When the sensor is placed inside the PCM sample it is essential to avoid the interference of the sensor and the phase change process. The sensor can act as a nucleating agent so it can affect the subcooling degree and suppress the real behaviour of the PCM; hence small size of the temperature sensor was one of the main selection criteria. An RS 621-2158 (RS Components, Corby, UK) thermocouple type K

117

(Chromel-Alumel type) was selected primarily due to its size (0.2 mm probe diameter), and then its robustness and easy availability. The technical specifications of the selected sensor are given in Table 7.1.

| Parameter | Value |
|---|---|
| Thermocouple type | K |
| Minimum temperature sensed | -50 °C |
| Maximum temperature sensed | 1100 °C |
| Accuracy class | ±1.5 °C |
| Probe diameter | 0.2 mm |
| Probe length | 1000 mm |
| Package |  |

***Table 7.1:*** *Specifications of the RS 621-2158 thermocouple type K sensor.*
.

Despite the history of thermocouple usage in previous T-history studies, an initial assumption that thermocouples were not suitable for T-history temperature measurements was made at this stage of the project. Namely, the implicit tolerances of thermocouples, without any errors introduced by measurement systems, do not go below ±0.5 °C i.e. the value previously set as the desired technical goal for the temperature accuracy in the PCM related measurements (Mehling et al., 2006). Typically, the measurement system introduces errors on top of the implicit tolerance values of the sensors alone. Consequently, the assumption that the desired technical goal in terms of temperature accuracy in T-history measurements could not be obtained by using thermocouples was adopted as a logical one. However, a proper measurement system i.e. the instrumentation system 1 had to be developed and tested to verify the initial assumption.

## 7.1.2 Linearisation and signal conditioning

As explained in the previous chapter, the temperature dependent voltage produced by thermocouples cannot be directly measured primarily due to its nonlinearity and low value. Additionally, direct connection of thermocouple and voltmeter with copper wires introduces a new thermoelectric circuit in the form of two additional metallic junctions. Hence, a circuit that enables linearisation and cold junction compensation of the thermocouple signals had to be developed. The main part of this circuit was the thermocouple amplifier AD595CQ, an Integrated Circuit (IC) purchased from RS Components (RS Components, Corby, UK). This IC includes a complete linearisation amplifier and thermocouple cold junction compensator on a single chip. It produces a high level ($10 \, \mathrm{mV{}^\circ C^{-1}}$) output directly from a thermocouple signal. The detailed technical specifications of this IC are given in Table 7.2. Apart from linearisation and cold junction compensation, an additional conditioning of the thermocouple signal was implemented. Namely, the output of the AD595CQ IC was further amplified and then filtered to enable better data acquisition of the temperature signal captured by the thermocouple. The details of the thermocouple temperature processing circuit are shown in Figure 7.3. The circuit was designed using NI Multisim circuit design software (National Instruments, Newbury, UK). The complete conditioning of the thermocouple signal resulted in three clearly distinguishable stages of the temperature processing circuit: linearisation and cold junction compensation, amplification and filtering (Figure 7.3). As previously explained, the first stage is implemented through a direct connection of the thermocouple (TC_AL and TC_CR mark the connection points of type K thermocouple leads) and AD595CQ chip. The amplification was implemented using a standard operational amplifier TL084CN IC. This chip has four integrated operational amplifiers. One of those was used in the second stage as an inverting amplifier with the gain of -13 which was assured by using three resistors, $R_1$ with the value of 1 k$\Omega$ and $R_2$ and $R_3$ with the values of 12 k$\Omega$ and 1 k$\Omega$ (Figure 7.3). The gain of the inverting amplifier is given by Equation 7.1:

$$G = -\frac{R_2 + R_3}{R_1}.$$

(7.1)

| Parameter | Value |
|---|---|
| +Vs to −Vs maximum rating | 36 V |
| Common mode input voltage | -Vs-0.15 V (min), +Vs (max) |
| Differential input voltage | -Vs (min), +Vs (max) |
| Operating temperature range | -55 °C to 125 °C |
| Calibration error at 25 °C | ±1 °C |
| Package details |  |
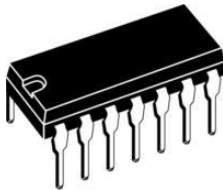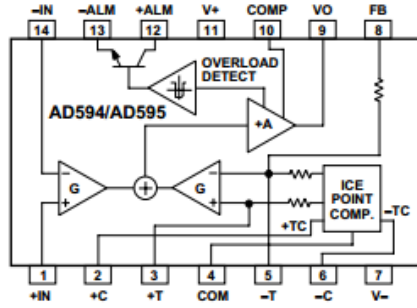
*Table 7.2:* *Specifications of the AD595CQ IC.*

The other three operational amplifiers were used as voltage followers preventing the loading between different stages of the thermocouple temperature processing circuit (Figure 7.3). In total all four operational amplifiers of the TL084CN IC were used in the thermocouple conditioning circuit. The detailed technical specifications of the TL084CN IC are given in Table 7.3. The final, filtering stage was implemented by using a simple *RC* low pass filter with the resistor $R_4$ (1 MΩ) and the capacitor $C_1$ (100 nF) as shown in Figure 7.3. The values of $R_4$ and $C_1$ were selected in order to tune the cut-off frequency of the low pass filter, given by Equation 7.2:

$$f_c = \frac{1}{2\pi R_4 C_1}$$
(7.2)

Namely, the thermocouple temperature signal is a Direct Current (DC) signal in its nature. Given the nature of the thermocouple temperature signal, the laboratory environment and the availability of *RC* components the low pass filter was designed to have a cut-off frequency of 1.59 Hz. The frequency response of the *RC* low pass filter is given in Figure 7.4. The filter was designed to cut the high frequencies from the thermocouple DC signal. The reason a simple *RC* low pass filter was used in this stage was the assumption that most of the signal filtering will be performed by using digital filters. The design and implementation of digital filtering is explained in the section 7.1.4.
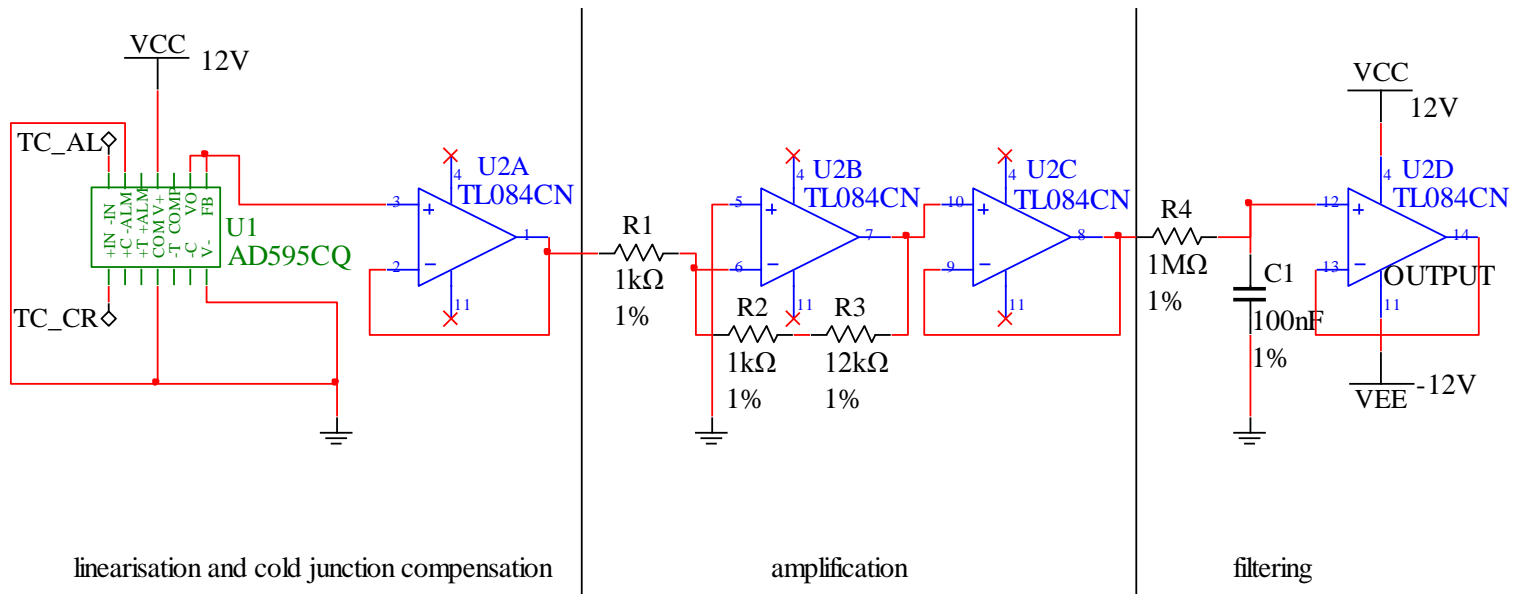
**Figure 7.3:** *Thermocouple temperature processing circuit.*

| Parameter | Value |
|---|---|
| Supply voltage maximum rating | ±18 V |
| Input voltage maximum rating | ±15 V |
| Input offset voltage at 25 °C | 3 mV (typ), 10 mV (max) |
| Input offset current at 25 °C | 5 pA(typ), 100 pA (max) |
| Input bias current at 25 °C | 30 pA(typ), 400 pA (max) |
| Common mode rejection ratio | 70 dB (min), 86 dB (typ) |
| Operating temperature range | 0 °C to 70 °C |
| Package details | |
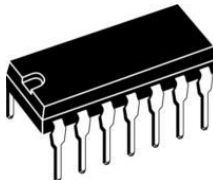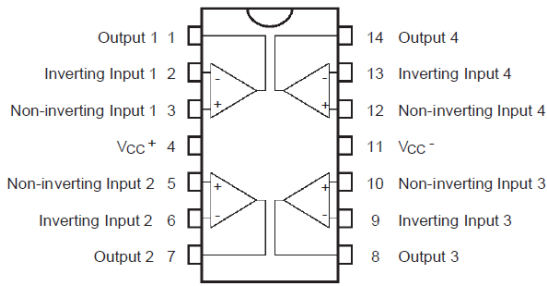


*Table 7.3: Specifications of the TL084CN IC.*
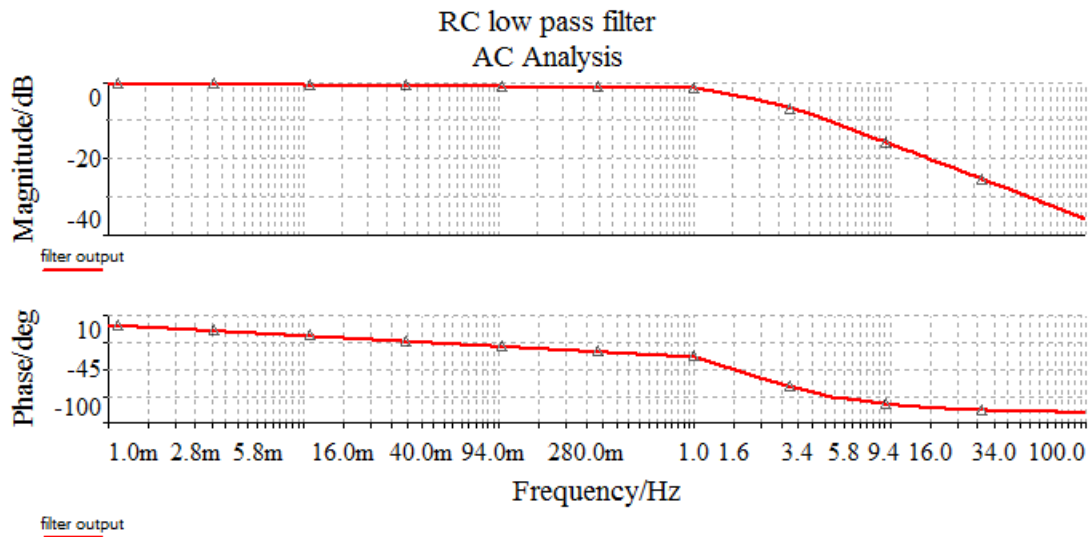


*Figure 7.4: Frequency response of the RC low pass filter of the thermocouple temperature processing circuit.*

Additionally, given the DC nature of the thermocouple temperature signal the sampling frequency of the signal was set to be 15 Hz. This frequency value was selected as suitable to preserve the quality of the signal given the Nyquist-Shannon sampling theorem.

Apart from the thermocouple temperature processing system, an important part of the instrumentation system 1 was the power source. Given the ICs used for the thermocouple signal conditioning the standard laboratory scale ISO-TECH IPS-4303 digital DC power supply (RS Components, Corby, UK) was used to power the temperature processing circuit with the dual ±12 V voltage supply (Figure 7.3). The specifications of the power supply instrument are given in Table 7.4.

| Parameter | Value |
|---|---|
| Variable DC voltage output | 0-30 V |
| Current output | 3 A (max) |
| Operating temperature range | 0 °C to 40 °C |
| Package details |  |

***Table 7.4:*** *Specifications of the ISO-TECH 4303 digital DC power supply.*

Once the thermocouple temperature processing circuit was designed and built a proper Data AcQuisition (DAQ) system had to be developed. The details of this system are explained in the next section.

# 7.1.3 Data acqusition

The data acquisition system was partially implemented in hardware and partially in software. Namely, the 16-bit NI Universal Serial Bus (USB) 6212 data acquisition card (National Instruments, Newbury, UK) was used in the hardware part of the system. The card has 16 single-ended i.e. 8 differential analogue input channels. The relevant technical specifications of the card are given in Table 7.5.

This card was selected because of its USB interface which provided an easy plug and play connection with the desktop personal computer (PC) to perform the data acquisition. The PC used for the data acquisition was a Dell Optiplex 755 Desktop PC (Dell, Round Rock, Texas), equipped with the 1.6 GHz Intel Pentium Dual Core

processor, 1 GB of Random Access Memory (RAM), and 80 GB hard drive. The PC was able to detect and install the DAQ card automatically once the card was connected through the USB interface. Another important feature of the data acquisition card was the possibility of complete software configuration.

| Parameter | Value |
|---|---|
| Analogue input channels | 16 (single-ended), 8 (differential) |
| Resolution | 16 bit |
| Sample rate | $400 \text{ kSs}^{-1}$ |
| Maxium voltage range | -10 V to 10 V |
| Package details |  |

*Table 7.5: Specifications of the NI USB 6212 DAQ card.*

The software part of the data acquisition system was implemented in NI LabVIEW version 8.5 (National Instruments, Newbury, UK). The LabVIEW software environment is often used in conjunction with NI DAQ cards in measurement and control systems. The aim of the data acquisition software was to enable data sampling at the specified sampling frequency as well as the output file data storage. Consequently, the proper code in the form of the LabView Virtual Instrument (VI) had to be implemented. The block diagram of the developed virtual instrument (PCM_DAQ.vi) is given below (Figure 7.5).
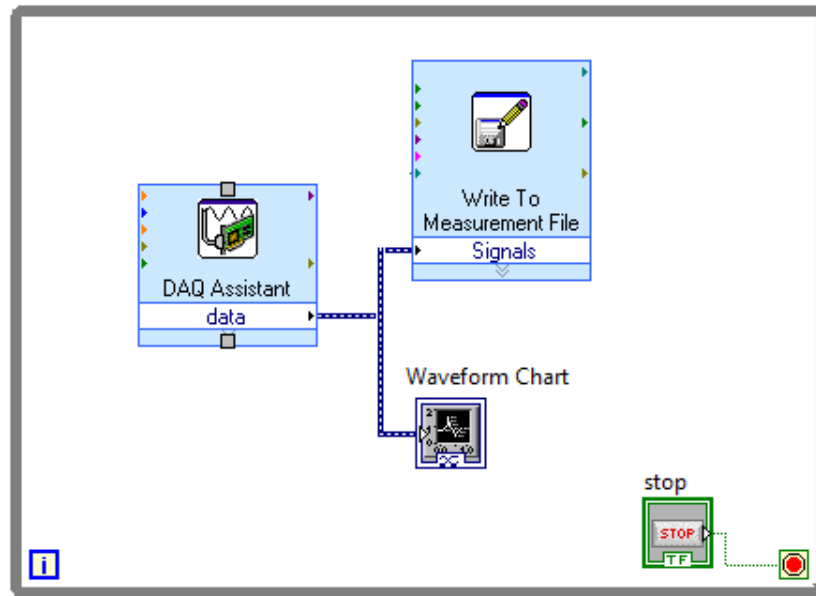
***Figure 7.5:*** *Block diagram of the PCM_DAQ.vi.*

The implemented PCM_DAQ.vi is rather simple given that the LabVIEW's built-in express VIs were used in its implementation. T-history measurements require the acquisition of temperature signals. These signals are DC signals in their nature. Given the nature of the selected sensing modalities (thermocouples and thermistors) it was clear that the signals to be measured in the advanced T-history studies will essentially be analogue voltages. Hence, one of the most important features of the developed PCM_DAQ.vi was to enable the DAQ card for the sampling of analogue voltages. This feature was implemented through the usage of LabVIEW's built-in DAQ Assistant express VI (Figure 7.5). The express VI provides the necessary support for software configuration of the DAQ cards. It offers the possibility to adjust several parameters in order to properly configure the acquisition of the required signals (Figure 7.6). The most important settings that can be adjusted by using this VI are *Channel settings and Timing Settings* (Figure 7.6)*.* In the channel settings one can configure the type and the number of channels i.e. signals to be sampled. Furthermore, the input range and the units of the selected signals can also be configured as well as their terminal settings. In the timing settings the acquisition mode, the sampling rate, and the size of the DAQ card buffer (samples to read) can be adjusted.
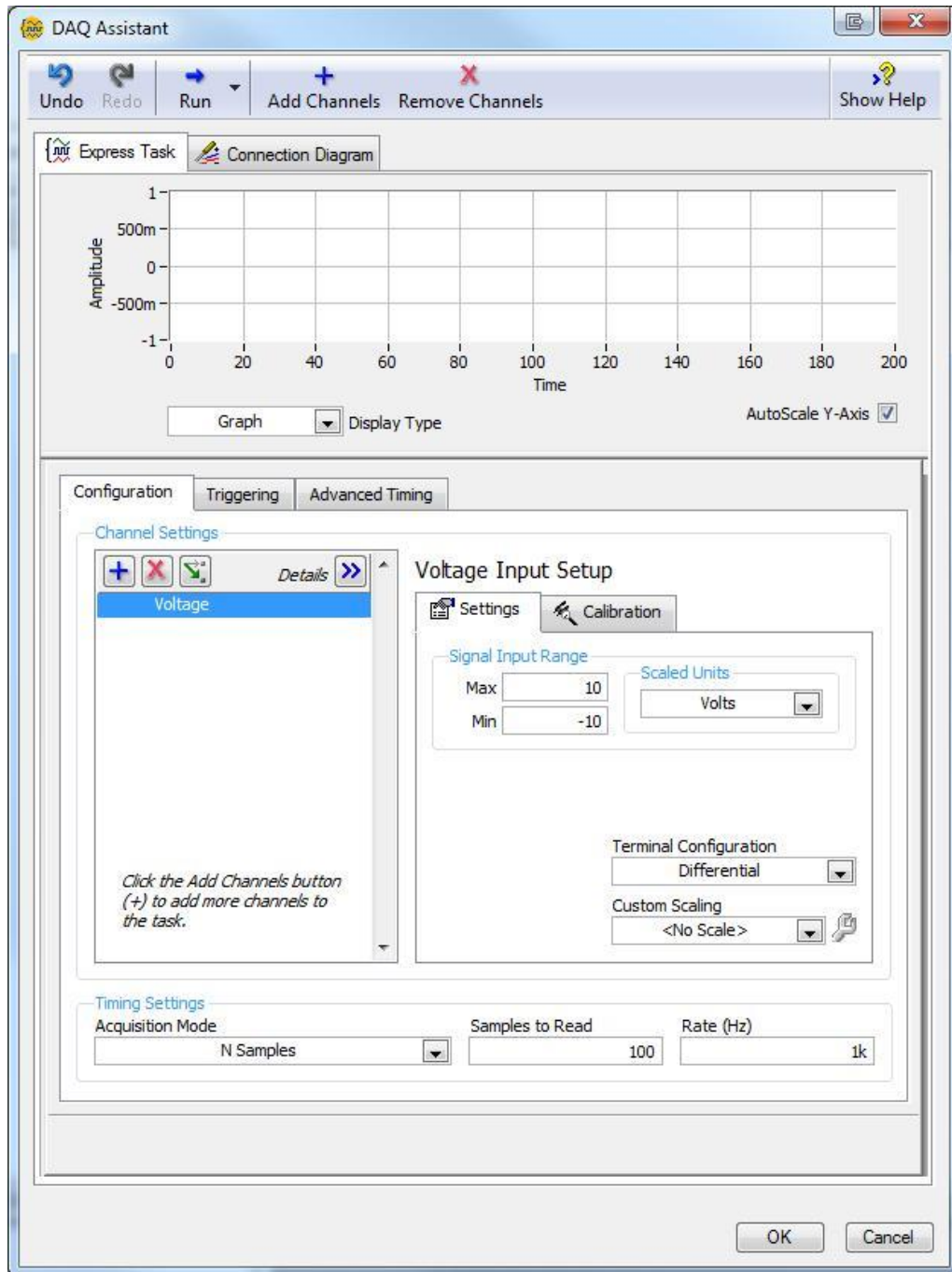
**Figure 7.6:** *The configuration panel of the LabVIEW's DAQ Assistant express VI.*

.

As explained earlier, given the expected T-history measurements and temperature signals the PCM_DAQ.vi was supposed to enable the acquisition of multiple analogue voltage signals. One of the parameters expected to change between T-history measurements was the number of sampled channels on the DAQ card i.e. the number of temperature signals and the other parameters were the sampling rate and the

input range of the signals. For this reason, it was concluded that the DAQ Assistant express VI should be used in PCM_DAQ.vi since it provided more than enough data acquisition settings. Naturally, the sampling rate, the number of channels, their input range and consequently the size of the DAQ card's buffer had to be adjusted before each T-history measurement. These four parameters were adopted as variable in the PCM_DAQ.vi. However, their adjustment represented a rather quick and easy task when the DAQ Assistant express VI was used. The other parameters, labeled as the fixed ones, were adjusted only once. These included the signal units, the terminal configuration of the channels, and the acquisition type. The signal units were set to Volts, the channel terminals were configured as Differential, the data acquisition was configured as Continuous.

Another important feature of the PCM_DAQ.vi was to enable the storage of the acquired data into an output file. This was easily implemented by using the Write To Measurement File express VI (Figure 7.5). This VI also provides the user with the option to select few parameters regarding the data storage (Figure 7.7).

In PCM_DAQ.vi the Write To Measurement File express VI was configured in such way to enable the user to choose the file for the storage of data. Moreover, in the case of the selection of an already existing data file, the software was configured to rename the existing file. The text file was selected as the desired file format. One header option in the entire storage file was also selected. The express VI was set to only store the actual voltage signals without the time data since those could be easily recovered based on the sampling frequency.

The last implemented feature in the PCM_DAQ.vi was to display the acquired data on the waveform chart (Figure 7.5).

The data acquisition, data storage, and data display were implemented to run continuously inside the while loop in the PCM_DAQ.vi. The continuous execution of the VI could be stopped once the stop button was pressed (Figure 7.5).

The implementation of the PCM_DAQ.vi was the final step in the development of the instrumentation system 1. Once the instrumentation system was fully designed and assembled as described in sections 7.1.1-7.1.3 its validation could be performed.
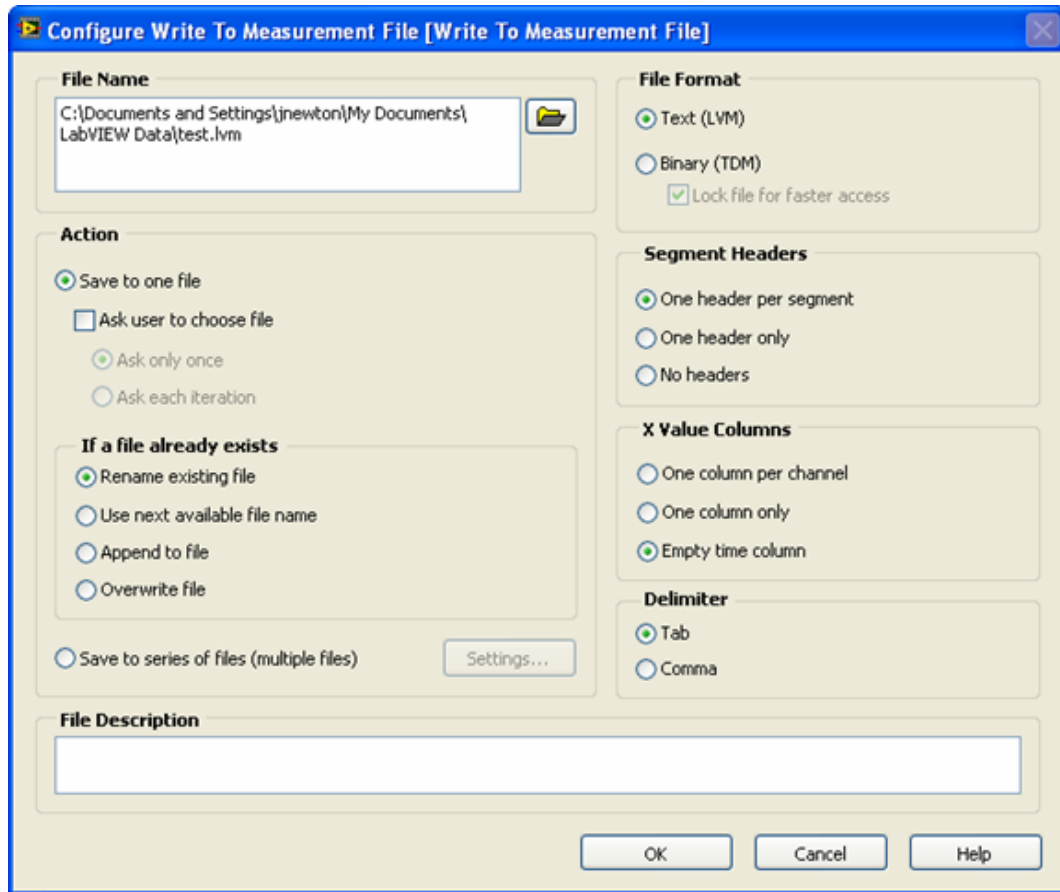
**Figure 7.7:** *The configuration panel of the LabVIEW's Write To Measurement File express VI.*

## 7.1.4 Validation

As explained at the beginning of this chapter, every instrumentation system had to be properly validated. This section explains the validation procedure for the instrumentation system 1. As previously noted, the value of ±0.5 °C in terms of the required temperature accuracy was selected as the validation criterion in the instrumentation development. Hence, in order to test the temperature accuracy of the instrumentation system 1 some temperature measurement had to be performed. It was decided that the instrumentation system 1 will be tested in the T-history measurement of a certain PCM. The selected PCM was a well-known commercially available organic material from Rubitherm's RT paraffin series, the RT21 (Rubitherm GmbH, Berlin, Germany). The material properties of RT21 are given in Table 7.6.

| Property | Value |
|---|---|
| Melting area | 18-23 °C |
| Congealing area | 22-19 °C |
| Typical phase change temperature | 21 °C |
| Heat storage capacity (15 to 30 °C) | 134 kJkg$^{-1}$ |
| Specific heat capacity | 2 kJkg$^{-1}$K$^{-1}$ |
| Density solid (at 15 °C) | 0.88 kgl$^{-1}$ |
| Density liquid (at 25 °C) | 0.77 kgl$^{-1}$ |
| Thermal conductivity | 0.2 Wm$^{-1}$K$^{-1}$ |

**Table 7.6:** *Material properties of organic paraffin RT21.*

The T-history measurement of RT21 was performed using the advanced T-history method based on the experimental setup explained in Chapter 6 and the instrumentation system 1.

The explanation of the basic T-history setup was given in Chapter 5 (Figure 5.6). It was explained that in any T-history measurement the sample and reference materials, placed in test tubes of a defined geometry (cylindrical) and at the same initial temperature $T_0$ ($T_0 > T_{pc} = T_m$), need to be subjected to the ambient temperature $T_{\infty,a}(t)$ or simply $T_a$ ($T_a < T_{pc}$). Furthermore, their temperature history needs to be recorded until both samples reach equilibrium with the ambient so the recorded curves can be compared and the heat release/storage capacity of the sample determined. Accordingly, the very first PCM measurement using the concepts of the advanced T-history method, developed in this study, needs to be explained in details at this point. Given this fact, it is only reasonable to firstly present the advanced T-history setup in details. This was not done earlier in the thesis because the presentation required the development of at least one measurement system. Provided that the development of the instrumentation system 1 was entirely explained, the details of the complete advanced T-history setup can be presented here.

Figure 5.6 showed the schematic diagram of a general T-history setup. However, as noted earlier, the experimental chamber Binder KMF 115 was used as the control modality in the advanced T-history method. This resulted in marginally different perspective of the advanced T-history setup than that of the standard setup given in Figure 5.6. Namely, the boundary between the exterior and the interior of the setup was distinctly established here.

The exterior of the advanced T-history setup is shown in Figure 7.8.



*Figure 7.8: Exterior of the advanced T-history setup.*

In this T-history implementation, the main parts of the exterior setup include: the environmental chamber, the sensors, the instrumentation system, the power supply, the DAQ card, and the personal computer (Figure 7.8).

The functional boundary between the exterior and interior setup is established through the port positioned on the left side of the environmental chamber (Figure 7.8). This port has a silicon plug which provides a secured placement of the sensors used in measurements as well as the hermetic seal of the chamber once the sensors are indrawn inside the chamber.

The interior of the advanced T-history setup is shown in Figure 7.9.
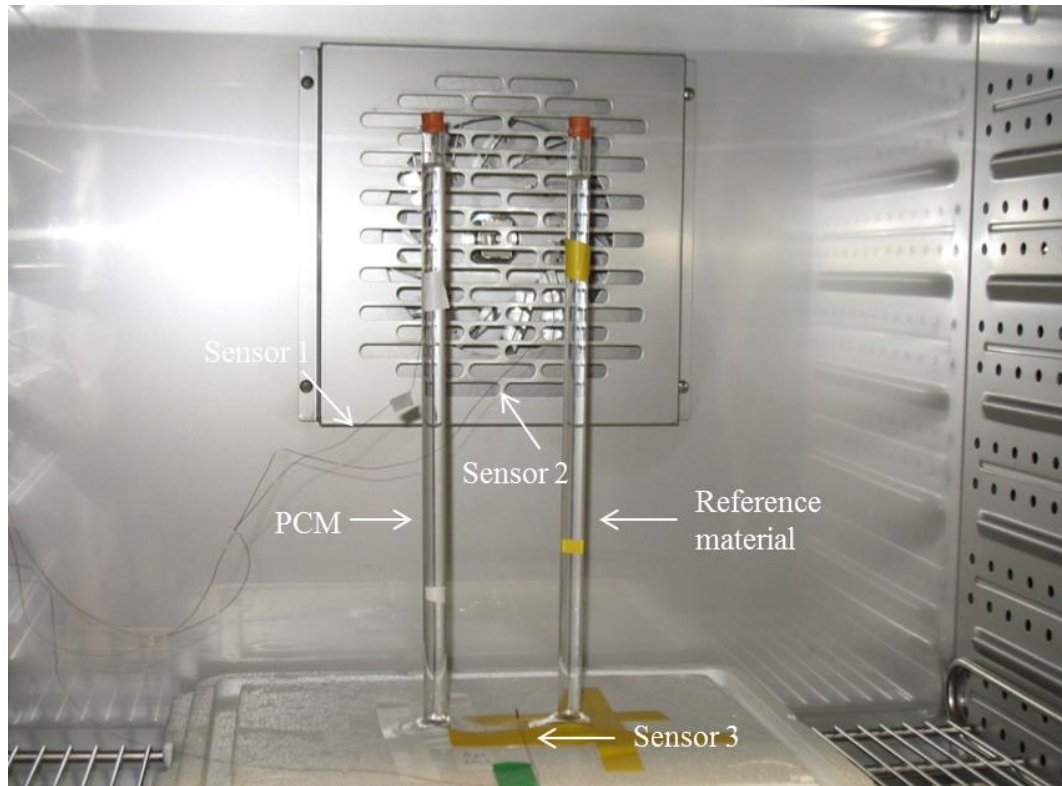


***Figure 7.9:*** *Interior of the advanced T-history setup (amended from Stankovic and Kyriacou, 2013, p. 2).*

Here, as in the basic T-history setup, the PCM and the reference material are put inside the test tubes and placed in the temperature controlled environment i.e. in the chamber's interior. The design, development, and specifications of the test tubes are explained in detail in section 6.2.3 and therefore not discussed here. However, it is important to mention that the test tubes were not directly placed on the chamber's floor but on the 50 mm thick polystyrene board to isolate their bottoms from the chamber's metallic surface.

The sensors (Sensors 1 and 2 in Figure 7.9) used for the temperature measurements of the samples (PCM and reference distilled water samples) were placed inside the test tubes along the central axes of the tubes and secured with the rubber stoppers used to seal the tubes. Namely, very small diameter holes were made with a needle through the center of the 10 mm long rubber stoppers. The sensors were tunneled through the holes and tightly secured at a depth of 120 mm from the top of the test tubes. A separate temperature sensor, identical with the ones used in the two

samples, was used to record the temperature inside the chamber (Sensor 3 in Figure 7.9). At least three sensors were required in any measurement using the advanced T-history method.

Given the presented specifics of the advanced T-history setup it is possible to describe the very first PCM measurement performed on the RT21 PCM in order to validate the instrumentation system 1. As noted earlier, some measurement parameters are fixed and defined in the explanation of the experimental setup, instrumentation and data acquisition systems. Other parameters are changeable between measurements. Accordingly, the specifics including the variable measurement parameters of the RT21 PCM measurement using RS 621-2158 (RS Components, Corby, UK) type K thermocouples are described now.

In the very first PCM measurement the RT21 and the reference material (distilled water) were put in 300 mm long test tubes and subjected to a temperature program with alternating heating and cooling cycles between 11 °C and 30 °C. At the beginning of every 2 h long cycle the chamber's temperature was sharply changed between the two mentioned temperature points. Given the size of the test tubes, it was presumed that both samples will reach the thermal equilibrium with the chamber's environment within the 2 h cycle. The samples' temperatures and the chamber's temperature were continuously recorded resulting in totally three (*no_of_chan*) data channels. Prior to the measurement, a prototype signals acquisition and pre-processing system for these three channels was built on the breadboard. Every channel on this prototype was implemented according to the schematic given in Figure 7.3. The three resulting signals from the developed prototype, although single-ended in nature, were connected to the differential inputs of the NI USB 6212 DAQ card (NI, Newbury, UK) and recorded using the developed PCM_DAQ.vi. The sampling frequency (*sampling_freq*) was 15 Hz. The expected input range of the signals was set between -10 V and 10 V. Finally, the size of the DAQ card's buffer (*buffer_size*) was set to 54 according to the formula given by Equation 7.3:

$$buffer\_size = \lceil 1.2 \cdot sampling\_freq \cdot no\_of\_chan \rceil. \quad (7.3)$$

The results obtained in the described measurement are given in the following subsection.

## 7.1.4.1 Results and discussion

The raw results from the RT21 T-history measurement using instrumentation system 1 captured by the PCM_DAQ.vi are displayed in Figure 7.10.
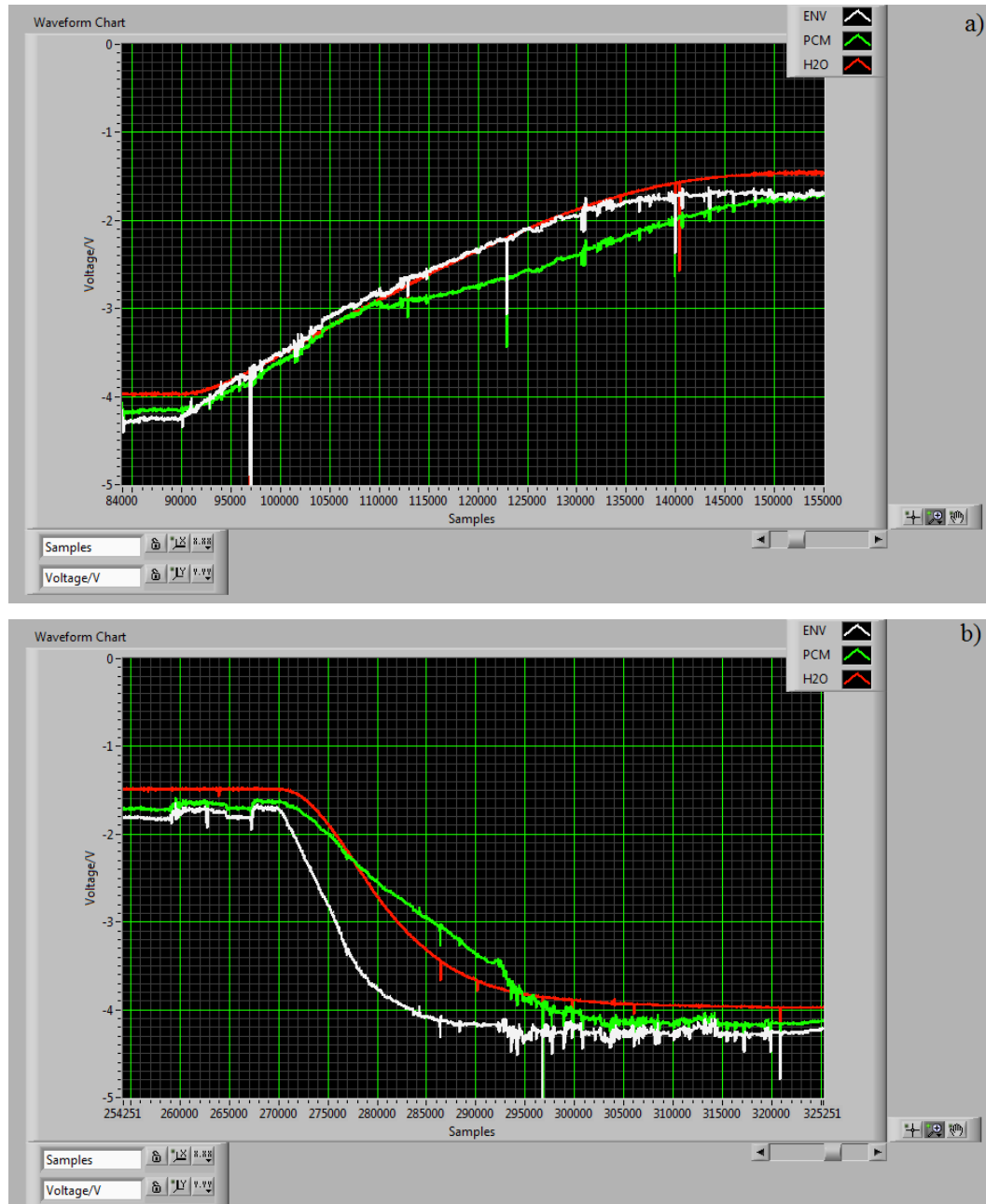


**Figure 7.10:** *Cooling (a) and heating (b) cycle in RT21 T-history measurement using instrumentation system 1 – raw results (ENV – environmental temperature, PCM – temperature of PCM sample, H2O –temperature of reference sample).*

The signals captured by PCM_DAQ.vi show the increase in voltage in a cooling cycle (Figure 7.10a) and decrease in a heating cycle (Figure 7.10b). This is due to the negative gain of -13 in the amplification stage of the instrumentation system 1 (Figure 7.3). Three different signals were captured in both cycles: temperature of the chamber's environment (ENV in Figure 7.10), temperature of the PCM (PCM in Figure 7.10), and temperature of the reference material i.e. distilled water (H2O in Figure 7.10). It is evident that the captured signals are noisy, especially the ones representing the environmental and the temperature of the PCM. Moreover, the signals don't reach the equilibrium state at the beginning and at the end of each cycle as expected. Hence, this could be justified by the nature of the raw signal (voltage) and the fact that equilibrium should be expected only in the case of temperature values.

Repetitive measurements using the above mentioned signal acquisition and pre-processing system have consistently produced low quality signals and therefore it was deduced that the instrumentation system 1 cannot meet the validation criteria (±0.5 °C accuracy). Nevertheless, the above presented raw results were subjected to some post-processing in order to obtain the temperature data. The post-processing of the signals was done using MATLAB. Considering the gain used in the amplification stage and the fact that the AD595CQ chip produces an output of 10 mV$°C^{-1}$ the conversion between voltage (expressed in V – *voltage*) and temperature (expressed in °C – *temperature*) for the obtained signals (ENV, PCM, and H2O in Figure 7.10) was rather easily implemented using Equation 7.4.

$$temperature = \frac{voltage}{G \cdot 10mV} = \frac{voltage}{-13 \cdot 10mV} \qquad (7.4)$$

The temperature data obtained from the raw voltage results after the conversion are given in Figure 7.11.

Moreover, the Samples scale (Figure 7.10) was converted into the Time scale (Figure 7.11) by using the sampling frequency value of 15 Hz in the post-processing phase.
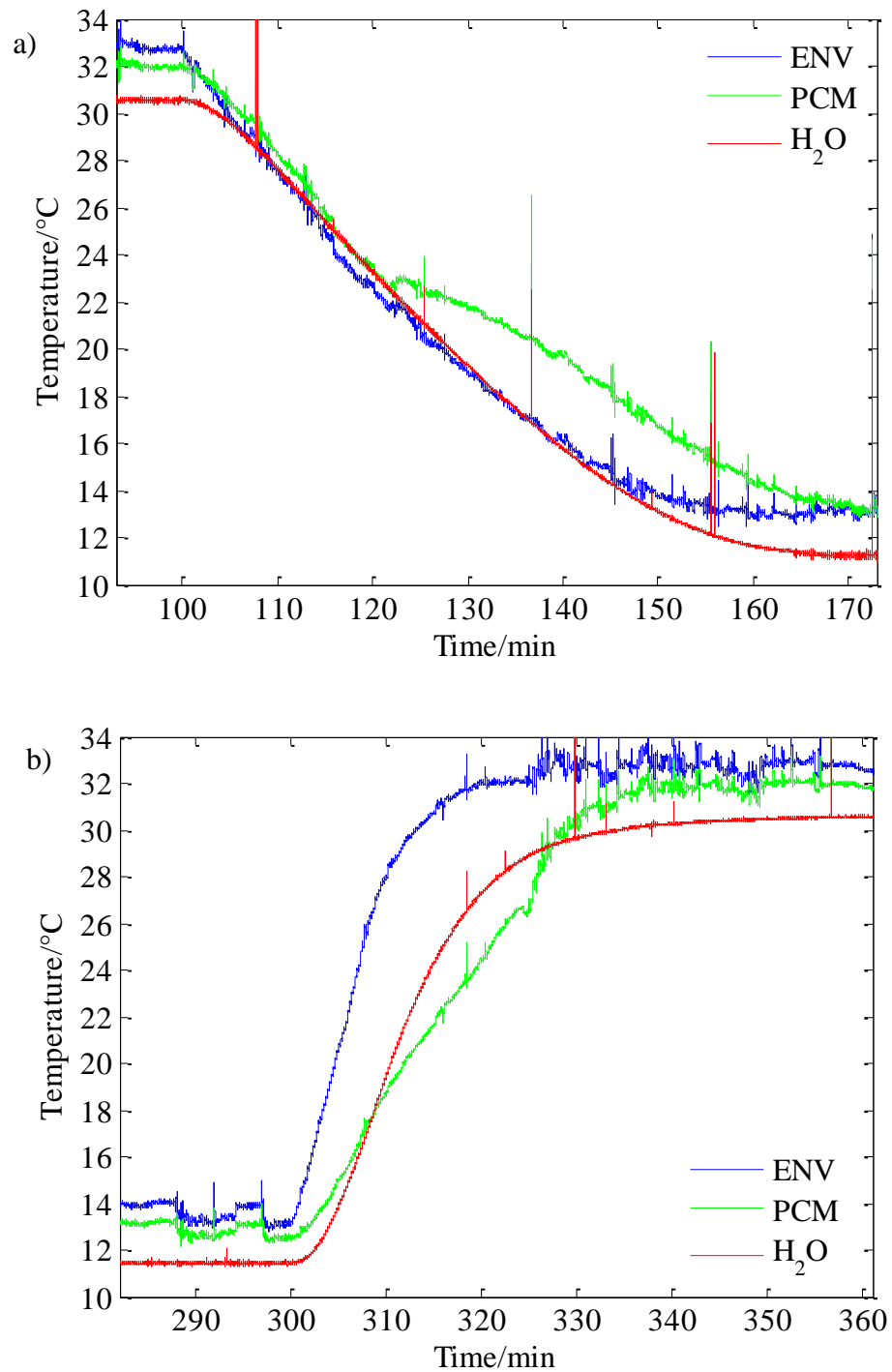
***Figure 7.11:*** *Cooling (a) and heating (b) cycle in RT21 T-history measurement using instrumentation system 1 – temperature results (ENV – environmental temperature, PCM – temperature of PCM sample, $H_2O$ – temperature of reference sample).*

The temperature data reflect a similar perspective as the voltage data. Apart from noise, it is clear that the signals don't reach the equilibrium state at the beginning and at the end of each cycle as expected at temperature levels of 30 °C and 11 °C. However, separately observed each signal shows a similar deviation at both temperature levels in both cooling and heating cycles (ENV – the smallest deviation, PCM – slightly greater deviation and $H_2O$ – the greatest deviation Figure 7.11). For this reason it was assumed that the observed deviations at in advance known temperatures of 30 °C and 11 °C could be used to calibrate the thermocouple signals. However, in order to achieve this additional post-processing had to be performed.

As mentioned in section 7.1.2 the reason a simple *RC* low pass filter was used in the filtering stage of the instrumentation system was the assumption that most of the signal filtering could be performed digitally. Hence, at this point a digital low pass filter with the cut-off frequency close to 0 Hz had to be designed and implemented to extract the explicit DC temperature signal originally captured by the thermocouples. The developed filter was a MATLAB's low pass generalised Butterworth filter based on the *maxflat* function. This filter type was selected due to its optimal maximally flat response. The cut-off frequency of the filter was 0.025 Hz. Its frequency response is given in Figure 7.12.
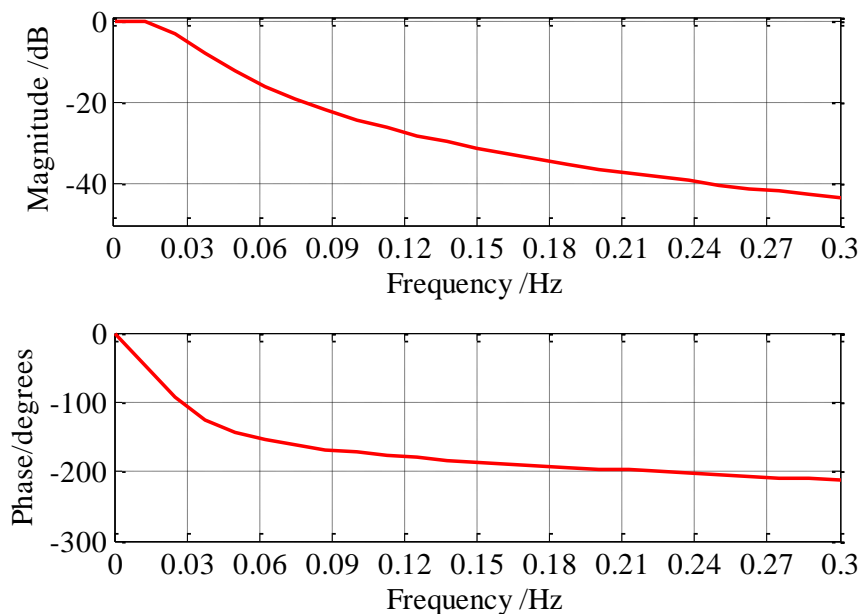


***Figure 7.12:*** *Frequency response of the digital low pass filter.*

The complete implementation details of the digital low pass filter in the form of the developed MATLAB's function are given in the APPENDIX A1.

Once the digital filtering was performed on the signals shown in Figure 7.11 the temperature calibration was enabled. Namely, a rather simplistic calibration protocol was developed. The mean value of the signal portion where the expected temperature value was supposed to be 30 °C was calculated. This was also performed for the signal portion with the intended value of 11 °C. Once these means were calculated their deviations from 30 °C and 11 °C were calculated (signal_dev_30 and signal_dev_11 values). These values were used to readjust the original signals by adding the value of the calibration parameter (*calibr_par*), calculated using Equation 7.5, to them.

$$calibr\_par = \pm \frac{signal\_dev\_30 + signal\_dev\_11}{2} \quad (7.5)$$

The calibration parameter was used with the sign "+" or "-" depending on the original direction of the signal's deviation (e.g. if the signal value at the expected 30 °C was higher than 30 °C the "-" sign was used in the calibration procedure, otherwise the "+" sign was used).

The temperature calibration protocol was implemented for all three signals (ENV, PCM, and $H_2O$) in both heating and cooling cycles. The obtained temperature results after the digital filtering and calibration are presented in Figure 7.13.

The signals in Figure 7.13 are of much better quality than those shown in Figure 7.11 especially the $H_2O$ signals which are nicely smoothed after the filtering. The filtering of initially much noisier ENV and PCM signals resulted in relatively non smooth data (Figure 7.13). The non-smoothness of these signals also affected the calibration procedure since the evaluation of the aforementioned mean values was affected by it as well as the corresponding *calibr_par* value. In summary, the estimated typical phase change temperature of RT21 in the case of cooling was 19.9 °C and in the case of heating 23.3 °C. This values deviate from 21 °C, the typical phase change temperature of RT21 as given by the manufacturer (Rubitherm GmbH, Berlin, Germany).
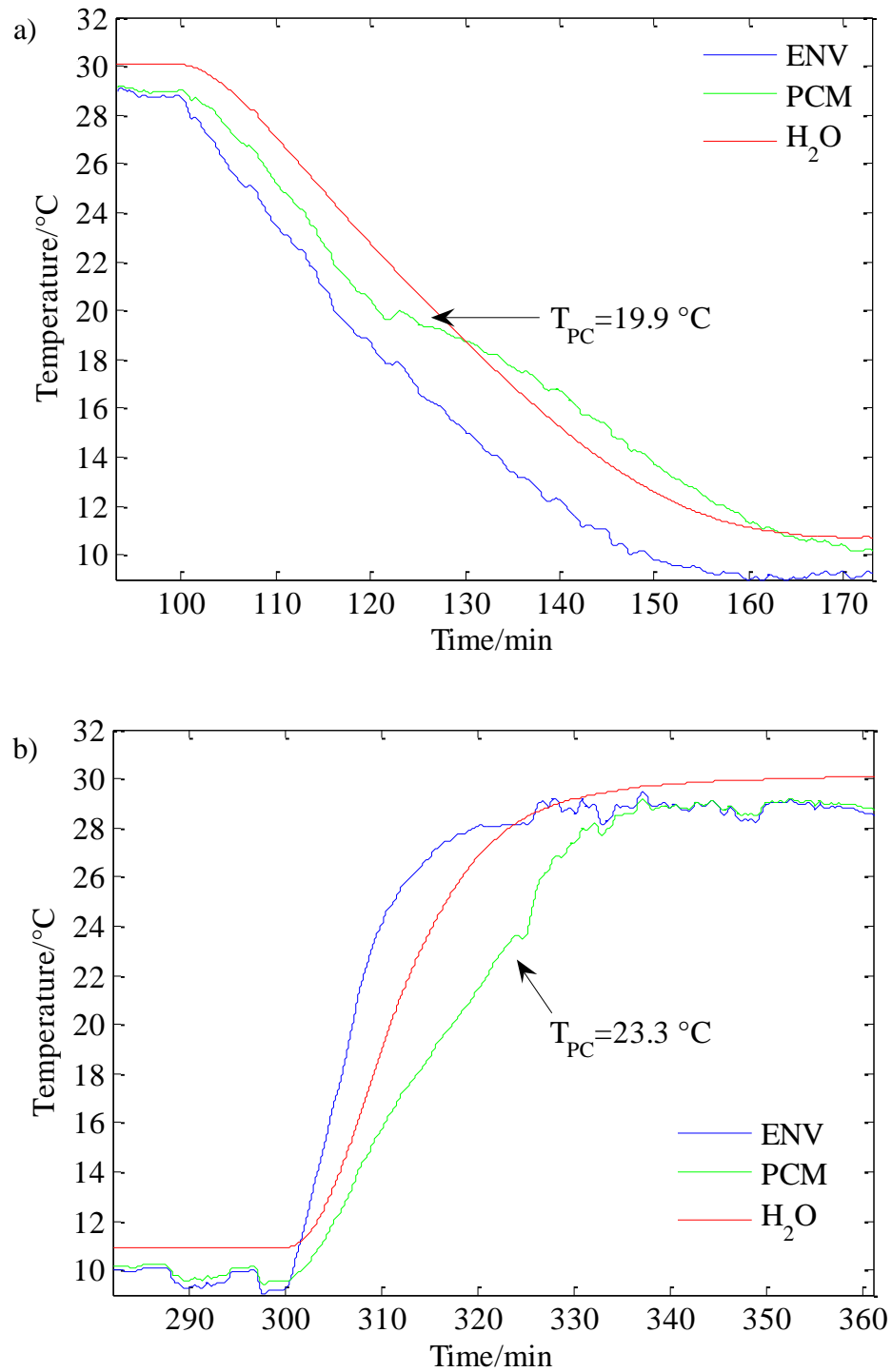
**Figure 7.13:** *Cooling (a) and heating (b) cycle in RT21 T-history measurement using instrumentation system 1 – filtered and calibrated temperature results (ENV – environmental temperature, PCM – temperature of PCM sample, H₂O – temperature of reference sample).*

The deviations in both cases with the deviations from the expected equilibrium temperatures (max ±1.9 °C) by far exceed the value of ±0.5 °C, previously adopted as the validation criterion of the instrumentation system. Hence, confirming the initial assumption that in terms of accuracy thermocouples were not suitable for the T-history temperature measurements. It was decided that the instrumentation system 1 is to be disregarded in any future PCM related measurement. The system was labeled as "*not accurate enough*" to be used in the advanced T-history method.

In addition, the thermocouples were also labeled as inappropriate sensing modalities to be used in the advanced T-history measurements, primarily due to their noise related issues. Consequently, no other thermocouple based instrumentation system was developed. Nonetheless, the proper instrumentation necessary for the implementation and successful application of the advanced T-history method had to be found. Accordingly, a different type of temperature sensors i.e. thermistors were considered. Hence, the development of the thermistor based instrumentation systems is thoroughly explained in the following sections.

## 7.2 Instrumentation system 2

One of the principal reasons for the development of the advanced T-history method was to enable more accurate characterisation of PCMs principally in terms of temperature and consequently in terms of heat release/storage capacity. As explained in Chapter 6, thermistors have great advantages over other common temperature sensing modalities due to their accuracy and high sensitivity making them particularly responsive to changes in temperature as required in T-history measurements. Another important advantage is the accessibility of small probes since small sensor size is also one of the provisional requirements in PCM related measurements. Given this thermistors were selected as the principal sensing modalities in the implementation of the advanced T-history method.

The main disadvantage of thermistors is their high nonlinearity. Consequently, a proper instrumentation system had to be developed to enable the temperature measurements. This instrumentation system was named instrumentation system 2. The

development process of the instrumentation system 2 was split into the same sub-processes as the development of the previously described instrumentation system 1: the sensor selection, linearisation and signal conditioning, and data acquisition (Figure 7.2). The details of these sub-processes as well as of the validation process will be explained in the following subsections.

## 7.2.1 Sensor selection

Once thermistors have been selected as the principal sensing modality in the development of the advanced T-history method a specific thermistor had to be chosen to perform the temperature measurements. As noted earlier, T-history requires the utilisation of narrow cylindrical test containers and small temperature probes. Moreover, the sensors need to be small to avoid the interference with the phase change process. Hence, at this point the sensor size was the main selection criterion. An NTC MA100BF103A thermistor model with a sensitivity of $5\,\%\,^\circ\text{C}^{-1}$ and a 0.762 mm diameter probe was selected (Newark Corporation, Newark, New Jersey). The technical specifications of the sensor are given in Table 7.7.

| Parameter | Value |
|---|---|
| Resistance at 25 °C | 10 kΩ |
| Sensitivity | $5\,\%\,^\circ\text{C}^{-1}$ |
| Minimum temperature sensed | 0 °C |
| Maximum temperature sensed | 50 °C |
| Accuracy class | ±0.1 °C |
| Probe diameter | 0.762 mm |
| Probe length | 609.6 mm |
| Package |  |

***Table 7.7:*** *Specifications of the NTC MA100BF103A thermistor.*

Given the nonlinearity of thermistors, a proper linearisation and signal conditioning circuit had to be designed and developed once the particular sensor was selected. The details of the linearisation and conditioning procedures are discussed in the following subsection.

## 7.2.2 Linearisation and signal conditioning

As explained in the previous chapter, thermistors are essentially resistive elements whose resistance changes with temperature. The resistance-temperature relation of thermistors can be expressed in various forms. For the selected MA100BF103A sensor, the temperature dependence of the thermistor resistance $R_t$ is given by the table of resistances. Its nominal resistance at 25 °C is 10 kΩ. Given that the MA100BF103A is an NTC thermistor, its $R_t(T)$ relation is negative and highly nonlinear preventing straightforward temperature measurements. Hereof, a linearisation circuit as the main part of the instrumentation system 2 had to be developed.

The principle function of the linearisation circuit was to transform the nonlinear thermistor's resistance-temperature change into a linear voltage-temperature dependency. The accuracy of such transformation depended on various factors including, the circuit itself, the circuit component values, and the linearising temperature range. In this study the linearising range was fixed between 10 °C and 39 °C to match the application requirements i.e. the temperature range between 9 °C and 37 °C as discussed in section 6.2.1. The linearising temperature range was marginally shifted in comparison to the application temperature range because the majority of the measured temperatures were expected to fall in the upper portion of the application range. Considering that the linearising range was fixed, accurate temperature measurements had to be made through the development of proper circuits with optimal component values.

Various hardware linearisation techniques have been developed over the years based on voltage divider or bridge circuits as reported by Tsai et al. (2009) or 555 timers as reported by Nenova and Nenov (2009) as well as different software solutions as indicated by Khan et al. (2002). However, at the time the instrumentation system 2 was being developed there was no reported documentation on the utilisation and

evaluation of these linearisation techniques in the T-history related PCM measurements. Therefore, a certain linearisation technique had to be implemented.

One of the commonly used thermistor linearisation techniques is the circuit based on the Wheatstone Bridge (WB) configuration. Therefore this circuit was selected to implement the linearisation part of the instrumentation system 2.

The details of the WB based thermistor temperature processing circuit are shown in Figure 7.14. In the linearisation stage of the circuit the thermistor (NTC_Thermistor) was placed in a simple WB configuration with the resistors $R_1$, $R_2$, and $R_3$ (Figure 7.14). Prior to the development of the linearisation circuit the optimal values of the $R_1$, $R_2$, and $R_3$ resistors had to be determined. Namely, the aim was to provide fine linearisation and accuracy through minimisation of the thermistor's self-heating and nonlinearity errors. To achieve this few restrictions were adopted on top of the design rules and the restrictions imposed by the experimental setup, as explained in Chapter 6. The first and much stronger new restriction was to keep the thermistor's self-heating error $\Delta T$ below 0.05 °C in order to keep the sensor from permanent damage. This error defines the value of the thermistor's maximum permissible current $I_{max}$ as indicated by Equation 7.6:

$$I_{max} = \sqrt{\frac{\Delta T C}{R_{t,min}}}, \qquad (7.6)$$

where $C$ denotes the thermistor's dissipation constant. Critical value (in air) of this constant for the selected thermistor is 2.5 $x$ $10^{-3}$ W°C$^{-1}$ (Newark Corporation, Newark, New Jersey). $R_{t,min}$ denotes the thermistor's minimal resistance in the operating temperature range. The thermistor's maximum permissible current $I_{max}$ can be calculated using Equation 7.6, as was done here, or it can be given as part of the thermistor's specification. In any case, the adopted restriction can be expressed in the form of Equation 7.7:

$$I_t < I_{max}, \qquad (7.7)$$

where $I_t$ denotes the thermistor's operating current.
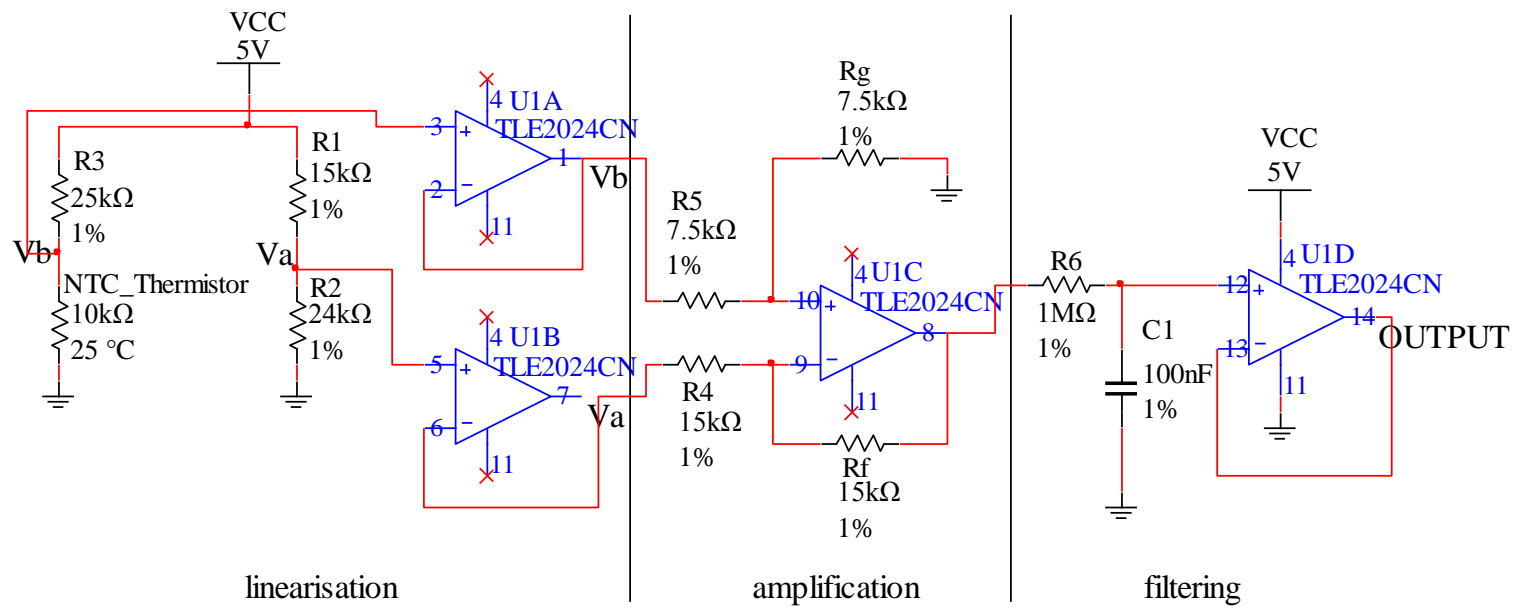
**Figure 7.14:** *The WB based thermistor temperature processing circuit.*

The second newly adopted restriction was to minimise the non-linearity errors. This implied the linearisation of the *OUTPUT* voltage-temperature characteristic (see Figure 7.14) or otherwise known as the transfer function *f(T)*. The *f(T)* function is linear in a particular region if its second derivative with respect to temperature equals zero in that same region as shown in Equation 7.8:

$$\frac{\partial^2 f(T)}{\partial T^2} = 0. \tag{7.8}$$

Due to the rather complicated form of *f(T)* which includes three unknowns and one variable parameter $R_t$ in the case of WB linearisation circuit the determination of the second derivative analytically was identified as non-feasible; therefore a numerical approach was used to determine the optimal values of the resistors $R_1$, $R_2$, and $R_3$.

Prior to the explanation of the concrete steps undertaken to evaluate the optimal values of $R_1$, $R_2$, and $R_3$ it is essential to mention that the additional restriction to keep the supply voltage $V_{CC}$ equal to the standard value of 5 V was adopted. This was done in order to be able to use a simple mobile charger to power the instrumentation system 2 and consequently minimise the system's power dissipation. The mobile charger powering solution was adopted as more convenient than the laboratory power supply used for the instrumentation system 1.

The selection of the fixed supply level of 5 V is important since it affected the calculation of the optimal values for $R_1$, $R_2$, and $R_3$. However, prior to these calculations the development of the auxiliary power circuit (Figure 7.15) which enabled the utilisation of the mobile charger as the sole power supply needs to be explained.

Namely, mobile chargers usually output a single supply voltage floating around the level of 5 V. The auxiliary power circuit (Figure 7.15) was developed to stabilise the output of the mobile charger at a sharp 5 V±10 % level. To achieve this MC7805CT voltage regulator chip (RS Components, Corby, UK) was used with the selected values of specific input and output capacitors (Figure 7.15). The technical specifications of the chip are given in Table 7.8. The configuration similar to the one in Figure 7.15 was seen in few Power Supply Units (PSUs) of old disassembled computers. It was presumed that such configuration will be suitable to provide the

necessary power to the instrumentation system 2 given the inherently low thermistor currents.
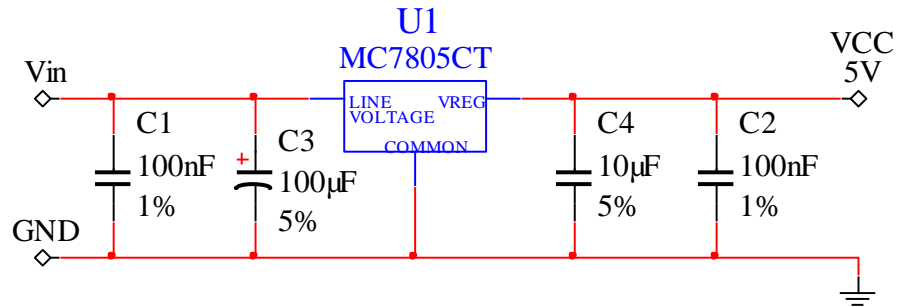


**Figure 7.15:** *Auxiliary power supply circuit.*

| Parameter | Value |
|---|---|
| Input voltage | 35 V (max) |
| Output voltage | 5 V |
| Output voltage tolerance | ±4 % |
| Output current | 1 A (max) |
| Operating temperature range | 0 °C to 125 °C |
| Package details |  |
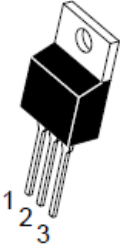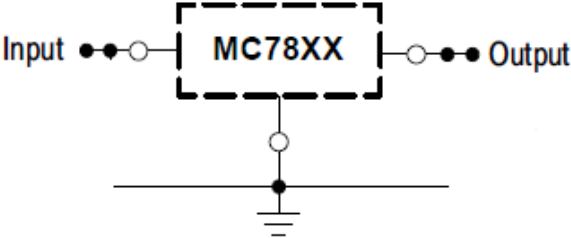
**Table 7.8:** *Specifications of the MC7805CT IC.*

Once its design was completed the auxiliary power supply circuit was implemented on the breadboard and kept ready for any thermistor based PCM measurement.

Given the explanation of the power circuit the estimation of the optimal values for the $R_1$, $R_2$, and $R_3$ resistors in the WB based thermistor temperature circuit can now be explained in detail.

Since a WB is essentially a form of voltage divider the adopted limitation of the thermistor's self-heating error and consequently the maximum permissible current $I_{max}$ automatically imposed the restriction on the value of $R_3$. This restriction is expressed by Equation 7.9:

$$R_3 > \frac{V_{cc}}{I_{max}} - R_{t,min},$$ (7.9)

where $R_{t,min}$ represents the minimum value of the thermistor's resistance which in the case of NTC thermistors occurs at the highest operating temperature. Once the calculations were made it was clear that $R_3$ needs to be higher than 24.78 k$\Omega$. This restriction did not allow any flexibility for the reduction of non-linearity errors of the *OUTPUT* voltage (see Figure 7.14). Namely, a WB based linearisation model was developed in MATLAB to determine the optimal values of the components $R_1$, $R_2$, and $R_3$ by taking into the account all the previously discussed restrictions. The implementation details of the model are given in the APPENDIX A2. The implementation of all the restrictions apart from the one expressed by Equation 7.8 was rather straightforward. As for the implementation of the Equation 7.8 the determination of the second derivative analytically was identified as non-feasible as previously discussed in this section. Therefore a numerical approach was used. Namely, the restriction regarding the nonlinearity error minimisation was implemented through the determination of the *f(T)* dependency for different combinations of circuit component values. Then the transfer function was fitted using the least square method and the optimal component values were determined based on the best linear fitting, i.e. the one that produced the minimal norm of the residuals.

The MATLAB model showed that any higher resistance of $R_3$ than the minimal value prescribed by Equation 7.9 increases the non-linearity error i.e. the norm of residuals. The model showed that the circuit configuration is such that the minimisation of the self-heating error highly restricts the minimisation of the nonlinearity errors.

Following the model results, the value of 25 k$\Omega$ was selected for the resistance $R_3$. This gave the fixed value for the voltage $V_b$ (see Figure 7.14) and completely determined the shape of the transfer function *f(T)*. Further on, the only possible manipulation, modification of the voltage $V_a$, was done in order to shift the *OUTPUT*

voltage (see Figure 7.14) to a range more suitable for measurements from 0.8 V to 2.2 V. This was done by using the values of 15 kΩ and 24 kΩ for $R_1$ and $R_2$.

Once the optimal values for the WB resistors were determined additional signal conditioning was performed. The output of the WB is a differential signal. Hence, in the amplification stage a differential amplifier had to be designed. This was achieved through the utilisation of the TLE2024CN operational amplifier chip in a differential amplifier configuration (Figure 7.14). The technical specifications of this chip are given in Table 7.9.

| Parameter | Value |
|---|---|
| Supply voltage maximum rating | ±18 V (dual), 5 V(single) |
| Input voltage maximum rating | ±15 V |
| Input offset voltage at 25 °C ($V_{cc}$=5 V) | 1.1 mV (max) |
| Input offset current at 25 °C ($V_{cc}$=5 V) | 0.6 nA(typ), 6 nA (max) |
| Input bias current at 25 °C ($V_{cc}$=5 V) | 45 nA(typ), 70 nA (max) |
| Common mode rejection ratio ($V_{cc}$=5 V) | 80 dB (min), 90 dB (typ) |
| Operating temperature range | 0 °C to 70 °C |
| Package details |  |
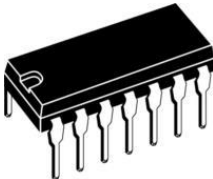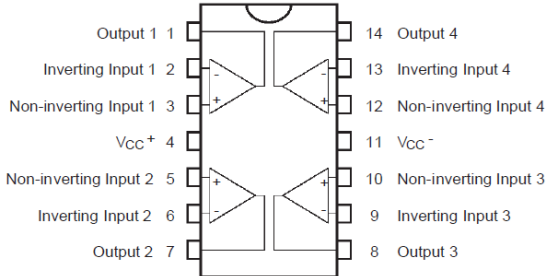
*Table 7.9: Specifications of the TLE20244CN IC.*

The principal reason this chip was selected was its relatively good performance with the single 5 V supply provided by the mobile charger as discussed before. The values for the resistor elements $R_4$, $R_f$, $R_5$, and $R_g$ were selected in such way that the gain of the differential amplifier (Equation 7.10) equalled one and therefore the *OUTPUT* of the entire circuit equalled the output voltage of the WB bridge (Figure 7.14).

$$G = \frac{R_f}{R_4} \qquad (7.8)$$

After the amplification stage the filtering stage was designed. The used low pass *RC* filter had the same features as the one in the filtering stage of the instrumentation system 1 and therefore its details are not discussed here to avoid repetition. Also, as in the instrumentation system 1, the voltage followers were used to prevent the loading between different stages of the WB based thermistor temperature processing circuit (Figure 7.14). The final *OUTPUT* of the circuit was a single-ended voltage.

## 7.2.3 Data acquisition

The same elements including the NI USB 6212 DAQ card and the developed PCM_DAQ.vi were used for the data acquisition in all measurements utilising the instrumentation system 2. Consequently, the details of the data acquisition are not discussed again. However, the variable parameters of the data acquisition discussed in section 7.1.3 will be mentioned prior to each measurement.

## 7.2.4 Validation

As in the case of the instrumentation system 1, the instrumentation system 2 had to be validated against the ±0.5 °C validation criterion. To perform the validation the T-history measurement of the RT21 PCM was conducted. The material properties of RT21 were previously given in Table 7.6. The T-history setup in this measurement was very similar to the one explained in section 7.1.4 with the exception of few minor changes. Instead of using the laboratory power supply (see Table 7.4), the instrumentation system 2 was powered by the mobile charger using the auxiliary power supply circuit (see Figure 7.15). The reasons behind such arrangement were discussed in the linearisation and signal conditioning section 7.2.2.

Furthermore, the RT21 and the reference material (distilled water) were put in the same test tubes as explained in section 7.1.4 and again subjected to a temperature program with alternating 2 h long heating and cooling cycles between 11 °C and 30 °C. Three channels (the samples' temperatures and the chamber's temperature) were again continuously recorded using the three-channel breadboard prototype developed

according to the schematic given in Figure 7.14. The signals from the prototype, again single-ended in nature, were connected to the differential inputs of the NI USB 6212 DAQ card and recorded using the developed PCM_DAQ.vi. The sampling frequency was 10 Hz. The expected input range of the signals was set between 0 V and 5 V. Finally, the size of the DAQ card's buffer was set to 36 according to the formula given by Equation 7.3.

The results from the validation measurement are presented in the following subsection.

## 7.2.4.1 Results and discussion

The raw results from the RT21 (subjected to the alternating cooling and heating cycles between 11 and 30 °C) T-history measurement using instrumentation system 2 captured by the PCM_DAQ.vi are displayed in Figure 7.16. This figure shows only a portion of the measured cycles captured during the real-time data acquisition. In total, 10 cooling and 10 heating cycles were recorded.

As in the thermocouple measurements, the signals captured by PCM_DAQ.vi show the increase in voltage in the cooling cycles and decrease in the heating cycles (Figure 7.16). However, unlike in the instrumentation system 1 this happens due to the NTC nature of the used thermistors. Three standard T-history signals were recorded in all cycles: temperature of the chamber's environment (ENV in Figure 7.16), temperature of the PCM (PCM in Figure 7.16), and temperature of the reference material i.e. distilled water (H2O in Figure 7.16). The captured signals are evidently less noisy and of better quality than the best thermocouple signals were (Figure 7.10). Hence, it was presumed that the instrumentation system 2 could give satisfying T-history results in terms of temperature.
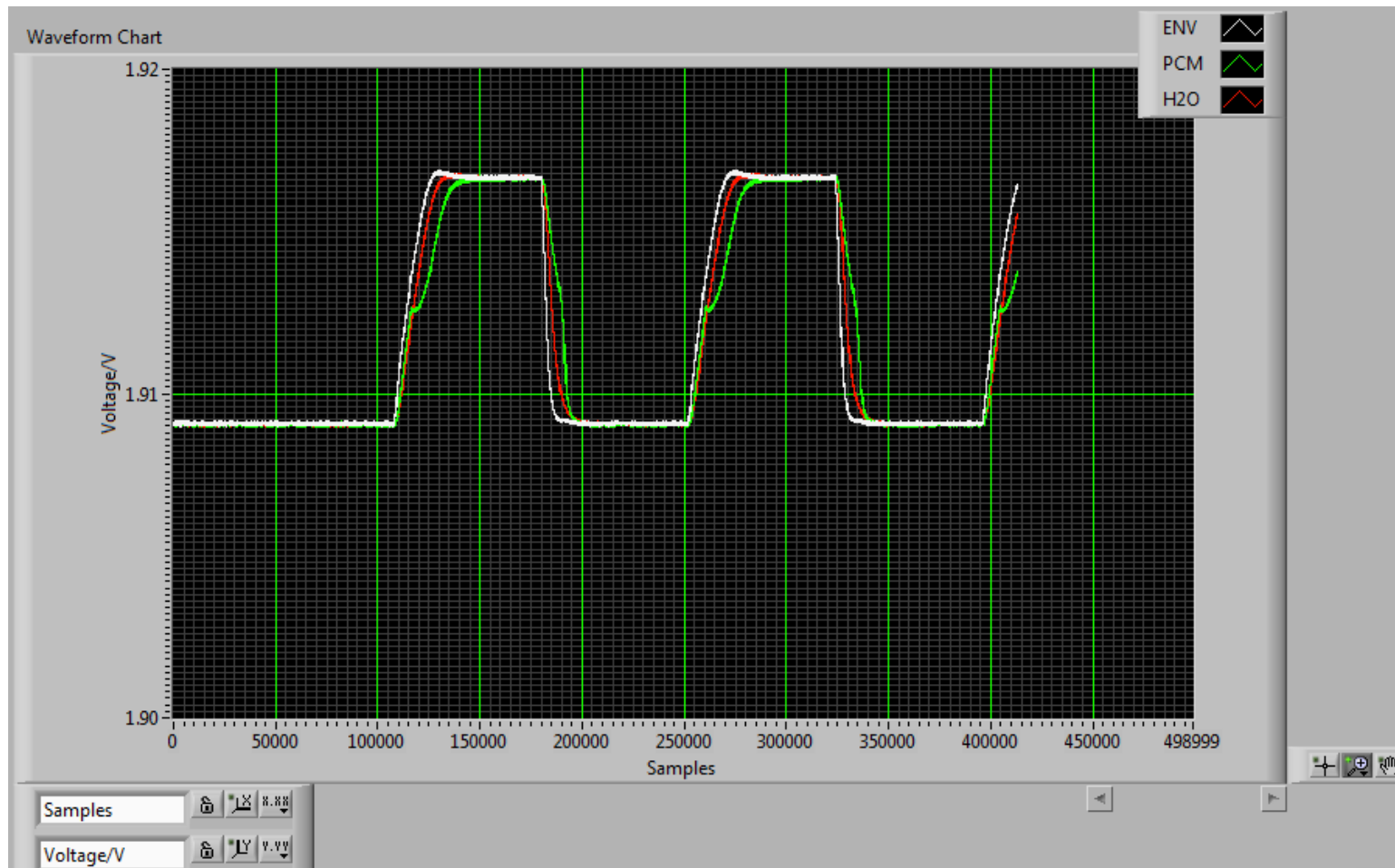
***Figure 7.16:*** *Alternating cooling and heating cycles in RT21 T-history measurement using instrumentation system 2 – raw results (ENV – environmental temperature, PCM – temperature of PCM sample, H2O – temperature of reference sample).*

Furthermore, the raw results were subjected to the post-processing in order to obtain the temperature data. The post-processing of the signals was done using MATLAB as in the case of the thermocouple measurements. However, unlike before the temperature conversion of the voltage data was not straightforward due to the thermistors' nonlinearity. To obtain the temperature data a proper calibration of each sensor had to be performed. Consequently, a certain calibration protocol had to be adopted.

It was decided that prior to or post any PCM T-history measurement each sensor should be subjected to 1 °C step temperature program from 10 °C to 39 °C (or above) inside the precisely controlled environment of the chamber. The length of each 1 °C temperature step was supposed to be 5 min which was enough to assure the temperature stability inside the chamber. The recorded *OUTPUT* voltage data were to be evaluated at known temperatures (10-39 °C in 1 °C step) and the calibration curves and equations were to be determined using the least squares method for data fitting. The calculation of absolute errors between expected and fitted measured temperature data was also to be performed. A special MATLAB script had to be developed to implement the voltage-temperature conversion based on the calibration data. The details of this script are given in the APPENDIX A3.

Accordingly, the calibration measurement was performed post the T-history measurement of the RT21. The raw results are shown in Figure 7.17. These represent the signals from three sensors (ENV, PCM, and H2O) as the sensors were subjected to the previously described step temperature program. Given that the temperature of each step in this measurement was known in advance, the measured data were used to determine the calibration curves and equations necessary for the voltage-temperature conversion.

Firstly, the data were filtered using the previously developed digital low pass filter described in section 7.1.4.1. The filtered data are shown in Figure 7.18. The digital filter proved to be of good efficiency to clean the originally measured data.
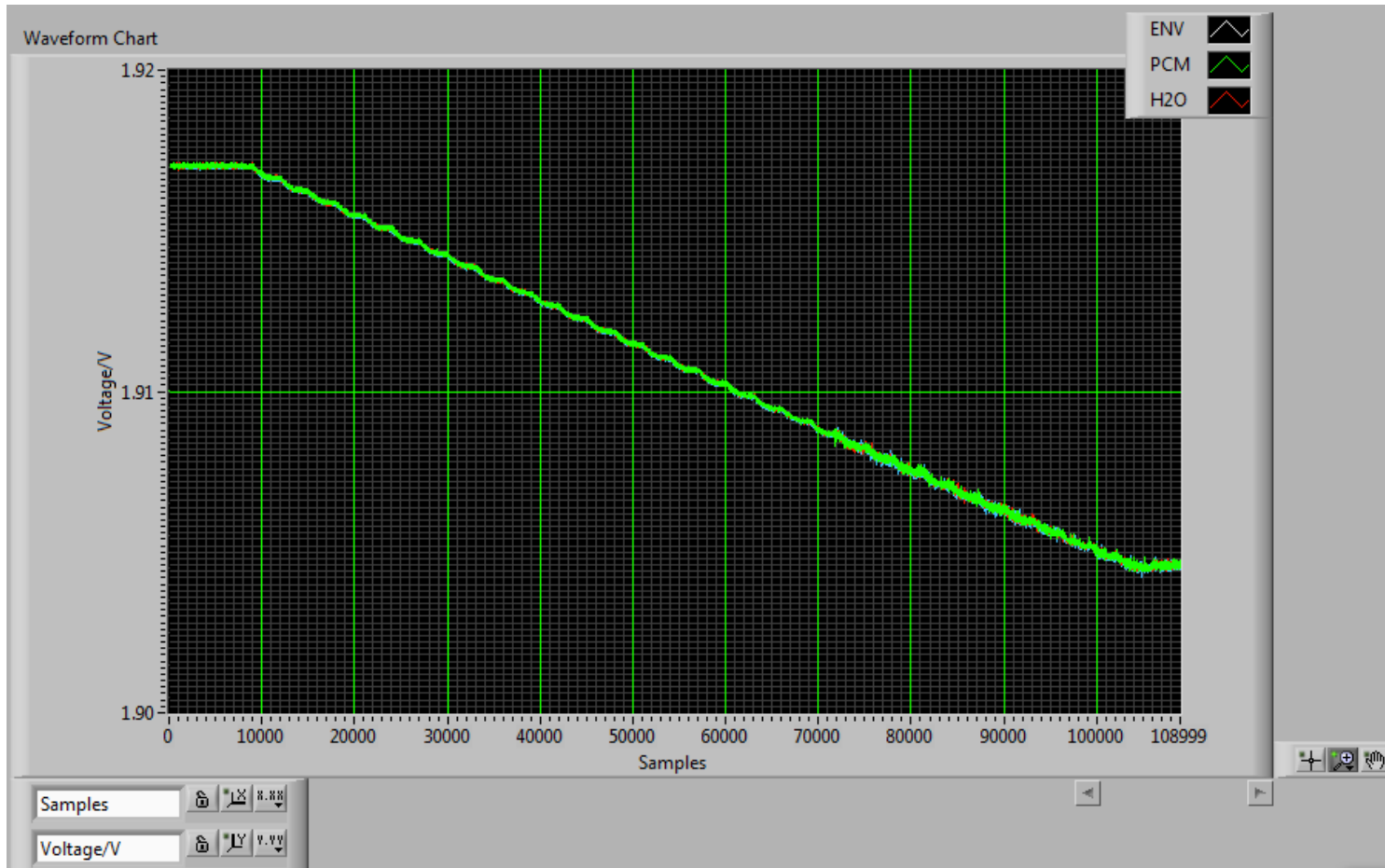
*Figure 7.17:* *The calibration temperature measurement using instrumentation system 2 – raw results (ENV – signal from the sensor later used for environmental temperature measurement, PCM – signal from the sensor later used for the temperature measurement of PCM sample, H2O – signal from the sensor later used for the temperature measurement of reference sample).*
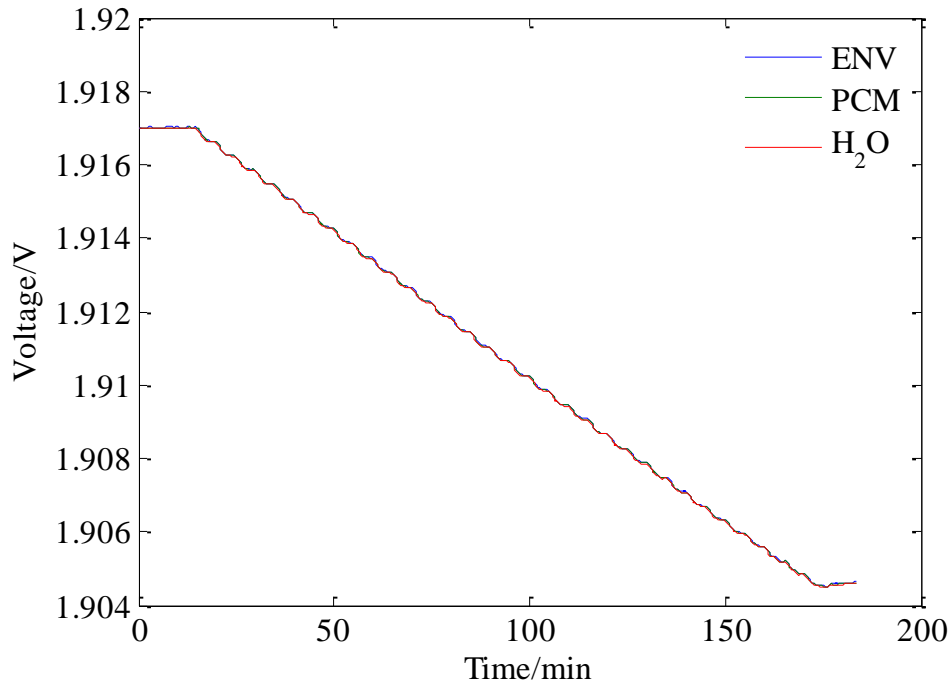
***Figure 7.18:*** *The calibration temperature measurement using instrumentation system 2 – filtered results (ENV – signal from the sensor used for environmental temperature measurement, PCM – signal from the sensor used for the temperature measurement of PCM sample, $H_2O$ – signal from the sensor used for the temperature measurement of reference sample).*

Furthermore, the filtered data of each signal were used to extract the voltage data at each specified temperature level of the consecutive steps. The extracted voltage data at specified temperatures were then fitted using the least square method to obtain the voltage-temperature conversion equations for each signal. These operations were implemented in the aforementioned thermistor calibration script written in MATLAB (see APPENDIX A3 for the code listing of the implemented script). Additionally, the absolute errors between the expected and fitted measured temperature data were also calculated. The calculated errors for each signal i.e. measurement channel (ENV, PCM, and $H_2O$) are shown in Figure 7.19.
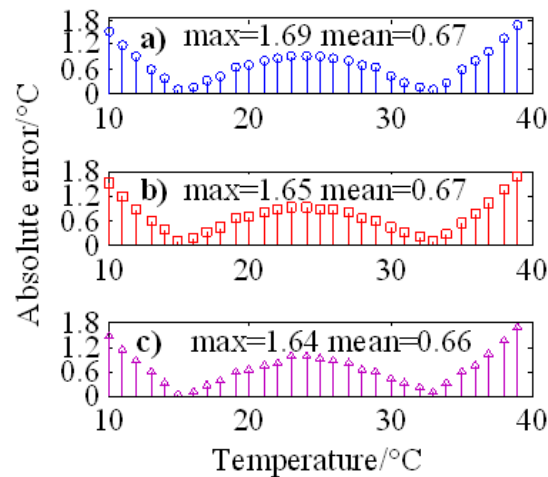
***Figure 7.19:*** *Calibration measurement based absolute error values for the temperature channels based on the instrumentation system 2. a) Channel used for environment temperature measurement. b) Channel used for the temperature measurement of PCM sample. c) Channel used for the temperature measurement of reference sample (amended from Stankovic and Kyriacou, 2012, p. 5).*

As shown in Figure 7.19 the worst-case scenario results (Figure 7.19a) indicated the mean and maximum error of 0.67 °C and 1.69 °C respectively. This was regarded unacceptable due to the error magnitude exceeding the originally established ±0.5 °C margin of success i.e. the validation criterion. Nevertheless, it was decided that the already measured T-history data (see Figure 7.16) should be converted to temperature values using the voltage-temperature conversion equations obtained from the calibration measurement.

The raw data (see Figure 7.16) were firstly filtered using the digital filter described in section 7.1.4.1. Following this, the results were averaged to obtain the 1 s data samples from the initially 0.1 s samples imposed by the 10 Hz sampling frequency. Finally, the results from 10 recorded cooling cycles were also averaged to minimise random errors and improve measurement precision. The mean data obtained by the 10-cycle averaging were converted to temperature. The final results are shown in Figure 7.20. It was presumed that given the error results in Figure 7.19 the T-history data from the cooling cycles alone should be enough for the final validation of the instrumentation system 2.
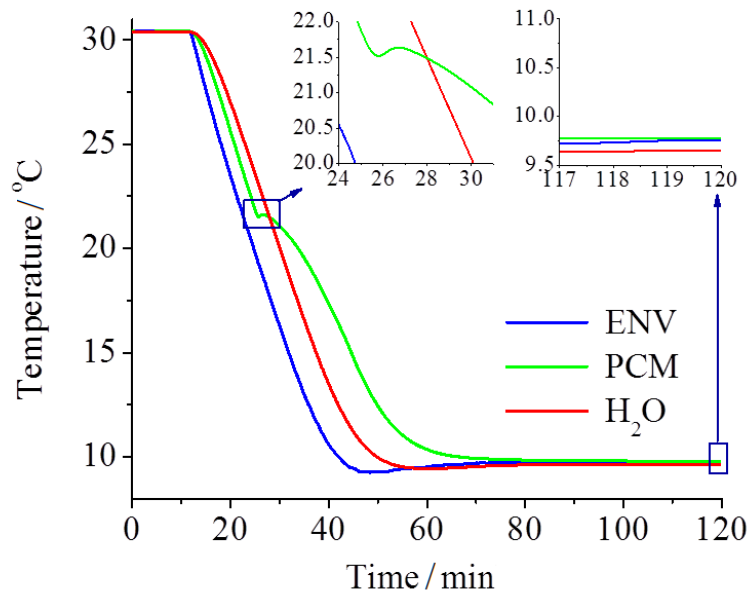
***Figure 7.20:*** *The cooling cycle in RT21 T-history measurement using instrumentation system 2 – post-processed results (ENV – environmental temperature, PCM – temperature of PCM sample, $H_2O$ – temperature of reference sample).*

It is clear that all T-history curves during the first 10 min showed temperature higher than 30 °C which was the expected first equilibrium temperature in the cooling cycle of the T-history measurement (see Figure 7.20). The section around the phase change was zoomed-in for better visibility. At the temperature of 21 °C (the typical phase change temperature of RT21) the PCM curve showed the temperature value of 21.65 °C. The recorder nucleation temperature of the PCM curve was 21.55 °C indicating a very small degree of subcooling. The section around the second equilibrium temperature of 11 °C was also zoomed-in. At the expected 11 °C all three curves showed a deviation greater than ±1.3 °C (see Figure 7.20).

Given the presented results, it was evident that the instrumentation system 2 did not meet the ±0.5 °C accuracy validation criterion and therefore was labeled as non-suitable for future PCM related measurements. However, the general quality of the signals obtained in the measurements described in this section suggested that thermistors are suitable to be used as sensing modalities in the advanced T-history method. Consequently, another instrumentation system for thermistor linearisation and conditioning had to be developed.

# 7.3 Instrumentation system 3

Given the unsuccessful validation of the instrumentation system 2, another system for the conditioning of the inherently nonlinear thermistor signals was developed. This system was named instrumentation system 3. The development process of the instrumentation system 3 could be split into the same sub-processes as the development of the previously described instrumentation system 1 and 2 (see Figure 7.2). However, some of this sub-processes are identical to the ones described in sections 7.1 and 7.2, and although mentioned, will not be discussed in detail here.

## 7.3.1 Sensor selection

As previously explained, the quality of the signals obtained in the measurements described in the section 7.2.4.1 identified thermistors as the suitable sensing modalities in the measurement based on the advanced T-history method. The technical specifications of the selected NTC MA100BF103A thermistor were previously given in Table 7.7.

## 7.3.2 Linearisation and signal conditioning

As explained in the previous chapter, given the thermistors' high nonlinearity an essential part of any temperature measurement system based on these sensors is the linearisation circuit. As shown in section 7.2 the linearisation based on the Wheatstone bridge configuration proved to be unreliable for the advanced T-history measurements. Hence, a different approach had to be adopted.

Namely, following the design rules described in Chapter 6 and the same set of restrictions given in section 7.2.2, a new linearisation circuit had to be designed. Given the condition in the instrumentation system 2 where the minimisation of self-heating error highly restricted the minimisation of the nonlinearity errors a more flexible linearising configuration than the WB was desirable. In such configuration the self-heating and the non-linearity errors could be considered simultaneously due to the existence of a minimum of two resistors which would influence both the maximum

permissible thermistor current $I_{max}$ and the shape of the transfer function $f(T)$. The necessary linearising configuration was found in the form of the Serial Parallel Resistor (SPR) connection circuit. This circuit was selected to implement the linearisation part of the instrumentation system 3.

The details of the SPR based thermistor temperature processing circuit are shown in Figure 7.21. The linearisation stage of the instrumentation system 3 (Figure 7.21) was simpler than the WB configuration (Figure 7.14) with the resistors $R_1$, $R_2$, and $R_3$ (Figure 7.21). In the SPR configuration the input voltage $V_{CC}$ is divided between the resistor $R_1$ and the parallel connection of the resistor $R_2$ and the NTC thermistor. The output of the SPR connection is the voltage across the parallel resistor connection. Prior to the development of the linearisation circuit the optimal values of the $R_1$ and $R_2$ had to be determined. As in the case of the WB based circuit, an SPR linearisation model was developed in MATLAB to determine the optimal values of the components $R_1$ and $R_2$, taking into account the restrictions regarding the self-heating, nonlinearity errors, and the power supply as described in section 7.2.2. The implementation details of the model are given in the APPENDIX A4.

The model was based on the calculation of the $f(T)$ functions for different combination of resistor values $R_1$ and $R_2$. The resistor values were changed in small steps of 20 $\Omega$ and then the calculated $f(T)$ functions were fitted with linear polynomial functions using the least squares method. The best fitting function i.e. the one that gave the minimum norm of residuals was used to retrieve the optimal $R_1$ and $R_2$ values. The model gave the values of 53 k$\Omega$ and 8.88 k$\Omega$ for $R_1$ and $R_2$. For the fixed value of resistance $R_1$ the transfer function showed both linear and exponential behaviour in the same temperature range depending on the values of $R_2$. Figure 7.22 shows that for an optimal value of $R_1$ the output voltage-temperature dependency i.e. the transfer function shows relatively linear behaviour for the values of $R_2$ below 20 k$\Omega$ (Figure 7.22a). The best linearity is achieved for the optimal value of $R_2$ as seen in Figure 7.22b.
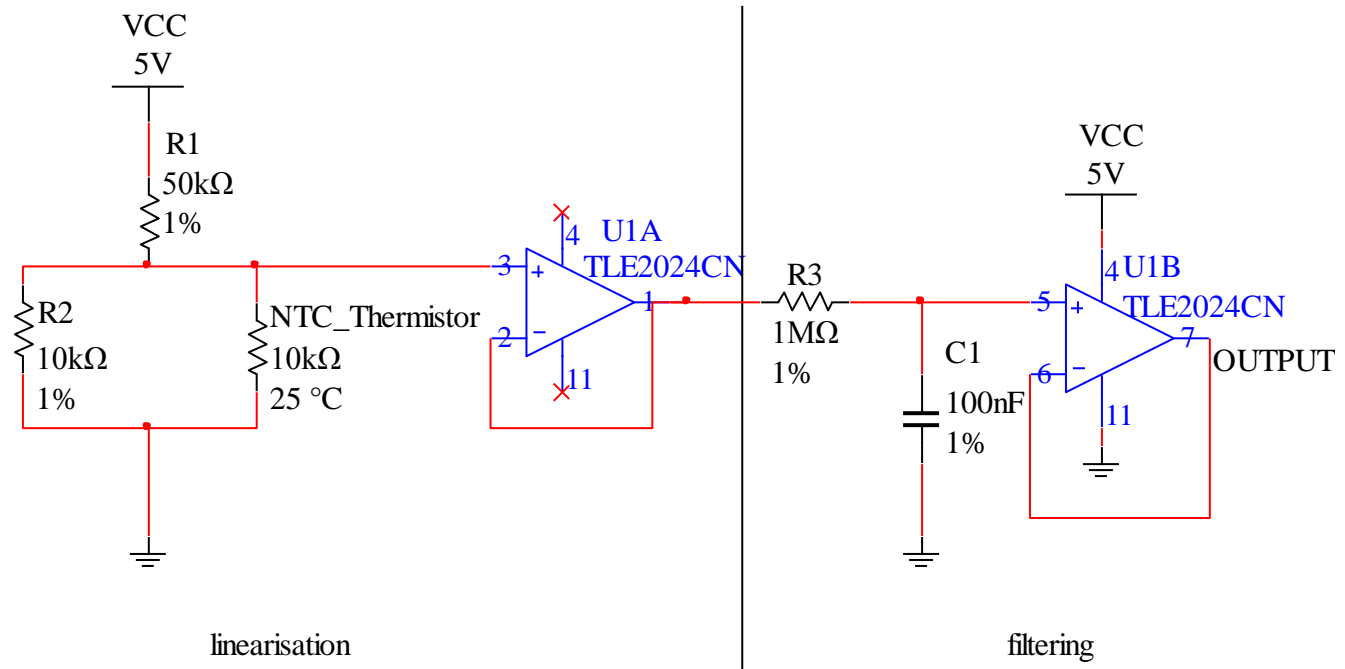
*Figure 7.21*: *The SPR based thermistor temperature processing circuit.*
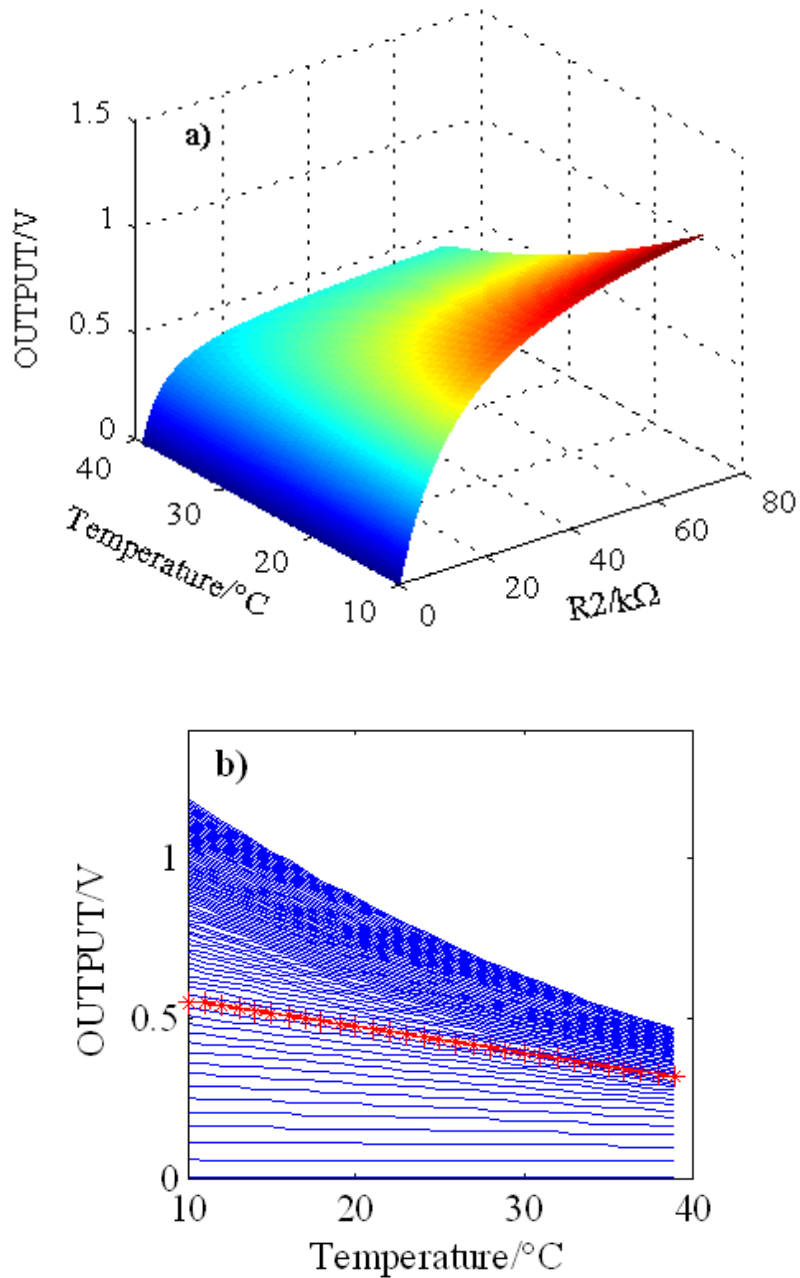
**Figure 7.22:** *The voltage-temperature dependencies i.e. the transform functions f(T) for optimal serial parallel resistor circuit component value $R_1=53\,k\Omega$ and variable values of $R_2$. a) 3D view. b) 2D view with the optimal transform function for $R_2=8.88\,k\Omega$ shown in asterisk marked line (amended from Stankovic and Kyriacou, 2012, p. 4).*

Given the optimal values from the model the resistance values of $50\,k\Omega$ and $10\,k\Omega$ for $R_1$ and $R_2$ were chosen for the SPR linearisation circuit. Given the expected voltage range of the output of the SPR connection (Figure 7.21) the amplification stage

was not necessary and therefore omitted in the development of the instrumentation system 3. In the filtering stage the used low pass *RC* filter had the same features as the one in the filtering stage of the instrumentation system 1 and 2. Also, as in the instrumentation system 1 and 2, the voltage followers were used to prevent the loading between different stages of the SPR based thermistor temperature processing circuit (Figure 7.21). The voltage followers were implemented using the TLE2024CN chips (see Table 7.9 for specification details). The final *OUTPUT* of the circuit in this case was also single-ended voltage.

## 7.3.3 Data acquisition

As in the case of instrumentation system 1 and 2 the same elements including the NI USB 6212 DAQ card and the developed PCM_DAQ.vi were planned to be used for the data acquisition in the measurements utilising the instrumentation system 3. Hence, the details of the data acquisition are not discussed. As before, the changeable parameters of the data acquisition system discussed in section 7.1.3 will be mentioned prior to each measurement.

## 7.3.4 Validation

As with the instrumentation system 1 and 2, the instrumentation system 3 had to be validated against the ±0.5 °C validation criterion. To perform the validation the T-history measurement of the RT21 PCM (see Table 7.6 for material data) was conducted. The T-history setup in this measurement was similar to the one explained in section 7.2.4. The only difference was that the SPR based instrumentation system 3 was used instead of the WB based instrumentation system 2. The RT21 and the reference material (distilled water) were again subjected to a temperature program with alternating 2 h long heating and cooling cycles between 11 °C and 30 °C. Three channels (the samples' temperatures and the chamber's temperature) were recorded continuously using the three-channel breadboard prototype developed according to the schematic given in Figure 7.21. The data acquisition parameters were exactly the same as in the measurements described in section 7.2.4.

The results from the validation measurement are presented in the following subsection.

## 7.3.4.1 Results and discussion

The raw results from the RT21 T-history measurement using instrumentation system 3 captured by the PCM_DAQ.vi are displayed in Figure 7.23. The figure shows only three measured cycles captured during the real-time data acquisition while 10 cooling and 10 heating cycles were recorded in total.

The voltage range of the recorded signals corresponding to the 11 to 30 °C was around 0.2 V. This was an order of magnitude larger than the matching range of the signals captured using the instrumentation system 2 (see Figure 7.16). Consequently, it was evident that the instrumentation system 3 was much more sensitive than the instrumentation system 2. Hence, it was presumed that additionally it will be more accurate as well. However, this assumption had to be proven.

Furthermore, the raw results were subjected to the post-processing in order to obtain the temperature data. The post-processing of the signals was once more done using MATLAB. The same calibration protocol as described in section 7.2.4.1 was implemented. Each sensor used in T-history was subjected to 1 °C step temperature program from 10 °C to 39 °C inside the chamber. The calibration measured data were used in the same manner as described in section 7.2.4.1 to determine the voltage-temperature conversion equations for each sensing channel. This was done as before by using the MATLAB calibration script (see APPENDIX A3). The absolute errors between the expected and fitted measured temperature data were also evaluated. The calculated errors for each signal i.e. measurement channel (ENV, PCM, and $H_2O$) are shown in Figure 7.24.

As shown in Figure 7.24 the worst-case scenario results (Figure 7.24b) indicated the mean and maximum error of 0.07 °C and 0.26 °C respectively. This was smaller than the originally established ±0.5 °C validation criterion.
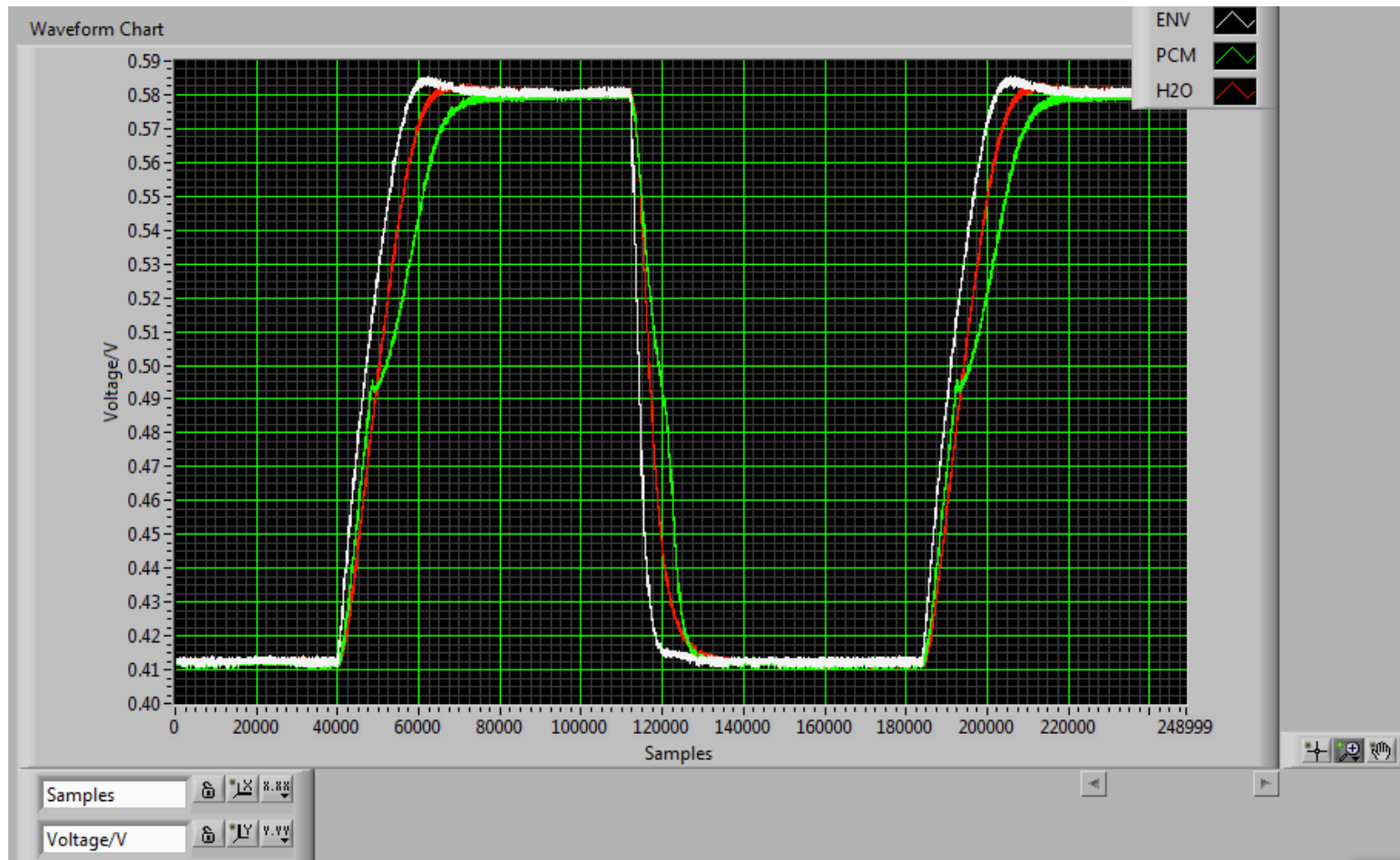
***Figure 7.23:*** *Alternating cooling and heating cycles in RT21 T-history measurement using instrumentation system 3 – raw results (ENV – environmental temperature, PCM – temperature of PCM sample, H2O – temperature of reference sample).*
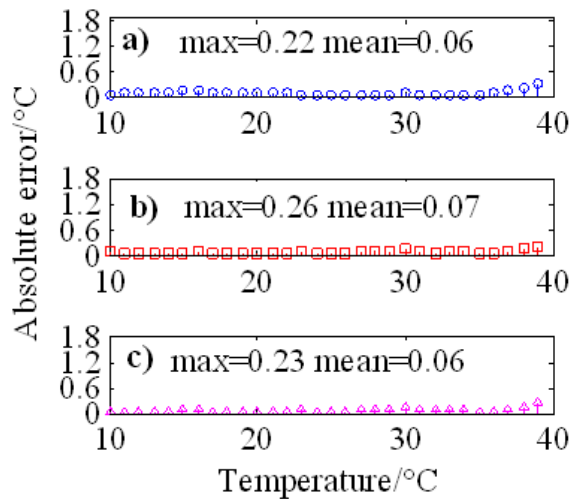
**Figure 7.24:** *Calibration measurement based absolute error values for the temperature channels based on the instrumentation system 3. a) Channel used for environment temperature measurement. b) Channel used for the temperature measurement of PCM sample. c) Channel used for the temperature measurement of reference sample (amended from Stankovic and Kyriacou, 2012, p. 5).*

Moreover, the measured T-history data (see Figure 7.23) were post-processed to determine their corresponding temperature values. The raw data (see Figure 7.23) were firstly filtered using the digital filter described in section 7.1.4.1. Then the results were averaged to obtain the 1 s data samples from the initially 0.1 s samples. Finally, the results from 10 recorded cooling cycles were averaged to obtain the mean cooling cycle data to be converted to temperature. The final results are shown in Figure 7.25. The T-history data from the cooling cycles alone are represented since the heating data showed the same trend in terms of temperature accuracy.

All T-history curves were aligned at the 30 °C as expected during the first 10 min of the equilibrium state (see Figure 7.25). At the expected temperature of 21 °C (the typical phase change temperature of RT21) the PCM curve showed the temperature value of 21.2 °C. The nucleation temperature was 21.1 °C. Hence, a small degree of subcooling was detected. At the expected 11 °C all three curves showed a deviation smaller than ±0.1 °C (see Figure 7.25).
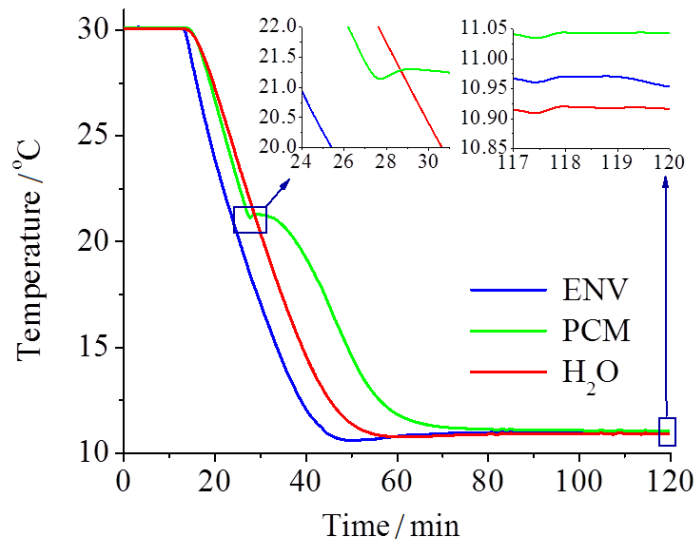
**Figure 7.25:** *The cooling cycle in RT21 T-history measurement using instrumentation system 3 – post-processed results (ENV – environmental temperature, PCM – temperature of PCM sample, $H_2O$ – temperature of reference sample).*

Given the presented results, it was concluded that the validation process was finally successful and the instrumentation system 3 was adopted as the integral part of the advanced T-history setup.

# 7.4 Summary

The development of the instrumentation system of the advanced T-history method was described in this chapter.

The instrumentation development was explained in terms of the necessary sub-processes that had to be performed to complete the instrumentation system. These included the selection of the specific sensors, the development of the necessary linearisation and conditioning circuits, the development of the data acquisition system and finally the validation of the instrumentation system. As indicated in the previous chapters, the value of ±0.5 °C was set as the desired technical goal for the temperature accuracy in the PCM related measurements (Mehling et al., 2006). This value was also selected as the validation criterion in the instrumentation development. Consequently, the development of the proper instrumentation system had to be performed in an

iterative procedure until the validation criterion was not met. This resulted in the development of three different instrumentation systems: one using thermocouples i.e. the instrumentation system 1 and two using thermistors, instrumentation system 2 and 3. The details of the development and validation procedures of each instrumentation system were presented. Given the temperature accuracy requirement ($\pm0.5$ °C) the only acceptable system was the instrumentation system 3 which was adopted as the definitive instrumentation system of the advanced T-history setup. Once the $\pm0.5$ °C temperature accuracy goal was achieved the advanced T-history method could be used for PCM characterisation. Hence, the testing of various organic PCMs using the advanced T-history method is discussed in detail in the following chapter.

# Chapter 8

# INVESTIGATION
# OF THERMO-PHYSICAL PROPERTIES
# OF ORGANIC PCMs

Once the validation process in the design strategy flowchart (see Figure 6.1) was identified as successful and the instrumentation system 3 adopted as an integral part of the advanced T-history setup two final processes in the development of the advanced T-history method could be implemented. Namely, the successful development of the advanced T-history setup and its validation in terms of temperature accuracy (±0.5 °C criterion) was not enough to designate the development of the advanced T-history method as completed. The new setup had to be tested to verify the main hypothesis underlying this project that a better planned experimental tests in terms of more accurate and precise sensing and control modalities will be able to provide more comprehensive and reliable results than those currently described in the literature. The tests were performed by following the basic measurement premises which were described in section 5.1 and summarised as the design rules in the design strategy flowchart (see Figure 6.1). As explained in section 6.1 the basic measurement premises given in section 5.1 were listed as the main part of the design rules (see Figure 6.1). In this way, each step in the development of the advanced T-history method was continuously bound by the main criteria that need to be satisfied in any PCM measurement. Several organic and inorganic PCMs were tested using the advanced setup. However, given the distinguishable properties of the organic and inorganic materials the testing of organic PCMs is described in this chapter and followed by the explanation of testing of inorganic PCMs in the next chapter.

At this point, the T-history setup was validated and was fully ready to perform measurements on PCMs. However, the measurements so far gave the temperature

history curves which only presented a part of the necessary PCM characterisation. The temperature data had to be properly evaluated to determine the basic thermo-physical properties of investigated materials predominantly the phase change temperature (range) and the energy stored/released. Hence, a proper data evaluation technique had to be implemented. Given its relevance, the implementation of the computational data evaluation technique is explained prior to any measurements. Additionally, considering the need to balance between the various measurements' parameters as explained in section 5.1 thorough parametric studies were performed on the well-known organic PCM RT21, introduced in the previous chapter. The details of the parametric studies are also explained in this chapter as well as the in-depth characterisation of few organic PCMs from Rubitherm's RT series (Rubitherm GmbH, Berlin, Germany) and Entropy Solutions' PT series (Entropy Solutions Inc., Plymouth, Minnesota).

# 8.1 Data evaluation technique

The original T-history method has undergone several improvements over the years as explained in chapter 5. Most of those improvements focused on the development of the appropriate evaluation techniques necessary to convert the raw temperature history curves into the meaningful PCM data in terms of phase change temperature (range) and associated heat capacity. The achievements regarding the data processing of the T-history curves were summarised in subsection 5.3.1. Various improvements were discussed including two most extensive and relatively opposing data evaluation techniques, the time delay technique (Marin et al., 2003) and the thermal delay technique (Kravvaritis et al., 2010). In both techniques the T-history curves (that of the environment, of the PCM, and of the reference material) are used to determine the available heat capacity of the PCM in question. As previously explained Marin et al. (2003) observed the temperature variation of the sample and reference over very small and fixed temperature intervals $\Delta T_i$ corresponding to time intervals $t_{i+1}$-$t_i$ and $t'_{i+1}$-$t'_i$ for PCM and reference respectively. The authors used the time delay between the moments when sample and reference reach the specified temperature and the theoretical basis of the T-history method (Equation 5.8) to calculate enthalpy changes $\Delta h_p(T_i)$ of the PCM

in the corresponding temperature intervals $\Delta T_i$ (Figure 8.1). On the other hand, Kravvaritis et al. (2010) observed the temperature variation of the sample and reference over very small and fixed time intervals $\Delta t_i$ corresponding to thermal intervals $T_{m,i}-T_{m,i+1}$ and $T_{r,i}-T_{r,i+1}$ for PCM and reference respectively. Moreover, they used the thermal delay (i.e. temperature difference) between PCM (at temperature $T_{m,i}$) and reference (at temperature $T_{r,i}$) at the specified moment in time to evaluate the effective PCM thermal capacity (Figure 8.1). Considering the arguments presented in section 5.1 one of the aims in this study was to obtain the PCM data in the form of heat released/stored in given temperature intervals for both cooling and heating cases. Given this, the obtained temperature accuracy and precision of the T-history curves (as discussed in subsection 7.3.4.1) and the time resolution of those curves (minimum sampling frequency 10 Hz) it was concluded that the time delay evaluation technique is the most suitable for data processing in the advanced T-history method. Hence, its adaptation for the advanced T-history method will be explained further.



***Figure 8.1:*** *The conceptual differences between time delay and thermal delay techniques used in evaluation of T-history curves.*

The Equation 8.1 and Equations 5.13-5.14 represent the basis for the implementation of the time delay technique adapted for the advanced T-history method.

$$\Delta h_p(T_i) = \frac{m_w c_{p,w} + m_t c_{p,t}}{m_p} \frac{I_1}{I'_1} \Delta T_i - \frac{m_t}{m_p} c_{p,t} \Delta T_i \qquad (8.1)$$

As noted earlier, the $\Delta h_p(T_i)$ represents enthalpy changes of the PCM in the corresponding temperature intervals $\Delta T_i$; $m_p$ or simply $m$, $m_w$ and, $m_t$ are the masses of the PCM sample, the reference (distilled water) and the test tubes, respectively; $c_{p,w}$ or $c_{p,r}$ and $c_{p,t}$ are the mean specific heats of the reference and the tube materials; and $I_1$ and $I'_1$ are the values of the corresponding integration areas obtained by integration of the PCM and reference T-history curves (Figure 8.2).
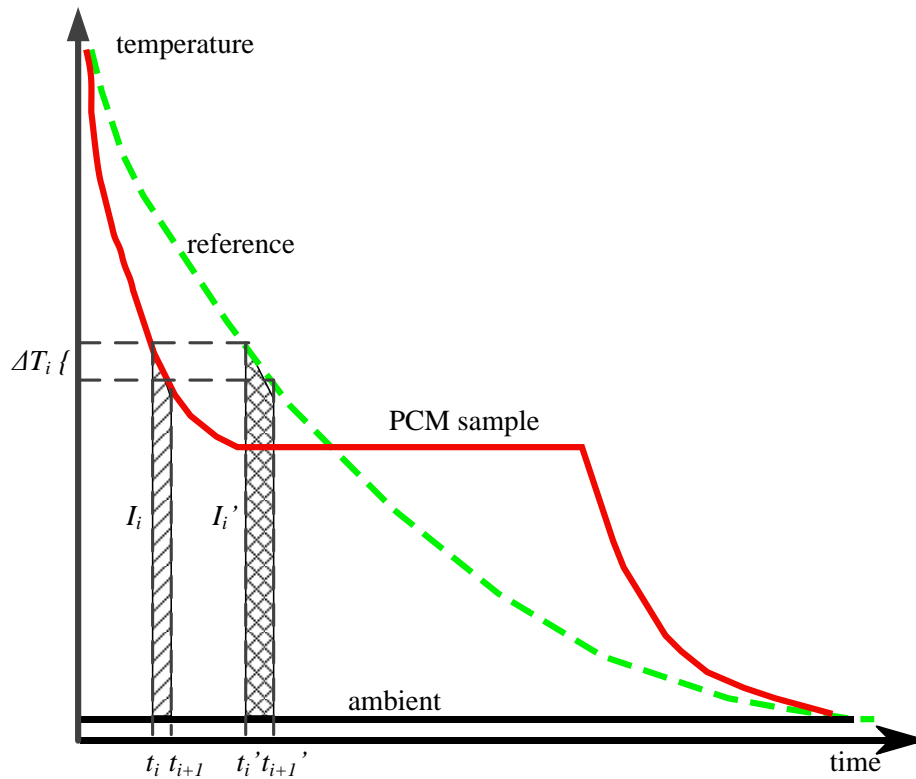


**Figure 8.2:** *The graphic representation of the time delay technique used in evaluation of T-history curves.*

169

Considering that the measurements carried out using the advanced T-history setup occur at constant pressure it was evident that the output of the time delay evaluation technique i.e. the enthalpy changes $\Delta h_p(T_i)$ of the PCM in the corresponding temperature intervals $\Delta T_i$ represent exactly the heat released/stored in the PCM in given temperature intervals. As previously explained this was labelled as the desired output of the PCM characterisation using the advanced T-history method. Hence, the time delay technique had to be implemented in such a way to enable the calculation of both heat released upon cooling and heat stored upon heating of the PCM. Furthermore, the selection of the temperature evaluation interval $\Delta T_i$ had to be flexible.

The technique was implemented in MATLAB and the code listings of the important functions are given in the APPENDIX A5 and A6. The most important implemented function is the *time_delay* function which calculates the heat released/stored in given temperature intervals upon either cooling or heating depending on its input parameter *Mode*. If this parameter has the value '*c*' then the output of the function *time_delay* is the heat released in given temperature intervals upon cooling. Otherwise, its output is heat stored in given temperature intervals upon heating. The other relevant inputs of this function are the measured T-history data, the temperature evaluation range i.e. the temperature range in which the heat is estimated, the width of the temperature intervals in which the heat is given, the temperature sensitivity with which the calculations are performed, and the parameters which contain the information about the masses of the PCM, reference, and test tubes as well as the information about the heat capacities of the reference and tube materials.

Another important function is the *enthalpy_calc* function which enables the determination and file storage of enthalpy-temperature curves $H(T)$ from the heat released/stored in given intervals data. This function is predominantly based on the Equation 5.13.

Once the time delay technique was adapted and implemented for the advanced T-history method measurements to verify this method could be performed. The verification experiments are described in detail in the following sections.

## 8.2 Parametric studies of RT21

As previously explained in section 5.1 PCM related measurements are very sensitive to various measurement parameters. Additionally, the need to balance between the parameters like the sample size and the measurement heating/cooling rates to maintain the thermal equilibrium inside the samples was also explained in the same section. Hence, it was decided to perform several measurements of the well-known PCM RT21 (see Table 7.6 for material specifications) using the advanced T-history method. The measurements were to be performed on the same PCM but with varying measurement parameters in order to discover which parameters affect the PCM characterisation and to which extent. Initially it was planned to carry out a set of parametric studies of RT21 by varying the parameters like the size and position of the sensors used for temperature measurements as well as the size of the investigated samples. However, after some measurements it was established that few other parametric studies need to be performed. Accordingly, all the performed studies are explained in detail in this section.

## 8.2.1 Sensor size study – results and discussion

To investigate the effects of the size of the sensors used in PCM measurements two different T-history measurements were performed. In the first one the standard MA100BF103A sensors were used while in the second one the MA100GG103A sensors were used. Both sensors have exactly the same characteristics minus the probe diameter. As given in the Table 7.7 the diameter of the MA100BF103A is 0.762 mm while the sensor MA100GG103A has larger diameter of 2 mm. By using the sensors of the same characteristics the instrumentation system 3 could be used in both measurements and given the precise control environment of the advanced T-history setup the only variable parameter in the measurements would be the sensor size.

In both cases (with the 0.762 mm and the 2 mm diameter sensors) the T-history measurement of RT21 were performed using the advanced T-history method based on the experimental setup explained in Chapter 6 and the instrumentation system 3 explained in section 7.3. In terms of T-history setup arrangements the same general

procedure as explained in subsection 7.1.4 was followed in both measurements. Namely, in both T-history measurements the RT21 and the reference (distilled water with the specific heat capacity $c_{p,w}$ of 4.185 kJkg$^{-1}$K$^{-1}$) were placed in 300 mm long SIMAX glass test tubes (the specific heat capacity of the SIMAX glass $c_{p,t}$ being 0.98 kJkg$^{-1}$K$^{-1}$). The design details and specifications of the test tubes were given in subsection 6.2.3. The mass of the PCM test tube was 28.8 g and the mass of the reference tube was 29.3 g. The masses were measured using the lab scale with the 0.01 g precision. The same tubes were used in both T-history measurements. The placement of sensors was done as explained in subsection 7.1.4. Since three temperatures (the environmental ENV, that of the PCM, and that of the reference H$_2$O) were measured in total in both measurements the same instrumentation system 3 prototype as in the measurement described in subsection 7.3.4 was used. Additionally, the data acquisition was done by using the system described in subsection 7.1.3 and the PCM_DAQ.vi. The variable parameters of the PCM_DAQ.vi were the same in both measurements. The sampling frequency was 10 Hz. The expected input range of the signals was set between 0 V and 5 V. Finally, the size of the DAQ card's buffer was set to 36 according to the formula given by Equation 7.3.

Prior to the T-history measurements it was decided that the calibration measurements for both 0.762 mm and 2 mm diameter sensors should be performed. As in previous measurements explained in section 7.2.4.1 and 7.3.4.1 the sensors were subjected to 1 °C step temperature program from 10 °C to 39 °C inside the chamber. The calibration data were used in the same way as in section 7.2.4.1 to determine the voltage-temperature conversion equations for each sensing channel. Once these preparations were made the T-history measurements could be performed.

In the T-history measurement with the 0.762 mm diameter sensor the RT21 and the reference were subjected to the alternating cooling and heating 2 h long cycles between 11 and 30 °C. In total, 10 cooling and 10 heating cycles were recorded. The respective masses of the sample ($m_p$) and reference ($m_w$) were 19.6 g and 24.3 g. Once the data were recorded the post-processing was performed in the same way as described in section 7.2.4.1 to obtain the relevant T-history curves. For the T-history measurement with 2 mm sensors only the MA100BF103A sensors were replaced with

the MA100GG103A sensors and everything else remained the same. The masses of the PCM and reference were measured again but resulted in small changes in the order of $10^{-2}$ g. As before, the recorded voltage data were post-processed using the appropriate temperature conversion equations to obtain the T-history curves.

The 10 cooling cycles from the measurement with 0.762 mm diameter sensors were averaged as well as the 10 heating cycles to obtain the respective cooling and heating cycle data for this measurement. The same was done with the data from the measurements with the 2 mm diameter sensors. The cooling cycle data from both measurements were compared as well as the heating cycle data. In the case of heating the data from both measurements were almost identical with the temperature difference in the order of $10^{-2}$ °C. On the other hand, in the cooling data the only significant difference between the measurements was observed for the temperatures of the PCM (Figure 8.3).
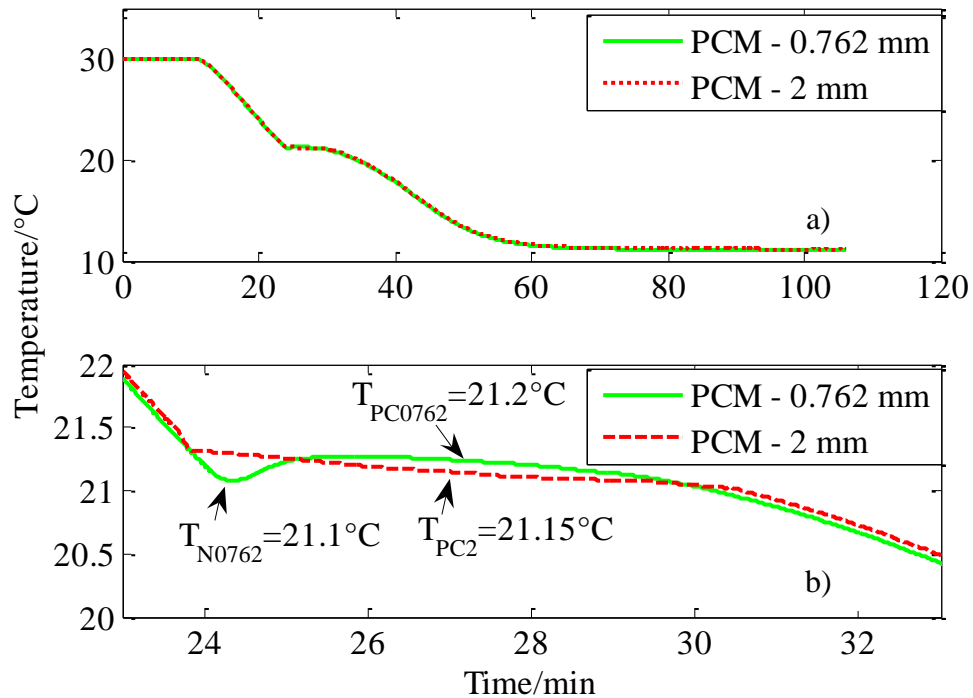


***Figure 8.3:*** *Comparison of the PCM cooling cycle data from RT21 T-history measurements with the 0.762 mm diameter sensor (PCM - 0.762 mm) and with the 2 mm diameter sensor (PCM - 2 mm). a) Normal view. b) Zoomed-in view.*

In normal view (Figure 8.3a) the difference between the data cannot even be observed. Hence a zoomed-in view was provided (Figure 8.3b). It is evident that the main difference between the measurements with different size sensors occurs during the phase change of the PCM i.e. during its solidification process. In the measurement with the 0.762 mm diameter sensor the observed typical phase change temperature ($T_{PC0762}$ in Figure 8.3b) was 21.2 °C while the nucleation temperature ($T_{N0762}$ in Figure 8.3b) was 21.1 °C. Hence, the observed degree of subcooling in this measurement was negligible 0.1 °C but still existent. The phase change plateau was flatter in the measurement with the larger 2 mm diameter sensors resulting in the typical phase change temperature of 21.15 °C ($T_{PC2}$ in Figure 8.3b). Given the flatness of the phase change plateau the nucleation temperature could not be observed in this measurement resulting in the zero degree of subcooling hence lower than in the measurement with the smaller sensors.

It was concluded that the sensor size indeed affects the degree of subcooling. Namely, the sensor, if used inside the PCM sample during T-history characterisation measurement, can act as a nucleating agent (seed) and suppress the naturally existing subcooling phenomenon i.e. lower the real degree of subcooling of the PCM sample. The larger the size of the sensor (i.e. the size of the nucleating seed) the solidification starts sooner without reaching the nucleation temperature as it would be the case in the naturally occurring solidification process and this consequently results in the lower degree of subcooling of the investigated PCM than the real one. Hence, it was decided that in the future PCM characterisation measurements using the advanced T-history method only the smaller size MA100BF103A sensors will be used in order to minimise the sensor effect on the natural course of the phase change process.

Furthermore, another observation was made in this parametric study. Namely, in the case of T-history measurements with the 0.762 mm diameter sensors the observed subcooling lasted only for 1 min (Figure 8.3b) and consequently could not be observed if the data sampling frequency was not high enough. However, the 10 Hz sampling frequency used in the aforementioned T-history measurements was adequate to register the 1 min long subcooling effect. Hence, it was also decided to use the same sampling frequency in the future measurements.

## 8.2.2 Sensor position study – results and discussion

One of the ways to avoid the interaction of the sensors and the investigated samples in T-history measurements is to place the sensors on the surface of the test tubes instead inside the PCM and reference samples. In the DSC instruments the measurement sensors are usually placed on the surface of the test crucibles. However, the size of the DSC samples is much smaller than the size of the samples investigated in T-history measurements. Hence, it is reasonable to use surface measurements in the case of small DSC samples and adequate heating/cooling rates. The aim of this parametric study was to verify if the surface temperature measurements can be adequate in T-history studies. The investigated PCM was again RT21. The measurement was performed in an almost identical way as the measurement with the 0.762 mm MA100BF103A sensors described in subsection 8.2.1. The only difference was that the prototype of the instrumentation system 3 had to be expanded to accommodate three more temperature channels. Namely, apart from the standard channels for the measurement of the environmental temperature (ENV or ENV-in in this case), that of the PCM (PCM or PCM-in in this case), and that of the reference ($H_2O$ or $H_2O$-in in this case) three additional channels were used in this test. An additional channel to record the environmental temperature was added (labeled as ENV-s) as well as the channels to record the surface temperatures of the PCM (PCM-s) and reference ($H_2O$-s) (Figure 8.4). The MA100BF103A sensors were used for all six channels. The instrumentation prototype was expanded by using the same processing circuit (Figure 7.21) for each added channel. The channels were connected to the analogue inputs of the DAQ card in differential mode. The parameters of the PCM_DAQ.vi had to be adjusted to enable it for the acquisition of six analog voltage channels. The sampling frequency was 10 Hz and the input voltage range was set from 0 to 5 V as in the measurement with the 0.762 mm MA100BF103A sensors described in subsection 8.2.1. The size of the DAQ card's buffer was set to 72 to accommodate the three extra channels as given by Equation 7.3.
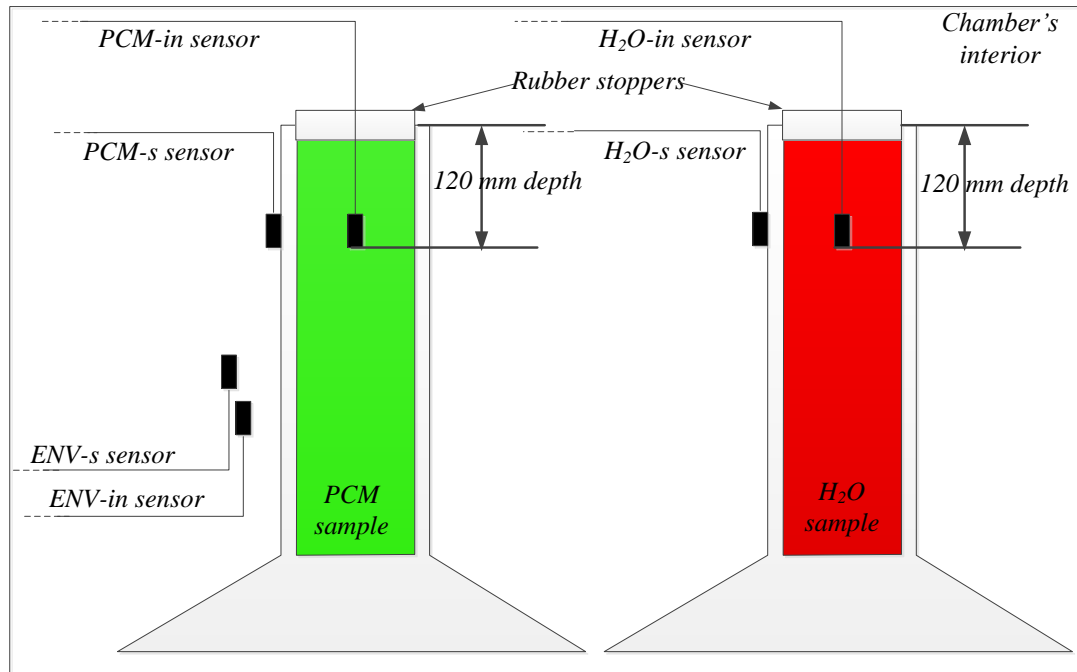
***Figure 8.4:*** *Sensor position study with sensors placed inside and on the surface of the measured PCM and reference ($H_2O$) samples – schematic diagram (ENV-in and ENV-s – sensors for the measurement of environmental temperatures, PCM-in and PCM-s – sensors for the measurement of temperatures inside and on the surface of the PCM sample, $H_2O$-in and $H_2O$-s – sensors for the measurement of temperatures inside and on the surface of the reference sample).*

As in the subsection 8.2.1, prior to the T-history measurement, an adequate calibration measurement was performed. All six sensors were subjected to 1 °C step temperature program from 10 °C to 39 °C inside the chamber. Once more the calibration data were used as described in section 7.2.4.1 to determine the voltage-temperature conversion equations for each sensing channel.

Once the calibration was performed, the RT21 and reference samples were measured. Given that the same test tubes were used as in the MA100BF103A T-history measurement in subsection 8.2.1 the masses of the samples were almost identical, 19.5 g (PCM mass) and 24.3 g (reference mass).

The sensors labeled as PCM-in and $H_2O$-in were placed inside the PCM and reference samples respectively and secured at the 120 mm depth from the top of the tubes (Figure 8.4) following the procedure described in subsection 7.1.4. The sensors labeled PCM-s and $H_2O$-s were placed on the surface of the respective test tubes at the same level as the PCM-in and $H_2O$-in sensors (Figure 8.4). The good thermal contact between the sensors and the tubes was secured by using a thermally conductive paste purchased from Omega (Omega, 2012) and simple adhesive tape. The sensors labeled ENV-in and ENV-s were placed inside the chamber in close proximity to one another (Figure 8.4).

Once the aforementioned arrangements were made the RT21 and the reference were subjected to the alternating cooling (10 cycles) and heating (10 cycles) 2 h long cycles between 11 and 30 °C. The recorded data were post-processed in the same way as described in section 7.2.4.1 to obtain the relevant T-history curves. The 10 recorded cooling cycles were averaged as well as the 10 heating cycles to minimise errors and obtain the respective cooling and heating cycle data for this measurement.

The obtained T-history curves are shown in Figure 8.5. The difference between the data recorded by the sensors inside and on the surface of the samples is evident in the case of both cooling (Figure 8.5a) and heating (Figure 8.5b) cycles. Both environmental temperature sensors (ENV-in and ENV-s in Figure 8.5) recorded almost identical temperature values. This confirmed that the temperature distribution inside the environmental chamber is rather uniform. Additionally, it demonstrated the consistency of the temperature circuit (Figure 7.21) used to build the instrumentation system 3 prototype.

The cooling PCM curve recorded by the sensor inside the sample (PCM-in in Figure 8.5a) shows that the typical phase change temperature of the material is around 21 °C as expected for RT21 (Rubitherm GmbH, Berlin, Germany). The cooling curve recorded by the sensor placed on the surface of the PCM tube (PCM-s in Figure 8.5a) shows lower temperature than the one of the PCM-in curve (Figure 8.5a) during the entire cooling cycle. It also shows the typical phase change temperature of around 20 °C i.e. 1 °C deviation from the typical phase change temperature expected for RT21.
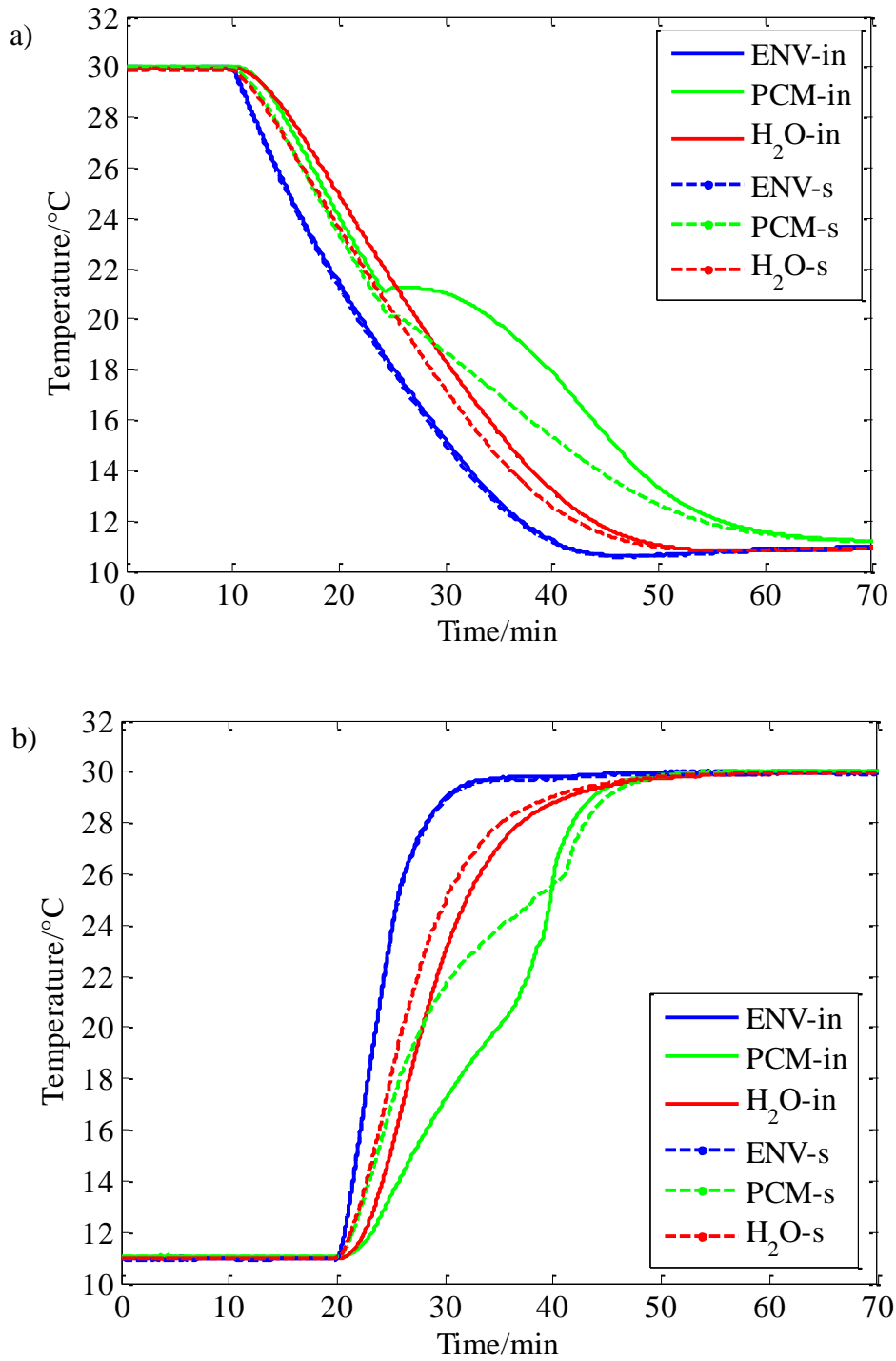
***Figure 8.5:*** *Cooling (a) and heating (b) cycle in RT21 T-history sensor position study (ENV-in and ENV-s – environmental temperatures, PCM-in and PCM-s – temperatures inside and on the surface of the PCM sample, $H_2O$-in and $H_2O$-s – temperatures inside and on the surface of the reference sample).*

The deviation in the case of heating curves (PCM-in and PCM-s in Figure 8.5b) is even larger. The heating curve PCM-s generally shows higher temperature during the heating cycle than the PCM-in curve (Figure 8.5b). It can also be concluded that the phase change range is much wider in the case of PCM-s curve than in the case of PCM-in curve (Figure 8.5b).

The reference curve recorded by the sensor placed on the surface of the reference tube ($H_2O$-s) shows lower temperature than the reference curve recorded by the sensor placed inside the reference sample ($H_2O$-in) during the entire cooling cycle (Figure 8.5a). On the other hand the $H_2O$-s curve shows higher temperature than the $H_2O$-in curve during the heating cycle (Figure 8.5b).

The tendency of surface curves to show lower temperature than the inside curves upon cooling and higher temperature upon heating is completely logical given that the cooling and heating of the samples occurs by firstly changing the environmental temperature. Hence, it is expected that the surfaces of the test tubes are cooler than the insides upon cooling and also warmer upon heating.

Despite the obvious deviations between the surface and inside curves (PCM-s, $H_2O$-s, PCM-in, and $H_2O$-in Figure 8.5) it was decided to further evaluate the recorded T-history curves to obtain the relevant PCM heat release/storage data. The evaluation was performed using the evaluation technique described in section 8.1. The heat released/stored was evaluated between 15 °C to 30 °C. The width of the temperature interval in which heat data were to be given was set to 0.5 °C. Although the temperature interval could be smaller given the accuracy and precision of the measured T-history curves the value of 0.5 °C was selected in order to maintain the good precision of the heat data but also to have good visibility of the data presented. The results of the evaluation process are shown in Figure 8.6.
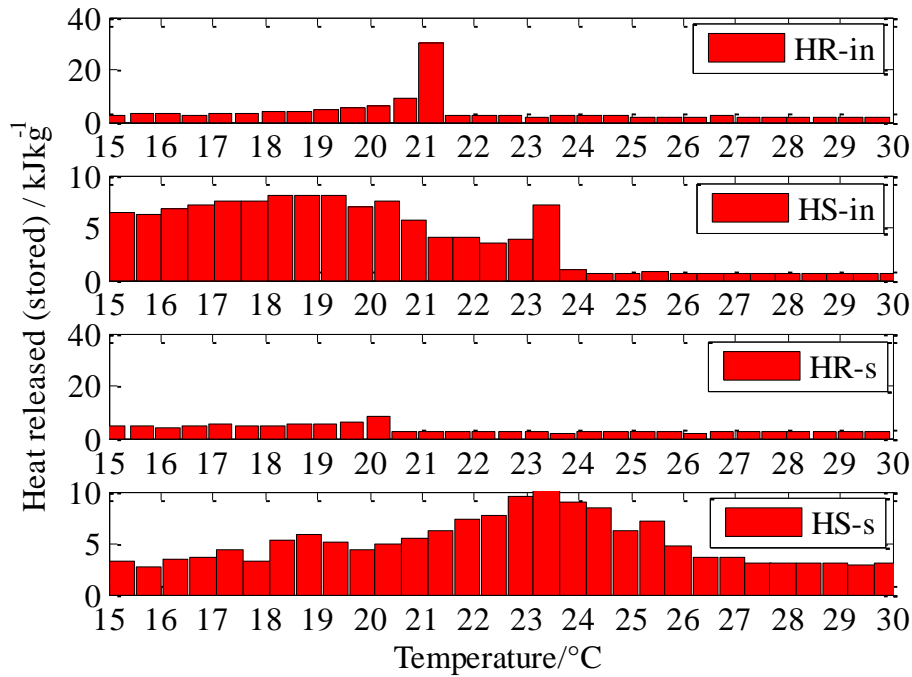
*Figure 8.6: Heat released (stored) in given temperature intervals from RT21 T-history sensor position study (HR-in – heat released based on the cooling cycle data obtained from sensors placed inside the samples, HS-in – heat stored based on the heating cycle data obtained from sensors placed inside the samples, HR-s – heat released based on the cooling cycle data obtained from sensors placed on the surface of the samples, HS-in – heat stored based on the heating cycle data obtained from sensors placed on the surface of the samples).*

The heat released upon cooling in given temperature intervals (HR-in in Figure 8.6) was calculated from the ENV-in, PCM-in, and $H_2O$-in T-history curves (Figure 8.5a). The peak value in heat released occurs in the temperature interval from 21 °C to 21.5 °C (HR-in in Figure 8.6) as expected for RT21. The heat stored upon heating in given temperature intervals (HS-in in Figure 8.6) was calculated from the ENV-in, PCM-in, and $H_2O$-in T-history curves (Figure 8.5b). In this case the latent heat storage is distributed in a wider temperature range ending at 23.5 °C. The width of the melting temperature range and the end of melting is in relative agreement with the melting area between 18 and 23 °C for RT21 as given in Table 7.6. The heat released upon cooling in given temperature intervals (HR-s in Figure 8.6) was calculated from the ENV-s, PCM-s, and $H_2O$-s T-history curves (Figure 8.5a). The peak value in this case is in the temperature interval from 20 °C to 20.5 °C showing that the temperature

measurements on the surface of the test tubes result in the shift of the congealing area for RT21 towards lower temperatures as expected in the case of surface measurement. Moreover, the peak value in the case of HR-s in much lower than in the case of HR-in (Figure 8.6) leading to the conclusion that the surface T-history measurements result in lower and incorrect overall heat capacity of the investigated material. The heat stored upon heating in given temperature intervals (HS-s in Figure 8.6) was calculated from the ENV-s, PCM-s, and $H_2O$-s T-history curves (Figure 8.5b). In this case the melting range is shifted towards higher temperatures ending at rather high temperature of 26 °C in comparison to the expected melting area of RT21 (Table 7.6). Additionally, the HS-s shows higher values in the corresponding temperature intervals than the HS-in (Figure 8.6). This once more leads to the conclusion that the T-history surface measurement result in the misleading PCM characterisation in terms of both temperature and heat release/storage data. Hence, it was concluded that the measurements with the sensors placed on the surface of the test tubes cannot be performed as part of the advanced T-history setup. It was decided that further T-history measurements will be performed only with the sensors placed inside the PCM and reference samples.

Apart from the shortcomings of the surface measurements another observation was made in this parametric study. Namely, this was the first time the T-history data were utilised to estimate the heat capacity of the investigated material resulting in the data given in Figure 8.6. Although the difference between the heat released and the heat stored data was expected especially in the case of surface measurement the interesting part was that the hysteresis between the HR-in and HS-in data was rather evident (Figure 8.6). The argument was made that the observed hysteresis could only be apparent due to the possible thermal gradients occurring inside the investigated PCM sample. It was decided that another parametric test to investigate the aforementioned hysteresis needs to be performed.

The factors that can result in the existence of thermal gradients in PCM samples were explained in detail in section 5.1. Since one of the major aims of the overall study was to test the large size PCM sample the reduction of sample size was not possible. Hence, a reduction in cooling/heating rates used in T-history experiments had to be

implemented. As explained in chapter 6 the heating and cooling rates of the environmental chamber are fixed (0.5 Kmin$^{-1}$ for cooling and 1.3 Kmin$^{-1}$ for heating) and cannot be changed. Also the recommended heating/cooling rates for the PCM related studies are 1 Kmin$^{-1}$ (RAL, 2010). The cooling rate of the chamber is not as the recommended value; however it is lower and therefore should provide reduced temperature gradients inside the investigated samples as required in PCM measurements. Adversely, the heating rate of the chamber is higher than the recommended value and it was identified as the possible source of the previously observed hysteresis problem. Hence it was decided to lower the heating/cooling rates of the PCM samples in the T-history measurements by means of the insulation of the test tubes. It was concluded that the test tubes need to be insulated with the thermally insulating tape of the appropriate thickness in order to avoid the creation of temperature gradients inside the PCM samples. The study to determine the optimal thickness of the insulating tape was performed and described in detail in the next subsection.

## 8.2.3 Insulation thickness study – results and discussion

As discussed in the previous subsection, it was concluded that the test tubes in the advanced T-history setup need to be properly insulated to reduce the temperature gradients inside the samples and enable accurate PCM characterisation. The aim of this study was to find the optimal thickness of the thermally insulating tape used to wrap the test tubes. For this the results of the measurements with different thicknesses of the insulating tapes had to be compared. The RT21 T-history results obtained in the measurement with the 0.762 mm diameter sensors described in subsection 8.2.1 were selected to be a part of the comparison procedure since no insulation (i.e. insulation thickness of 0 mm) was used on the test tubes in this measurement. Two additional T-history measurements of RT21 were performed in the exactly same manner as the measurement with the 0.762 mm diameter sensors described in subsection 8.2.1. The only difference was that in the first of these measurements the test tubes were wrapped

with the adhesive polyethylene foam-tape purchased from RS Components (RS Components, 2010) with the tape's thickness of 3 mm while the tape's thickness was 6 mm in the second measurement. As before, prior to each T-history measurement the proper calibration measurement with 1 °C step temperature program from 10 °C to 39 °C inside the chamber was performed to assure the accuracy of the sensors used in T-history measurements. Given that the same sample and reference were used as in the MA100BF103A T-history measurement described in subsection 8.2.1 the masses of the samples were checked prior to each measurement and in both cases remained almost unchanged, 19.5 g (PCM mass) and 24.3 g (reference mass). In total, 10 cooling and 10 heating 6 h long cycles (to take the extra insulation into the account) were recorded in both measurements and averaged to determine the T-history cooling and heating cycle data. For comparison purposes, the obtained results and the results from the MA100BF103A T-history measurement described in subsection 8.2.1 are shown in Figure 8.7.

Clearly, the environmental temperature in all three measurements is almost identical upon both cooling and heating as expected (ENV – 0 mm ins, ENV – 3 mm ins, and ENV – 6 mm ins in Figure 8.7). It is also evident that the time to reach equilibrium state for both PCM and reference samples increases as the insulation thickness increases in both cooling and heating cycles (PCM – 0 mm ins, $H_2O$ – 0 mm ins, PCM – 3 mm ins, $H_2O$ – 3 mm ins, PCM – 6 mm ins, and $H_2O$ – 6 mm ins in Figure 8.7). The corresponding PCM and $H_2O$ curves become less steep as the insulation thickness increases in both cooling and heating measurements (Figure 8.7) indicating slower cooling/heating processes. The phase change temperature was not affected to a great extent by the varying insulation thicknesses. Nevertheless, to further investigate the effects of different insulation thicknesses, the T-history curves from all three aforementioned measurements were evaluated in the 15 °C to 30 °C using the evaluation technique described in section 8.1 and the temperature interval of 0.5 °C to obtain the heat released/stored data in given temperature intervals (Figure 8.8).
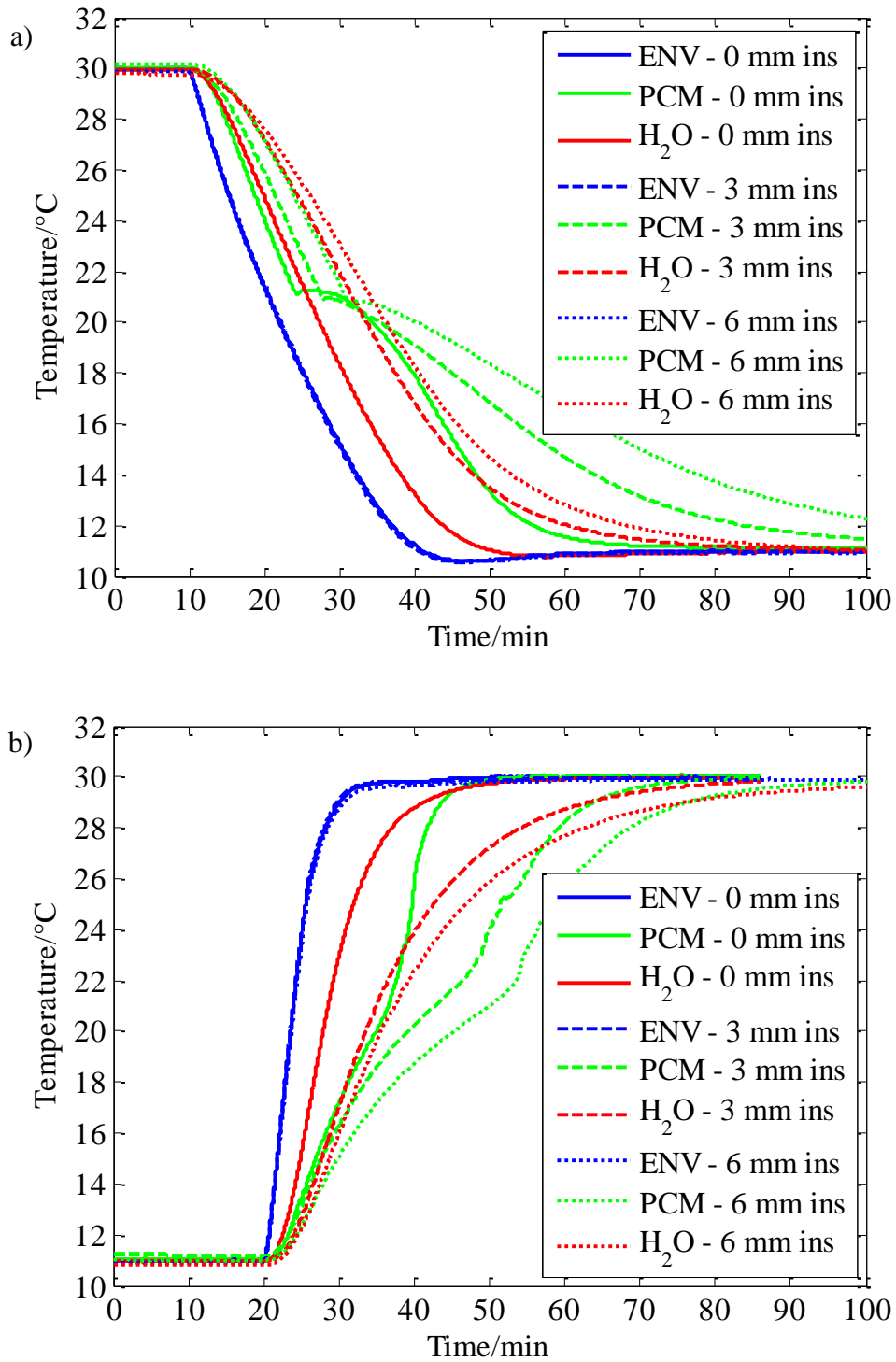
**Figure 8.7:** *Cooling (a) and heating (b) cycles in RT21 T-history studies with various insulation thicknesses (0, 3, and 6 mm) (ENV – environmental temperatures, PCM – temperatures of the PCM sample, $H_2O$ – temperatures of the reference sample).*
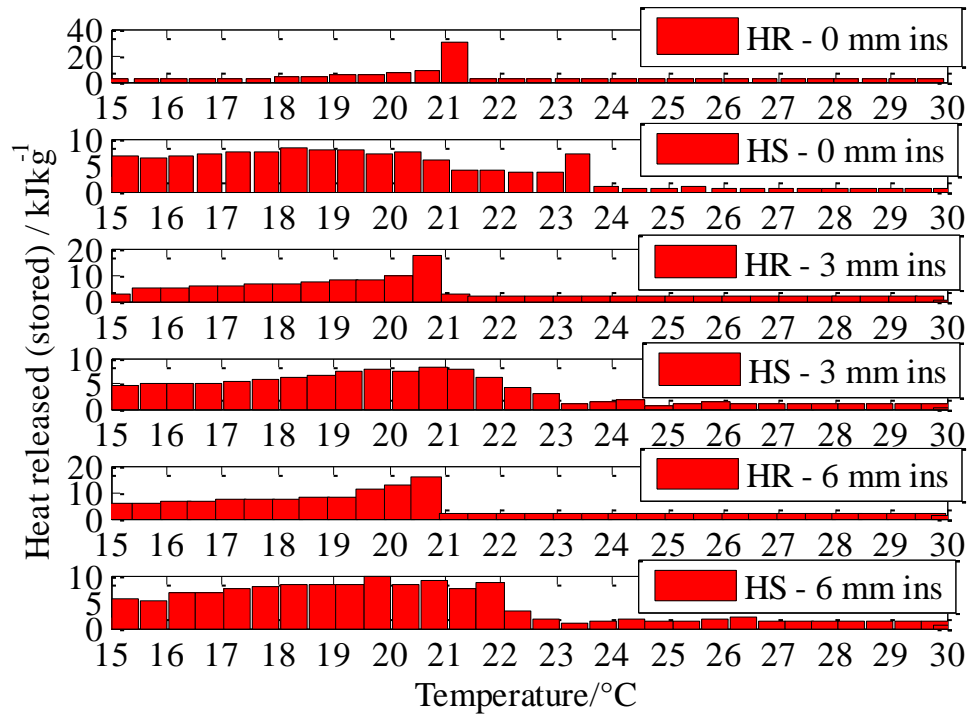
***Figure 8.8:*** *Heat released (stored) in given temperature intervals from RT21 T-history studies with various insulation thicknesses (0, 3, and 6 mm) (HR – heat released upon cooling, HS – heat stored upon heating).*

The heat released upon cooling in given temperature intervals in the measurement with no insulation (HR – 0 mm ins in Figure 8.8) was calculated from the ENV – 0 mm ins, PCM – 0 mm ins, and $H_2O$ – 0 mm ins T-history curves (Figure 8.7a). The peak value in heat released occurs in the temperature interval from 21 °C to 21.5 °C (HR – 0 mm ins in Figure 8.8) which is in agreement with the typical phase change temperature of RT21 (Table 7.6). The heat stored upon heating in given temperature intervals in the same measurement (HS – 0 mm ins in Figure 8.8) was calculated from the ENV – 0 mm ins, PCM – 0 mm ins, and $H_2O$ – 0 mm ins T-history curves (Figure 8.7b). In this case the latent heat storage is distributed in a wider temperature range ending at 23.5 °C. The hysteresis between the HR – 0 mm ins and HS – 0 mm ins is evident. The heat released upon cooling in given temperature intervals in the measurement with 3 mm thick insulation (HR – 3 mm ins in Figure 8.8) was calculated from the ENV – 3 mm ins, PCM – 3 mm ins, and $H_2O$ – 3 mm ins T-history curves (Figure 8.7a). The peak value in heat released in this case is in the

temperature interval from 20.5 °C to 21 °C (HR – 3 mm ins in Figure 8.8) which is also in agreement with the typical phase change temperature of RT21 (Table 7.6). The value of the highest peak is lower than in the case of HR – 0 mm ins (Figure 8.8). However, the latent heat release in this case occurs in a wider 19 °C to 21 °C temperature range. The heat stored upon heating in given temperature intervals in the measurement with 3 mm thick insulation (HS – 3 mm ins in Figure 8.8) was calculated from the ENV – 3 mm ins, PCM – 3 mm ins, and $H_2O$ – 3 mm ins T-history curves (Figure 8.7b). In this case the latent heat storage occurs in a temperature range ending at 22.5 °C (Figure 8.8). The hysteresis between the HR – 6 mm ins and HS – 6 mm ins is even smaller than in the measurement with the 3 mm thick insulation (Figure 8.8).

Furthermore, the heat released/stored data (HR and HS in Figure 8.8) were used to calculate the corresponding enthalpy curves upon cooling and heating in all three aforementioned measurements. The enthalpy was calculated using the function *calc_enthalpy* described in section 8.1. The results are shown in Figure 8.9.

All the enthalpy-temperature curves were normalised to 0 kJkg$^{-1}$ at 15 °C (Figure 8.9). From the enthalpy curves it is evident that the increase of the insulation thickness resulted in reduction of the hysteresis between the cooling and heating data in the case of RT21 T-history measurements. In the case of the measurement with the 6 mm thick insulation the cooling and heating enthalpy curves were almost aligned (Cooling enthalpy – 6 mm ins and Heating enthalpy – 6 mm ins in Figure 8.9). Hence it was concluded that the 6 mm value represents the optimal value to be used for the insulation thickness in the advanced T-history studies. Another indicator that the 6 mm value represents the optimal value was the fact that in the measurement with the 6 mm insulation the total heat released/stored in the temperature range between the 15 °C and 30 °C was in the range between 130 and 140 kJkg$^{-1}$ (Figure 8.9). This was in much better agreement ($\pm 5$ %) with the value of 134 kJkg$^{-1}$ (Table 7.6) than the values around 120 kJkg$^{-1}$ ($\pm 12$ %) obtained from the measurements with the 0 and 3 mm thick insulations (Figure 8.9).
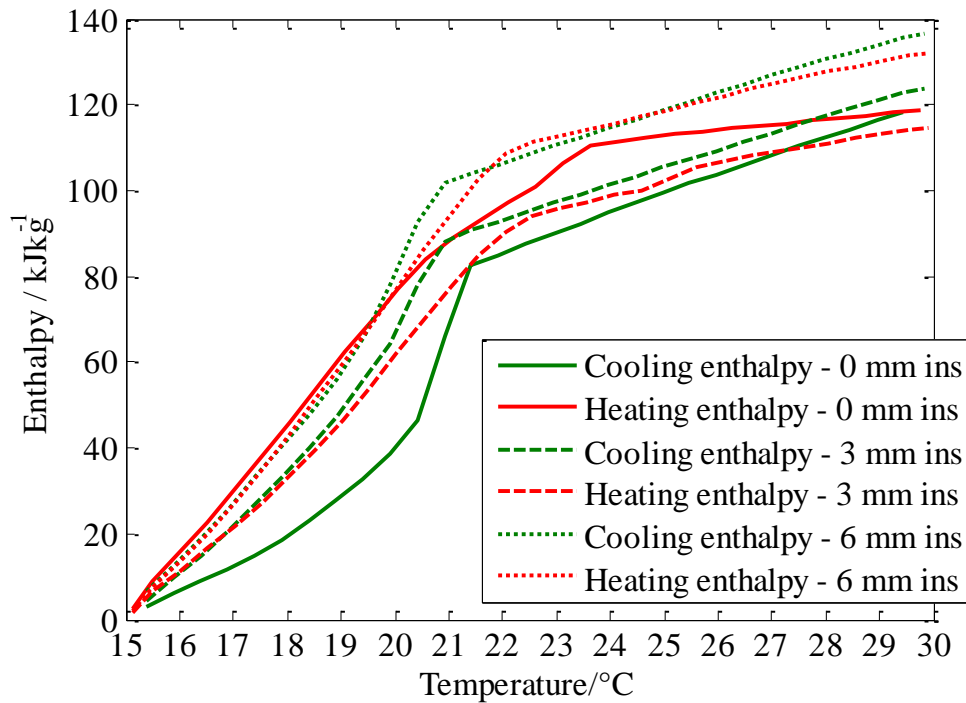
***Figure 8.9:*** *Enthalpy-temperature curves upon cooling and heating from RT21 T-history studies with various insulation thicknesses (0, 3, and 6 mm) with the normalised enthalpy value of 0 kJkg$^{-1}$at 15 °C.*

Given the low and similar values of thermal conductivities of different PCMs it was decided that the 6 mm insulation will be used as optimal even in the experiments with other PCMs and not just RT21.

## 8.2.4 Sample mass study – results and discussion

As mentioned in chapter 5 the size of the tested samples is around 1000 times larger in T-history experiments than in DSC ones. Hence, as explained in chapter 6 the test tubes were designed and built to enable the testing of relatively large representative PCM samples. The aim in this parametric study was to test the dependency of the PCM characterisation on the size of the samples. In all previous studies RT21 samples were placed in the test tubes with 300 mm height resulting in the sample's mass of 19.5 g. As part of this study another RT21 T-history measurement was performed by using the same setup and parameters as in the measurement with the 6 mm thick insulating tape described in the previous subsection 8.2.3. The only difference was that in this

measurement the PCM sample and reference were placed in the 430 mm long test tubes resulting in their respective masses of 41.4 g and 47.5 g. It is evident that the sample mass in this case (41.4 g) was greater than in the former case (19.5 g). As before, 10 cooling and 10 heating 6 h long cycles were recorded in this measurement and averaged to determine the corresponding T-history cooling and heating cycle data. The data from this measurement were compared to those obtained by the measurement of RT21 placed in 300 mm long test tube wrapped with the 6 mm thick tape described in subsection 8.2.3. The results of this comparison are shown in Figure 8.10.

The environmental temperatures in both measurements are almost identical upon both cooling and heating as expected (ENV – small sample and ENV – large sample in Figure 8.10). The difference between the corresponding PCM and $H_2O$ curves is evident (Figure 8.10). However, the significant difference can only be observed in terms of time needed by samples to reach equilibrium state (Figure 8.10). The larger samples (both PCM and reference) as expected needed more time (around 50 min) to reach the equilibrium states (Figure 8.10). On the other hand, by observing the T-history curves it can be concluded that the phase change temperature was not significantly affected by the samples' masses. To investigate the effect of the samples' masses, the T-history curves from both aforementioned measurements were evaluated in the 15 °C to 30 °C range using the evaluation technique described in section 8.1 and the temperature evaluation interval of 0.5 °C to obtain the heat released/stored data in given temperature intervals (Figure 8.11).

The heat released upon cooling in given temperature intervals in the measurement with the smaller mass samples (HR – small sample in Figure 8.11) was calculated from the ENV – small sample, PCM – small sample, and $H_2O$ – small sample T-history curves (Figure 8.10a). The peak value in heat released occurs in the temperature interval from 20.5 °C to 21 °C (HR – small sample in Figure 8.11) corresponding to the typical phase change temperature of RT21 (Table 7.6).
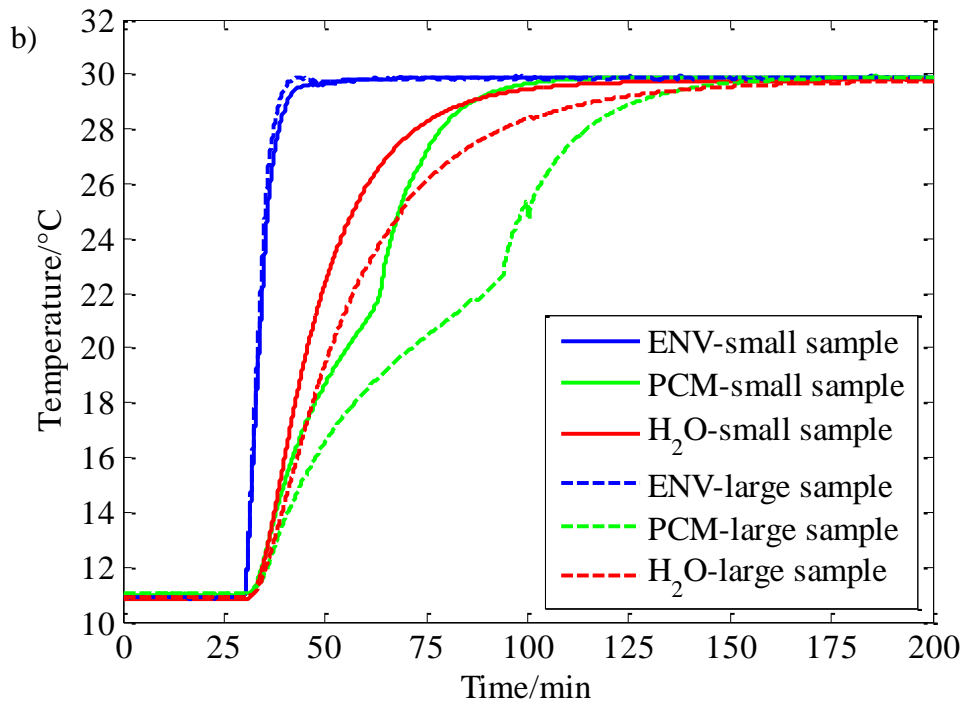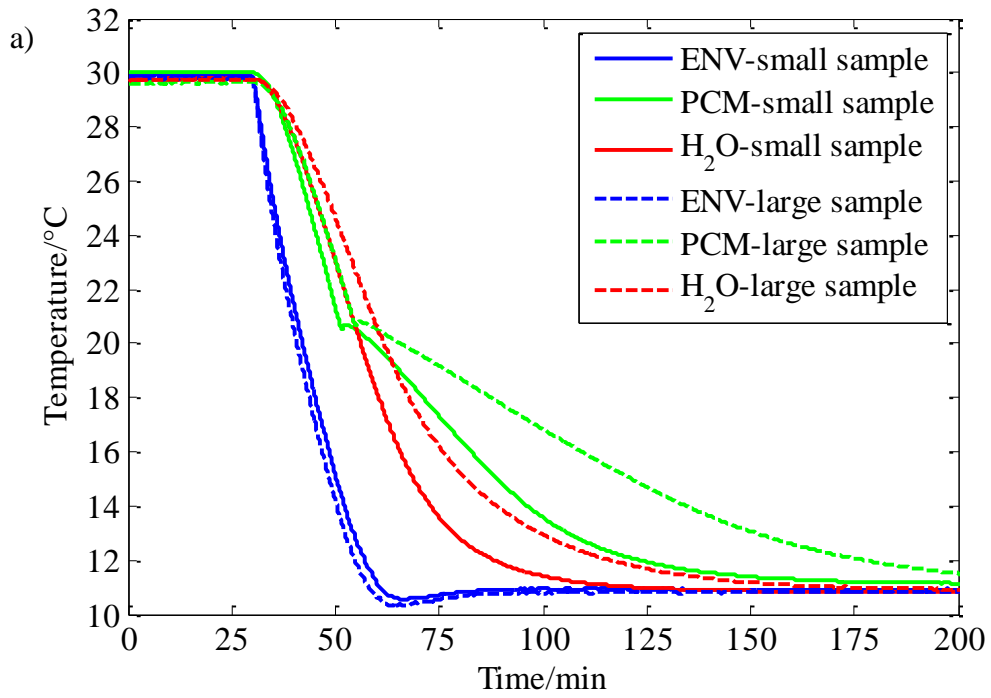
**Figure 8.10:** *Cooling (a) and heating (b) cycles in RT21 T-history studies with different masses of the PCM samples (ENV – environmental temperatures, PCM – temperatures of the PCM sample, $H_2O$ – temperatures of the reference sample).*
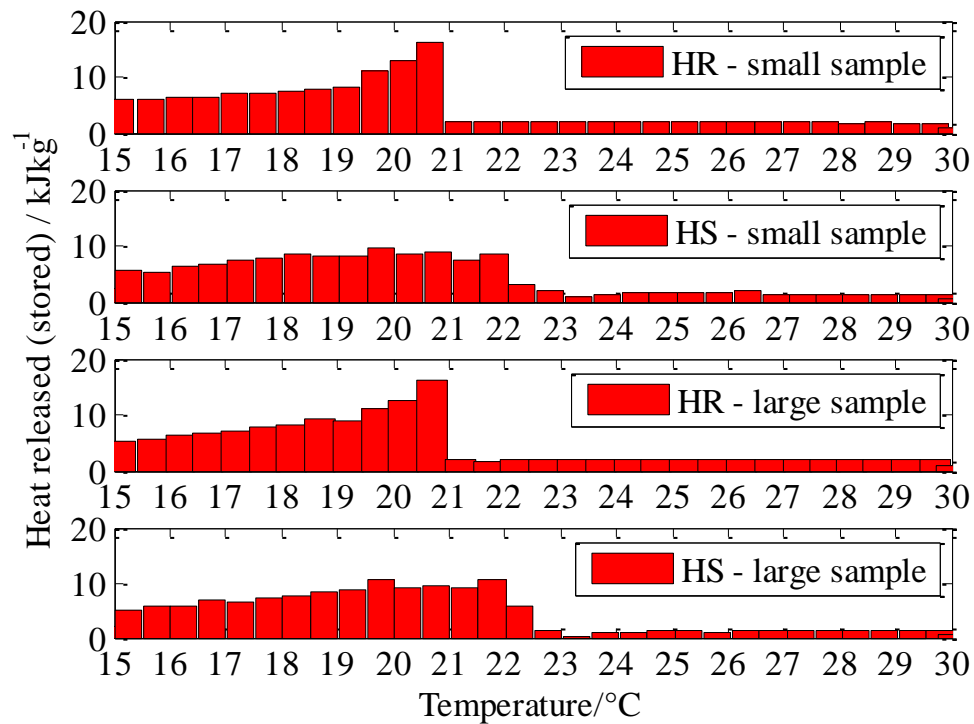
*Figure 8.11: Heat released (stored) in given temperature intervals from RT21 T-history studies with different masses of the PCM samples (HR – heat released upon cooling, HS – heat stored upon heating).*

The heat stored upon heating in given temperature intervals in the same measurement (HS – small sample in Figure 8.11) was evaluated based on the ENV – small sample, PCM – small sample, and $H_2O$ – small sample T-history curves (Figure 8.10b). In this case the latent heat storage is distributed in a slightly wider temperature range ending at 22.5 °C. The heat released upon cooling in given temperature intervals in the measurement with larger samples (HR – large sample in Figure 8.11) was calculated from the ENV – large sample, PCM – large sample, and $H_2O$ – large sample T-history curves (Figure 8.10a). The heat stored upon heating in given temperature intervals in the same measurement (HS – large sample in Figure 8.11) was calculated from the ENV – large sample, PCM – large sample, and $H_2O$ – large sample T-history curves (Figure 8.10b). The HR – large sample and HS – large sample data are almost the same as the corresponding HR – small sample and HS – small sample data (Figure 8.11) in terms of both temperature and heat released/stored values. This indicates that

the samples' mass does not affect the result of the PCM characterisation in the case of advanced T-history method.

Moreover, the heat released/stored data (HR and HS in Figure 8.11) were used to determine the corresponding enthalpy curves upon cooling and heating in the case of both measurements with small (19.5 g) and large (41.4 g) PCM samples. This was done by using the function *calc_enthalpy* described in section 8.1. The results are shown in Figure 8.12.
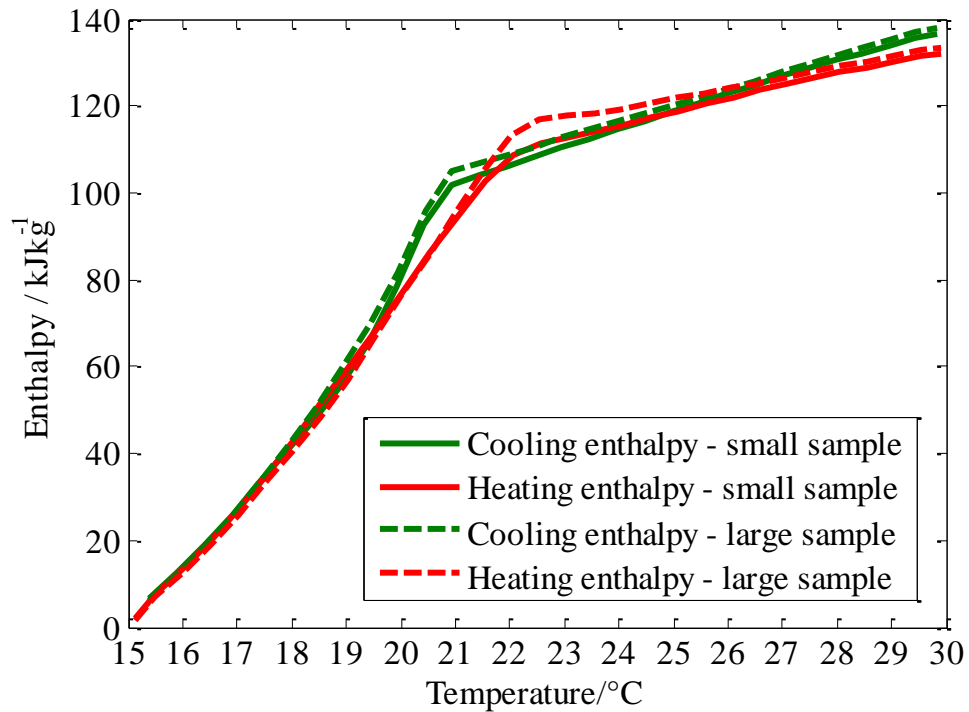


*Figure 8.12:* *Enthalpy-temperature curves upon cooling and heating from RT21 T-history studies with different masses of the PCM samples with the normalised enthalpy value of 0 kJkg$^{-1}$ at 15 °C.*

All enthalpy-temperature curves were normalised to 0 kJkg$^{-1}$ at 15 °C (Figure 8.12). The difference between the corresponding enthalpy curves (Cooling enthalpy and Heating enthalpy curves in Figure 8.12) is very small. The biggest difference in enthalpy values (4 kJkg$^{-1}$) was observed at 22.5 °C between the Heating enthalpy – small sample and Heating enthalpy – large sample in Figure 8.12. However this represents only 3 % of the expected value (134 kJkg$^{-1}$) for the total heat released/stored in the temperature range between the 15 °C and 30 °C for the RT21 (Table 7.6). Hence it was concluded that the samples' mass does not significantly affect the PCM

characterisation. Given this and the aim of this research to investigate large PCM samples (larger than 20 g) it was decided that the 430 mm long test tubes will be used in all future PCM characterisation experiments.

Additionally, the total heat released/stored in the temperature range between the 15 °C and 30 °C in the case of both cooling and heating was in the range between 130 and 140 kJkg$^{-1}$ (Figure 8.12) in the case of both small and large samples. This is in good agreement (±5 %) with the expected value of 134 kJkg$^{-1}$ (Table 7.6).

# 8.3 Investigation studies of RT organic series

Once the set of parametric studies, described in section 8.2, was performed and the conclusions regarding the parameters that mostly affect the measurement drawn the advanced T-history method was ready to be used for reliable PCM characterisation. It was decided that two organic materials from the Rubitherms's RT series (Rubitherm GmbH, Berlin, Germany) will be firstly tested. The previously tested RT21 and the new RT27 were selected due to their phase change temperature ranges that could be useful for building applications. Given that these applications were of the most interest for this study as discussed in the introductory chapters the selection of RT21 and RT27 was logical. These two materials have been commercially available for some time and form a part of various PCM objects sold by Rubitherm (Rubitherm GmbH, Berlin, Germany). Furthermore, other researchers (Kravvaritis et al., 2011) have tested these two materials. Hence it was concluded that the advanced T-history tests need to be performed on these materials to further validate the advanced T-history method.

## 8.3.1 RT21 characterisation – results and discussion

The T-history curves obtained from the measurement with the larger samples described in subsection 8.2.4 were used to represent the characterisation of RT21. The relevant T-history curves (ENV – large sample, PCM – large sample, and H$_2$O – large sample in Figure 8.10) are now given separately (ENV, PCM, and H$_2$O in Figure 8.13).
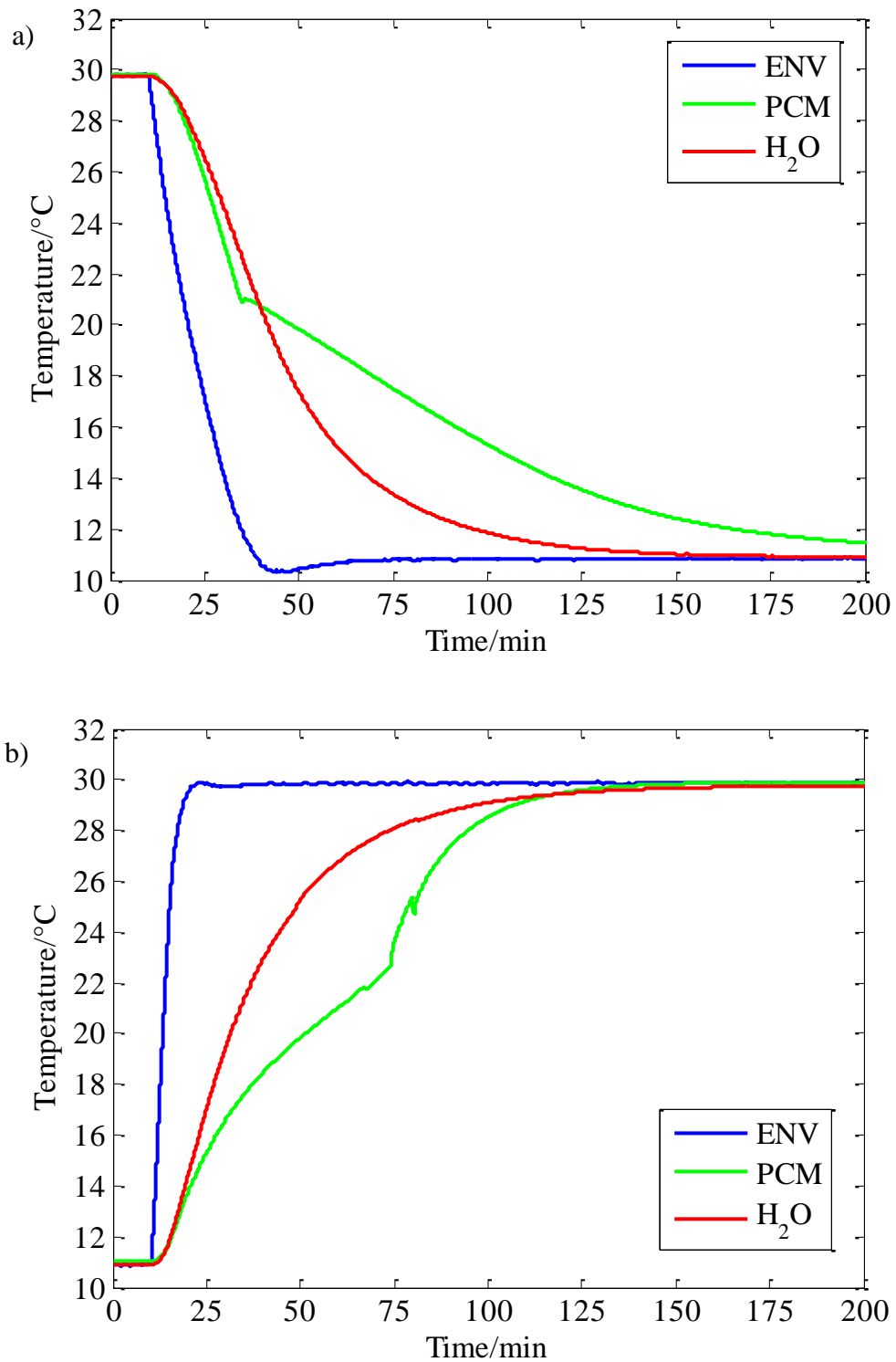
**Figure 8.13:** *Cooling (a) and heating (b) cycles in the advanced T-history characterisation of RT21 (ENV – environmental temperature, PCM – temperature of the PCM sample, H₂O – temperature of the reference sample).*

The reason these data were reused to properly represent the RT21 material is that the measurement with the larger samples described in subsection 8.2.4 represents an adequate measurement for PCM characterisation based on the advanced T-history method given the size of the samples and the reduced hysteresis between the cooling and heating data due to the appropriate insulation.

According to the T-history curves from the cooling cycle (Figure 8.13a) the typical phase change temperature of RT21 is 21 °C. This is in a perfect agreement with the RT21 specifications given by the manufacturer (Table 7.6). In addition, a very small 0.1 °C degree of subcooling was observed between the typical phase change temperature of 21 °C and the nucleation temperature of 20.9 °C (PCM in Figure 8.13a). The manufacturer does not report any degree of subcooling for RT21 (Rubitherm GmbH, Berlin, Germany). This could be due to the reason that the degree of subcooling is negligible (0.1 °C) or due to the fact that the subcooling was only detected because the MA100BF103A sensors used in the advanced T-history method were small enough not to interfere with the natural course of the phase change process upon characterisation. As discussed in subsection 8.2.1 the size of the sensors used in T-history studies affects the subcooling phenomenon.

Researchers usually give the PCM characterisation data obtained from measurements upon cooling. Arkar and Medved (2005) reported significant variation in the typical phase change temperature for the RT20 (former name of RT21) depending on the cooling rate used in their DSC tests. In the case of 1 K/min cooling rate (in the range of the cooling/heating rates used in the measurements presented here) the typical phase change temperature reported by Arkar and Medved (2005) was 19.7 °C. On the other hand, the same temperature reported by Kravvaritis et al. (2011) from their T-history studies was around 21 °C. Since the 19.7 °C is much lower than 21 °C the conclusion was made that that the results of DSC tests significantly depend on the position of the temperature sensors inside the DSC instruments. As mentioned in chapter 5 the sensors in the DSC instruments are usually placed on the surface of the test crucibles. This could explain the reason for the lower phase change temperature of 19.7 °C reported by Arkar and Medved (2005) given the observations discussed in subsection 8.2.2.

Furthermore, to achieve another aim of this research and as the result of the PCM characterisation based on the advanced T-history method, the results obtained upon heating (Figure 8.13b) are to be always presented with the results obtained from cooling (Figure 8.13a). According to the T-history curves from the heating cycle (Figure 8.13b) the phase change occurs in slightly wider temperature range ending at 22.5 °C. This observation is in agreement with the melting/congealing range of RT21 given by the manufacturer (Table 7.6).

As discussed in chapters 5 and 6 one of the aims of the study was to represent the PCM characterisation data in the form of the heat released/stored in given temperature intervals upon both cooling and heating. Hence, the relevant heat released/stored data in given intervals (0.5 °C wide) (HR – large sample and HS – large sample in Figure 8.11) were also reused and given separately (HR and HS in Figure 8.14).
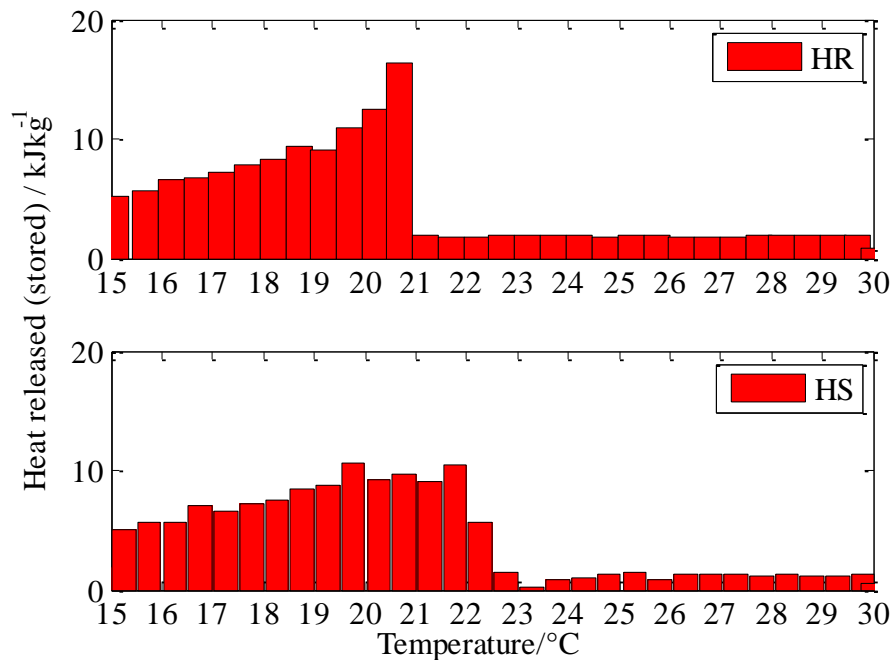


**Figure 8.14:** *Heat released (stored) data obtained from the advanced T-history characterisation of RT21 (HR – heat released upon cooling, HS – heat stored upon heating).*

It is evident that the heat stored upon heating is distributed in a wider temperature range than the heat released upon cooling (Figure 8.14) as expected from

the data given by the manufacturer for RT21 (Table 7.6). However in terms of the actual values of the heat data in the corresponding intervals the results between heat released and heat stored are rather close given the scales of *y*-axes (Figure 8.14). Relatively large heat values are present in the HR data and attributed to the intervals between 20 °C and 21 °C (Figure 8.14). However, this relatively high heat values are compensated in HS data by the heat values attributed to the intervals between 21 °C and 22.5 °C degrees (Figure 8.14). This results in wider phase change range upon heating for RT21 but similar heat content once the heat is evaluated in the temperature ranges wider than the phase change range.

Furthermore, as the enthalpy-temperature curves are often necessary for the design and modeling of any TES systems based on PCMs these curves will also be presented as part of the characterisation data for each investigated PCM. Following this, the relevant enthalpy data upon cooling and heating (Cooling enthalpy – large sample and Heating enthalpy – large sample in Figure 8.12) were reused and given separately (Cooling enthalpy and Heating enthalpy in Figure 8.15). As explained is subsection 8.2.4 all enthalpy-temperature curves were normalised to 0 kJkg$^{-1}$ at 15 °C and evaluated between 15 °C and 30 °C (Figure 8.15). The reason this was done is that the manufacturer provides the data for the heat capacity of the RT21 evaluated between 15 °C and 30 °C (Table 7.6). Hence the same was done here. The difference (hysteresis) between the corresponding enthalpy curves (Cooling enthalpy and Heating enthalpy curves in Figure 8.15) is relatively small. It is mostly observed at the upper end temperatures of the phase change ranges (21 °C in the case of cooling and 22.5 °C in the case of heating enthalpy curve in Figure 8.15).

As explained in subsection 8.2.4 the originally recorded T-history data in the measurement with the larger samples (10 cooling and 10 heating cycles) were standardly averaged and the mean data obtained by averaging and the corresponding evaluations were presented in Figures 8.10-8.12 and also in Figures 8.13-8.15. The mean value of the total heat released upon cooling between 15 °C and 30 °C was 138 kJkg$^{-1}$. This value showed a deviation of ±3 % from the expected value (134 kJkg$^{-1}$) for the total heat released/stored in the temperature range between the 15 °C and 30 °C for the RT21 (Table 7.6). The mean value of the total heat stored upon heating

between 15 °C and 30 °C was 133 kJkg$^{-1}$. This value showed a deviation of ±0.8 % from the expected value for RT21 (Table 7.6). Given that the deviation values were less than ±10 % it was concluded that the PCM characterisation based on the advanced T-history method results in accurate and reliable data.
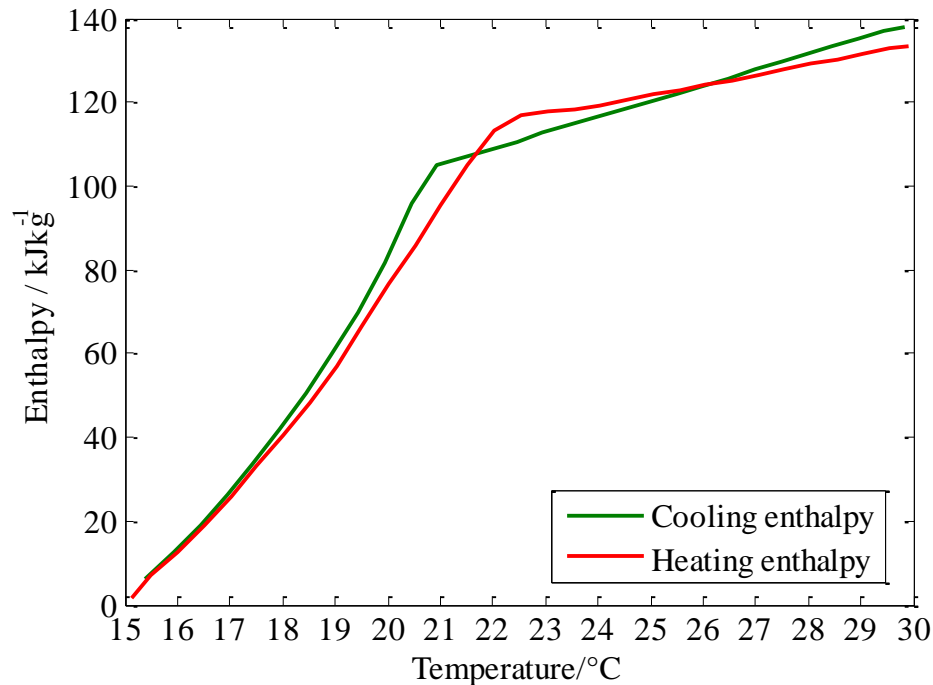


***Figure 8.15:*** *Enthalpy-temperature curves upon cooling and heating obtained from the advanced T-history characterisation of RT21 with the normalised enthalpy value of 0 kJkg$^{-1}$at 15 °C.*

In addition, the T-history curves obtained in each separate cooling and heating cycle were evaluated by using the functions described in section 8.1 and the total heat released/stored in the temperature range between the 15 °C and 30 °C for the RT21 calculated for each cycle. The results are shown in Figure 8.16.

It was evident that the heat content values from the first cycle are always higher than the values from the consecutive cycles. Moreover, the heat values decline with the increasing cycle number. The possible explanation for this could be the fact that before the first cycle a clean sensor is placed inside the sample. After the first cycle, the sensor undergoes at least one solidification process within the sample and it appears to be acting as a nucleating seed in the consecutive cycles. This means that it should be presumed that the first cycle within each measurement reflects the most natural

behavior of the PCM sample. Hence, the data obtained from the first cycle should be taken as the most accurate. The value of the total heat released upon cooling between 15 °C and 30 °C estimated from the data obtained in the first cooling cycle was 140 kJkg$^{-1}$ (Figure 8.16). This value showed a deviation of ±4.5 % from the expected value (134 kJkg$^{-1}$) for the RT21 (Table 7.6). The value of the total heat stored upon heating between 15 °C and 30 °C estimated from the data obtained in the first heating cycle was 137 kJkg$^{-1}$. This value showed a deviation of ±2.2 % from the expected value for RT21 (Table 7.6). Given these deviation values and the aforementioned explanation about the sensor acting as a nucleating seed it was concluded that the data from the first cycle should be used as the most accurate in all future PCM characterisation studies. It was decided that the PCMs in the future experiments will be subjected to the T-history program with 10 alternating cooling and heating cycles in order to test the stability of the investigated PCMs. However, only the data obtained in the first cycle should be taken as relevant for the most accurate PCM characterisation.
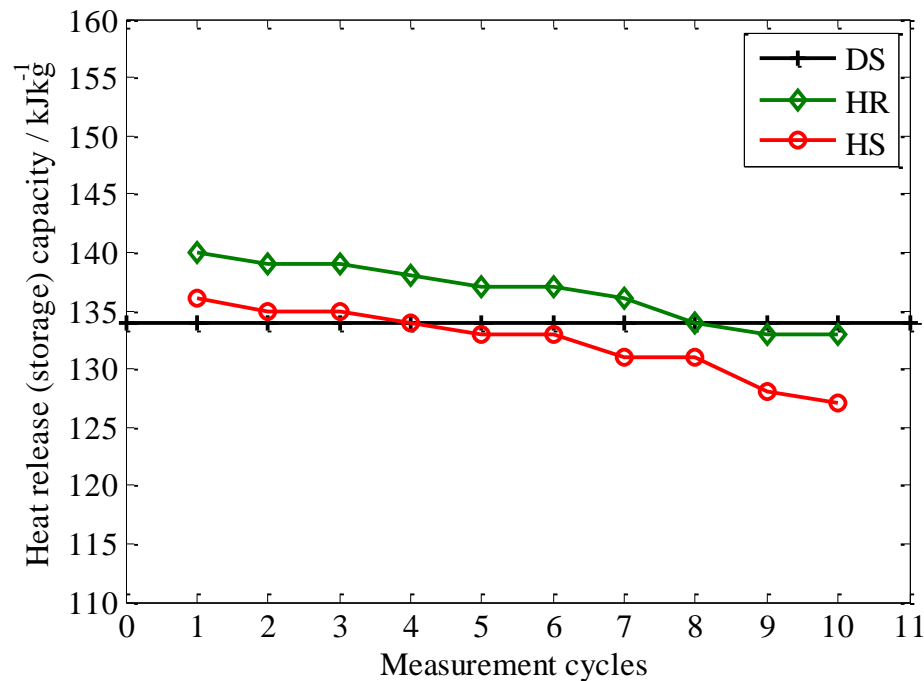


***Figure 8.16:*** *The total heat released/stored between 15 °C and 30 °C estimated from the corresponding cycle data from the advanced T-history based characterisation measurement of RT21 (DS – heat data sheet value, HR – heat released upon cooling, and HS – heat stored upon heating).*

.

Furthermore, as discussed in section 5.1 the calculated heat released/stored data are usually given as the heat released/stored per mass (Figure 8.16). Following the suggestions in the RAL procedure (RAL, 2010) it was decided that as part of the advanced T-history characterisation of PCMs these data should also be given in the form of the heat released/stored per volume. This could be done by multiplying the heat released/stored data per mass with the minimum PCM density in the temperature range of interest. Hence, the total heat released/stored per volume data are given for the investigated PCM RT21. The value of the total heat released per volume upon cooling between 15 °C and 30 °C was 107.8 kJl$^{-1}$. The value of the total heat stored per volume upon heating between 15 °C and 30 °C was 105.5 kJl$^{-1}$.

Finally, in order to test the damage criteria regarding enthalpy, temperature, and mass changes as explained in section 5.1 two more T-history measurements of RT21 were performed with the exactly same parameters as the measurement with large samples described in section 8.2.4. The data from different cycles were evaluated and the corresponding total heat released/stored values between 15 °C and 30 °C calculated. The calculated data showed the same trend as in Figure 8.15 confirming once more that the data obtained from the first cycle should be used as the most accurate. Moreover the changes in enthalpy, temperature and mass profiles of the PCM sample between measurements were estimated. Firstly, the maximum changes in the corresponding total enthalpies upon cooling and heating between 15 °C and 30 °C were ±1.5 % (<±10 %). Secondly, the maximum change in temperature profiles was ±0.2 °C (<±1 °C). Thirdly, the maximum change in mass of the PCM samples was ±0.5 % (<±3 %). Once the damage criteria established in section 5.1 were satisfied the RT21 characterisation was finally labeled as successful.

## 8.3.2 RT27 characterisation – results and discussion

The other material that was tested from Rubitherm's RT series was RT27 (Rubitherm GmbH, Berlin, Germany). The material specifications for the RT27 are given in Table 8.1.

| Property | Value |
|---|---|
| Melting area | 25-28 °C |
| Congealing area | 28-25 °C |
| Typical phase change temperature | 27 °C |
| Heat storage capacity (15 to 30 °C) | 184 kJkg$^{-1}$ |
| Specific heat capacity | 2 kJkg$^{-1}$K$^{-1}$ |
| Density solid (at 15 °C) | 0.88 kgl$^{-1}$ |
| Density liquid (at 40 °C) | 0.76 kgl$^{-1}$ |
| Thermal conductivity | 0.2 Wm$^{-1}$K$^{-1}$ |

***Table 8.1:*** *Material properties of organic paraffin RT27.*

The characterisation measurement of RT27 using the advanced T-history method was performed with the almost identical parameters as in the RT21 measurement with the larger samples described in section 8.2.4 except that different PCM (RT27) was investigated in this measurement. Once more the PCM and distilled water, placed in the 430 mm long test tubes insulated by 6 mm thick tape, were subjected to the alternating cooling and heating 6 h long cycles. Given the expected phase change range of the material the cycles were operated between 14 and 37 °C. The respective masses of the sample ($m_p$) and reference ($m_w$) were 39.2 g and 47.5 g. The sensors, their placement, and the instrumentation and data acquisition parameters were the same as in the MA100BF103A measurement described in subsection 8.2.1. As before, prior to the T-history measurement the proper calibration measurement with 1 °C step temperature program from 10 °C to 39 °C inside the chamber was performed to assure the accuracy of the sensors used in the T-history measurement. The calibration data and the recorded voltage data from the T-history measurement were used as described in section 7.2.4.1 to obtain the relevant T-history curves (Figure 8.17). The presented curves are from the first cooling and heating cycle due to the reasons explained in subsection 8.3.1.

According to the T-history curves from the cooling cycle (Figure 8.17a) the typical phase change temperature of RT27 is 27 °C. This is in a perfect agreement with the RT27 specifications given by the manufacturer (Table 8.1) and the results reported by Kravvaritis et al. (2011) for the same material. In the case of RT27 no subcooling was detected (PCM in Figure 8.17a). The manufacturer also does not report any degree of subcooling for RT27 (Rubitherm GmbH, Berlin, Germany).
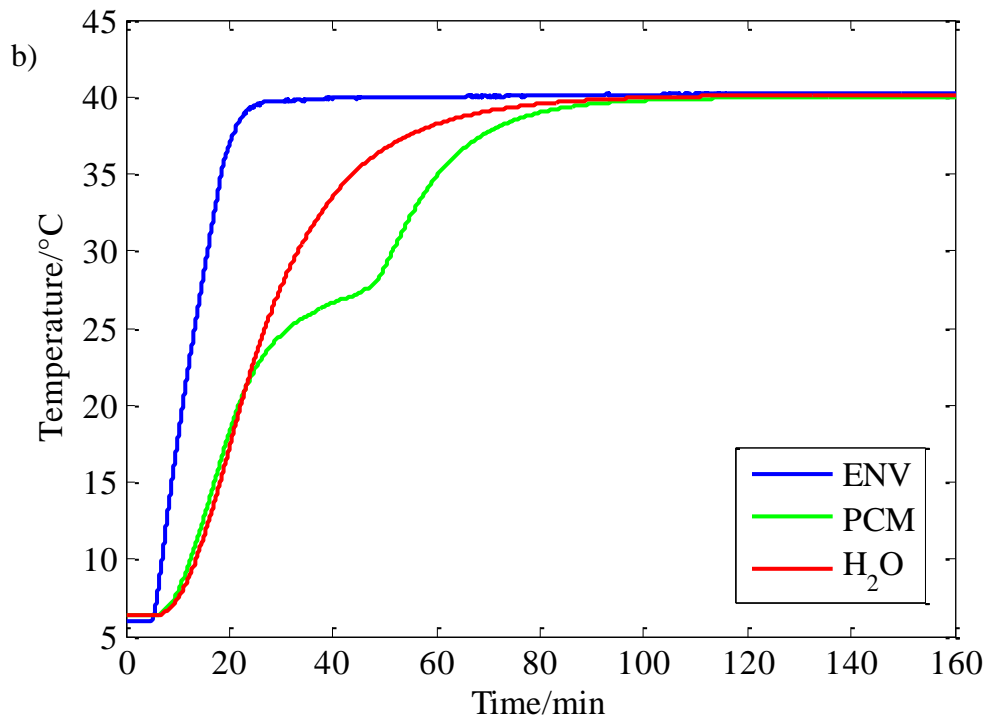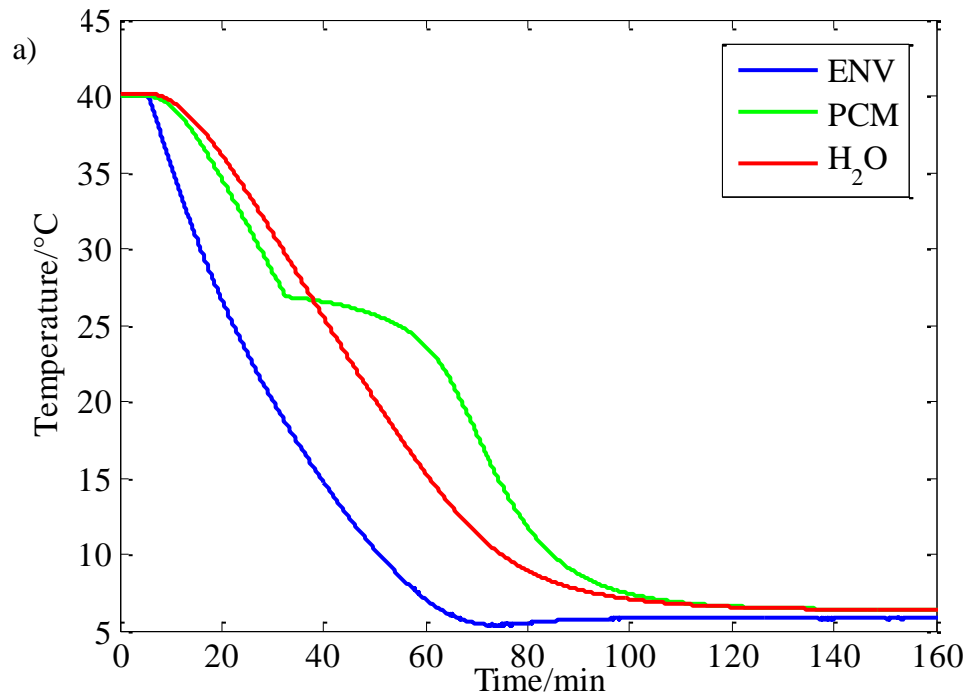
***Figure 8.17:*** *Cooling (a) and heating (b) cycles in the advanced T-history characterisation of RT27 (ENV – environmental temperature, PCM – temperature of the PCM sample, H₂O – temperature of the reference sample).*

As for the RT21, the results obtained upon heating are also presented (Figure 8.17b). According to the relevant T-history curve from the heating cycle (PCM in Figure 8.17b) the typical phase change temperature observed upon heating was 27.2 °C.

As in the case of RT21 characterisation, the heat released/stored in given temperature intervals data for RT27 upon both cooling and heating are also presented. The T-history curves (Figure 8.17) were evaluated in the 15 °C to 30 °C range using the evaluation technique described in section 8.1 and the temperature evaluation interval of 0.5 °C to obtain the heat released/stored data in given temperature intervals upon both cooling and heating (Figure 8.18).

The heat released upon cooling and heat stored upon heating values in given temperature intervals (HR and HS in Figure 8.18) were calculated from the respective ENV, PCM, and $H_2O$ T-history curves (Figure 8.17a and 8.17b). According to the HR data in Figure 8.18 the congealing area of RT27 is in the range from 25 °C to 27.5 °C. This is for a 0.5 °C smaller than the congealing range reported by the manufacturer (Table 8.1). However it was concluded that the observed congealing range could be more accurate given the precision and accuracy of the sensors as well as the precision of the data evaluation procedure used in the advanced T-history method. According to the HS data in Figure 8.18 the melting area of RT27 is in the slightly wider range from 25 °C to 28 °C and in perfect agreement with the data reported by the manufacturer (Table 8.1). The HR and HS data show very similar behaviour in terms of the heat data values in the corresponding intervals given the scales of $y$-axes (Figure 8.18). The slightly higher values in HR data attributed to the intervals between 26 °C and 27 °C are compensated by the higher values in HS data attributed to the intervals between 27 °C and 28 °C degrees (Figure 8.18)

The aforementioned observations are due to the marginally wider phase change range upon heating for RT27. However, the total heat contents in the case of cooling and heating are expected to be very similar once the heat is evaluated in the temperature ranges wider than the phase change range.
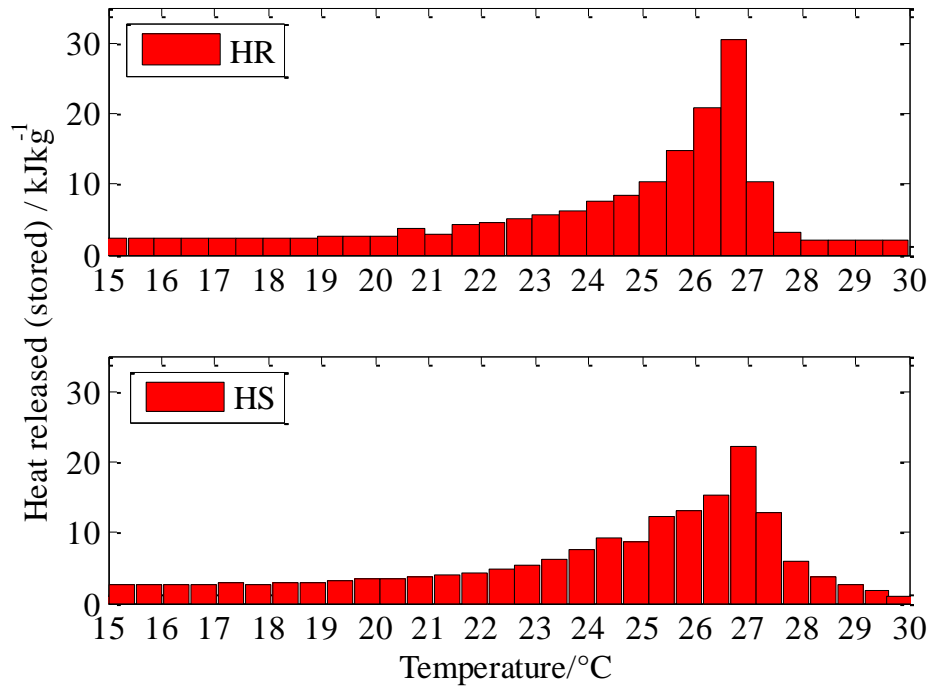
**Figure 8.18:** *Heat released (stored) data obtained from the advanced T-history characterisation of RT27 (HR – heat released upon cooling, HS – heat stored upon heating).*

As for the RT21, the relevant enthalpy data upon cooling and heating were evaluated from the heat released/stored data in given temperature intervals (Figure 8.18) and presented in Figure 8.19. Since the manufacturer provides the data for the heat capacity of the RT27 evaluated between 15 °C and 30 °C (Table 8.1) the enthalpy-temperature curves were normalised to 0 kJkg$^{-1}$ at 15 °C and evaluated between 15 °C and 30 °C (Cooling enthalpy and Heating enthalpy in Figure 8.19). The difference (hysteresis) between the corresponding enthalpy curves (Cooling enthalpy and Heating enthalpy in Figure 8.15) is very small in terms of both temperature and enthalpy values labeling the RT27 as a good quality PCM with no effects like subcooling or hysteresis. The value of the total heat released upon cooling between 15 °C and 30 °C for the RT27 was 175 kJkg$^{-1}$. This value showed a deviation of ±4.9 % from the expected value (184 kJkg$^{-1}$) for the total heat released/stored in the temperature range between the 15 °C and 30 °C for the RT27 (Table 8.1). The value of the total heat stored upon heating between 15 °C and 30 °C was 179 kJkg$^{-1}$. This value showed a deviation of ±2.7 % from the expected value for RT27 (Table 8.1). Given that the deviation values

were less than ±10 % it was once more confirmed that the PCM characterisation based on the advanced T-history method results in accurate and reliable data.
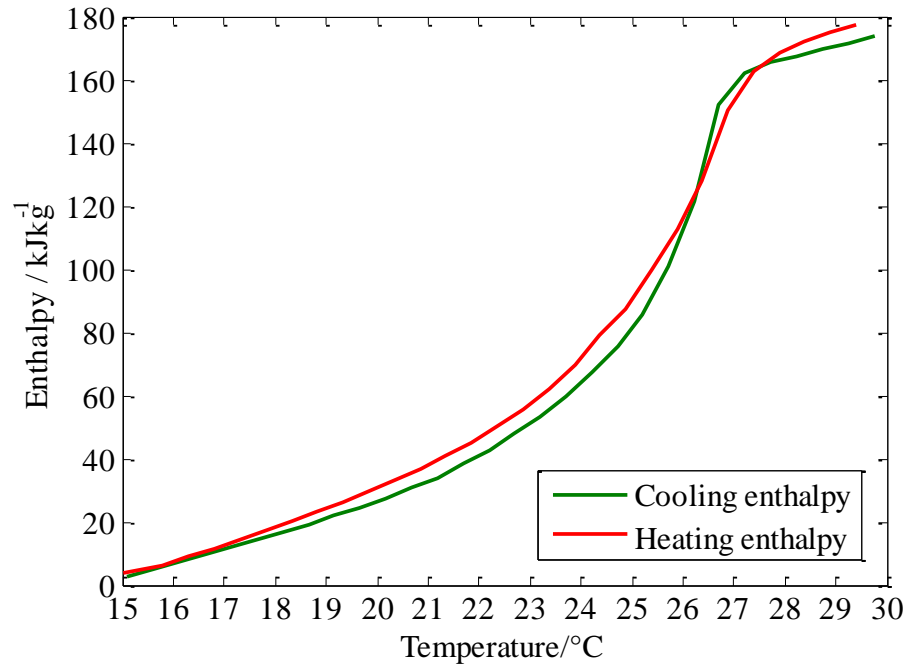


***Figure 8.19:*** *Enthalpy-temperature curves upon cooling and heating obtained from the advanced T-history characterisation of RT27 with the normalised enthalpy value of 0 kJkg⁻¹ at 15 °C.*

As in the case of RT21 the heat released/stored per volume data were also estimated for RT27. The value of the total heat released per volume upon cooling between 15 °C and 30 °C was 133 kJl⁻¹. The value of the total heat stored per volume upon heating between 15 °C and 30 °C was 136 kJl⁻¹.

Finally, in order to test the damage criteria regarding enthalpy, temperature, and mass changes as explained in section 5.1 two additional T-history measurements of RT27 were performed with the exactly same parameters as in the measurement previously described in this subsection. The changes in enthalpy, temperature and mass profiles of the PCM sample between measurements were estimated. Firstly, the maximum changes in the corresponding total enthalpies upon cooling and heating between 15 °C and 30 °C were ±4.2 % (<±10 %). Secondly, the maximum change in temperature profiles was ±0.2 °C (<±1 °C). Thirdly, the maximum change in mass of

the PCM samples was ±0.3 % (<±3 %). Once the damage criteria established in section 5.1 were satisfied the RT27 characterisation was labeled as successful.

# 8.4 Investigation studies of PT bio-organic series

Once the advanced T-history method was successfully validated in the PCM characterisation measurements of the well-known materials from the Rubitherm's organic RT series (Rubitherm GmbH, Berlin, Germany), this method could also be used for testing of other relatively unknown PCMs. The decision was made to test the PCMs from the PT bio-organic series produced by Entropy Solutions (Entropy Solutions Inc., Plymouth, Minnesota). These materials are relatively new on the PCM market and untested by researchers. According to the manufacturer the biggest advantages of these materials is their natural vegetable based origin resulting in 100 % renewable PCMs with high latent heat contents (Entropy Solutions Inc., Plymouth, Minnesota) making them rather suitable for various PCM applications. It was decided that three bio-organic materials from the PT series (Entropy Solutions Inc., Plymouth, Minnesota) will be tested, PT20, PT27, and PT28. These materials were selected based on their expected phase change temperature ranges. Namely, these materials appeared to be very suitable for building applications which were, as mentioned in the introductory chapters, of the most interest for this research.

## 8.4.1 PT20 characterisation – results and discussion

The first material that was tested from the PT series was PT20 (Entropy Solutions Inc., Plymouth, Minnesota). The material specifications of PT20 are given in Table 8.2.

| Property | Value |
|---|---|
| Typical phase change temperature | 20 °C |
| Heat storage capacity | 180 kJkg$^{-1}$ |
| Specific heat capacity (solid) | 2.59 kJkg$^{-1}$K$^{-1}$ |
| Specific heat capacity (liquid) | 2.89 kJkg$^{-1}$K$^{-1}$ |
| Density | 0.86 kgl$^{-1}$ |

**Table 8.2:** *Material properties of bio-organic PCM PT20.*

The characterisation measurement of PT20 using the advanced T-history method was performed with almost the same parameters as the RT21 and RT27 characterisation measurements. The PCM and distilled water, placed in the 430 mm long test tubes insulated by 6 mm thick tape, were subjected to the alternating cooling and heating 6 h long cycles. Given the relative novelty of the PT series the cycles were operated in wider temperature range than in the case of RT PCMs. The operating temperature range was between 8 °C and 40 °C. The respective masses of the sample ($m_p$) and reference ($m_w$) were 42.6 g and 47.4 g. As before, prior to the T-history measurement, the proper calibration measurement was performed with 1 °C step temperature program but now from 6 °C to 41 °C since the operating range was between 8 °C and 40 °C. The calibration of sensors was performed as described in subsection 7.2.4.1. Given the width of the operating temperature range the variable *NUMBER_OF_TEMP_POINTS* in the calibration script (see APPENDIX A3) had greater value than in any previous experiment. This resulted in the slightly higher maximum absolute error of 0.46 °C for the temperature sensors than before (< 0.3 °C). However this value did not exceed the ±0.5 °C temperature validation criterion for the advanced T-history measurements. Hence, the calibration data could be used to obtain the T-history curves. Once this was performed, the difference between the cooling and heating T-history curves was evident. It was assumed that it was due to the temperature gradients formed inside the investigated PCM sample. Therefore another T-history characterisation measurement of PT20 was performed with the only difference that the 10 mm thick insulating tape was used to wrap the test tubes. The obtained T-history results (Figure 8.20) were almost identical as in the 6 mm thick insulation case leading to the conclusion that the hysteresis between the cooling and heating T-history curves is the real property of the investigated PT20 PCM.

According to the T-history curves from the cooling cycle (Figure 8.20a) the typical phase change temperature of PT20 is 18.9 °C. This value deviates from the expected value of 20 °C (Table 8.2). Subcooling was not observed for PT20 (PCM in Figure 8.20a). The manufacturer also does not report any degree of subcooling for PT20 (Entropy Solutions Inc., Plymouth, Minnesota). The results obtained upon heating are also presented (Figure 8.20b). According to the PCM T-history curve from

the heating cycle (Figure 8.20b) the typical phase change temperature is 19.9 °C which is in a good agreement with the value reported by the manufacturer (Table 8.2). Hence, it was presumed that the manufacturer reported the PT20 characterisation data obtained only upon heating.

As in the case of RT series characterisation measurement, the heat released/stored in given temperature intervals data for PT20 upon both cooling and heating are also presented. The T-history curves (Figure 8.20) were evaluated in the 15 °C to 30 °C range using the evaluation technique described in section 8.1 and the temperature evaluation interval of 0.5 °C to obtain the heat released/stored data in given temperature intervals upon both cooling and heating (Figure 8.21). The reason 15 °C to 30 °C range was selected is that the same range was used in the case of RT series PCMs. The manufacturer does not provide any information regarding the temperature ranges used for the evaluation of heat capacity data of PT20 (Entropy Solutions Inc., Plymouth, Minnesota). Hence the same range as in the case of RT PCMs was used to enable some comparison between the respective PCMs.

The heat released upon cooling and heat stored upon heating values in given temperature intervals (HR and HS in Figure 8.21) were calculated from the respective ENV, PCM, and $H_2O$ T-history curves (Figure 8.20a and 8.20b). According to the HR data in Figure 8.21 the congealing area of PT20 is in the range from 18 °C to 20 °C. The melting area of PT20 is marginally shifted in comparison to the congealing area towards the 18.5 °C to 20.5 °C (Figure 8.21). The HR and HS data show similar behaviour to a certain degree in terms of the heat data values in the corresponding intervals given the scales of *y*-axes (Figure 8.21). The heat value in the interval between 18.5 °C and 19 °C in HR data is evidently larger than in any interval in HS data (Figure 8.21). This confirms that the hysteresis between the cooling and heating data in the case of PT20 is small but still real and existent.
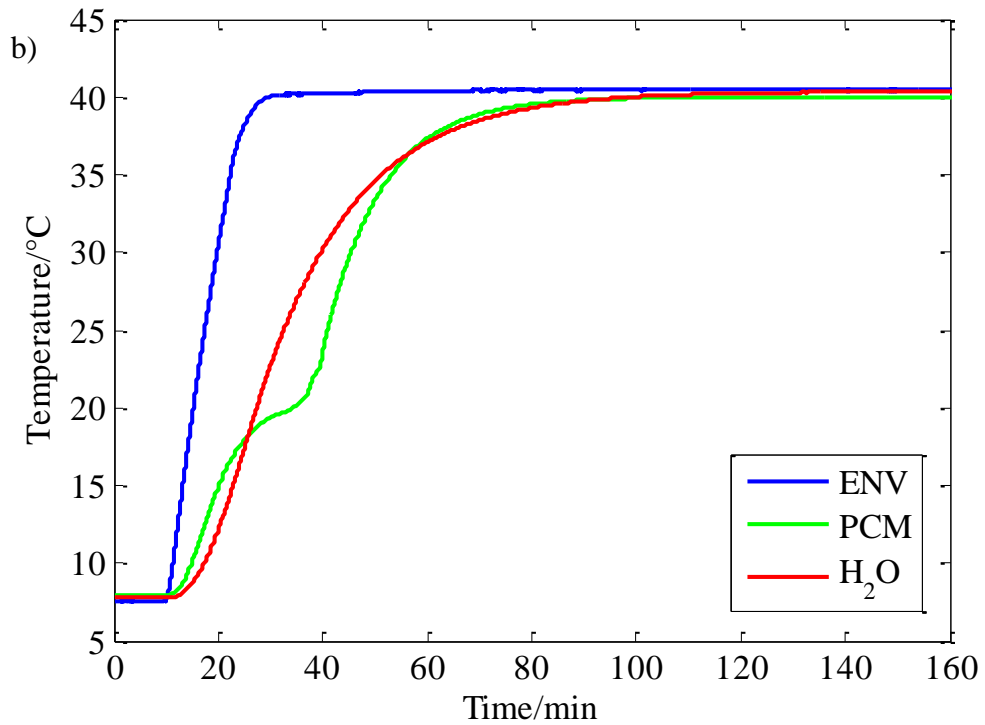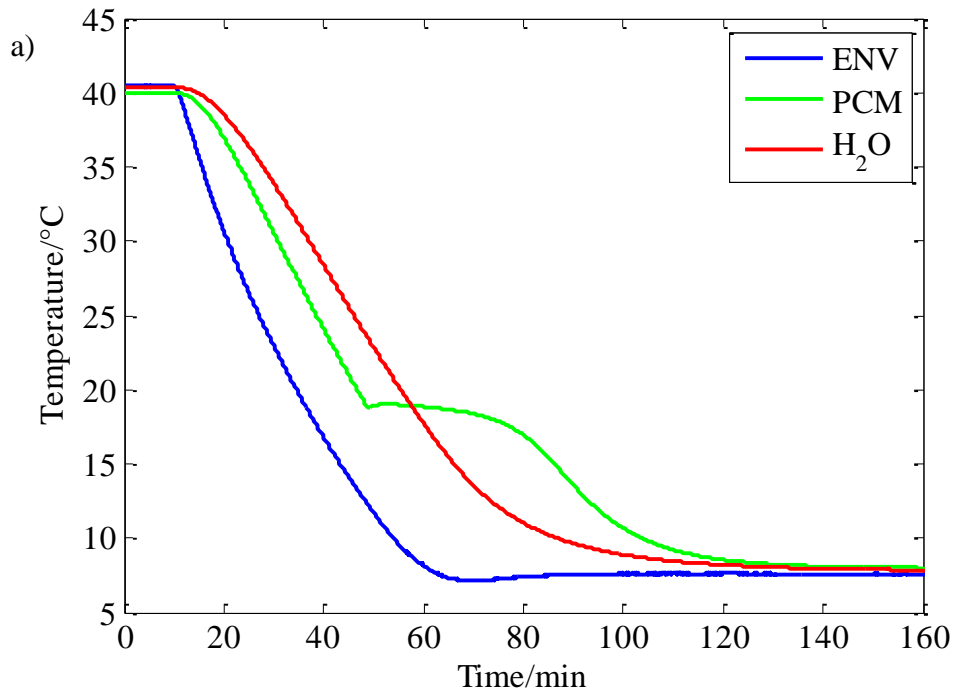
***Figure 8.20:*** *Cooling (a) and heating (b) cycles in the advanced T-history characterisation of PT20 (ENV – environmental temperature, PCM – temperature of the PCM sample, H₂O – temperature of the reference sample).*
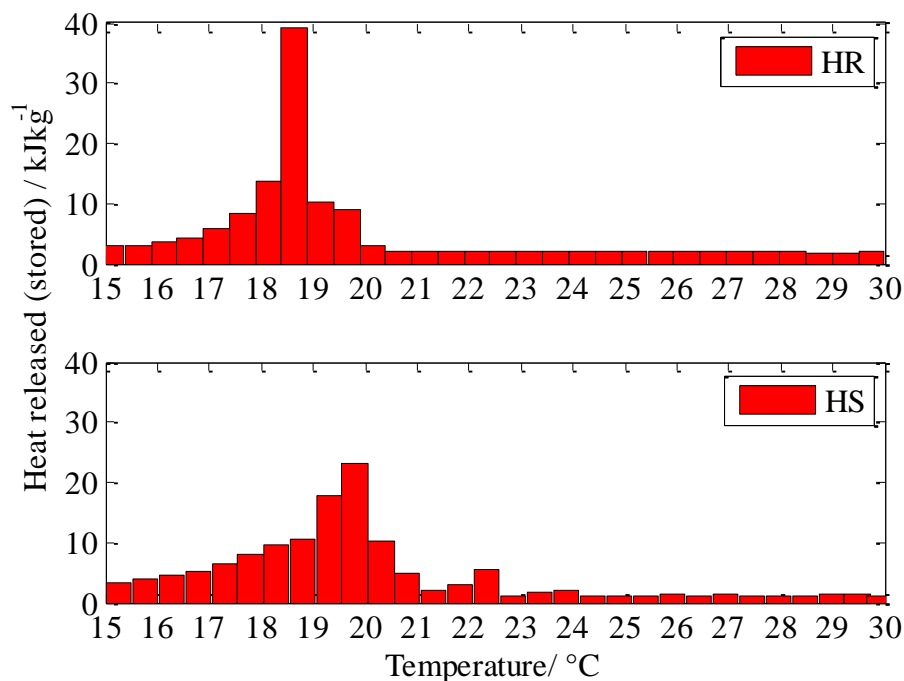
***Figure 8.21:*** *Heat released (stored) data obtained from the advanced T-history characterisation of PT20 (HR – heat released upon cooling, HS – heat stored upon heating).*

As in the case of RT21 and RT27 characterisations, the relevant enthalpy data upon cooling and heating were evaluated from the heat released/stored data in given temperature intervals (Figure 8.21) and presented in Figure 8.22. The enthalpy-temperature curves were normalised to 0 kJkg$^{-1}$ at 15 °C and evaluated between 15 °C and 30 °C (Cooling enthalpy and Heating enthalpy in Figure 8.22). The difference (hysteresis) between the corresponding enthalpy curves (Cooling enthalpy and Heating enthalpy in Figure 8.22) is evident and mainly due to the difference in temperature values given the earlier observed differences in the congealing and melting ranges of PT20. The value of the total heat released upon cooling between 15 °C and 30 °C for the PT20 was 140 kJkg$^{-1}$ while the value of the total heat stored upon heating in the same range was 138 kJkg$^{-1}$. These values were not close to the value of 180 kJkg$^{-1}$ (Table 8.2). However since the manufacturer does not provide any information regarding the temperature ranges used for the evaluation of heat capacity data of PT20 (Entropy Solutions Inc., Plymouth, Minnesota) those values cannot be compared. On the other hand the total heat released/stored data between 15 °C and 30 °C for the PT20

were almost identical to the same data reported for RT21. This showed that the PT20 could be used as the concurrent material to the RT21 in terms of both heat content and phase change temperature range. The advantage of PT20 over RT21 would be its bio origin and 100 % renewability.
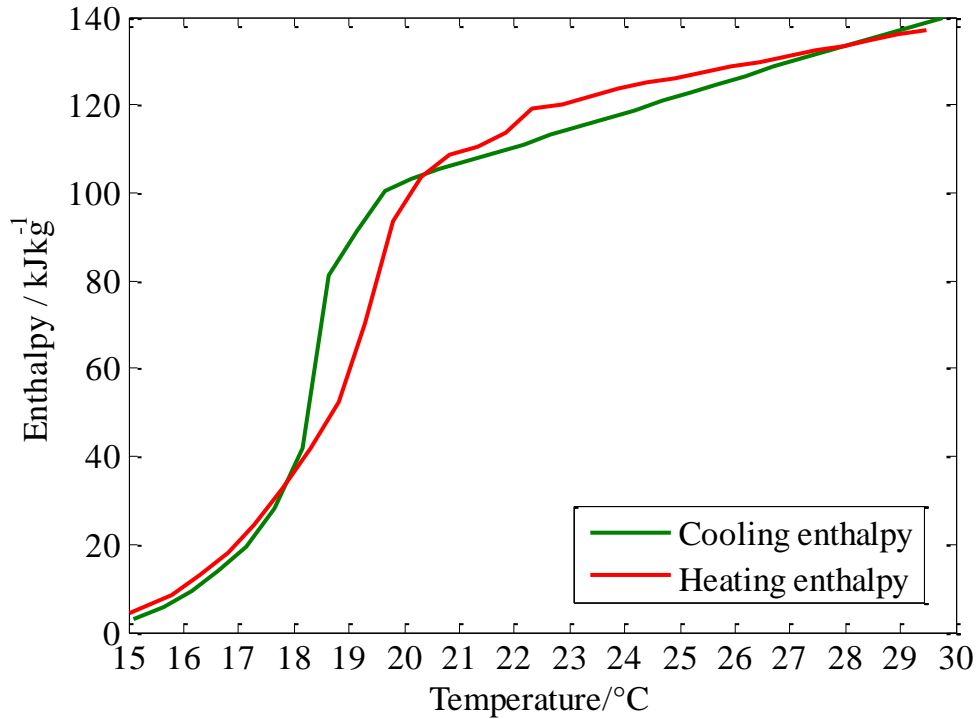


***Figure 8.22:*** *Enthalpy-temperature curves upon cooling and heating obtained from the advanced T-history characterisation of PT20 with the normalised enthalpy value of 0 kJkg⁻¹ at 15 °C.*

As in the case of previous characterisation reports the heat released/stored per volume data were also estimated for PT20. The value of the total heat released per volume upon cooling between 15 °C and 30 °C was 120.4 kJl⁻¹. The value of the total heat stored per volume upon heating between 15 °C and 30 °C was 118.7 kJl⁻¹.

Finally, in order to test the damage criteria regarding enthalpy, temperature, and mass changes two additional T-history measurements of PT20 with the insulation thickness of 10 mm were performed. The maximum changes in the corresponding total enthalpies upon cooling and heating between 15 °C and 30 °C were ±3 % (<±10 %). The maximum change in temperature profiles was ±0.3 °C (<±1 °C). Thirdly, the

maximum change in mass of the PCM samples was ±0.2 % (<±3 %). Once the damage criteria were checked the PT20 characterisation was completed.

## 8.4.2 PT27 characterisation – results and discussion

The second material that was tested from the PT series was PT27 (Entropy Solutions Inc., Plymouth, Minnesota). The material specifications of PT27 are given in Table 8.3.

| Property | Value |
|---|---|
| Typical phase change temperature | 27 °C |
| Heat storage capacity | 200 kJkg$^{-1}$ |
| Specific heat capacity (solid) | 2.46 kJkg$^{-1}$K$^{-1}$ |
| Specific heat capacity (liquid) | 2.63 kJkg$^{-1}$K$^{-1}$ |
| Density | 0.86 kgl$^{-1}$ |

*Table 8.3:* *Material properties of bio-organic PCM PT27.*

The characterisation measurement of PT27 using the advanced T-history method was performed with minor changes in regard to the PT20 characterisation. The PCM and distilled water, placed in the 430 mm long test tubes insulated by 10 mm thick tape, were subjected to the alternating cooling and heating 6 h long cycles between 8 °C and 40 °C. The respective masses of the sample ($m_p$) and reference ($m_w$) were 42.1 g and 47.4 g. As before, prior to the T-history measurement, the proper calibration measurement was performed with 1 °C step temperature program from 6 °C to 41 °C. Hence, the calibration data were used to obtain the T-history curves (Figure 8.23).

According to the T-history curves from the cooling cycle (Figure 8.23a) the typical phase change temperature of PT27 is 24 °C. This value deviates from the expected value of 27 °C (Table 8.2). Small degree of subcooling (0.5 °C) was also observed between the phase change temperature and the nucleation temperature (23.5 °C). The manufacturer does not report any degree of subcooling for PT27 (Entropy Solutions Inc., Plymouth, Minnesota). According to the PCM T-history curve from the heating cycle (Figure 8.23b) the typical phase change temperature is 25.5 °C which is in a better agreement with the value of 27 °C (Table 8.2). Hence, it was once more presumed that the manufacturer reported the PT27 characterisation data obtained only upon heating.
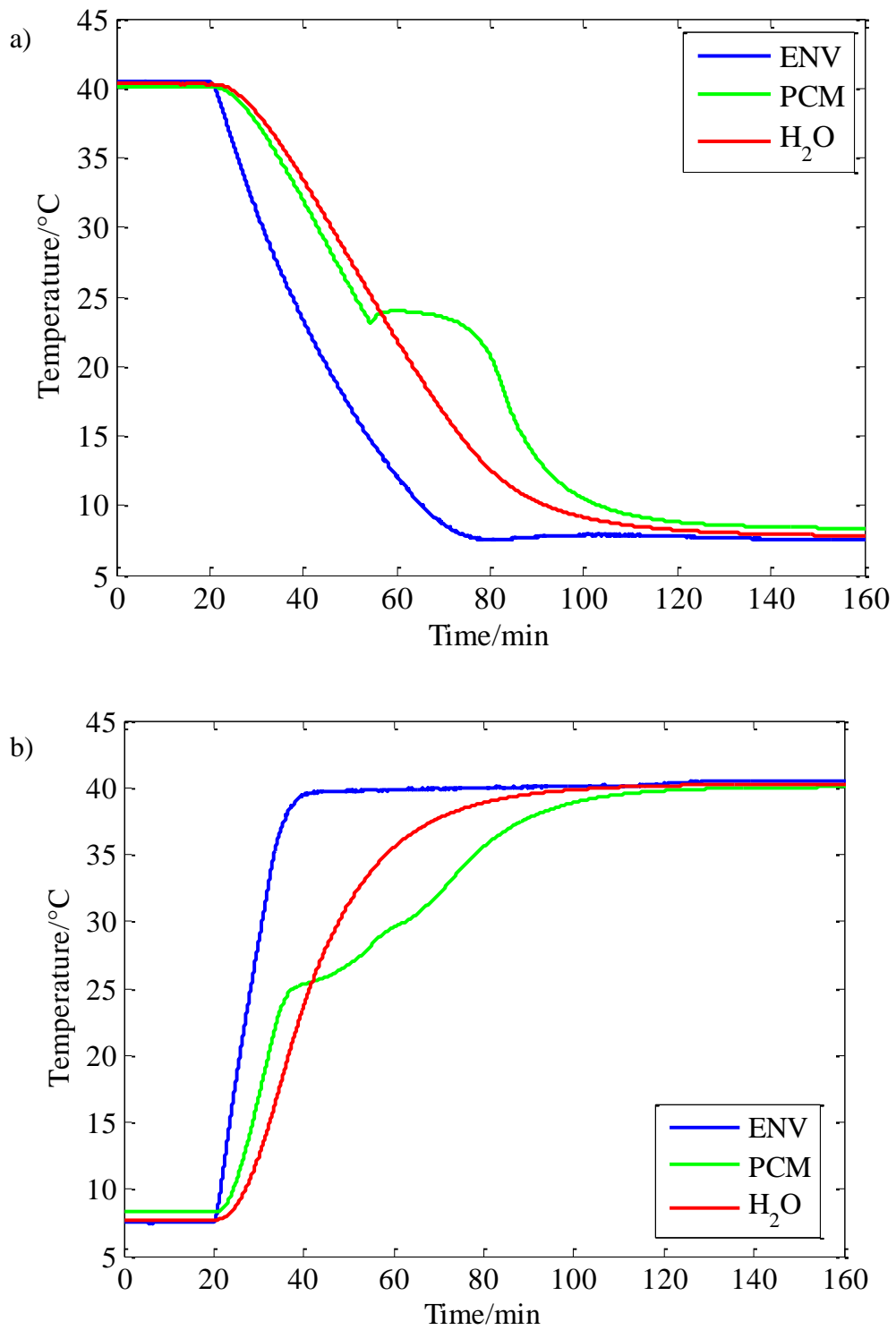
**Figure 8.23:** *Cooling (a) and heating (b) cycles in the advanced T-history characterisation of PT27 (ENV – environmental temperature, PCM – temperature of the PCM sample, H₂O – temperature of the reference sample).*

As in previous characterisation measurements, the heat released/stored in given temperature intervals data for PT27 upon both cooling and heating are also presented. The T-history curves (Figure 8.23) were evaluated in the 15 °C to 30 °C range with the temperature evaluation interval of 0.5 °C to obtain the heat released/stored data in given temperature intervals upon both cooling and heating (Figure 8.24).
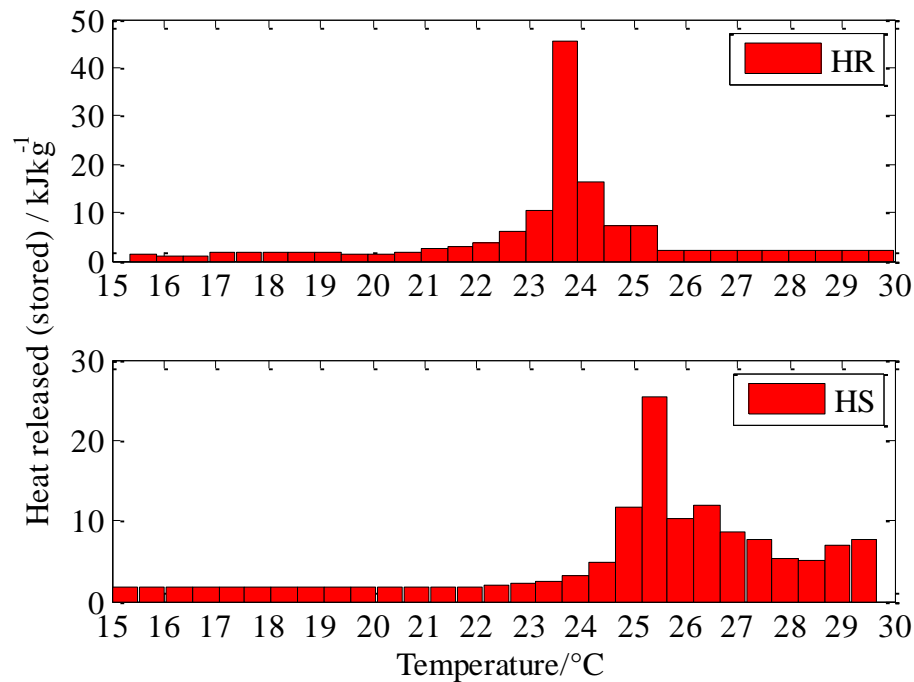


***Figure 8.24:*** *Heat released (stored) data obtained from the advanced T-history characterisation of PT27 (HR – heat released upon cooling, HS – heat stored upon heating).*

The heat released upon cooling and heat stored upon heating values in given temperature intervals (HR and HS in Figure 8.24) were calculated from the respective ENV, PCM, and $H_2O$ T-history curves (Figure 8.23a and 8.23b). According to the HR data in Figure 8.24 the congealing area of PT27 is in the range from 23.5 °C to 24.5 °C. The melting area of PT27 is wider and shifted towards the 24.5 °C to 27.5 °C range or even beyond that (Figure 8.24). These values show an evident and real hysteresis between the cooling and heating data in the case of PT27. The hysteresis is not reported by the manufacturer (Entropy Solutions Inc., Plymouth, Minnesota). This and the lack of the subcooling report confirmed that the manufacturer gave the PT27 data obtained only upon heating. As discussed in section 5.1 it is essential for the TES system

development that the PCM characterisation data upon both heating and cooling are reported along with any existing hysteresis between the data.

The enthalpy data upon cooling and heating were evaluated from the heat released/stored data in given temperature intervals (Figure 8.24) and presented as Cooling enthalpy and Heating enthalpy in Figure 8.25.
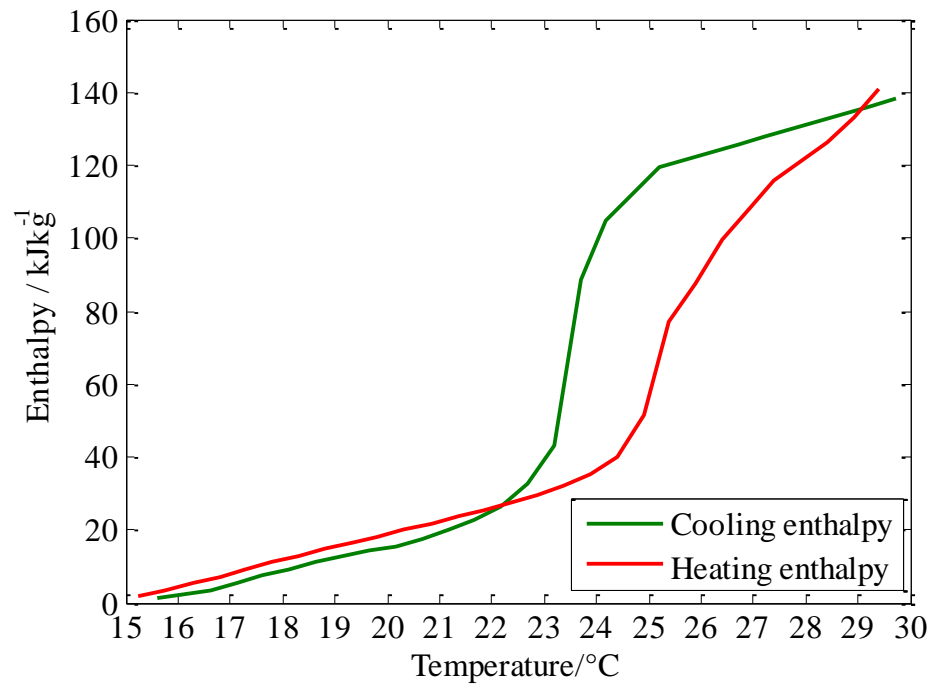


***Figure 8.25:*** *Enthalpy-temperature curves upon cooling and heating obtained from the advanced T-history characterisation of PT27 with the normalised enthalpy value of 0 kJkg<sup>-1</sup>at 15 °C.*

The difference (hysteresis) between the corresponding enthalpy curves (Cooling enthalpy and Heating enthalpy in Figure 8.25) is rather significant and mainly due to the difference in temperature values given the differences in the congealing and melting ranges of PT27. The value of the total heat released upon cooling between 15 °C and 30 °C for the PT27 was 140 kJkg$^{-1}$ while the value of the total heat stored upon heating in the same range was 141 kJkg$^{-1}$.These values were not close to the value of 200 kJkg$^{-1}$ (Table 8.3). However since the information regarding the temperature ranges used for the evaluation of the heat capacity data of PT27 are not provided (Table 8.3) the heat values cannot be compared. The total heat data are only marginally higher than the ones reported for PT20. On the other hand, the total heat released/stored data

between 15 °C and 30 °C for the PT27 are smaller than in the case of the corresponding RT material (RT27) making RT27 the more competitive PCM.

The heat released/stored per volume data were also estimated for PT27. The value of the total heat released per volume upon cooling between 15 °C and 30 °C was 120.4 kJl$^{-1}$. The value of the total heat stored per volume upon heating between 15 °C and 30 °C was 121.3 kJl$^{-1}$.

Finally, in order to test the damage criteria regarding enthalpy, temperature, and mass changes two additional T-history measurements of PT27 were performed. The maximum changes in the corresponding total enthalpies upon cooling and heating between 15 °C and 30 °C were ±3.4 % (<±10 %). The maximum change in temperature profiles was ±0.5 °C (<±1 °C). Thirdly, the maximum change in mass of the PCM samples was ±0.2 % (<±3 %). Once the damage criteria were checked the PT27 characterisation was finished.

## 8.4.3 PT28 characterisation – results and discussion

The last material that was tested from the PT series was PT28 (Entropy Solutions Inc., Plymouth, Minnesota). The material specifications of PT28 are given in Table 8.4.

| Property | Value |
|---|---|
| Typical phase change temperature | 29 °C |
| Heat storage capacity | 205 kJkg$^{-1}$ |
| Specific heat capacity (solid) | 2.34 kJkg$^{-1}$K$^{-1}$ |
| Specific heat capacity (liquid) | 2.54 kJkg$^{-1}$K$^{-1}$ |
| Density | 0.86 kgl$^{-1}$ |

*Table 8.4: Material properties of bio-organic PCM PT28.*

The characterisation measurement of PT28 using the advanced T-history method was performed in the same manner as the PT27 characterisation. The PCM and distilled water, placed in the 430 mm long test tubes insulated by 10 mm thick tape, were subjected to the alternating cooling and heating 6 h long cycles between 8 °C and 40 °C. The respective masses of the sample ($m_p$) and reference ($m_w$) were 42.2 g and 47.4 g. As before, prior to the T-history measurement, the proper calibration measurement was performed with 1 °C step temperature program from 6 °C to 41 °C. Hence, the calibration data were used to obtain the T-history curves (Figure 8.26).
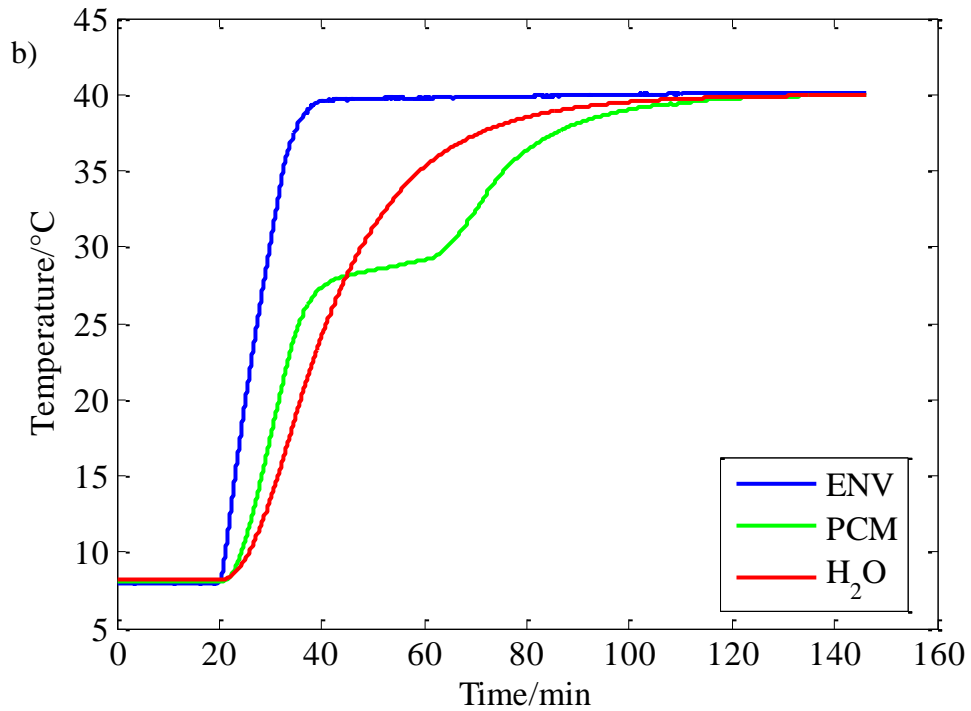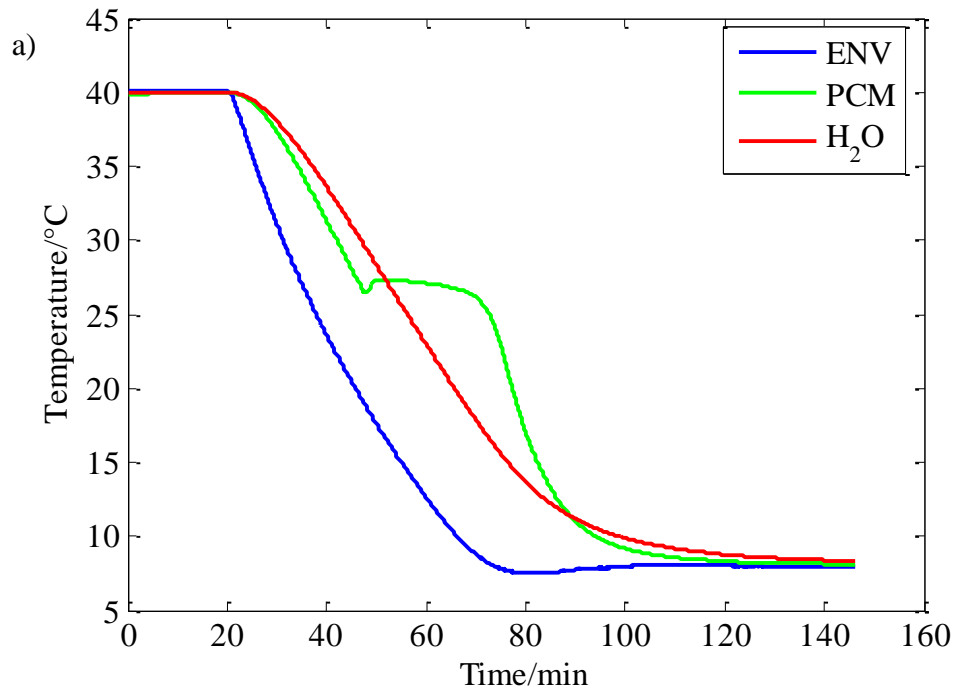
**Figure 8.26:** *Cooling (a) and heating (b) cycles in the advanced T-history characterisation of PT28 (ENV – environmental temperature, PCM – temperature of the PCM sample, H₂O – temperature of the reference sample).*

According to the T-history curves from the cooling cycle (Figure 8.26a) the typical phase change temperature of PT28 is 27.3 °C. This value deviates from the expected value of 29 °C (Table 8.3). Small degree of subcooling (0.4 °C) was also observed between the phase change temperature and the nucleation temperature (26.9 °C). The manufacturer does not report any degree of subcooling for PT28 (Entropy Solutions Inc., Plymouth, Minnesota). According to the PCM T-history curve from the heating cycle (Figure 8.26b) the typical phase change temperature is 28.5 °C which is close to the value of 29 °C (Table 8.3). Given these values it was again confirmed the manufacturer (Entropy Solutions Inc., Plymouth, Minnesota) reports only the PCM characterisation data obtained upon heating.

The heat released/stored data in given temperature intervals for PT28 upon both cooling and heating are also presented. The T-history curves (Figure 8.26) were evaluated in the 15 °C to 30 °C range with the temperature evaluation interval of 0.5 °C to obtain the heat released/stored data in given temperature intervals upon both cooling and heating (Figure 8.27).
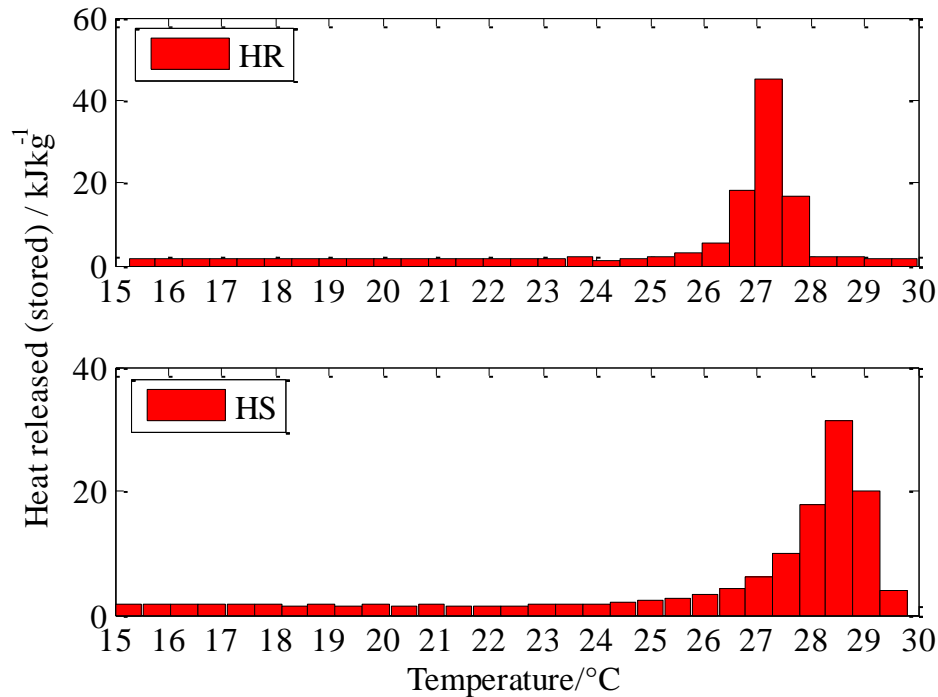


*Figure 8.27: Heat released (stored) data obtained from the advanced T-history characterisation of PT28 (HR – heat released upon cooling, HS – heat stored upon heating).*

The heat released upon cooling and heat stored upon heating values in given temperature intervals (HR and HS in Figure 8.27) were calculated based on the ENV, PCM, and $H_2O$ T-history curves (Figure 8.26a and 8.26b). According to the HR data in Figure 8.27 the congealing area of PT28 is in the range from 26.5 °C to 28 °C. The melting area of PT28 is wider and shifted towards the 27.5 °C to 29.5 °C range (Figure 8.27). As in the case of PT27 the hysteresis between the cooling and heating data, although not reported by the manufacturer (Entropy Solutions Inc., Plymouth, Minnesota), is real.

The enthalpy data upon cooling and heating were evaluated from the heat released/stored data in given temperature intervals (Figure 8.27) and presented as Cooling enthalpy and Heating enthalpy in Figure 8.28.
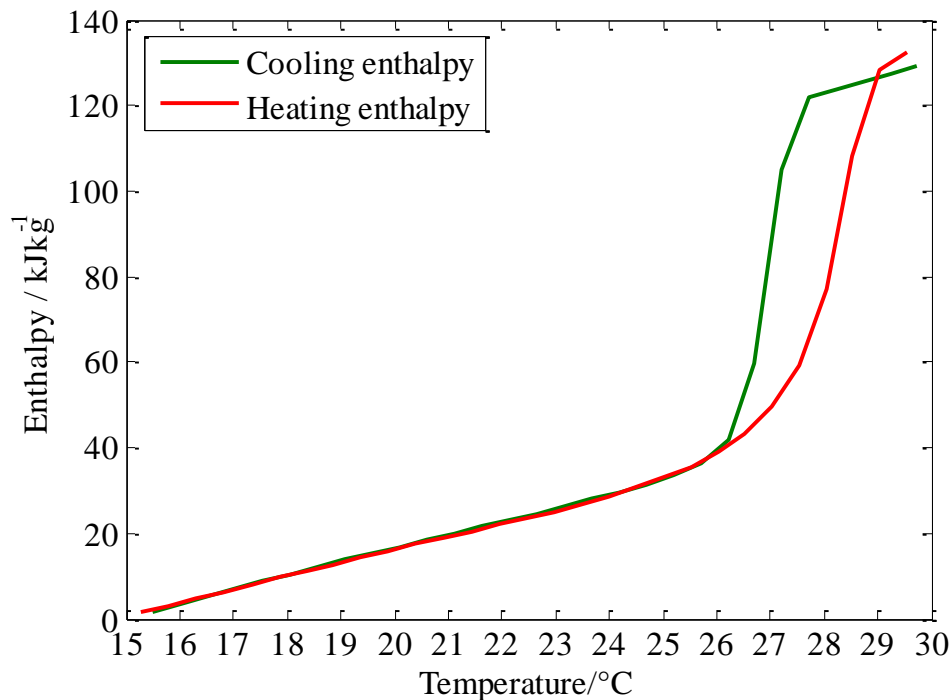


***Figure 8.28:*** *Enthalpy-temperature curves upon cooling and heating obtained from the advanced T-history characterisation of PT28 with the normalised enthalpy value of 0 kJkg$^{-1}$at 15 °C.*

The difference (hysteresis) between the corresponding enthalpy curves (Cooling enthalpy and Heating enthalpy in Figure 8.28) is evident especially in terms of temperature values. The value of the total heat released upon cooling between 15 °C and 30 °C for the PT28 was 130 kJkg$^{-1}$ while the value of the total heat stored upon

heating in the same range was 133 kJkg$^{-1}$. These values were not close to the value of 205 kJkg$^{-1}$ (Table 8.3). However given the lack of information regarding the temperature ranges used for the evaluation of the heat capacity data of PT28 (Table 8.3) the heat values cannot be compared. The total heat data are similar (±10%) to the values reported for PT20 and PT27. This indicates that the materials from the PT series show rather similar behaviour in terms of the heat capacity values regardless of their phase change ranges. Consequently, as in PT27 case the total heat released/stored data for the PT28 are smaller than the corresponding RT27 data.

The heat released/stored per volume data were also estimated for PT28. The value of the total heat released per volume upon cooling between 15 °C and 30 °C was 111.8 kJl$^{-1}$. The value of the total heat stored per volume upon heating between 15 °C and 30 °C was 114.4 kJl$^{-1}$.

Finally, for the damage criteria tests regarding enthalpy, temperature, and mass changes two additional T-history measurements of PT28 were performed. The maximum changes in the corresponding total enthalpies upon cooling and heating between 15 °C and 30 °C were ±2.9 % (<±10 %). The maximum change in temperature profiles was ±0.4 °C (<±1 °C). Thirdly, the maximum change in mass of the PCM samples was ±0.2 % (<±3 %). Once the damage criteria were checked the PT28 characterisation was completed.

# 8.5 Summary

The comprehensive studies of various organic PCMs were described in this chapter. The temperature history curves present only a part of the PCM characterisation. The temperature data need to be properly evaluated to determine the basic thermo-physical properties of investigated materials predominantly the phase change temperature (range) and the energy stored/released. Hence, the implementation of the technique used for the data evaluation of the T-history curves was described in this chapter.

Additionally, considering the need to balance between various measurements' parameters in PCM related experiments, as explained in section 5.1, thorough parametric studies had to be performed on the well-known organic PCM RT21. The

parametric studies, carried out by varying the parameters like the size and position of the sensors, the thickness of the insulating tape used to wrap the test tubes and the size of the samples used in measurements, were described in detail.

Moreover the details of the in-depth characterisation of organic RT21 and RT27 (Rubitherm GmbH, Berlin, Germany) as well as bio-organic PT20, PT27, and PT28 PCMs (Entropy Solutions Inc., Plymouth, Minnesota) were also given in this chapter.

# Chapter 9

# INVESTIGATION

# OF THERMO-PHYSICAL PROPERTIES

# OF INORGANIC PCMs

In addition to the tests performed on the organic materials, the advanced T-history method was used to characterise some inorganic PCMs as well. As explained in chapter 8, the T-history measurements produce the temperature history curves which form only a part of the PCM characterisation. The temperature data need to be properly evaluated to determine the basic thermo-physical properties of investigated materials (phase change range and heat content). Given the distinguishable properties of the inorganic and organic PCMs especially in terms of the subcooling phenomenon the computational technique explained in section 8.1 had to be adapted to take the subcooling into the account and therefore enable proper characterisation of inorganic PCMs. The details regarding the adaptation procedure are described in this chapter.

Once the data evaluation procedure was adjusted for the characterisation of inorganic materials and properly implemented, the in-depth characterisation studies of inorganic PCMs could be performed. Two inorganic PCMs from Rubitherm's SP series (Rubitherm GmbH, Berlin, Germany) were investigated and their characterisation data presented in detail.

In addition, given that the new evaluation procedure was developed to take the subcooling into the account the T-history data of PT27 and PT28 (see subsections 8.4.2 and 8.4.3) from the Entropy Solutions' PT series (Entropy Solutions Inc., Plymouth, Minnesota) were re-evaluated and the obtained results also presented.

# 9.1 Data evaluation technique

The evaluation technique transforms the T-history measurement data into the meaningful PCM data in terms of phase change temperature (range) and associated heat capacity. As explained in section 8.1, the time delay technique developed by Marin et al. (2003) was selected as the most suitable and hence adapted for data processing in the advanced T-history method. The implementation of this technique was described in detail in section 8.1. However, given the distinguishable properties between the inorganic and organic PCMs predominantly in terms of the subcooling phenomenon the computational technique from section 8.1 had to be further modified. Namely, the computational procedure used for the calculation of PCM data had to take the degree of subcooling, observed in the cooling T-history curves, into consideration.

As suggested in section 5.1, for the proper PCM characterisation the subcooling should be eliminated from the heat released/stored PCM data and given separately with reference to the sample mass (Mehling and Cabeza, 2008; RAL, 2010). Although this suggestion was given as early as in 2008 the reported PCM characterisation data are not generally presented in this form. Hence, one of the aims of this study was to determine and present the degree of subcooling and the data regarding the heat lost due to this phenomenon for all investigated PCM with the significant subcooling. The procedure for the elimination of the subcooling effect was suggested by Mehling and Cabeza (2008) (see Figure 5.1). Namely, according to them the effect of subcooling should be eliminated from the heat stored/released graphs and given separately as the degree of subcooling while the heat lost upon subcooling should be attributed to the solidification temperature. However, a slightly different approach was used here for the development of the time delay evaluation procedure that takes the subcooling into consideration. This approach is presented in Figure 9.1.

The approach used at this point follows the main principles of the heat exchange during the solidification process. According to Mehling and Cabeza (2008) the heat lost upon subcooling is attributed to the entire section between the typical phase change temperature and the nucleation temperature (Figure 5.1). On the other hand, given the typical PCM T-history cooling curve and the heat exchange principles the heat

attributed to the interval between the typical phase change temperature ($T_{PC}$ in Figure 9.1) and the nucleation temperature ($T_N$ in Figure 9.1) is not lost due to subcooling as indicated in Figure 5.1 but rather normally released in the PCM cooling process. This portion of heat is labeled as the heat released between the $T_{PC}$ and $T_N$ (Figure 9.1). The heat that is truly lost upon subcooling is the heat attributed to the temperature interval between the $T_N$ and $T_{PC}$ (heat lost upon subcooling in Figure 9.1). This portion of heat is used to raise the temperature of the PCM from $T_N$ to $T_{PC}$ during cooling and therefore lost as the usable PCM heat content. Considering the earlier established format to represent the PCM data in the form of the heat released/stored in given temperature intervals upon cooling and heating it was decided that the heat released between $T_{PC}$ and $T_N$ (Figure 9.1) should be added to the heat released data attributed to the temperature intervals between the $T_N$ and $T_{PC}$. Usually this heat will overlap with the higher heat content released in the phase change range (Figure 9.1). The heat lost upon subcooling (Figure 9.1) needs to be given separately and naturally attributed to temperature intervals between the $T_N$ and $T_{PC}$. The degree of subcooling is easily estimated and given as the difference between the corresponding $T_{PC}$ and $T_N$ temperatures.
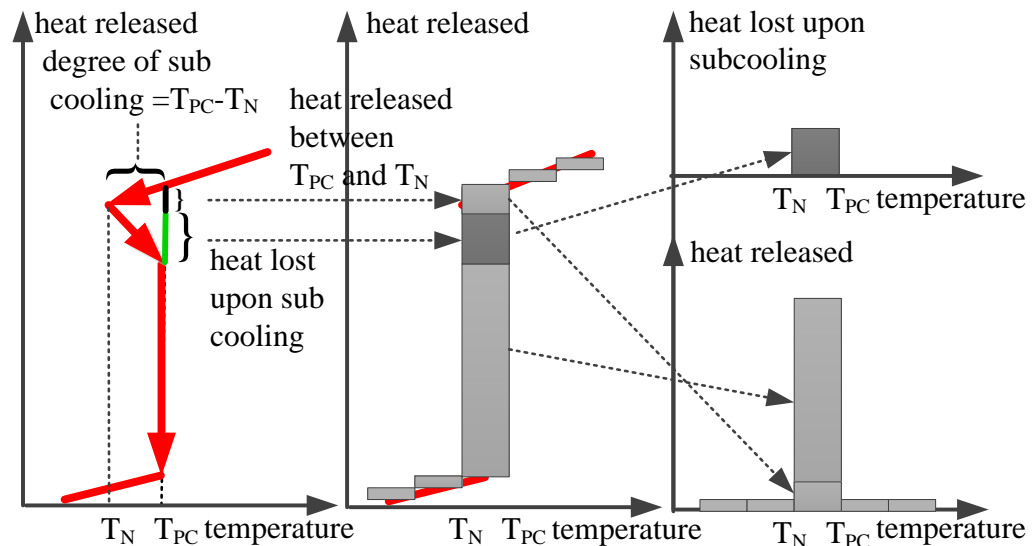


***Figure 9.1:*** *The procedure for the determination of the heat released/stored of PCMs in given temperature intervals and the degree of subcooling as well as the accompanying heat loss.*

223

The *time_delay* function described in section 8.1 had to be adjusted to accommodate the aforementioned changes. For this, the new *time_delay_sc* function was implemented. The implementation details are given in APPENDIX A7. The changes to the previous *time_delay* function were made only for the evaluation of the cooling T-history data (to take the subcooling into the account). The evaluation of the heating T-history data was unchanged in the new function.

Once the *time_delay_sc* function was implemented the advanced T-history method could be used for the characterisation of inorganic PCMs as described in the following section.

# 9.2 Investigation studies of SP inorganic series

Two inorganic materials from the Rubitherms's SP series (Rubitherm GmbH, Berlin, Germany) were tested. The SP22 and SP25 were selected due to their phase change temperature ranges being suitable for building applications. As RT21 and RT27, these two materials are commercially available and form a part of various PCM objects sold by Rubitherm (Rubitherm GmbH, Berlin, Germany).

## 9.2.1 SP22 characterisation – results and discussion

The first material that was tested from the SP series was SP22 (Rubitherm GmbH, Berlin, Germany). The material specifications of SP22 are given in Table 9.1.

| Property | Value |
|---|---|
| Melting area | 22-23 °C |
| Congealing area | 21-20 °C |
| Typical phase change temperature | 22 °C |
| Heat storage capacity (15 to 30 °C) | 150 kJkg$^{-1}$ |
| Specific heat capacity | 2 kJkg$^{-1}$K$^{-1}$ |
| Density solid (at 15 °C) | 1.5 kgl$^{-1}$ |
| Density liquid (at 35 °C) | 1.4 kgl$^{-1}$ |
| Thermal conductivity | 0.6 Wm$^{-1}$K$^{-1}$ |

***Table 9.1:*** *Material properties of inorganic PCM SP22.*

The characterisation of SP22 using the advanced T-history method was performed by in the same way as the characterisation measurements of PT27 and PT28 described in section 8.4. The PCM and distilled water, placed in the 430 mm long test tubes insulated by 10 mm thick tape, were subjected to the alternating cooling and heating 6 h long cycles. The cycles were operated between 8 °C and 30 °C in this case. The respective masses of the sample ($m_p$) and reference ($m_w$) were 72.7 g and 47.3 g. The mass of the PCM sample was greater in this case because the density of the inorganic material is much larger than the density of the investigated organic PCMs. As before, prior to the T-history measurement, the proper calibration measurement was performed with 1 °C step temperature program from 6 °C to 36 °C. The calibration data were used to obtain the T-history curves (Figure 9.2).

According to the T-history curves from the cooling cycle (Figure 9.2a) the typical phase change temperature of SP22 is 19.9 °C. This value is different from the expected typical value of 22 °C but deviates only by a small margin (0.1 °C) from the lower boundary temperature of the expected congealing range (Table 9.1). In addition, significant degree of subcooling of 5.9 °C was observed between the phase change temperature and the nucleation temperature of 14 °C. The manufacturer does not report any degree of subcooling for SP22 (Rubitherm GmbH, Berlin, Germany). However, even when the data given in Figure 9.2a represent the T-history curves from the first cooling cycle of SP22 (due to the reasons explained in subsection 9.3.1) the subcooling was detected in all consecutive cooling cycles although to a marginally smaller degree. This observation confirmed that after the first solidification cycle the sensor within the PCM sample acts as a nucleating seed and therefore reduces the subcooling in the subsequent cycles. However, given the fact that subcooling was observed in all cooling cycles the theoretical PCM T-history curve (Ideal PCM in Figure 9.2a) made by excluding the subcooling from the real PCM cooling curve (PCM in Figure 9.2a) was also given. This curve was used later to evaluate the data regarding the heat release without taking the subcooling into the account. According to the PCM T-history curve from the heating cycle (Figure 9.2b) the typical phase change temperature is 22.6 °C which is in agreement with the expected typical value of 22 °C and the melting area data (Table 9.1).
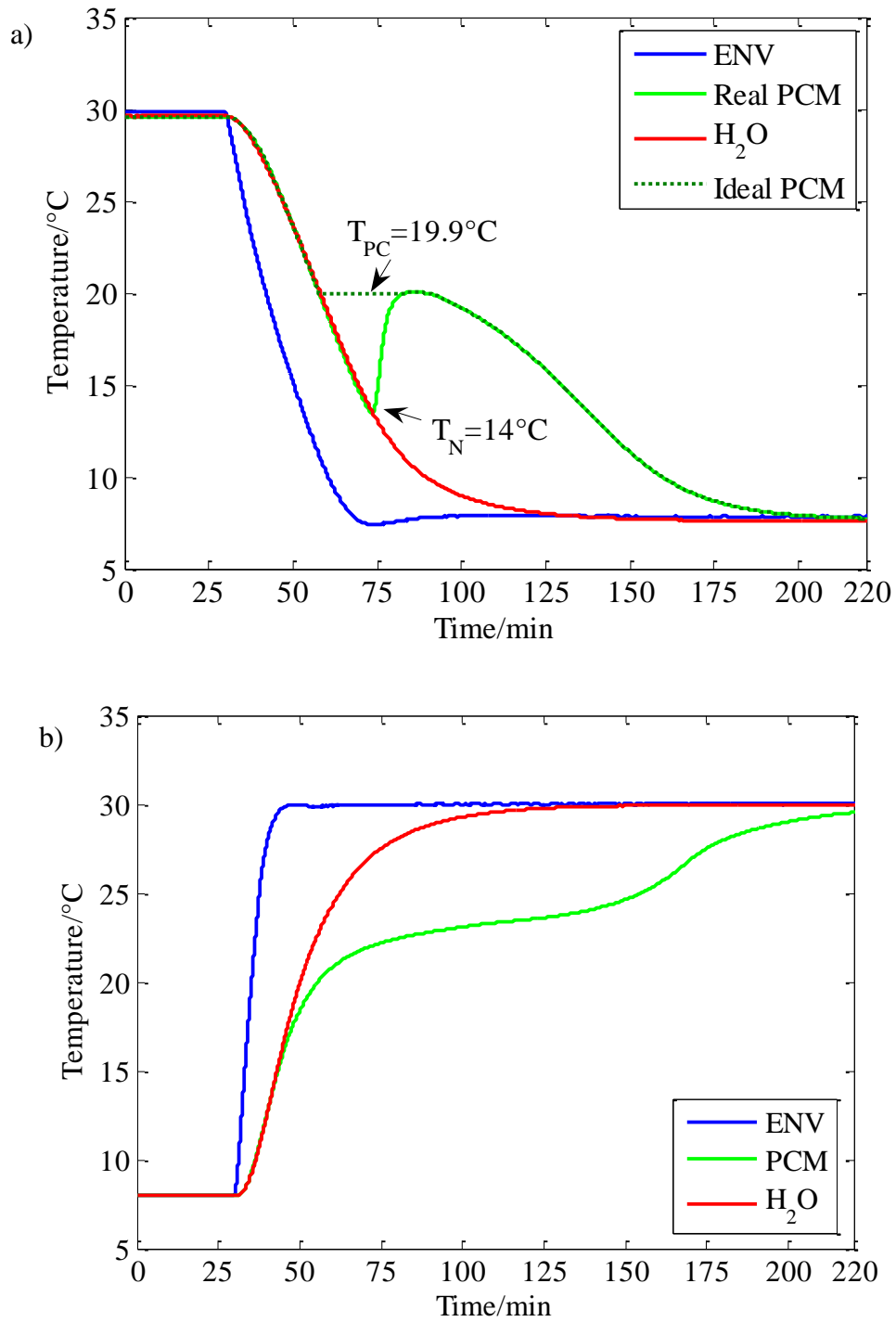
**Figure 9.2:** *Cooling (a) and heating (b) cycles in the advanced T-history characterisation of SP22 (ENV – environmental temperature, PCM – temperature of the PCM sample, Ideal PCM – temperature of the PCM sample upon cooling if subcooling is neglected, $H_2O$ – temperature of the reference sample).*

The T-history data (Figure 9.2) and the evaluation technique described in section 9.1 were used to determine the heat released/stored in given temperature intervals data for SP22. In the case of cooling the ENV, Ideal PCM, and $H_2O$ T-history curves (Figure 9.2a) were used to calculate the heat released data without taking the subcooling into the account (HR in Figure 9.3a). The corresponding ENV, PCM, and $H_2O$ T-history curves (Figure 9.2a) were used to calculate the heat released data and the heat lost upon subcooling (HR and SC in Figure 9.3b). The heat stored data (HS) in both cases (HS in Figure 9.3a and 9.3b) have been calculated based on the T-history heating curves (Figure 9.2b). The T-history curves (Figure 9.2) were evaluated in the 15 °C to 30 °C range with the temperature evaluation interval of 0.5 °C to obtain the heat released/stored data in given temperature intervals (Figure 9.3).

According to the HR data in Figure 9.3a the congealing area of SP22 is in the range from 19 °C to 20.5 °C which is slightly shifted and wider in comparison to the expected 20 °C to 21 °C range (Table 9.1). According to the HR data in Figure 9.3b the congealing area of SP22 is in the range from 19 °C to 20 °C which is slightly shifted in comparison to the expected 20 °C to 21 °C range (Table 9.1) but 1 °C wide as expected. Furthermore, according to the SC data in Figure 9.3b non-negligible portion of heat (19 kJkg$^{-1}$) is lost upon subcooling between 20 °C and 14 °C. The melting area of SP22 is wider than the congealing area and shifted towards the 22 °C to 23.5 °C range (Figure 9.3). This range is 0.5 °C wider than the melting area reported by the manufacturer (Table 9.1). Given the data presented in Figure 9.3 it was concluded that the hysteresis between the cooling and heating data in the case of SP22 especially when subcooling is taken into account is real and significant.

The enthalpy data upon cooling and heating (Figure 9.4) were evaluated from the data given in Figure 9.3. The cooling enthalpy curve was calculated with taking the subcooling into the account (Cooling enthalpy WSC and Cooling enthalpy WSC in Figure 9.4). The Cooling enthalpy WOSC data (Figure 9.4) were calculated from the HR data in Figure 9.3a, while the Cooling enthalpy WSC data (Figure 9.4) were calculated from the HR and SC data in Figure 9.3b.
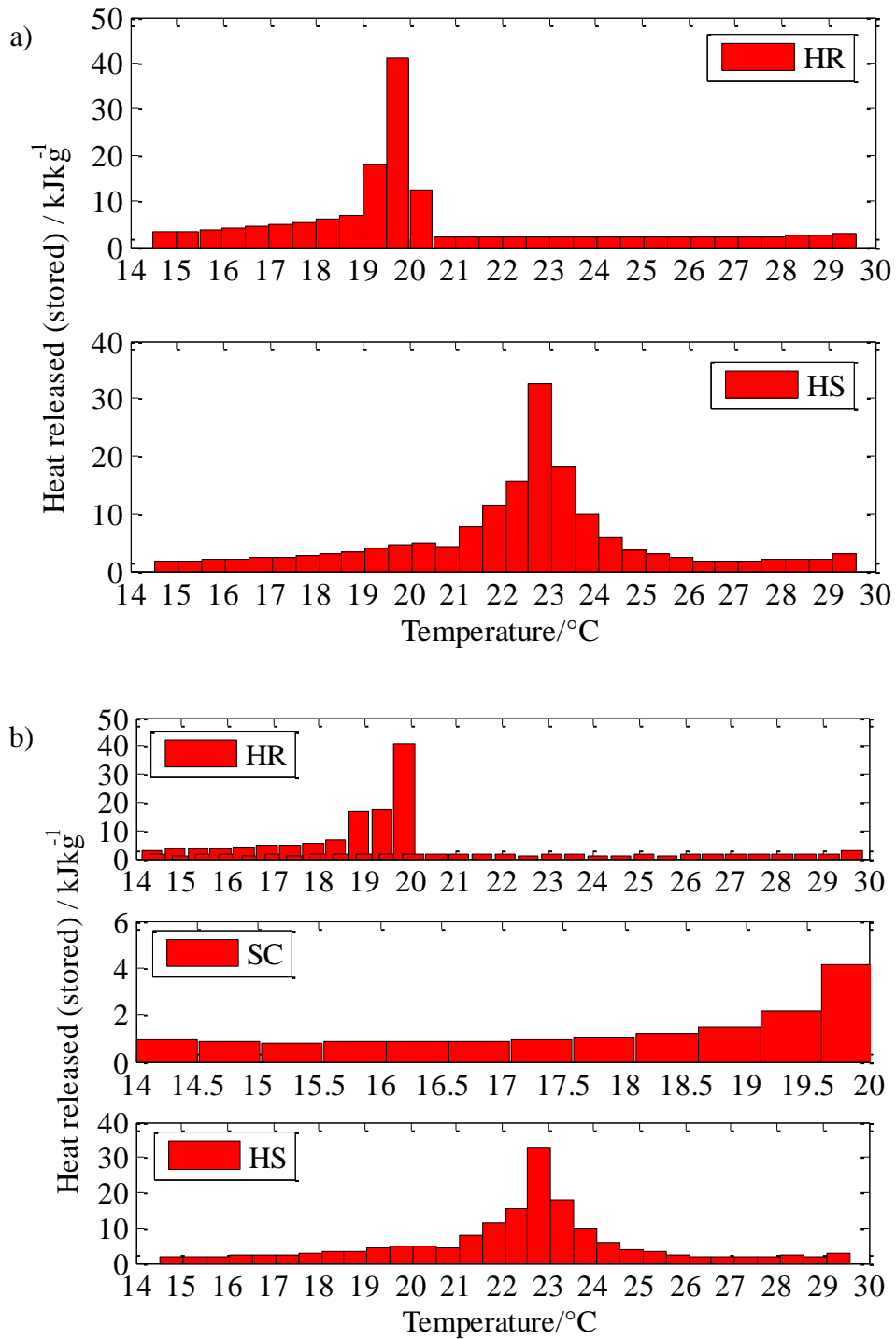
***Figure 9.3:*** *Heat released (stored) data obtained from the advanced T-history characterisation of SP22. a) Case when subcooling is neglected. b) Case when subcooling is taken into account (HR – heat released upon cooling, HS – heat stored upon heating, SC – heat lost upon subcooling).*
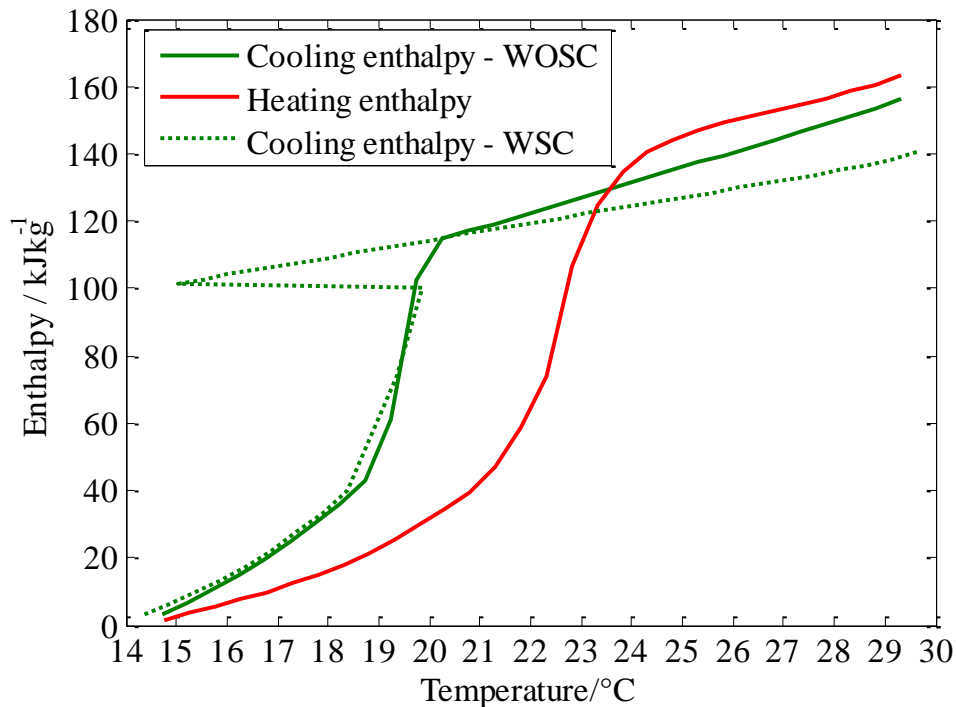
***Figure 9.4:*** *Enthalpy-temperature curves upon cooling and heating obtained from the advanced T-history characterisation of SP22 with the normalised enthalpy value of 0 kJkg$^{-1}$ at 15 °C (Cooling enthalpy WOSC – enthalpy curve upon cooling in the case when subcooling is neglected, Heating enthalpy – enthalpy curve upon heating, Cooling enthalpy WSC – enthalpy curve upon cooling in the case when subcooling is taken into account).*

The difference (hysteresis) between the cooling and heating enthalpy curves is evident especially in the case when subcooling is taken into the account (Figure 9.4) The value of the total heat released upon cooling between 15 °C and 30 °C for the SP22 was 159 kJkg$^{-1}$ in the case when subcooling is neglected and 140 kJkg$^{-1}$ when subcooling was considered. The first value showed a deviation of ±6 % and the second value showed a deviation of ±6.7 % from the expected value of 150 kJkg$^{-1}$ (Table 9.1). The value of the total heat stored upon heating in the interval between 15 °C and 30 °C was 162 kJkg$^{-1}$. This value showed a deviation of ±8 % from the expected value (Table 9.1). The deviation values in all cases were within the ±10 % margin. The difference between the respective values obtained upon cooling and heating was larger in the case when subcooling was not neglected. However given that heat lost upon subcooling is not negligible (11.7 % of the heat stored upon heating) it had to be taken into the account. Nevertheless, even when subcooling is considered the total heat

229

released/stored data for the SP22 are equal (cooling case) or larger (heating) than the respective RT21 data. This makes SP22 marginally more competitive material once the information regarding the subcooling and hysteresis are taken into account. Only then the usage of SP22 can result in the development of successful and reliable PCM based TES systems.

The heat released/stored per volume data were also estimated for SP22. The value of the total heat released per volume upon cooling (subcooling considered) between 15 °C and 30 °C was 196 $kJl^{-1}$. The value of the total heat stored per volume upon heating between 15 °C and 30 °C was 226.8 $kJl^{-1}$. Given the larger densities of inorganic materials these values are much larger than in the case of organic PCMs.

Finally, for the damage criteria tests regarding enthalpy, temperature, and mass changes two additional T-history measurements of SP22 were performed. The maximum changes in the corresponding total enthalpies upon cooling and heating between 15 °C and 30 °C were ±8.3 % (<±10 %). The maximum change in temperature profiles was ±0.6 °C (<±1 °C). Thirdly, the maximum change in mass of the PCM samples was ±1.2 % (<±3 %). Once the damage criteria were checked the SP22 characterisation was completed.

## 9.2.2 SP25 characterisation – results and discussion

The second material that was tested from the SP series was SP25 (Rubitherm GmbH, Berlin, Germany). The material specifications of SP25 are given in Table 9.2.

| Property | Value |
|---|---|
| Melting area | 24-26 °C |
| Congealing area | 24-23 °C |
| Typical phase change temperature | 24 °C |
| Heat storage capacity (15 to 30 °C) | 180 $kJkg^{-1}$ |
| Specific heat capacity | 2 $kJkg^{-1}K^{-1}$ |
| Density solid (at 15 °C) | 1.5 $kgl^{-1}$ |
| Density liquid (at 30 °C) | 1.4 $kgl^{-1}$ |
| Thermal conductivity | 0.6 $Wm^{-1}K^{-1}$ |

*Table 9.2: Material properties of inorganic PCM SP25.*

The characterisation of SP25 using the advanced T-history method was performed by in the same way as the characterisation measurement of SP22. The PCM

and distilled water, placed in the 430 mm long test tubes insulated by 10 mm thick tape, were subjected to the alternating cooling and heating 6 h long cycles. The cycles were operated between 6 °C and 40 °C in this case. The respective masses of the sample ($m_p$) and reference ($m_w$) were 71.2 g and 47.3 g. As before, prior to the T-history measurement, the proper calibration measurement was performed with 1 °C step temperature program from 6 °C to 36 °C. The calibration data were used to obtain the T-history curves (Figure 9.5).

According to the T-history curves from the cooling cycle (Figure 9.5a) the typical phase change temperature of SP25 is 24.6 °C. This value is marginally different from the expected typical value of 24 °C and the expected congealing range (Table 9.2). The observed degree of subcooling between the phase change temperature and the nucleation temperature of 9 °C is rather large (15.6 °C). As in SP22 case, the manufacturer does not report any degree of subcooling for SP25 (Rubitherm GmbH, Berlin, Germany). However, the subcooling was detected in the first and all consecutive cooling cycles. Hence, the theoretical PCM T-history curve (Ideal PCM in Figure 9.5a) made by excluding the subcooling from the real PCM cooling curve (PCM in Figure 9.5a) was presented as in the previous subsection. This curve was used to evaluate the heat release data without taking the subcooling into the account. According to the PCM T-history curve from the heating cycle (Figure 9.5b) the typical phase change temperature is 26.7 °C which is 0.7 °C higher than the upper boundary temperature of the expected melting area (Table 9.2).

The T-history data (Figure 9.5) and the evaluation technique described in section 9.1 were used to determine the heat released/stored in given temperature intervals data for SP25. As in SP22 case, the ENV, Ideal PCM, and $H_2O$ T-history curves (Figure 9.5a) were used to calculate the heat released data without taking the subcooling into the account (HR in Figure 9.6a). The corresponding ENV, PCM, and $H_2O$ T-history curves (Figure 9.5a) were used to calculate the heat released data and the heat lost upon subcooling (HR and SC in Figure 9.6b).
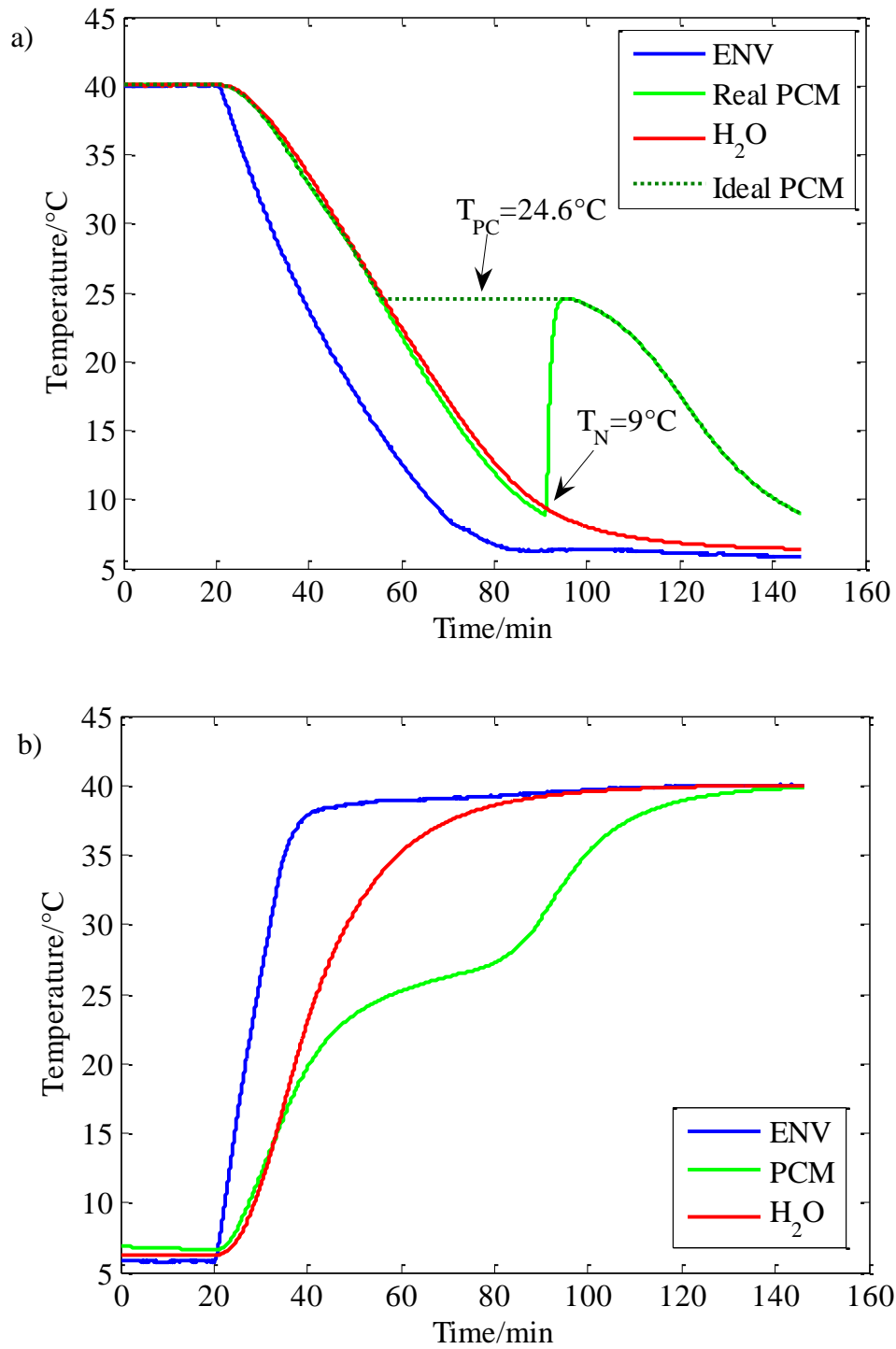
**Figure 9.5:** *Cooling (a) and heating (b) cycles in the advanced T-history characterisation of SP25 (ENV – environmental temperature, PCM – temperature of the PCM sample, Ideal PCM – temperature of the PCM sample upon cooling if subcooling is neglected, $H_2O$ – temperature of the reference sample).*

The heat stored data (HS) in both cases (HS in Figure 9.6a and 9.6b) have been calculated based on the T-history heating curves (Figure 9.5b). Given the detected degree of subcooling and the nucleation temperature, the evaluation of the T-history curves (Figure 9.5) was done in the 9 °C to 30 °C range. The temperature evaluation interval was 0.5 °C.

According to the HR data in Figure 9.6a the congealing area of SP25 is in the range from 24.5 °C to 26 °C which is shifted towards higher temperatures in comparison to the expected 23 °C to 24 °C range (Table 9.2). However this was expected given that the HR data in Figure 9.6a were estimated using the Ideal PCM T-history curve in Figure 9.5a. According to the HR data in Figure 9.6b the congealing area of SP25 is in the range from 23.5 °C to 25 °C which is wider but in a better agreement with the expected 23 °C to 24 °C range (Table 9.2). Furthermore, according to the SC data in Figure 9.6b large portion of heat (22 kJkg$^{-1}$) is lost upon subcooling between 24.5 °C and 9 °C. The melting area of SP25 is wider than the congealing area and shifted towards the 24 °C to 27 °C range (Figure 9.6). This range is 1 °C wider than the melting area reported by the manufacturer (Table 9.2). As in the SP22 case, the hysteresis between the cooling and heating SP25 data especially when subcooling is taken into account is real.

The enthalpy data upon cooling and heating (Figure 9.7) were evaluated from the data given in Figure 9.6. The cooling enthalpy curves were estimated in both cases without and with taking the subcooling into the account (Cooling enthalpy WOSC and Cooling enthalpy WSC in Figure 9.7). As explained in the previous subsection, the Cooling enthalpy WOSC data (Figure 9.7) were calculated from the HR data in Figure 9.6a, while the Cooling enthalpy WSC data (Figure 9.7) were calculated from the HR and SC data in Figure 9.6b.
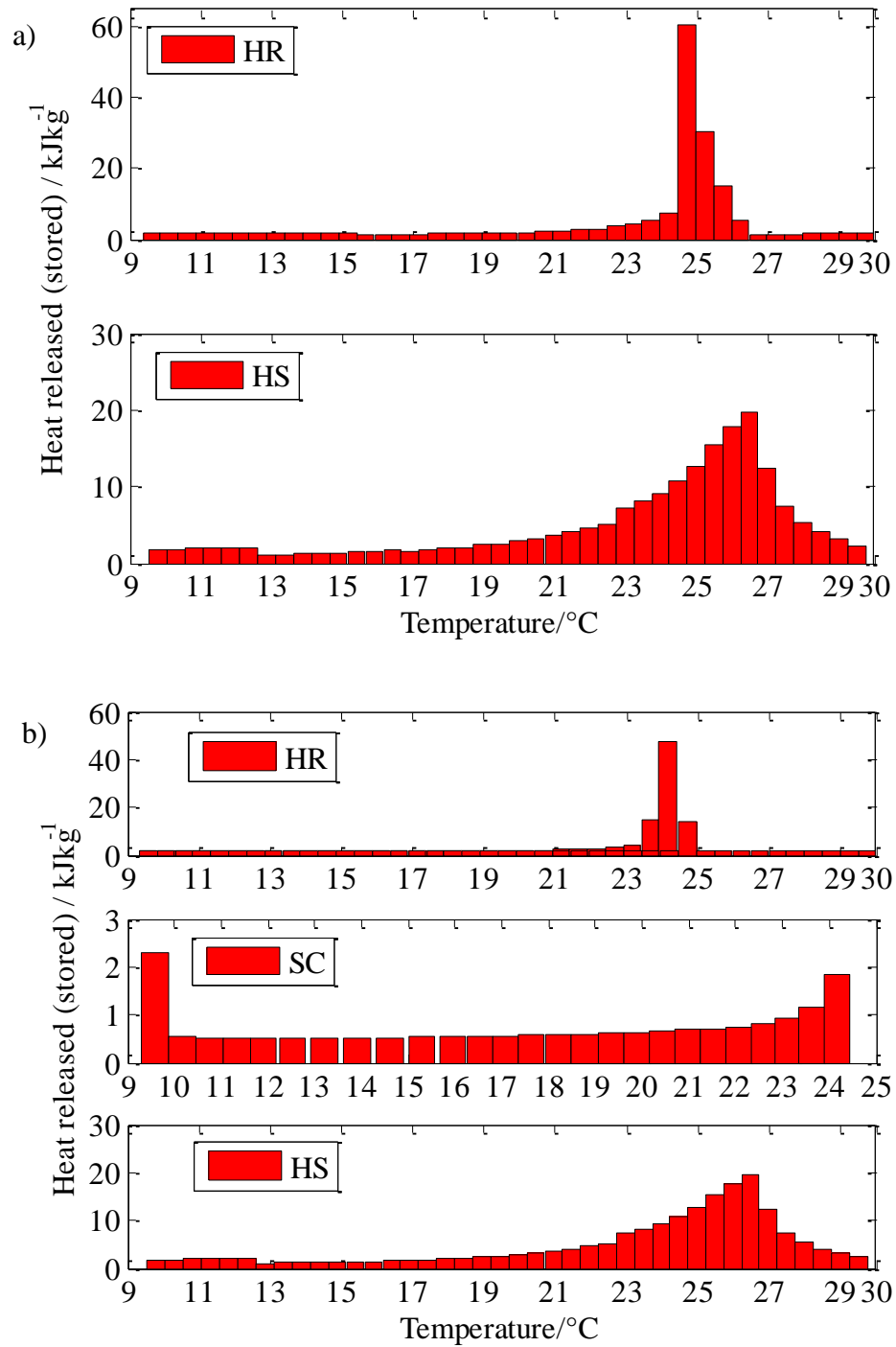
***Figure 9.6:*** *Heat released (stored) data obtained from the advanced T-history characterisation of SP25. a) Case when subcooling is neglected. b) Case when subcooling is taken into account (HR – heat released upon cooling, HS – heat stored upon heating, SC – heat lost upon subcooling).*
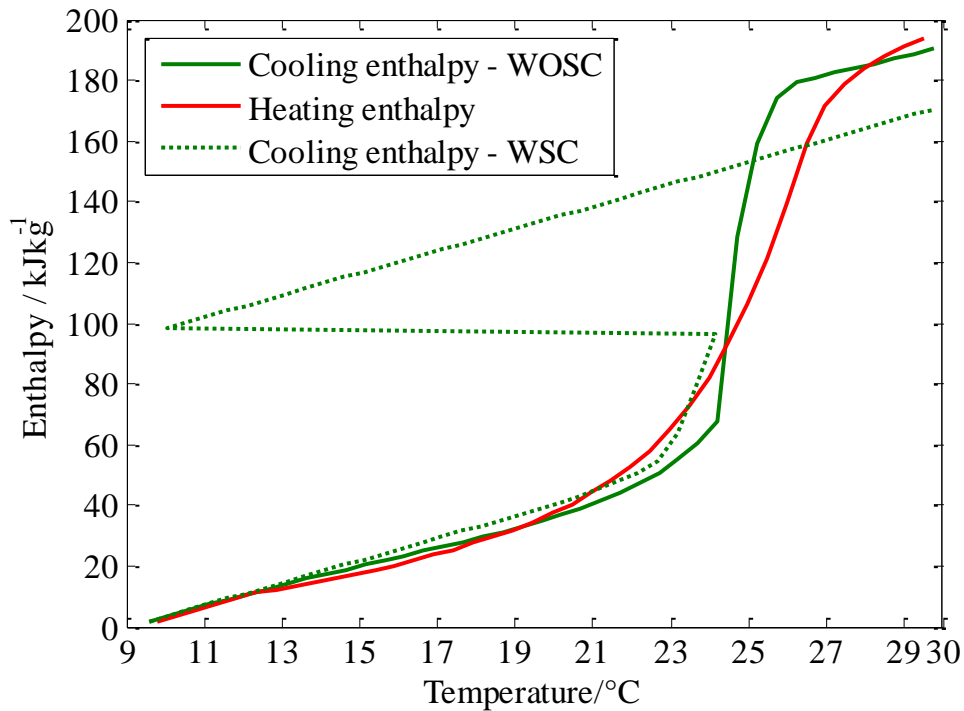
***Figure 9.7:*** *Enthalpy-temperature curves upon cooling and heating obtained from the advanced T-history characterisation of SP25 with the normalised enthalpy value of 0 kJkg$^{-1}$ at 15 °C (Cooling enthalpy WOSC – enthalpy curve upon cooling in the case when subcooling is neglected, Heating enthalpy – enthalpy curve upon heating, Cooling enthalpy WSC – enthalpy curve upon cooling in the case when subcooling is taken into account).*

The difference (hysteresis) between the cooling and heating enthalpy curves is evident especially in the case when subcooling is taken into the account (Figure 9.7) The value of the total heat released upon cooling between 9 °C and 30 °C for the SP25 was 192 kJkg$^{-1}$ in the case when subcooling is neglected and 170 kJkg$^{-1}$ when subcooling was considered. The value of the total heat stored upon heating between 9 °C and 30 °C was 197 kJkg$^{-1}$. The calculated values of the total heat released upon cooling without considering subcooling and of the total heat stored upon heating were larger than the expected value of 180 kJkg$^{-1}$ (Table 9.2) but this was expected since the evaluation range was wider than the 15 °C to 30 °C range reported by the manufacturer. As in the SP22 case, the difference between the respective values obtained upon cooling and heating was larger in the case when subcooling was considered. However given that heat lost upon subcooling is not negligible (11.2 % of the heat stored upon heating) once more it had to be taken into the account. Given the

arguments presented in section 5.1, the information regarding the subcooling and hysteresis needs to be provided for the reliable utilisation of SP25.

The heat released/stored per volume data were also estimated for SP25. The value of the total heat released per volume upon cooling (subcooling considered) between 9 °C and 30 °C was 238 kJl[-1]. The value of the total heat stored per volume upon heating between 9 °C and 30 °C was 268.8 kJl[-1]. These values are much larger than in the case of organic PCMs due to difference in densities between organic and inorganic PCMs.

Finally, for the damage criteria tests regarding enthalpy, temperature, and mass changes two additional T-history measurements of SP25 were performed. The maximum changes in the corresponding total enthalpies upon cooling and heating between 9 °C and 30 °C were ±6.8 % (<±10 %). The maximum change in temperature profiles was ±0.6 °C (<±1 °C). Thirdly, the maximum change in mass of the PCM samples was ±0.8 % (<±3 %). Once the damage criteria were checked the SP25 characterisation was completed.

# 9.3 Re-evaluation studies of PT bio-organic series

Given that some degree of subcooling was observed in the case of PT27 and PT28 PCMs from the PT bio-organic series (Entropy Solutions Inc., Plymouth, Minnesota) it was decided that the T-history curves obtained in the characterisation measurements of PT27 and PT28 (Figure 8.22 and 8.25) were re-evaluated using the data evaluation technique described in section 9.1. This was done in order to check if the relatively low degree of subcooling as observed in the case of PT27 and PT28 affects the heat capacity of these materials to the relevant extent. The results of the re-evaluation are presented in the following subsections.

## 9.3.1 PT27 re-evaluation – results and discussion

Given that the observed degree of subcooling between the phase change temperature (24 °C) and the nucleation temperature (23.5 °C) for PT27 was 0.5 °C the temperature interval used in the re-evaluation procedure was 0.3 °C. The T-history curves

(Figure 8.22) were evaluated in the 15 °C to 30 °C range with the temperature evaluation interval of 0.3 °C to obtain the heat released/stored data in given temperature intervals (Figure 9.8).
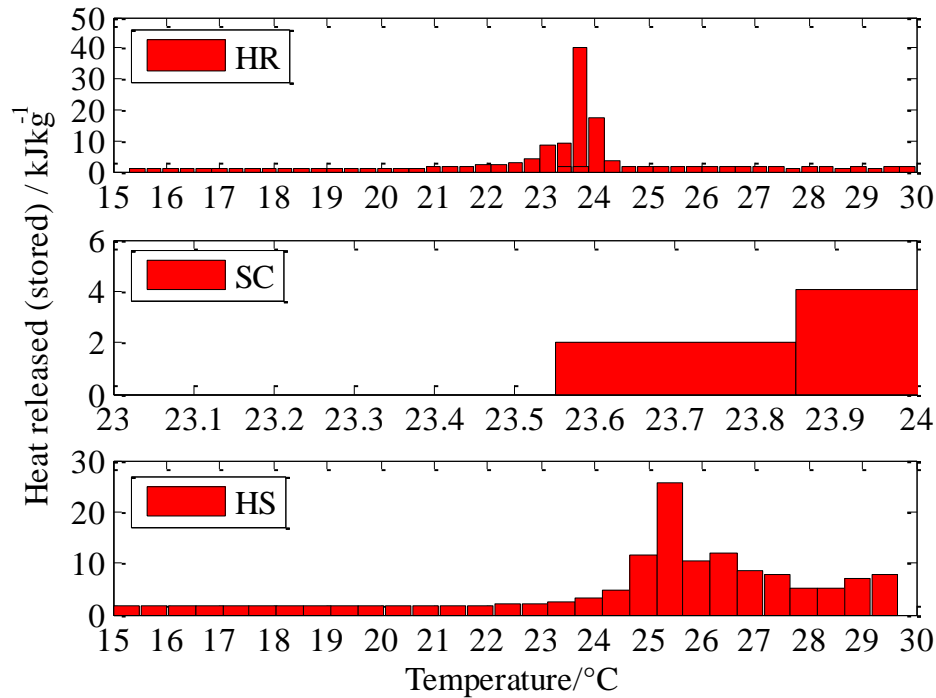


***Figure 9.8:*** *Heat released (stored) data obtained from the re-evaluation of PT27 (HR – heat released upon cooling, HS – heat stored upon heating, SC – heat lost upon subcooling).*

The temperature evaluation interval of 0.3 °C resulted in more precise heat released/stored in given temperature intervals (HR and HS in Figure 9.8) than the corresponding HR and HS data presented in Figure 8.23. Additionally, the heat lost upon subcooling was also determined (SC in Figure 9.8). According to the SC data in Figure 9.8 small portion of heat (6 kJkg$^{-1}$) is lost upon subcooling between 23.5 °C and 24 °C.

The enthalpy data upon cooling with taking subcooling into account (Cooling enthalpy WSC in Figure 9.9) were evaluated from the HR and SC data given in Figure 9.8. The calculated cooling enthalpy curve with taking the subcooling into the account (Cooling enthalpy WSC in Figure 9.9) was compared with the respective enthalpy data obtained without considering subcooling (Figure 8.24). The Cooling

enthalpy from Figure 8.24 is presented as the Cooling enthalpy WOSC while the Heating enthalpy from Figure 8.24 is presented as the Heating enthalpy in Figure 9.9.
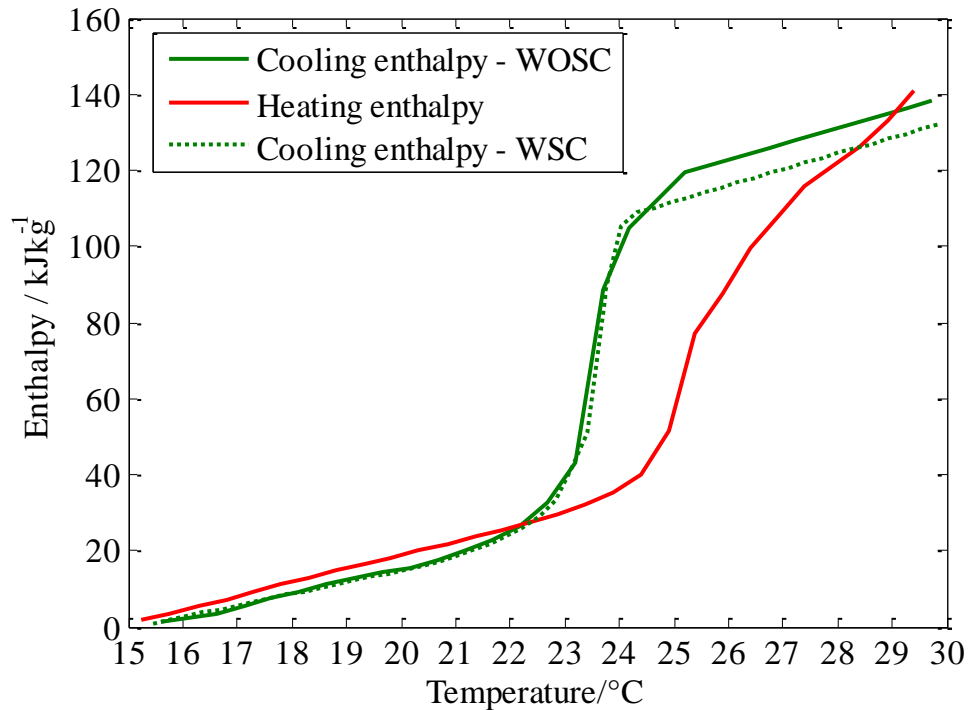


***Figure 9.9****: Enthalpy-temperature curves upon cooling and heating obtained from the re-evaluation of PT27 with the normalised enthalpy value of 0 kJkg$^{-1}$ at 15 °C (Cooling enthalpy WOSC – enthalpy curve upon cooling in the case when subcooling is neglected, Heating enthalpy – enthalpy curve upon heating, Cooling enthalpy WSC – enthalpy curve upon cooling in the case when subcooling is taken into account).*

The difference (hysteresis) between the cooling and heating enthalpy curves is increased in the case when subcooling is taken into the account (Figure 9.9) The former value of the total heat released upon cooling between 15 °C and 30 °C for the PT27 of 140 kJkg$^{-1}$ was reduced to 134 kJkg$^{-1}$ once the heat lost upon subcooling was taken into account. The heat lost upon subcooling in the case of PT27 (6 kJkg$^{-1}$) represents a small fraction (4.2 %) of the heat stored upon heating (141 kJkg$^{-1}$). Given that the degree of subcooling was only 0.5 °C and the fraction of heat lost less than 5% it was concluded that the subcooling can be neglected in PT27 case. Nevertheless, it is always better to estimate the subcooling for the investigated PCM and then decide whether it should be neglected or not.

## 9.3.2 PT28 re-evaluation – results and discussion

Given that the observed degree of subcooling between the phase change temperature (27.3 °C) and the nucleation temperature (26.9 °C) for PT28 was 0.4 °C the temperature interval used in the re-evaluation procedure was 0.3 °C. The T-history curves (Figure 8.25) were evaluated in the 15 °C to 30 °C range with the temperature evaluation interval of 0.3 °C to obtain the heat released/stored data in given temperature intervals (Figure 9.10).
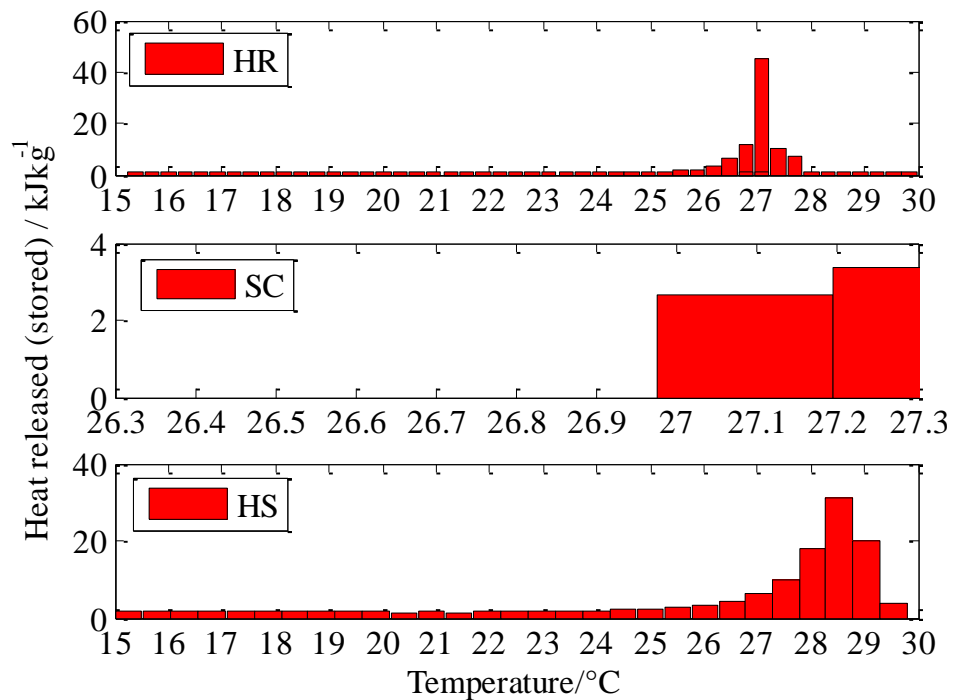


***Figure 9.10:*** *Heat released (stored) data obtained from the re-evaluation of PT28 (HR – heat released upon cooling, HS – heat stored upon heating, SC – heat lost upon subcooling).*

As in the case of PT27 described in the subsection 9.3.1 the temperature evaluation interval of 0.3 °C resulted in more precise heat released/stored in given temperature intervals (HR and HS in Figure 9.10) than the corresponding HR and HS data presented in Figure 8.26. Additionally, the heat lost upon subcooling was also determined (SC in Figure 9.10). According to the SC data in Figure 9.10 small portion of heat (6 kJkg$^{-1}$) is lost upon subcooling between 27 °C and 27.3 °C.

The enthalpy data upon cooling with taking subcooling into account (Cooling enthalpy WSC in Figure 9.11) were evaluated from the HR and SC data given in Figure 9.10.
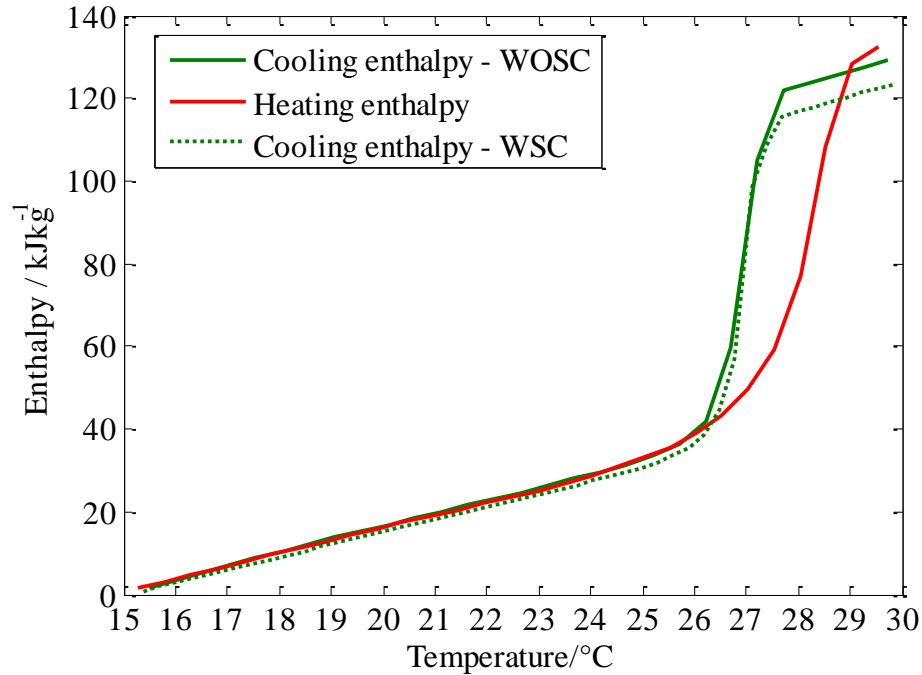


*Figure 9.11: Enthalpy-temperature curves upon cooling and heating obtained from the re-evaluation of PT28 with the normalised enthalpy value of 0 kJkg$^{-1}$at 15 °C (Cooling enthalpy WOSC – enthalpy curve upon cooling in the case when subcooling is neglected, Heating enthalpy – enthalpy curve upon heating, Cooling enthalpy WSC – enthalpy curve upon cooling in the case when subcooling is taken into account).*

The calculated cooling enthalpy curve with taking the subcooling into the account (Cooling enthalpy WSC in Figure 9.11) was compared with the respective enthalpy data obtained without considering subcooling (Figure 8.27). The Cooling enthalpy from Figure 8.27 is presented as the Cooling enthalpy WOSC while the Heating enthalpy from Figure 8.27 is presented as the Heating enthalpy in Figure 9.11.

As in the PT27 case, the difference (hysteresis) between the cooling and heating enthalpy curves is increased in the case when subcooling is taken into the account (Figure 9.11) The former value of the total heat released upon cooling between 15 °C and 30 °C for the PT28 of 130 kJkg$^{-1}$ was reduced to 124 kJkg$^{-1}$ once the heat lost upon subcooling was taken into account. The heat lost upon subcooling in the case of PT28 (6 kJkg$^{-1}$) represents a small fraction (4.5 %) of the heat stored upon heating

($133 \, \text{kJkg}^{-1}$). Given that the degree of subcooling was only 0.4 °C and the fraction of heat lost less than 5% it was concluded that the subcooling can also be neglected in the PT28 case.

# 9.4 Summary

The comprehensive studies of inorganic PCMs from the Rubitherm's SP series (Rubitherm GmbH, Berlin, Germany) were described in this chapter.

Given the relatively large degree of subcooling, expected in the case characterisation studies of inorganic PCMs, the data evaluation technique that takes the subcooling into the account and therefore enables proper characterisation of inorganic PCMs had to be developed. The details regarding the implementation of the appropriate technique were described in this chapter.

Furthermore, the details regarding the in-depth characterisation of inorganic SP22 and SP25 (Rubitherm GmbH, Berlin, Germany) were given in this chapter.

Finally, given the development of the new data evaluation technique the re-evalution of the organic PT27 and PT28 PCMs was performed. This was done because the investigation of these two materials in the previous chapter 8 resulted in the detection of small degree of subcooling. The results of the re-evaluation were also presented in this chapter.

# Chapter 10

# INVESTIGATION
# OF OPTICAL TRANSMITTANCE
# PROPERTIES OF PCMs

As explained in chapter 3 a rather challenging type of PCM based TES applications are solar applications. In these applications the PCMs are integrated with different glazing systems or used as window curtains in order to reduce the solar gain in buildings. Namely, the growing architectural trend to design buildings with the extensive glass areas has led to the issues regarding the low thermal masses of the building envelopes. The high thermal mass values are desirable to reduce the temperature fluctuations and hence increase the thermal comfort within buildings. Moreover, the reduction in temperature fluctuations is directly related with the reduced energy consumption.

One of the ways to achieve higher thermal mass in buildings with large glazed areas is through the utilisation of PCMs incorporated into the cavities of the glazing systems. The latent energy released/stored in the phase change process improves the storage potential of the glazing units and hence enhances the thermal mass of such systems. As mentioned in chapter 3 some of the pioneering works in this field were reported by Ismail and Henriquez (2001) and Weinläder et al. (2005). Furthermore, the company Greenlite Glass Systems (Greenlite Glass Systems, Port Coquitlam, British Columbia) recently commercialised the PCM enhanced glass façade system, called GLASS X. However, there is a lack of in-depth knowledge/information on the real-time performance of the PCM glazing solutions. One of the main problems associated with the PCM enhanced glazing systems is the change in the material's transparency accompanying the phase change. Generally, the transparency of the solid PCMs is lower than that of the liquid materials (Weinläder et al., 2005). Therefore the comprehensive knowledge of optical properties of PCMs is necessary. For this reason

pilot optical tests to determine the transmittance properties of PCMs in different phases were performed on two materials from the Rubitherm's RT series (Rubitherm GmbH, Berlin, Germany), the RT27 and RT21.

The details of the performed optical tests are given in the following sections.

# 10.1 Optical investigation studies of RT organic series

The optical PCM data published in literature usually include the transmittance values in VISible (VIS) part of the electromagnetic spectrum in the case of fully solid or fully liquid PCM (Weinläder et al., 2005). The assumption was made in this study that a more comprehensive optical investigation of PCMs should enable better and more reliable utilisation of these materials in glazing systems. Therefore it was decided that optical characterisation measurements of the PCM should provide data in terms of the transmittance values in a wider wavelength range from 280 and 700 nm to include the part of the Ultra-Violet (UV) and the entire visible electromagnetic spectrum. Moreover, the data should be provided for the range of temperatures in order to investigate the particular PCM applicability for solar glazing in three cases: PCM in its liquid form, PCM in its solid form and PCM going through the phase change i.e. the mushy form.

The high performance PerkinElmer LAMBDA 1050 spectrophotometer (PerkinElmer, Cambridge, UK) was used to measure the transmittance spectra of the PCMs. The specifications of the device are given in Table 10.1.

This device was selected due to its high sensitivity and wide spectral range available for the transmittance measurements. The spectrophotometer does not provide temperature control of the investigated samples upon transmittance measurements. This represented an issue given that the objective of the optical study was to provide the transmittance spectra at different temperatures for the investigated PCMs. Hence a proper experimental protocol had to be implemented in order to obtain information regarding the optical behaviour of PCMs at different temperatures.

| Parameter | Value |
|---|---|
| Wavelength range | 175-3300 nm |
| Wavelength resolution | 0.2 nm |
| Package details |  |

***Table 10.1:*** *Specifications of the PerkinElmer LAMBDA 1050 spectrophotometer.*

Namely, prior to any transmittance measurement, the PCM sample placed in a glass cuvette with the volumetric capacity of 10 ml was maintained inside the environmental chamber for 2 h. It was presumed that this time was long enough for the sample to reach full thermal equilibrium at the specified temperature inside the chamber given the size of the testing cuvettes (10 ml). The temperature maintained inside the chamber was also the initial temperature at which the transmittance measurement was to start. After the 2 h inside chamber the sample was placed inside the spectrophotometer and continuous transmittance scans were performed until a moment labelled as the stable spectrum was obtained. The stable spectrum moment was the time when the difference in spectral data between the consecutive scans became negligible. Given the previously established wavelength range from 280 to 700 nm each scan inside the spectrophotometer lasted for about 5 min. As previously mentioned the PCM temperature could not be controlled within the spectrophotometer. Nevertheless, the air temperature inside the spectrophotometer was measured in every test (set of transmittance scans from the moment the sample at certain initial temperature was placed inside the spectrophotometer to the moment labelled as the stable spectrum) to enable the correct interpretation of the obtained results.

## 10.1.1 RT27 optical characterisation – results and discussion

The first investigated material was RT27. The material properties are given in Table 8.1. The recorded optical behaviour of RT27 at different temperatures and consequently in different states is shown in Figure 10.1.
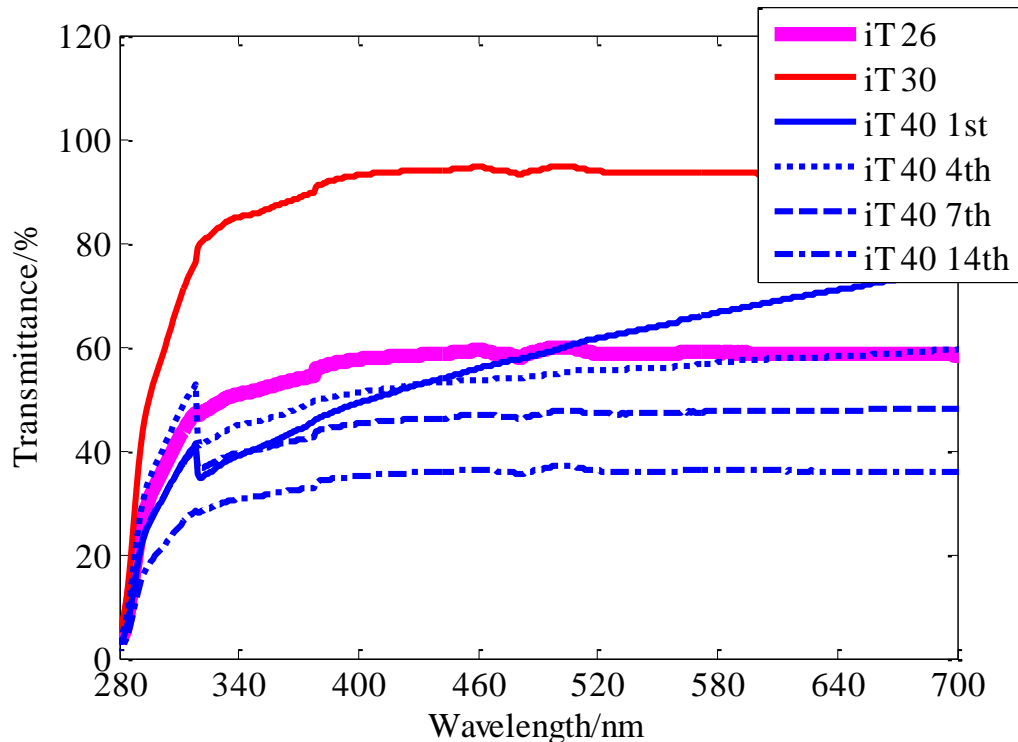


***Figure 10.1:*** *Transmittance – wavelength dependency for RT27 for different initial temperatures of the PCM sample; iT 26 – initial PCM temperature at 26 °C; iT 30 – initial PCM temperature at 30 °C; iT 40 1st – initial PCM temperature at 40 °C, 1ˢᵗ scan; iT 40 4th – initial PCM temperature at 40 °C, 4ᵗʰ scan; iT 40 7th – initial PCM temperature at 40 °C, 7ᵗʰ scan; iT 40 14th – initial PCM temperature at 40 °C, 14ᵗʰ scan (amended from Gowreesunker et al.,2013, p. 3).*

The obtained data were used as part of the experimental and numerical study of the optical and thermal aspects of a PCM-glazed unit and published in paper reported by Gowreesunker et al. (2013).

The first test was performed with the RT27 at the initial temperature of 26 °C. Once the sample was taken out from the chamber it was checked and the visual inspection showed that the PCM started to change its phase from liquid to solid. The

sample was then placed inside the spectrophotometer. The air temperature inside the instrument was 25 ±1 °C as recorded by a standard mercury thermometer. Three transmittance scans were performed resulting in very similar spectral data. The data from all three scans were averaged and presented as curve iT 26 in Figure 10.1. Given the experimental conditions in this test and the thermal RT27 data presented in subsection 8.3.2, curve iT 26 in Figure 10.1 corresponds to the mushy region of the RT27. In the second test, the fully liquid PCM with the initial temperature of 30 °C was placed inside the spectrometer with the inside air temperature of 27 ± 1 °C. Five consecutive scans were performed resulting again in similar transmittance values. The data from five scans were averaged and represented by curve iT 30 in Figure 10.1. This curve represents the transparency data of the liquid PCM sample. The third test was performed with the investigated material at an initial temperature of 40 °C. The sample was taken out of the chamber and placed inside the spectrophotometer with the inside air temperature of 23 ±1 °C. Initial scans resulted in very unstable spectral data. Hence, in total, fourteen scans were performed until the moment a stable spectrum was obtained. To have better visibility, only the $1^{st}$, $4^{th}$, $7^{th}$ and $14^{th}$ scan data were shown in Figure 10.1 as curves iT 40 1st, iT 40 4th, iT 40 7th, and iT 40 14th, respectively. The curve iT 40 14th in Figure 10.1 corresponds to the stable transmittance spectrum in the third test when, upon visual inspection performed after the test, the sample was in solid phase. Based on different measurements at various temperatures, it was concluded that the spectral data were very unstable during transitional processes inside the investigated material i.e. when the large differences between the initial temperature of the PCM and the air temperature inside the spectrophotometer were present. Furthermore, another observation was made. Namely, as the transmittance values change for the RT27 in different phases the spectral distribution over the entire spectrum (i.e. the shape of the transmittance spectra) stays relatively constant (Figure 10.1).

The transmittance of the liquid RT27 in the visible region was around 90 % (iT 30 in Figure 10.1). On the other hand, the respective transmittance of the RT27 corresponding to the mushy and solid states were 60 % and 38 % (iT 26 and iT 40 14th in Figure 10.1). The results obtained for the solid (38 %) and liquid (90 %) phases,

shown in Figure 10.1, are in a relatively good agreement with the solid (50 %) and liquid (90 %) transmittance values provided by Weinläder et al. (2005) for similar material RT25. The difference between the transmittance values in solid and liquid phases is evident in both cases. However, given the thermal properties of the investigated RT27 material presented in subsection 8.3.2 and the minimal transmittance value of 38 % it was concluded that the RT27 could be used in a carefully designed glazing systems.

Additionally, the obtained optical RT27 data (Figure 10.1) were used and observed from a different perspective (Figure 10.2).
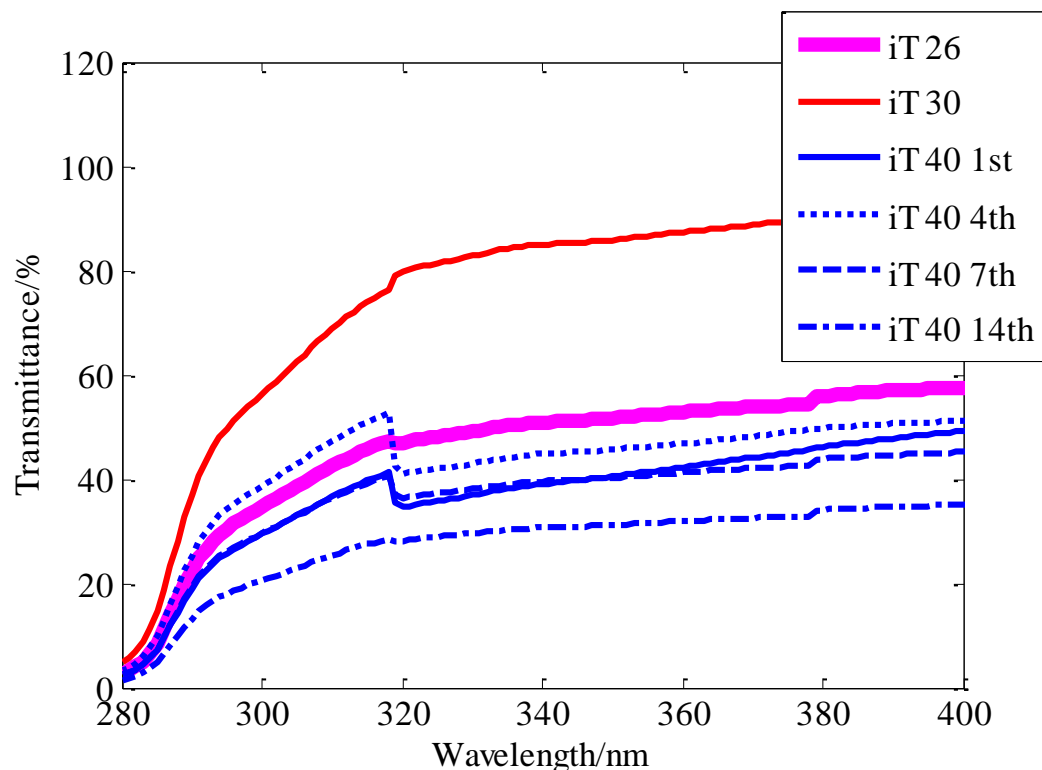


***Figure 10.2:*** *Transmittance – UV wavelength dependency for RT27 for different initial temperatures of the PCM sample; iT 26 – initial PCM temperature at 26 °C; iT 30 – initial PCM temperature at 30 °C; iT 40 1st – initial PCM temperature at 40 °C, 1$^{st}$ scan; iT 40 4th – initial PCM temperature at 40 °C, 4$^{th}$ scan; iT 40 7th – initial PCM temperature at 40 °C, 7$^{th}$ scan; iT 40 14th – initial PCM temperature at 40 °C, 14$^{th}$ scan.*

Namely, it is widely accepted that the protection from the UV radiation is an ongoing problem given the health damaging effects imposed by UV radiation. Glass envelopes represent the first line of defence against the UV radiation of the indoor

environments exposed to sunlight. However, the strength of this type of protection remains questionable given that glass is able to absorb only a portion of the UV radiation. Therefore an additional aim of this study was to check if the utilisation of PCMs in glazing units could be beneficial in terms of protection from the UV radiation.

For this reason the RT27 optical data (Figure 10.1) were zoomed-in to display the relevant transmittance data in the upper UV range from 280 nm to 400 nm (Figure 10.2). The RT27 transmittance data were compared to the corresponding data obtained from the measurement of the pure glass sample at room temperature (Figure 10.3). The comparison was performed to investigate the potential benefits of the RT27.
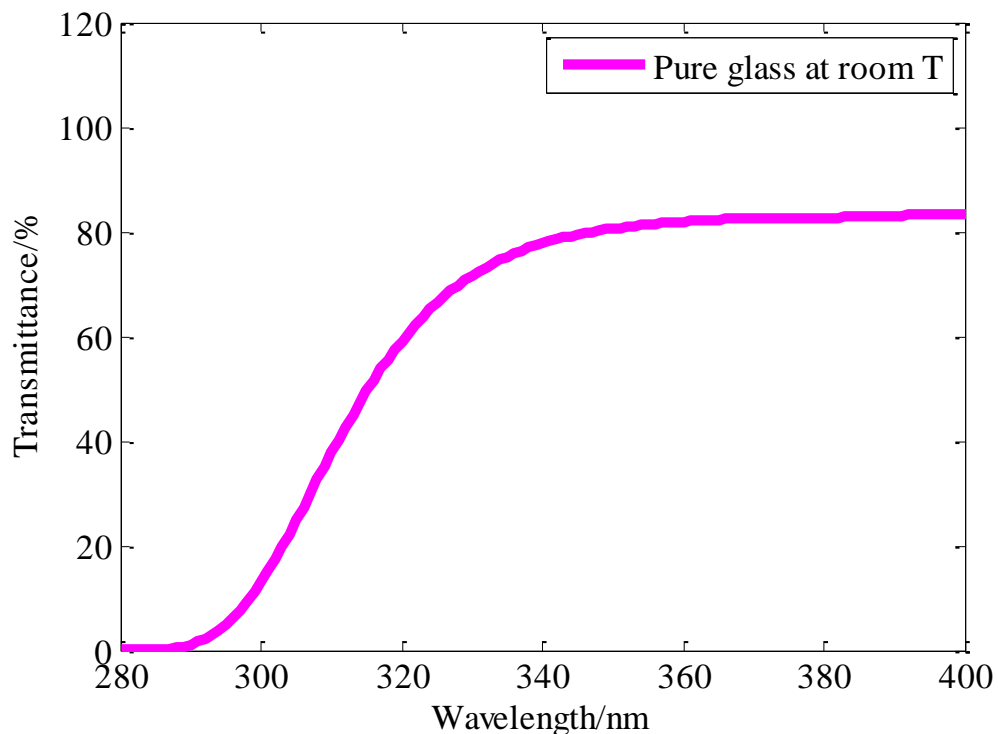


*Figure 10.3: Transmittance – UV wavelength dependency for pure glass at room temperature.*

According to the Figure 10.3 pure glass absorbs 20 % of the UV radiation in the upper Ultra-Violet A range (UVA) between 340 and 400 nm. The absorbed portion in the lower UVA range between 315 and 340 nm is between 40 and 20 %. The glass is much more absorbent (between 100 and 40 %) in the Ultra-Violet B (UVB) range between 280 and 315 nm. It becomes fully absorbent for UV radiation at wavelengths

below 290 nm (Figure 10.3). The RT27 in liquid form behaves similarly to pure glass (curve iT 30 in Figure 10.2). However, the RT27 in solid and mushy states (curves iT 40 14th and iT 26 in Figure 10.2) offers better UV protection than glass alone (around 40 % in the entire UVB region and between 100 and 50 % in the UVA range). The successful application of PCMs in the glazing units requires the materials to undergo through a phase change to release/store latent energy. Hence it is expected that the materials will be in solid and especially in mushy form for a significantly long time periods. Given this and the optical properties of the RT27 in the UV range it was concluded that the protection from the UV radiation could be an additional beneficial factor of PCM utilisation in glazing systems.

## 10.1.2 RT21 optical characterisation – results and discussion

Given the successful optical characterisation of RT27, it was decided to perform the optical investigations of another material from the Rubitherm's RT series, RT21 (Rubitherm GmbH, Berlin, Germany). The material properties are given in Table 7.6. The recorded optical behavior of RT21 at different temperatures is shown in Figure 10.4.

The first test was performed with the investigated material at an initial temperature of 18 °C. The sample was taken out of the chamber. Upon visual inspection the sample looked fully solid as expected (Table 7.6). It was placed inside the spectrophotometer with the inside air temperature of $26 \pm 1$ °C. As in the case of RT27, several consecutive scans were performed but rapid changes between the subsequent scans were rather evident. The stable spectrum was obtained after the 4$^{th}$ scan (curve iT 18 4th in Figure 10.4). This could be explained by the fact that a fully solid sample was placed in the spectrophotometer with the inside air temperature at least 4 °C higher than the typical phase change temperature of the investigated RT21 sample (Table 7.6). Given the size of the sample (10 ml cuvette) the relatively high temperature driving range (between 18 and 26 °C) led to the rapid phase change process of the investigated sample. Hence, it was concluded that the data from the 1$^{st}$,

$2^{nd}$, $3^{rd}$ and $4^{th}$ scan (curves iT 18 1st, iT 18 2nd, iT 18 3rd, and iT18 4th in Figure 10.4) could be attributed to the solid, mushy, and fully liquid state of the RT21.
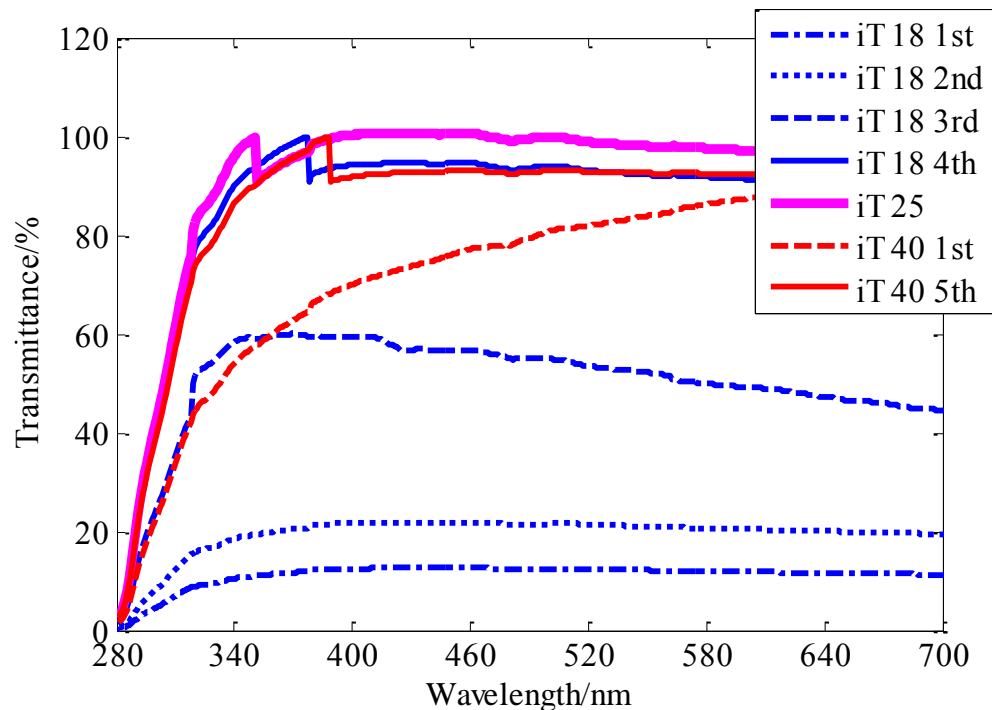


***Figure 10.4:*** *Transmittance – wavelength dependency for RT21 for different initial temperatures of the PCM sample; iT 18 1st – initial PCM temperature at 18 °C, 1ˢᵗ scan; iT 18 2nd – initial PCM temperature at 18 °C, $2^{nd}$ scan; iT 18 3rd – initial PCM temperature at 18 °C, $3^{rd}$ scan; iT 18 4th – initial PCM temperature at 18 °C, $4^{th}$ scan; iT 25 – initial PCM temperature at 25 °C; iT 40 1st – initial PCM temperature at 40 °C, $1^{st}$ scan; iT 40 5th – initial PCM temperature at 40 °C, $5^{th}$ scan.*

Two more tests were performed to verify this observation. The second test was performed with the RT21 at the initial temperature of 25 °C. Once the sample was taken out from the chamber it was checked and the visual inspection showed that the PCM was fully liquid. The sample was then placed inside the spectrophotometer with air temperature inside the instrument of 25 ±1 °C. Three consecutive transmittance scans were performed resulting in stable, almost identical spectral data. Given that the initial temperature of the PCM and the air temperature inside the spectrophotometer were same the observed behaviour was completely expected. The data from all three scans were averaged and presented as curve iT 25 in Figure 10.4. This curve was very similar to the curve iT 18 4th in Figure 10.4 confirming the earlier made observation that the curve iT 18 4th in Figure 10.4 should be attributed to the liquid form of RT21.

The third test was performed with the investigated material at the initial temperature of 40 °C. The fully liquid sample was taken out of the chamber and placed inside the spectrophotometer with the inside air temperature of 25 ±1 °C. Initial scans resulted in very unstable spectral data. This could be attributed to the large temperature difference between 40 and 25 °C. As in the case of RT27 measurements the temperature difference between the initial temperature of PCM and the air temperature inside the spectrophotometer resulted in cooling process of the PCM. The cooling process included the unstable temperature conditions within the PCM leading to the unstable spectral data regardless of the fully liquid form of the material at both the beginning and the end of the test. The stable spectrum was obtained after the 5$^{th}$ scan (iT 40 5th in Figure 10.4). To have better visibility, only the 1$^{st}$ and 5$^{th}$ scan data were shown in Figure 10.4 as curves iT 40 1st and iT 40 5th, respectively. The curve iT 40 5th corresponds to the PCM in equilibrium state and fully liquid form. Its similarity with the curves iT 18 4th in Figure 10.4 once more confirmed that curve iT 18 4th should be attributed to the PCM in liquid form. Given the PCM behaviour in the third test it was once more concluded that the spectral data have a tendency to be very unstable during both phase change and any temperature transitional processes inside the investigated material i.e. when the large differences between the initial temperature of the PCM and the air temperature inside the spectrophotometer are present. On the other hand and similarly to the RT27 case, as the transmittance values of RT21 change due to the phase changes the spectral distribution over the entire spectrum (i.e. the shape of the transmittance spectra) stays relatively constant (Figure 10.4).

The transmittance of the liquid RT21 in the visible region was between 100 and 90 % (curves iT 18 4th, iT 25 and iT 40 5th in Figure 10.1). On the other hand, the transmittance of the RT21 corresponding to the mushy state was between 60 and 40 % (curve iT 18 3rd in Figure 10.4). The solid state transmittance in the visible region was rather low 10 % (iT 18 1st in Figure 10.1). The results obtained for the liquid phase are in a very good agreement with the liquid transmittance values (90 %) of RT27 presented in the previous subsection and RT25 provided by Weinläder et al. (2005). However, the difference between the transmittance values in solid and liquid phases in the case of RT21 is rather large (around 80 %). Hence, it was concluded that the RT21

is not a good material to be used in PCM glazing units. Nevertheless, the obtained optical RT21 data (Figure 10.4) were used and zoomed-in to display the relevant transmittance data in the upper UV range from 280 nm to 400 nm (Figure 10.5).
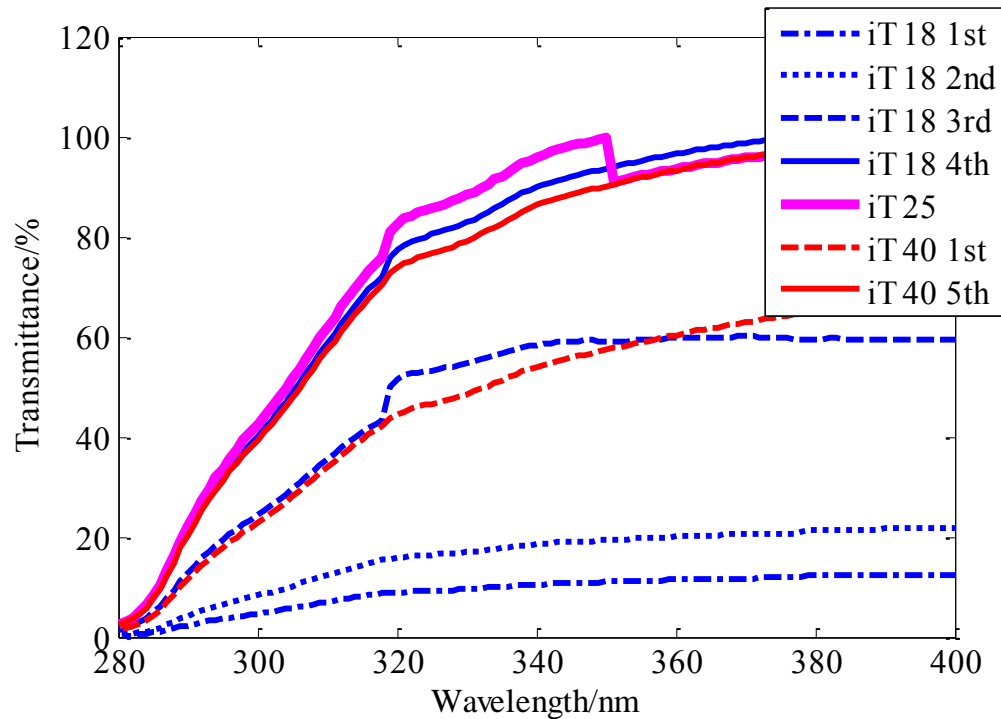


***Figure 10.5:*** *Transmittance – UV wavelength dependency for RT21 for different initial temperatures of the PCM sample; iT 18 1st – initial PCM temperature at 18 °C, 1ˢᵗ scan; iT 18 2nd – initial PCM temperature at 18 °C, 2ⁿᵈ scan; iT 18 3rd – initial PCM temperature at 18 °C, 3ʳᵈ scan; iT 18 4th – initial PCM temperature at 18 °C, 4ᵗʰ scan; iT 25 – initial PCM temperature at 25 °C; iT 40 1st – initial PCM temperature at 40 °C, 1ˢᵗ scan; iT 40 5th – initial PCM temperature at 40 °C, 5ᵗʰ scan.*

As in the case of RT27, the RT27 in liquid form behaves similarly to pure glass (Figure 10.3 and 10.5). The solid RT21 offers much better UV protection than glass being 70 % more absorbent. However, given its low transmittance in the visible region the benefits of RT21 utilisation in glazing systems are impractical.

# 10.2 Summary

As explained in chapter 3 solar applications implemented with PCMs incorporated into the glazing units represent a rather challenging application type. The PCMs are used due to their high latent energy potential to enhance the thermal mass of the building

envelopes in such applications. However, despite the commercialised solutions and those reported in research papers (Greenlite Glass Systems, Port Coquitlam, British Columbia; Ismail and Henriquez, 2001; Weinläder et al., 2005) the main problems associated with the PCM enhanced glazing systems remains in the change of the material's transparency during the phase change process. Therefore the knowledge of optical properties of PCMs in terms of the transmittance values over a range of temperature is necessary to reflect the behaviour of PCMs in different phases. Moreover this knowledge appears to be essential in the investigation of the particular PCM's applicability for the development of glazing systems used in solar applications.

To investigate this hypothesis, the preliminary optical tests to investigate the transmittance properties of the organic materials from the Rubitherm's RT series (Rubitherm GmbH, Berlin, Germany) were performed in this study. Two materials, RT27 and RT21 were investigated and the obtained optical results in conjunction with the details regarding the investigation procedure were presented in this chapter. Finally, the optical investigation studies showed that the phase change temperature is one of the most determinative factors of material's applicability in PCM enhanced glazing units used in solar applications.

# Chapter 11

# CONCLUSIONS AND DISCUSSION

One of the major limiting factors for both modelling and implementation of efficient PCM based TES systems as well as for the prediction of long-term behaviour of such systems is the inaccuracy/lack of the experimentally determined material data especially in terms of phase change temperature and enthalpy. This represents a serious problem since in addition to the benefits regarding the development of efficient PCM based TES systems the accurate knowledge of thermo-physical properties of existing materials is essential for the understanding of their limitations and hence for the development of new PCMs. The existing PCM thermal investigation methods have significant drawbacks and limitations as thoroughly explained in chapter 5. The aim of this research was to overcome at least some of the shortcomings of the existing PCM thermal investigation procedures. Hence an advanced PCM characterisation methodology based on the T-history method (Zhang et al., 1999) was developed and extensively used to verify the hypothesis that a better planned PCM experimental tests in terms of more accurate and precise sensing and control modalities should provide more comprehensive and reliable results than those described in the literature so far.

At the very early stage of the research project, a parametric test based on the simulations implemented using the Stefan's solution (one of the earliest phase change problem analytical solutions) was performed. The test was implemented to verify which PCM properties mostly affect the PCM behavior and founded on the notion that the influence of certain PCM parameters should reflect similarly in the highly complex TES systems as in simple solutions like Stefan's. The results of the early parametric study showed that the phase change temperature and the phase change enthalpy are the most important and dominant PCM properties. Once these two thermo-physical properties were validated as the most significant PCM properties the research was

continued towards the development of the advanced thermal PCM characterisation methodology.

The design strategy for the implementation of the advanced T-history method was developed (see section 6.1). The integral part of the design strategy was the development of the design rules which represented a set of input parameters to be taken into consideration prior to the development of the advanced T-history setup. These parameters included the basic measurement premises presented in chapter 5. Since PCM characterisation could be considered successful only if the size of the investigated sample was representative, its temperature and heat stored/released correctly determined and the thermal equilibrium maintained within the sample upon measurements these requirements had to be and were taken into the account as the design rules. This was done so the development of the entire advanced T-history setup could be continuously bound by the main criteria that need to be satisfied in any PCM measurement. An additional design rule to keep the Biot number below 0.1 was adopted to satisfy the requirement imposed by the original T-history method (Zhang et al., 1999). After the design rules were established the experimental setup of the advanced T-history was developed (see section 6.2). The development of the experimental setup included the investigation and selection of the control and sensing modalities and design and development of the testing containers. The BINDER KMF 115 (Binder GmbH, Tuttlingen, Germany) environmental chamber was selected as the control modality after the careful considerations of the T-history setups reported in literature and the established design rules. The chamber was selected primarily due to its temperature accuracy of ±0.2 °C. This was the first time the accuracy of the T-history control facility could be guaranteed to that degree. The selection of the sensing modalities was also done based on the design rules and the T-history studies reported in literature. It was decided that both thermocouples and thermistors will be used in the advanced T-history method. Considering the design rule regarding the sample size another objective of this research to test the PCM samples larger than those reported in literature was established. To achieve this, the testing containers were properly designed and custom built. It was determined that the height of the testing tubes was essential in enabling the measurements of larger samples. Hence the developed test

tubes were 300 mm and 430 mm long. Two different sizes were selected to enable the measurements of different size samples. The development of the test tubes was also based on the previously adopted design rules.

Once the advanced T-history setup was assembled the proper instrumentation system to enable the correct temperature measurements of the PCM samples was developed. Following the previously established design rules the value of ±0.5 °C was set as the desired temperature accuracy in the PCM related measurements and adopted as the validation criterion in the instrumentation development.

The instrumentation system 1 was developed for the thermocouple temperature measurements (see section 7.1). The development of the instrumentation system included the sensor selection (an RS 621-2158 type K thermocouple was selected due to its small 0.2 mm probe diameter) and the design and implementation of the linearisation/signal conditioning and data acquisition systems. A new LabView virtual instrument PCM_DAQ.vi was developed to allow the continuous acquisition of T-history signals. The measurement prototype based on the instrumentation system 1 was built and used to perform the first PCM measurement using the advanced T-history setup. The measurement was performed on the well-known organic RT21 PCM from the Rubitherm's RT series (Rubitherm GmbH, Berlin, Germany). The raw voltage results obtained in the measurement were subjected to some post-processing in order to obtain the temperature data. The post-processing of signals included filtering and calibration. The low pass generalised Butterworth filter based on the *maxflat* function was implemented in MATLAB and was used to clean the raw voltage signals. The temperature deviations of the obtained T-history curves (max ±1.9 °C) by far exceeded the validation value of ±0.5 °C. Hence the conclusion was made that the instrumentation system 1 was not accurate enough to be used in the advanced T-history method. Moreover, the measurement results confirmed that despite the usage reports in the literature the thermocouples were not suitable for high-accuracy T-history temperature measurements due to their accuracy and noise related issues. Following these observations a different type of temperature sensors was considered for the successful implementation of the advanced T-history method.

The instrumentation system 2 was developed for the thermistor based temperature measurements (see section 7.2). The selected sensors were MA100BF103A NTC thermistors due to their high sensitivity of 5 %°C$^{-1}$ and small 0.762 mm diameter probes. Given the thermistor high nonlinearities the Wheatstone Bridge (WB) based linearisation and signal conditioning circuit was developed. For the optimal development of the linearisation circuit a proper linearisation model was implemented in MATLAB. The measurement prototype based on the instrumentation system 2 was built and used to perform the T-history measurement of RT21. This appears to be the first time, apart from the studies reported as parts of this project (Stankovic and Kyriacou, 2012; Stankovic and Kyriacou, 2013), thermistors were used as the sensing modality in the T-history based measurements. The raw voltage results obtained in the measurement were subjected to proper filtering using the previously developed digital low-pass filter. The calibration measurements were performed and processed using the calibration script developed in MATLAB to obtain the temperature data from the raw T-history data. The temperature deviations of the obtained T-history curves (greater than ±1.3 °C) also exceeded the validation value of ±0.5 °C. The results showed that the instrumentation system 2 could not be used in PCM measurements. Nevertheless, the general quality of the obtained results showed the promising results that thermistors were suitable to be used as sensing modalities in the advanced T-history method.

The instrumentation system 3 was developed to achieve more accurate thermistor based temperature measurements (see section 7.3). New linearisation and signal conditioning circuit based on the Serial-Parallel Resistor (SPR) connection was developed using the new linearisation model implemented in MATLAB. The measurement prototype based on the instrumentation system 3 was built and used to for the T-history measurement of RT21. The raw voltage results obtained in the measurement were subjected to proper filtering and calibration procedures to determine the T-history curves. The obtained temperature deviations (lower than ±0.3 °C) were well below the validation value of ±0.5 °C. The results showed that the validation process was finally successful. This appears to be the first time, apart from the studies reported as parts of this project (Stankovic and Kyriacou, 2012; Stankovic and

Kyriacou, 2013), high temperature accuracy was successfully demonstrated in the T-history related measurements partially supporting the hypothesis that better planned PCM studies in terms of control and sensing modalities lead to more reliable data. Consequently, the instrumentation system 3 was adopted as the instrumentation system of the advanced T-history method.

The successful outcome of the validation process led to a set of comprehensive studies of organic PCMs using the advanced T-history method. At this stage of research the computational data evaluation technique was implemented to determine the basic thermo-physical PCM properties predominantly the phase change temperature (range) and the energy stored/released based on the measured T-history data. For this purpose, the time delay data evaluation procedure developed by Marin et al. (2003) was adapted to enable the calculation of heat released/stored in given temperature intervals upon cooling and heating of PCMs and implemented using MATLAB.

Following the successful implementation of the data evaluation procedure, a set of parametric studies of the well-known RT21 PCM were performed to discover which parameters mostly influence the PCM characterisation and to what extent. The first parametric study was carried out to investigate how the size of the sensors used in T-history based measurements affects the PCM characterisation results. The data from two different measurements of RT21, one with the smaller 0.762 mm diameter probe sensors and the other with the larger 2 mm diameter probe sensors were compared. The results showed that the sensor size indeed affects the degree of subcooling in the investigated PCM samples. Regardless of the speculations that the degree of subcooling could be dependent on the sample size, this appears to be the first experimental demonstration that the sensor if used inside the PCM sample during T-history characterisation measurement acts as a nucleating agent and therefore suppresses the naturally existing subcooling phenomenon. Consequently, it was concluded that sensors used in the T-history studies need to be as small as possible. The second parametric study was performed to investigate how the position of the sensors used in T-history based measurements influences the PCM characterisation. Thus, the data from the internal and surface temperature measurements of RT21 were compared. The results showed that the T-history surface measurements result in the

misleading PCM characterisation data in terms of both temperature and heat release/storage capacity. This also appears to be the first experimental demonstration of the observed behaviour. It was concluded that the measurements with the sensors placed on the surface of the test tubes cannot be used in the advanced T-history measurements. The third parametric study was performed to determine the effects the insulation of the test tubes has on the PCM characterisation given the potential temperature gradients that could be created in PCM samples due to the high cooling/heating rates (see section 5.1). Hence, the data from the RT21 measurements with varying insulation thicknesses used on the test tubes were compared. The results evidently showed, for the first time, that insulation thickness extensively affects the PCM characterisation results especially in terms of the heat release/storage capacities and the observed hysteresis between cooling and heating data. The 6 mm insulation thickness was identified as the optimal value to be used in the advanced T-history measurements. It was concluded that proper insulation of the test tubes is necessary to avoid the creation of thermal gradients inside PCM samples. Given that one of the objectives of this project was to perform the measurements of the larger PCM samples than those reported in literature so far, the effects of the sample's mass were examined in the fourth parametric test. The results from the characterisation measurements of RT21 with sample masses of 19.5 and 41.4 g were compared and it was concluded that the sample mass does not affect the PCM characterisation results when advanced T-history method is used. Moreover, this was the first successful measurement of the larger PCM sample than those reported in literature thus enabling the future characterisation of PCMs in the same size margin.

The parametric tests enabled the usage of the advanced T-history method for the characterisation of various organic PCMs. Firstly, the well-known materials RT21 and RT27 were tested. The results including the details regarding the material's behaviour upon both cooling and heating, the heat release/storage in given 0.5 °C wide temperature intervals, the respective enthalpy-temperature curves, and the total heat released/stored with respect to mass and volume evaluated in the temperature interval between 15 and 30 °C were presented for both materials (see section 8.2). This appears to be the first time such comprehensive presentation of the PCM characterisation data

and moreover with the alike precision was given. The obtained results showed very good agreement with the PCM data provided by the manufacturer in terms of both temperature (within the $\pm 1\,°C$ margin) and heat release/storage content (within the $\pm 10\,\%$ margin) proving the validity of the advanced T-history method developed in this study. Moreover, the results supported the original hypothesis regarding the better planned PCM experimental tests. Another significant observation regarding the constant decline in heat capacity values in the consecutive cooling and heating cycles of RT21 was made. This once more supported the claims that the sensor inside PCM samples acts as a nucleating seed and hence needs to be as small as possible to avoid the interference with the natural course of the phase change process.

The encouraging results obtained from the measurement of the materials from the RT organic series led to the characterisation of the corresponding materials from the less investigated organic PT series. Three materials PT20, PT27, and PT28 were successfully tested and the comprehensive characterisation data presented for the first time (see section 8.4). The results showed that the materials from the PT series (particularly PT20 given the registered subcooling and hysteresis margins in the case of PT27 and PT28) are able to offer a competitive performance in terms of both heat content and phase change temperatures with the assertive advantages being the bio origin and 100 % renewability.

Following the successful characterisation of organic PCMs the advanced T-history method was used for the characterisation of inorganic materials as well. Given the distinguishable properties of the inorganic and organic PCMs especially in terms of the subcooling phenomenon the new computational technique was developed and implemented in MATLAB to take the subcooling into account and therefore enable proper characterisation of inorganic PCMs. Despite the existing suggestions and speculations (Mehling and Cabeza, 2008) this was the first implementation of the T-history data evaluation technique considering subcooling.

The comprehensive characterisation data were presented for two inorganic materials, SP22 and SP25 (see section 9.2). Here, in addition to the respective data given as in the case of organic PCMs, the degree of subcooling and the data regarding the heat lost upon it were also presented. The results showed that the non-negligible

portion of the total heat stored upon PCM heating (around 12 %) gets lost due to subcooling upon the PCM cooling process and hence needs to be adequately presented. This appears to be the first time, apart from the study reported as part of this project (Stankovic and Kyriacou, 2013), the subcooling was properly addressed in any PCM related measurement. These investigations showed that inorganic materials, even upon subcooling, appear to offer more competitive performance especially in terms of volumetric heat capacities than their organic counterparts.

Additionally, the PT27 and PT28 materials were re-evaluated using the newly developed data evaluation technique but it was concluded that the subcooling in the case of this materials can be neglected considering the observed degree of subcooling (0.5 °C) and heat lost (below 5 %) margins (see section 9.3).

Finally, pilot optical studies of RT27 and RT21 were performed to determine the respective transmittance values in a wide wavelength range (from 280 and 700 nm) at different temperatures. These tests were performed to investigate the potential of these materials for the utilisation in PCM enhanced glazing units, given the emerging popularity of PCM solar applications. Another objective was to verify the PCMs' potential for UV protection. Consequently, the transmittance spectra were presented for both PCMs in their respective liquid, mushy, and solid phases for the first time, apart from the study reported as part of this project (Gowreesunker et al., 2013). The results showed that the transmittance values decline as the sample undergoes the change from liquid to solid phase. The transmittance values (predominantly in the visible part of spectrum) in the solid phase are the deciding factor of the PCM's applicability for solar glazing. It was concluded that these values are also dependant on the PCM's phase change temperature (38 % in the case of RT27 versus 10 % in the case of RT21) resulting in the phase change temperature being one of the determinative factors of PCM's applicability in glazing units. In addition, it was concluded that PCMs in general provide better UV protection than glazing systems alone. However, the benefits of this highly depend on the applicability of the particular PCM given its transmittance properties in the visible part of the spectrum.

# 11.1 Future work

More PCM characterisation studies should be performed on different organic and inorganic materials to further validate the advanced T-history method. In an attempt to obtain more accurate and precise data than those presented in this study the goal of further efforts should be the minimisation of contact between the sensors and samples given that the sensor size was identified as one of the most influential parameters in T-history based investigations, as confirmed by several observations made in this study. This could be achieved in two ways. Either smaller sensors should be used or some reliable non-contact temperature measurements with high accuracy (±0.5 °C) provided. Regarding the utilisation of smaller sensors, the thermocouples appear to offer the smallest solutions in the case of conventional temperature sensors. However, the measurement results in this study showed that thermocouples were not suitable for high-accuracy T-history temperature measurements due to their accuracy and noise related issues. Given the importance of the reduction of sensor size the thermocouples could be further investigated. Smaller size thermistors than the 0.762 mm diameter probe ones, used in this study, would be an even a better solution. The best solution however would be the implementation of the high accuracy non-contact temperature measurement system. One observation that could be exploited in the future development of such measurement system was made in this study. Namely, upon the optical investigations the large temperature differences between the initial temperature of the investigated PCM and the air temperature inside the spectrophotometer always resulted in unstable and rapidly changing spectral data. An effort towards the discovery of potential correlations between the changes of the spectral transmittance data and evident changes of temperature inside PCM could be made in the future investigations.

To summarise, the advanced T-history method was developed and validated in a series of characterisation studies of both organic and inorganic phase change materials. In addition to experimental confirmation of various speculations regarding the parameters influencing the PCM characterisation, the utilisation of the advanced method proved that more accurate and precise PCM experimental tests provide more

comprehensive and reliable results than those described in the literature so far and hence enable the development of more efficient PCM based TES systems.

# APPENDIX A  Code listings of the MATLAB based scripts and functions

## A.1 The digital low pass filter function

```
% A digital low pass filter function
% Copyright S Stankovic

% *** function body *** %

function [filtered_data,fig_counter]=...
    filterData_LF_TF_MF(Input_Data,Sampling_Rate,...
    Cut_Off, Figure_Counter)

% input data processing

format long;
number_of_channels=size(Input_Data,2);
t=0:1/Sampling_Rate:(length(Input_Data)-1)/Sampling_Rate;
fig_counter=Figure_Counter+1;
figure(fig_counter);
plot (t, Input_Data');
title('Input data');

% Max flat filter design

n = 20;
Wn = Cut_Off*2/(Sampling_Rate);
m = 2;
[b,a]=maxflat(n,m,Wn);
fig_counter=fig_counter+1;
figure(fig_counter);
freqz(b,a,1000,Sampling_Rate);
title('TF MaxFlat filter response')

% data filtering

filtered_data=filtfilt(b,a,Input_Data);

% comparison of raw and filtered data

fig_counter=fig_counter+1;
```

```matlab
figure(fig_counter);
plot(filtered_data);
title('Filtered data');
fig_counter=fig_counter+1;
figure(fig_counter);
plot(Input_Data-filtered_data);
title('Noise');
for i=1:number_of_channels
    fig_counter=fig_counter+1;
    figure(fig_counter);
    plot(0:length(Input_Data)-1,Input_Data(:,i),
0:length(Input_Data)-1,filtered_data(:,i));
    title('Raw vs. Filtered data');
end
end
```

# A.2 The WB linearisation model

```matlab
% The WB linearisation model script
% Copyright S Stankovic

% memory cleaning

clear all; close all; clc;

% thermistor temperature-resistance dependency definition

format long;
T=10:39; % temperature values [Celsius] - linearising range
TK=T+273.15; % temperature [K]
Rtt=[32650.5 31032.1 29499.9 28052.4 26684.6 25391.2 ...
24168.2 23011.2 21916.3 20879.8 19898.3 18968.6 18087.6 ...
17252.6 16460.9 15710 14997.7 14321.6 13679.8 13070.4 ...
12491.6 11941.6 11418.9 10922 10449.5 10000 9572.32 ...
9165.29 8777.79 8408.68 8057.31 7722.43 7403.29 7098.42 ...
6808.36 6531.31 6265.75 6016.47 5776.05 5546.53 5327.34 ...
5117.97 4917.94 4726.77 4543.91 4369.33 4200.84 4040.81 ...
3889.51 3743.17 3603.1]; % Resistance values
Rt=Rtt(11:40);
RtMin=Rt(length(Rt))

% linerisation procedure

C=2.5*10^-3; % dissipation constant [W/Celsius]
deltaT=0.05; % max dissipation error
IMaxDesign=sqrt(deltaT*C/RtMin)*10^3 % [mA]
Vin=5;
R3Min=Vin/(IMaxDesign*10^-3)-RtMin;
R3=R3Min:20:100000;
R2=1:20:50000;
R3Design=-1; ResMin=10^6;
k=1;
for l=1:length(R3)
    VoutRt=Vin*Rt./(R3(l)+Rt);
    [p,SS]=polyfit(VoutRt',T',1);
    if (SS.normr<ResMin)
        ResMin=SS.normr;
        R3Design=R3(l);
        VDesign=Vin*Rt./(R3Design+Rt);
    end
    V=VoutRt';
end
k=k+1;
figure(k);
plot(VDesign,T);
```

# A.3 The thermistor calibration script

```matlab
% The thermistor calibration script
% Copyright S Stankovic

% memory cleaning

clear all; close all; clc;

% initialising the time counter

tStart=tic;

% setting of input paramters

FILE_PATH='C:\Eksperimenti\Calibration\';
INPUT_FILE_NAME='Calibration';
EXTENSION='.lvm';
HEADERLINES=23;
DELIMITER='\t'; % tab
END_OF_LINE='\n'; % end of line
CONVERSION='%f';
NUMBER_OF_CHANNELS=3;
SAMPLING_RATE=10; % Hz
GAIN=1; % circuit gain
NEGATIVE_GAIN=0;
LAST_TEMP=39;
START_TEMP=10;
NUMBER_OF_TEMP_POINTS=LAST_TEMP-START_TEMP+1; %
TIME_STEP_MIN=5; % in minutes
INITIAL_TIME_STEP_MIN=3.5; % in minutes
AVG_TIME_STEP_MIN=1; % in minutes
CUT_OFF_TIME_MIN=15-4.95; %in minutes
TIME_STEP=TIME_STEP_MIN*60*SAMPLING_RATE; % in seconds
INITIAL_TIME_STEP=INITIAL_TIME_STEP_MIN*60*SAMPLING_RATE;
AVG_TIME_STEP=AVG_TIME_STEP_MIN*60*SAMPLING_RATE; % in seconds
CUT_OFF_TIME=CUT_OFF_TIME_MIN*60*SAMPLING_RATE %in seconds

% calibration data pre processing

format long;
full_input_file_name=strcat(FILE_PATH,INPUT_FILE_NAME, ...
EXTENSION);
input_data=importdata(full_input_file_name,DELIMITER, ...
HEADERLINES);
v_input=input_data;
if (HEADERLINES~=0)
    v_sorted_input=zeros(length(v_input.data),0);
    for i=1:NUMBER_OF_CHANNELS
        v_sorted_input=[v_sorted_input v_input.data(:,i+1)];
    end
```

```matlab
    else
        v_sorted_input=v_input;
    end
    if (NEGATIVE_GAIN==1)
        v_input_sorted=v_sorted_input*(-1);
    else
        v_input_sorted=v_sorted_input;
    end
    t=0:1/SAMPLING_RATE:(length(v_input_sorted)-1)/SAMPLING_RATE;
    kk=1;
    kk=kk+1; figure (kk);
    axis([0 (length(v_input_sorted)-1)/SAMPLING_RATE 0 5]);
    hold on;
    plot (t, v_input_sorted'); % V vs t
    title('Input voltage data');
    data_length=length(v_input_sorted);% in seconds
    fs=SAMPLING_RATE;
    v_filtered=filterData_LF_TF_MF(v_input_sorted,fs,0.025, kk);
    v_out_cut=v_filtered(CUT_OFF_TIME:length(v_filtered), ...
        1:NUMBER_OF_CHANNELS); % cut first T step in time
    kk=kk+1;figure(kk);
    plot( v_out_cut);
    ylabel('Cut voltage data');
    data_length=length(v_out_cut); % in seconds
    title('Filtered and cut voltage data');
    t=0:(data_length-1); % time data
    start=START_TEMP;
    final=LAST_TEMP;

    % calibration data fitting

    v_out_avg_for_fitting=[];
    T_out_lin_avg_for_fitting=[];
    T=(start:final)';
    T_channels=zeros(0,NUMBER_OF_CHANNELS);
    for i=1:NUMBER_OF_CHANNELS
        T_channels=[T_channels T];
    end
    for i=1:(final-start+1)
        v_out_avg_for_fitting(i,1:NUMBER_OF_CHANNELS)= ...
            mean(v_out_cut(INITIAL_TIME_STEP+ ...
            TIME_STEP*(i-1):INITIAL_TIME_STEP+TIME_STEP*(i-1)+ ...
            AVG_TIME_STEP,1:NUMBER_OF_CHANNELS));
    end
    v_out_avg_for_fitting= ...
        v_out_avg_for_fitting(1:length(v_out_avg_for_fitting) ...
        -(LAST_TEMP-final),1:NUMBER_OF_CHANNELS); % 10 to 39
    kk=kk+1; figure(kk);
    plot(v_out_avg_for_fitting);
    ylabel('Voltage data for fitting');
    title('Data for fitting');
    for i=1:NUMBER_OF_CHANNELS
```

268

```matlab
    p_lin(:,i)=polyfit(v_out_avg_for_fitting(:,i),T,1);
    T_calc_lin(:,i)=polyval( p_lin(:,i), ...
        v_out_avg_for_fitting(:,i));
end
T_real=T;
T_real_Ch=T_channels;
V_real=v_out_avg_for_fitting;
table_lin=[V_real T_real T_calc_lin abs(T_real_Ch-T_calc_lin)];
for i=1:NUMBER_OF_CHANNELS
    max_lin_fit_error(:,i)= ...
max(table_lin(1:length(table_lin)-1,2*NUMBER_OF_CHANNELS+1+i));
max_lin_fit_error_real(:,i)=
...max(table_lin(:,2*NUMBER_OF_CHANNELS+1+i));
    T_lin_fit(:,i)=polyval( p_lin(:,i),v_out_cut(:,i));
end
kk=kk+1; figure(kk);
plot(T_lin_fit);
ylabel('Linear fit temperature');
kk=kk+1; figure(kk);
plot(T_real_Ch,abs(T_real_Ch-T_calc_lin));
ylabel('Absolute error for practical linear fit');
xlabel('Temperature');

tElapsed=toc(tStart);
```

# A.4 The SPR linearisation model

```matlab
% The SPR linearisation model script
% Copyright S Stankovic

% memory cleaning

clear all; close all; clc;

% initialising the time counter

tStart=tic;

% thermistor temperature-resistance dependency definition

format long;
T=10:39; % temperature values [Celsius] - linearising range
TK=T+273.15; % temperature [K]
Rtt=[32650.5 31032.1 29499.9 28052.4 26684.6 25391.2 ...
24168.2 23011.2 21916.3 20879.8 19898.3 18968.6 18087.6 ...
17252.6 16460.9 15710 14997.7 14321.6 13679.8 13070.4 ...
12491.6 11941.6 11418.9 10922 10449.5 10000 9572.32 ...
9165.29 8777.79 8408.68 8057.31 7722.43 7403.29 7098.42 ...
6808.36 6531.31 6265.75 6016.47 5776.05 5546.53 5327.34 ...
5117.97 4917.94 4726.77 4543.91 4369.33 4200.84 4040.81 ...
3889.51 3743.17 3603.1]; % Resistance values
Rt=Rtt(11:40);
RtMin=Rt(length(Rt));

% linerisation procedure

C=2.5*10^-3; % dissipation constant [W/Celsius]
deltaT=0.05; % max dissipation error
IMaxDesign=sqrt(deltaT*C/Rt(length(Rt)))*10^3 % [mA]
R1=1:20:100000;
R2=1:20:50000;
Vin=5;
R1Design=-1; R2Design=-1; ResMin=10^6;
k=1;
for l=1:length(R1)
    for m=1:length(R2)
        Rpar(m,:)=R2(m)*Rt./(R2(m)+Rt);
        VoutRt=Vin*Rpar./(R1(l)+Rpar);
        [p,SS]=polyfit(VoutRt(m,:)',T',1);
        if (SS.normr<ResMin)
            ResMin=SS.normr;
            R1Design=R1(l);
            R2Design=R2(m);
            RparDesign=R2Design*Rt./(R2Design+Rt);
            VDesign=Vin*RparDesign./(R1Design+RparDesign);
        end
```

```matlab
        end
    V=VoutRt';

% visualisation

    figure(k); k=k+1;
    mesh(V); % 3D view
    colormap('Jet');
    colorbar;
    shading interp;
    figure(gcf);
    hold on;
end
k=k+1;
figure(k);
plot(VDesign,T);

tElapsed=toc(tStart);
```

# A.5 The time delay evaluation function

```matlab
% Time delay evaluation function
% Copyright S Stankovic

% *** function body *** %

function [T_avg1, heat1, fig_counter]=time_delay(Mode,...
    Input_T,Input_High_T, Input_Low_T, Input_Delta_T,...
    Input_Sensitivity, M, N, Figure_Counter)

fig_counter=Figure_Counter;
T_avg1=0;
heat1=0;
T1=Input_T+273.15;

% heat released/stored evaluation

j=0; k=0; i=1; DELTA_tm=1;
if (Mode=='c')
    while (i+DELTA_tm<length(T1))
        if( ((T1(i,2)-273.15)<Input_High_T) &&...
                ((T1(i+DELTA_tm,2)-273.15)>Input_Low_T) &&...
                ((T1(i,3)-T1(i,1))>Input_Sensitivity) &&...
                ((T1(i+DELTA_tm,3)-...
                T1(i+DELTA_tm,1))>Input_Sensitivity))
            if( abs((T1(i+DELTA_tm,2)-T1(i,2)))...
                >=Input_Delta_T)
                tr_i=find(abs(T1(:,3)-...
                T1(i,2))<=Input_Sensitivity,1);
                tr_ip1=find(abs(T1(:,3)-T1(i+DELTA_tm,2))...
                <=Input_Sensitivity,1);
                tm_i=i;
                tm_ip1=DELTA_tm+i;
                j=j+1;
                heat1(j,1)=(M*DELTA_tm)/(tr_ip1-tr_i)-N;
                T_avg1(j,1)= (T1(i,2)+T1(i+DELTA_tm,2))/2;
                i=i+DELTA_tm;
                DELTA_tm=1;
            else
                DELTA_tm=DELTA_tm+1;
            end
        else
            i=i+1;
            DELTA_tm=1;
        end
    end
else
    while (i+DELTA_tm<length(T1))
        if( ((T1(i+DELTA_tm,2)-273.15)<Input_High_T)...
                && ((T1(i,2)-273.15)>Input_Low_T) &&...
```

```matlab
                    ((T1(i,1)-T1(i,3))>Input_Sensitivity)...
                    && ((T1(i+DELTA_tm,1)-...
                    T1(i+DELTA_tm,3))>Input_Sensitivity))
            if( abs((T1(i+DELTA_tm,2)-T1(i,2)))>=Input_Delta_T)
                j=j+1;
                tr_i=find(abs(T1(:,3)-...
                T1(i,2))<=Input_Sensitivity,1);
                tr_ip1=find(abs(T1(:,3)-T1(i+DELTA_tm,2))...
                    <=Input_Sensitivity,1);
                tm_i=i;
                tm_ip1=DELTA_tm+i;
                heat1(j,1)=(M*DELTA_tm)/(tr_ip1-tr_i)-N;
                T_avg1(j,1)= (T1(i,2)+T1(i+DELTA_tm,2))/2;
                i=i+DELTA_tm;
                DELTA_tm=1;
            else
                DELTA_tm=DELTA_tm+1;
            end
        else
            i=i+1;
            DELTA_tm=1;
        end
    end
end
T_avg1=T_avg1-273.15;
heat1=heat1.*Input_Delta_T;
end
```

# A.6 The enthalpy calculation function

```matlab
% Enthalpy calculation function
% Copyright S Stankovic

% *** function body *** %

function [calc_enthalpy, fig_counter]=...
    calc_enthalpy(Heat,Input_Delta_T,...
    Output_File_Path,Output_File_Name, Figure_Counter)

j=1; e_last_step=Heat(1,2);
e_calc(1,1)=Heat(1,2);
T_calc(1,1)=Heat(1,1);

% enthalpy evaluation

for i=1:length(cp_eff_calc)-1
    if (cp_eff_calc(i+1,1)-cp_eff_calc(i,1)>=Input_Delta_T)
        j=j+1;
        e_calc(j,1)=e_last_step+cp_eff_calc(i+1,2);
        e_last_step=e_calc(j,1);
        T_calc(j,1)=cp_eff_calc(i+1,1);
    else
        e_calc(j,1)=e_last_step+cp_eff_calc(i+1,2);
        e_last_step=e_calc(j,1);
    end
end
e_calculated=[T_calc e_calc];
fig_counter=Figure_Counter;
fig_counter=fig_counter+1;
figure(fig_counter);
plot(e_calculated(:,1),e_calculated(:,2),e_calculated(:,1),...
    e_calculated(:,2),'o');
title(Output_File_Name);
saveInto_Lvm_File([e_calculated(:,1) e_calculated(:,2)],...
    Output_File_Path, Output_File_Name);
calc_enthalpy=e_calculated;
end
```

# A.7 The time delay with subcooling evaluation function

```matlab
% Time delay with subcooling evaluation function
% Copyright S Stankovic

% *** function body *** %

function [T_avg1, heat1, fig_counter]=time_delay_sc(Mode,...
    Input_T,Input_High_T, Input_Low_T, Input_Delta_T,...
    Input_Sensitivity, M, N, Figure_Counter)

fig_counter=Figure_Counter;
T_avg1=0;
heat1=0;
T1=Input_T+273.15;

% heat released/stored evaluation

j=0; k=0; i=1; DELTA_tm=1;
if (Mode=='c')
    while (i+DELTA_tm<length(T1))
        if( ((T1(i,2)-273.15)<Input_High_T) &&...
                ((T1(i+DELTA_tm,2)-273.15)>Input_Low_T) &&...
                ((T1(i,3)-T1(i,1))>Input_Sensitivity) &&...
                ((T1(i+DELTA_tm,3)-...
                T1(i+DELTA_tm,1))>Input_Sensitivity))
            if( abs((T1(i+DELTA_tm,2)-T1(i,2)))...
                    >=Input_Delta_T)
                tr_i=find(abs(T1(:,3)-...
                    T1(i,2))<=Input_Sensitivity,1);
                tr_ip1=find(abs(T1(:,3)-T1(i+DELTA_tm,2))...
                    <=Input_Sensitivity,1);
                tm_i=i;
                tm_ip1=DELTA_tm+i;
                j=j+1;
                heat1(j,1)=(M*DELTA_tm)/(tr_ip1-tr_i)-N;
                T_avg1(j,1)= (T1(i,2)+T1(i+DELTA_tm,2))/2;
                i=i+DELTA_tm;
                DELTA_tm=1;
            else
                DELTA_tm=DELTA_tm+1;
            end
        else
            i=i+1;
            DELTA_tm=1;
        end
    end
    T_avg1=T_avg1-273.15;
    sorted_data=sortDoubleColumnData([T_avg1 heat1]);
    SC=0;
    k=0;j=0;
```

```matlab
    for i=1:length(sorted_data)
        if(sorted_data(i,2)<0)
            k=k+1;
            SC(k,1)=sorted_data(i,1);
            SC(k,2)=sorted_data(i,2);
        else
            j=j+1;
            HR(j,1)=sorted_data(i,1);
            HR(j,2)=sorted_data(i,2);
        end
    end
    if(SC~=0)
        TN=SC(1,1);
        TPC=SC(size(SC,1),1)
        clear heat1;
        heat1=[HR.*Input_Delta_T SC.*Input_Delta_T];
    end
else
    while (i+DELTA_tm<length(T1))
        if( ((T1(i+DELTA_tm,2)-273.15)<Input_High_T)...
                && ((T1(i,2)-273.15)>Input_Low_T) a&&...
                ((T1(i,1)-T1(i,3))>Input_Sensitivity)...
                && ((T1(i+DELTA_tm,1)-...
                T1(i+DELTA_tm,3))>Input_Sensitivity))
            if( abs((T1(i+DELTA_tm,2)-T1(i,2)))>=Input_Delta_T)
                j=j+1;
                tr_i=find(abs(T1(:,3)-...
                    T1(i,2))<=Input_Sensitivity,1);
                tr_ip1=find(abs(T1(:,3)-T1(i+DELTA_tm,2))...
                    <=Input_Sensitivity,1);
                tm_i=i;
                tm_ip1=DELTA_tm+i;
                heat1(j,1)=(M*DELTA_tm)/(tr_ip1-tr_i)-N;
                T_avg1(j,1)= (T1(i,2)+T1(i+DELTA_tm,2))/2;
                i=i+DELTA_tm;
                DELTA_tm=1;
            else
                DELTA_tm=DELTA_tm+1;
            end
        else
            i=i+1;
            DELTA_tm=1;
        end
    end
    T_avg1=T_avg1-273.15;
    heat1=heat1.*Input_Delta_T;
end
end
```

# APPENDIX B   Publication list

## Peer-reviewed journal and conference publications

STANKOVIC, S. B. and KYRIACOU, P. A. (2013) 'Improved measurement technique for the characterization of organic and inorganic phase change materials using the T-history method', *Applied Energy,* 109 (9), p. 433-440.

GOWREESUNKER, B. L., STANKOVIC, S. B., TASSOU, S. A., and KYRIACOU, P. A. (2013) 'Experimental and numerical investigations of the optical and thermal aspects of a PCM-glazed unit', *Energy and Buildings,* 61 (6), p. 239-249.

STANKOVIC, S. B. and KYRIACOU, P. A. (2012) 'The effects of thermistor linearization techniques on the T-history characterization of phase change materials', *Applied Thermal Engineering,* 44 (13), p. 78-84.

STANKOVIC, S. B. and KYRIACOU, P. A. (2012) 'Improved measurement technique for the characterisation of phase change materials using the T-history method' in INNOSTOCK 12th International Conference on Energy Storage, LLeida, Spain, University of Lleida, May 16-19, 2012, p. 206-207.

STANKOVIC, S. B. and KYRIACOU, P. A. (2011) 'Comparison of thermistor linearization techniques for accurate temperature measurement in phase change materials', *Journal of Physics: Conference series,* 301 (1), p. 1-6.

# Bibliography

ARKAR, C. and MEDVED, S. (2005) 'Influence of accuracy of thermal property data of a phase change material on the result of a numerical model of a packed bed latent heat storage with spheres', *Thermochimica Acta*, 438 (1-2), p. 192-201.

ARKAR, C., VIDRIH, B., and MEDVED, S. (2007) 'Efficiency of free-cooling using latent heat storage integrated into the ventilation system of a low energy building', *International Journal of Refrigeration*, 30 (1), p. 134-143.

AMAYA, J. (2009) *Development of Renewable Energy in Emerging Economies,* Boca Raton: Dissertation.com.

AZZOUZ, K., LEDUCQ, D., and GOBIN, D. (2009) 'Enhancing the performance of household refrigerators with latent heat storage: an experimental investigation', *International Journal of Refrigeration,* 32 (7), p. 1634-1644.

AGYENIM, F., HEWITT, N., EAMES, P., and SMYTH, M. (2010) 'A review of materials, heat transfer and phase change problem formulation for latent heat thermal energy storage systems (LHTESS)', *Renewable and Sustainable Energy Reviews*, 14 (2), p. 615-628.

ATKINS, P. (2010) The zeroth law The concept of temperature In: ATKINS, P. (2010) *THE LAWS OF THERMODYNAMICS: A Very Short Introduction*, New York: OUP Oxford.

AIR CONTAINER, Åkersberga, Sweden (2012) 'Providing your requirements by science', [Online], Available: http://www.aircontainer.com/ [Accessed Nov, 6 2012].

ANDRÉ, R., LEPARLOUËR, P., and MOREAU, S. (2012) 'The input of microcalorimetric techniques for the characterization of latent and sensible heat storage materials' in INNOSTOCK 12th International Conference on Energy Storage, LLeida, Spain, University of Lleida, May 16-19, 2012, p. 160-161.

BENTZ, D. P. and TURPIN, R. (2007) 'Potential application of phase change materials in concrete technology', *Cement and Concrete Composites*, 29 (7), p. 527-532.

BUTALA, V. and STRITIH, U. (2009) 'Experimental investigation of PCM cold storage', *Energy and Buildings*, 41 (3), p. 354-359.

BAETENS, R., JELLE, B. P., and GUSTAVSEN, A. (2010) 'Phase change materials for building applications: A state-of-the-art review', *Energy and Buildings*, 42(9), p. 1361-1368.

BAILEY, J. M. (2010) *Modelling Phase Change Material Thermal Storage Systems,* A Thesis Submitted to the School of Graduate Studies in Partial Fulfillment of the Requirements for the Degree Master of Applied Science, Hamilton: McMaster University.

BASF SE, Ludwigshafen, Germany (2012) 'Phase Change Materials', [Online], Available: http://www.micronal.de/portal/basf/ien/dt.jsp?setCursor=1_290798 [Accessed Nov, 3 2012].

BINDER GmbH, Tuttlingen, Germany (2012) 'Best conditions for your success', [Online], Available: http://www.binder-world.com/en/ [Accessed Nov, 6 2012].

BARRENECHE, C., NAVARRO, M. E., FERNANDEZ, A. I., and CABEZA, L. F. (2013) 'Improvement of the thermal inertia of building materials incorporating PCM. Evaluation in the macroscale', *Applied Energy*, 109 (9), p. 428-432.

CLAGGETT, T. J. and WORRALL, R. W. (1982) Thermocouples. In: LIPTAK, B. G. (ed.) (2003) *Instrument Engineers' Handbook, Vol. 1: Process Measurement and Analysis,* 4th edn., Boca Raton: CRC Press.

CABEZA, L. F., ILLA, J., ROCA, J., BADIA, F., MEHLING, H., HIEBLER, S., and ZIEGLER, F. (2001) 'Middle term immersion corrosion tests on metal-salt hydrate pairs used for latent heat storage in the 32 to 36°C temperature range', *Materials and Corrosion,* 52 (10), p. 748-754.

CLAGGETT, T. J., WORRALL, R. W., and SILVA GIRÃO, P. B. M. (2003) Thermistors. In: LIPTAK, B. G. (ed.) (2003) *Instrument Engineers' Handbook, Vol. 1: Process Measurement and Analysis,* 4th edn., Boca Raton: CRC Press.

CABEZA, L. F., CASTELLON, C., NOGUES, M., MEDRANO, M., LEPPERS, R., and ZUBILLAGA, O. (2007) 'Use of microencapsulated PCM in concrete walls for energy savings', *Energy and Buildings,* 39 (2), p. 113-119.

CHERALATHAN, M., VELRAJ, R., and RENGANARAYANAN, S. (2007) 'Performance analysis on industrial refrigeration system integrated with encapsulated PCM-base cool thermal energy storage system', *International Journal of Energy Research,* 31(14), p. 1398-1413.

CASTELLON, C., GÜNTHER, E., MEHLING, H, HIEBLER, S., and CABEZA, L. F. (2008) 'Determination of the enthalpy of PCM as a function of temperature using a heat-flux DSC-A study of different measurement procedures and their accuracy', *International Journal of Energy Research*, 32 (13), p. 1258–1265.

CHEN, C., GUO, H. F., LIU, Y. N., YUE, H. L., and WANG, C. D. (2008) 'A new kind of phase change material (PCM) for energy-storing wallboard', *Energy and Buildings,* 40 (5), p. 882-890.

CHIU, J. N. W. (2011) *Heat Transfer Aspects of Using Phase Change Material in Thermal Energy Storage Applications,* Licentiate thesis, Stockholm: KTH School of Industrial Engineering and Management.

CHEN, Z. H., YU, F., ZENG, X. R., and ZHANG, Z. G. (2012) 'Preparation, characterization and thermal properties of nanocapsules containing phase change material n-dodecanol by miniemulsion polymerization with polymerizable emulsifier', *Applied Energy,* 91 (1), p. 7-12.

CLIMATOR SWEDEN AB, Skövde, Sweden (2012) 'Climator', [Online], Available: http://www.climator.com/en/home/ [Accessed Nov, 6 2012].

COLORTEX GmbH, Pirmasens, Germany (2012) 'Colortex', [Online], Available: http://www.colortex.de/en/index.php [Accessed Nov, 10, 2012].

DINCER, I. (2000) 'Renewable energy and sustainable development: a crucial review', *Renewable and Sustainable Energy Reviews*, 4(2), p. 157-175.

DIMAANO, M. N. R. and WATANABE, T. (2002) 'The capric–lauric acid and pentadecane combination as phase change material for cooling applications', *Applied Thermal Engineering,* 22 (4), p. 365–377.

DELL, Round Rock, Texas (2010) 'Dell UK Official Site', [Online], Available: http://dell.co.uk/ [Accessed Nov, 9 2010].

DIXON GLASS LIMITED, Kent, UK (2010) 'Dixon Glass Limited', [Online], Available: http://www.dixonglass.co.uk/ [Accessed May, 15 2010].

DE GRACIA, A., BARRENECHE, C., FARID, M. M., and CABEZA, L. F. (2011) 'New equipment for testing steady and transient termal performance of multilayered building envelopes with PCM', *Energy and Buildings,* 43 (12), p. 3704-3709.

DINCER, I. and ROSEN, M. A. (2011) *Thermal Energy Storage: Systems and Applications*, 2nd edn., Chichester: John Wiley & Sons.

DUTIL, Y., ROUSSE, D. R., SALAH, N. B., LASSUE, S., and ZALEWSKI, L. (2011) 'A review on phase-change materials: Mathematical modeling and simulations', *Renewable and Sustainable Energy Reviews,* 15 (1), p. 112-130.

DELGADO, M., LAZARO, A., MAZO, J., MARIN, J. M., and ZALBA, B. (2012) 'Experimental analysis of a microencapsulated PCM slurry as thermal storage system and as heat transfer fluid in laminar flow', *Applied Thermal Engineering*, 36 (4), p. 370-377.

DOLADO, P., MAZO, J., LAZARO, A., MARIN, J. M., and ZALBA, B. (2012) 'Experimental validation of a theoretical model: Uncertainty propagation analysis to a PCM-air thermal energy storage unit', *Energy and Buildings,* 45 (2), p. 124-131.

ENTROPY SOLUTIONS Inc., Plymouth, Minnesota (2012) 'Pure Temp', [Online], Available: http://www.puretemp.com/ [Accessed Nov, 6 2012].

FUKAI, J., HAMADA, Y., MOROZUMI, Y., and MIYATAKE, O. (2003) 'Improvement of thermal characteristics of latent heat thermal energy storage units using carbon-fiber brushes: experiments and modeling', *International Journal of Heat and Mass Transfer*, 46 (23), p. 4513–4525.

FRAUNHOFER ISE, Freiburg, Germany (2013) 'Fraunhofer Institute', [Online], Available: http://www.fraunhofer.de/en.html [Accessed June, 7 2013].

GÜNTHER, E., HIEBLER, S., and MEHLING, H. (2006) 'Determination of the heat storage capacity of PCM and PCM-objects as a function of temperature', in ECOSTOCK 10th International Conference on Thermal Energy Storage, Stockton, CA, Richard Stockton College, May 31-June 2, 2006, p. 1-7.

GÜNTHER, E., MEHLING, H, and HIEBLER, S. (2007) 'Modeling of subcooling and solidification of phase change materials', *Modelling and Simulation in Materials Science and Engineering,* 15 (8), p. 879–892.

GIL, A., ARCE, P., MARTORELL, I., MEDRANO, M., and CABEZA, L. F. (2008) 'State of the art of high temperature storage in thermosolar plants', [Online], Available: http://intraweb.stockton.edu/eyos/energy_studies/content/docs/effstock09/Session_4_1_High_Temperature_Applications/26.pdf [Accessed October, 12 2012].

GÜNTHER, E., HIEBLER, S., MEHLING, H., and REDLICH, R. (2009) 'Enthalpy of phase change materials as a function of temperature: required accuracy and suitable measurement methods', *International Journal of Thermophysics*, 30 (4), p. 1257-1269.

GIN, B. and FARID, M. M. (2010) 'The use of PCM panels to improve storage condition of frozen food', *Journal of Food Engineering,* 100 (2), p. 372-376.

GOWREESUNKER, B. L., STANKOVIC, S. B., TASSOU, S. A., and KYRIACOU, P. A. (2013) 'Experimental and numerical investigations of the optical and thermal aspects of a PCM-glazed unit', *Energy and Buildings,* 61 (6), p. 239-249.

GREENLITE GLASS SYSTEMS, Port Coquitlam, British Columbia (2013) 'Energy Saving Glass/ GLASS X Crystal', [Online], Available: http://www.greenliteglass.com/products/energy-saving-glass/glass-x-crystal.html [Accessed May, 15 2013].

HIRAN, S., SUWONDO, A., and MANSOORI, G. (1994) 'Characterization of alkanes and paraffin waxes for application as phase change energy storage medium', *Energy Sources*, 16 (1), p. 117-128.

HU, H. and ARGYROPOULOS, S. A. (1996) 'Mathematical modelling of

solidification and melting: a review', *Modelling and Simulation in Materials Science and Engineering,* 4 (4), p. 371-396.

HASNAIN, S. M. (1998) 'Review on sustainable thermal energy storage technologies, Part II: cool thermal storage', *Energy Conversion and Management*, 39 (11), p. 1139-1153.

HONG, H, KIM, S. K., and K, Y. S. (2004) 'Accuracy improvement of T-history method for measuring heat of fusion of various materials', *International Journal of Refrigeration*, 27(4), p. 360-366.

HAMMOU, Z. A. and LACROIX, M. (2006) 'A hybrid thermal energy storage system for managing simultaneously solar and electric energy', *Energy Conversion and Management,* 47 (3), p. 273-288.

HALFORD, C. K. and BOEHM, R. F. (2007) 'Modeling of phase change material peak load shifting', *Energy and Buildings*, 39 (3), p. 298-305.

INABA, H. and TU, P. (1997) 'Evaluation of thermophysical characteristics on shape-stabilized paraffin as a solid-liquid phase change material', *Heat and Mass Transfer*, 32 (4), p. 307-312.

ISMAIL, K. A. R. and HENRIQUEZ, J. R. (2001) 'Thermally effective windows with moving phase change material curtains', *Applied Thermal Engineering*, 21 (18), p. 1909-1923.

KAYGUSUZ, K. and AYHAN, T. (1999) 'Experimental and theoretical investigation of combined solar heat pump system for residential heating', *Energy Conversion and Management,* 40 (13), p. 1377-1396.

KHAN, S. A., SHAHANI, D. T., and AGARWALA, A. K. (2002) 'Sensor calibration

and compensation using artificial neural network', *ISA Transactions*, 42 (2), p. 337-352.

KHUDHAIR, A. M. and FARID, M. M. (2004) 'A review on energy conservation in building applications with thermal storage by latent heat using phase change materials', *Energy Conversion and Management*, 45 (2), p. 263-275.

KHATEEB, S. A., AMIRUDDIN, S., FARID, M., SELMAN, J. R., and AL-HALLAJ, S. (2005) 'Thermal management of Li-ion battery with phase change material for electric scooters: experimental validation', *Journal of Power Sources*, 142 (1-2), p. 345-353.

KUZNIK, F., VIRGONE, J., and ROUX, J. J. (2008) 'Energetic efficiency of room wall containing PCM wallboard: a full scale experimental investigation', *Energy and Buildings*, 38 (1), p. 18-24.

KUMANO, H., HIRATA, T., and KUDOH, T. (2009) 'Effects of poly-vinyl alcohol on supercooling phenomena of water', *International Journal of Refrigeration*, 32 (3), p. 454-461.

KRAVVARITIS, E. D., ANTONOPOULOS, K. A., and TZIVANIDIS, C. (2010) 'Improvements to the measurement of the thermal properties of phase change materials', *Measurement Science and Technology*, 21 (4), p. 1-9.

KRAVVARITIS, E. D., ANTONOPOULOS, K. A., and TZIVANIDIS, C. (2011) 'Experimental determination of the effective thermal capacity function and other thermal properties for various phase change materials using the thermal delay method', *Applied Energy*, 88 (12), p. 4459–4469.

LIN, K. P., ZHANG, Y. P., XU, X., DI, H. F., YANG, R., and QIN, P. H (2005)

'Experimental study of under-floor electric heating system with shape-stabilized PCM plates', *Energy and Buildings,* 37 (3), p. 215-220.

LAZARO, A., GÜNTHER, E., MEHLING, H., HIEBLER, S., MARIN, J. M. (2006), and ZALBA, B. 'Verification of a T-history installation to measure enthalpy versus temperature curves of phase change materials', *Measurement Science and Technology*, 17(8), p. 2168–2174.

LIN, K. P., ZHANG, DI, H. F., and YANG, R. (2007) 'Study of an electrical heating system with ductless air supply and shape-stabilized PCM for thermal storage', *Energy Conversion and Management,* 48 (7), p. 2016-2024.

LOSADA-PEREZ, P., TRIPATHI, C. S. P., LEYS, J., CORDOYIANNIS, G., GLORIEUX, C., and THOEN, J. (2011) 'Measurements of heat capacity and enthalpy of Phase Change Materials by Adiabatic Scanning Calorimetry', International Journal of Thermophysics, 32(5), p. 913-924.

LAZARO, A., PENALOSA, C., SOLE, A., DIARCE, G., HAUSSMANN, T., FOIS, M., ZALBA, B., GSHWANDER, S., and CABEZA, L. F. (2012) 'Intercomparative test on phase change materials characterisation with differential scanning calorimeter', *Applied Energy*, 109 (9), p. 415-420.

LE DU, M., ZALEWSKI, L., LASSUE, S., DUTIL, Y., and ROUSSE, D. (2012) 'Thermophysical characterization of a composite phase change material: the specific case of Energain[®]' in INNOSTOCK 12th International Conference on Energy Storage, LLeida, Spain, University of Lleida, , May 16-19, 2012, p. 1-10.

LIU, M., SAMAN, W., and BRUNO, F. (2012) 'Development of a novel refrigeration system for refrigerated trucks incorporating phase change material', *Applied Energy,* 92 (4), p. 336-342.

LI, W. Q., QU, Z. G., ZHANG, B. L., ZHAO, K., and TAO, W.Q. (2013a) 'Thermal behavior of porous stainless-steel fiber felt saturated with phase change material', *Energy,* [Online], Available: http://dx.doi.org/10.1016/j.energy.2013.02.064 [Accessed May, 7 2013].

LI, Y., ZHANG, Y., LI, M., and, ZHANG, D. (2013b) 'Testing method of phase change temperature and heat of inorganic high temperature phase change materials', *Experimental Thermal and Fluid Science*, 44(1), p. 697-707.

FUENSANTA, M., PAIPHANSIRI, U., ROMERO-SANCHEZ, M. D., GUILLEM, C., LOPEZ-BUENDIA, A. M., and LANDFESTER, K. (2013) 'Thermal properties of a novel nanoencapsulated phase change material for thermal energy storage', *Thermochimica Acta,* [Online], Available: http://dx.doi.org/10.1016/j.tca.2013.04.028 [Accessed May 15, 2013].

MARIN, J. M., ZALBA, B., SERRANO, R., and SANCHEZ-VALVERDE, B. (2001) 'Design of experiments (DOE) for thermal energy storage (TES) with phase change materials (PCM)' in Planning Workshop, IEA, ECES IA Annex 17, Advanced Thermal Energy Storage Techniques – Feasibility studies and Demonstration Projects, LLeida, Spain, April 5-6, 2001, p. 1-5.

MARIN, J. M., ZALBA, B., CABEZA, L. F., and MEHLING, H. (2003) 'Determination of enthalpy-temperature curves of phase change materials with the temperature history method: improvement to temperature dependent properties', *Measurement Science and Technology*, 14(2), p.184-189.

MARIN, J. M., LAZARO, A., and ZALBA, B. (2005) 'New installation at the University of Zaragoza (Spain) of T-history method to measure the thermal properties' in 8th Workshop, IEA, ECES IA Annex 17, Advanced Thermal Energy Storage Techniques – Feasibility studies and Demonstration Projects, Kizkalesi, Turkey, April 18-20, 2005, p. 1-9.

MEHLING, H., EBERT, H. P., and SCHOSSIG, P. (2006) 'Development of standards for material testing and quality control of PCM', [Online], Available: http://195.20.235.12/pdf/Paperfinal.pdf [Accessed June, 7 2013].

MATSUI, T., YOSHIDA, M., YAMASAKI, H., and HATATE, Y. (2007) 'Thermal properties of multicomponent fatty acids as solid-liquid phase change materials for cooling applications', *Chemical Engineering Communications*, 194 (1), p. 129-139.

MEDVED, S. and ARKAR, C. (2008) 'Correlation between the local climate and the free cooling potential of latent heat storage', *Energy and Buildings,* 40 (4), p. 429-437.

MEHLING, H. and CABEZA, L. F. (2008) *Heat and cold storage with PCM: An up to date introduction into basics and applications,* Berlin: Springer Verlag.

MEHLING, H., HIEBLER, S, and GÜNTHER, E. (2010) 'New method to evaluate the heat storage density in latent heat storage for arbitrary temperature ranges', *Applied Thermal Engineering*, 30 (17-18), p. 2652–2657.

MORENO-ALVAREZ, L., HERRERA, J. N., and MENESES-FABIAN, C. (2010) 'A differential formulation of the T-History calorimetric method', *Measurement Science and Technology*, 21 (12), p. 1-4.

MALDONADO, P. A. (2011) *Application of passive thermal energy storage in buildings using PCM and awnings*, Master thesis, LLeida: University of Lleida.

MEHLING, H., GÜNTHER, E., and HIEBLER, S. (2012) 'A new measurement and evaluation method for DSC of PCM samples', [Online], Available: http://intraweb.stockton.edu/eyos/energy_studies/content/docs/effstock09/Session_3_2_PCM/12.pdf [Accessed Nov, 14, 2012].

NEEPER, D. A. (2000) 'Thermal dynamics of wallboard with latent heat storage', *Solar Energy*, 68 (5), p. 393-403.

NENOVA, Z. P. and NENOV, T. G. (2009) 'Linearization circuit of the thermistor connection', *IEEE Transactions on Instrumentation and Measurement*, 58 (2), p 441-449.

NEWARK CORPORATION, Newark, New Jersey (2010) 'Newark element 14', [Online], Available: http://www.newark.com/ [Accessed Nov, 9 2010].

NATIONAL INSTRUMENTS, Newbury, UK (2010) 'National Instruments United Kingdom', [Online], Available: http://uk.ni.com/ [Accessed Nov, 9 2010].

OZISIK, M. N. (1994) 'PHASE CHANGE PROBLEMS', in *Finite Difference Methods in Heat Transfer*, Boca Raton: CRC Press.

OMEGA (2012) 'OMEGA Your One-Stop Source for Process Measurement & Control', [Online], Available: http://www.omega.com [Accessed Sep, 15 2012].
ORO, E., DE GRACIA, A., CASTELL, A., FARID, M.M., and CABEZA, L. F. (2012) 'Review on phase change materials (PCMs) for cold thermal energy storage applications', *Applied Energy,* 99 (11), p.513-533.

OUTLAST TECHNOLOGIES LLC, Golden, Colorado (2012) 'Outlast', [Online], Available: http://www.outlast.com/ [Accessed Nov, 10 2012].

PASUPATHY, A., VELRAJ, R., and SEENIRAJ, R.V. (2008) 'Phase change material-based building architecture for thermal management in residential and commercial establishments', *Renewable and Sustainable Energy Reviews*, 12 (1), p. 39-64.

PCM PRODUCTS LIMITED, Yaxley, UK (2012) 'Phase Change Materials', [Online], Available: http://www.pcmproducts.net/home.htm [Accessed Nov, 6 2012].

PCM THERMAL SOLUTIONS, Chicago, Illinois (2012) 'PCM Thermal Solutions',

[Online], Available: http://www.pcm-solutions.com/shippingcontainers.html [Accessed Nov, 6 2012].

PERKINELMER, Cambridge, UK (2012) 'PerkinElmer', [Online], Available: http://www.perkinelmer.co.uk/ [Accessed Nov, 25, 2012].

POMIANOWSKI, M., HEISELBERG, P., and JENSEN, R. L. (2012) 'Dynamic heat storage and cooling capacity of a concrete deck with PCM and thermally activated building system', *Energy and Buildings,* 53 (10), p. 96-107.

RAVIKUMAR, M. and SRINIVASAN, P. (2005) 'Phase Change Material as a thermal energy storage material for cooling of buildings', [Online], Available: http://www.jatit.org/volumes/research-papers/Vol4No6/6Vol4No6.pdf [Accessed October, 28 2012].

RADY, M. A., ARQUIS, E., and LE BOT, C. (2010) 'Characterization of granular phase changing composites for thermal energy storage using the T-history method', *International Journal of Energy Research*, 34(4), p. 333-344.

RAL (2010) 'RAL Phase Change Material', [Online], Available: http://www.pcm-ral.de/en/ral-quality.html [Accessed June, 7 2010].

RS COMPONENTS, Corby, UK (2010) 'RS Components-Distributor of Electronic, Electrical, and Industrial Components', [Online], Available: http://int.rsdelivers.com/default.aspx/ [Accessed Nov, 9 2010].

RATHGEBER, C., HIMPEL, M., and HIEBLER, S. (2012) 'A new T-history calorimeter for phase change materials in the temperature range 50 °C to 200 °C' in INNOSTOCK 12th International Conference on Energy Storage, LLeida, Spain, University of Lleida, May 16-19, 2012, p. 200-201.

RUBITHERM GmbH, Berlin, Germany (2012),'Innovative PCM's and Thermal Technology', [Online], Available: http://www.rubitherm.de/english/ [Accessed Nov, 6 2012].

SHARMA, S. D., KITANO, H., and SAGARA, K. (2004) 'Phase Change Materials for Low Temperature Solar Thermal Applications', [Online], Available: http://www.eng.mie-u.ac.jp/research/activities/29/29_31.pdf [Accessed October, 14 2012].

SAMAN, W., BRUNO, F., and HALAWA, E. (2005) 'Thermal performance of PCM thermal storage unit for a roof integrated solar heating system', *Solar Energy,* 78 (2), p. 341-349.

SHARMA, A., TYAGI, V. V., CHEN, C. R., and BUDDHI, D. (2009) 'Review on thermal energy storage with phase change materials and applications', *Renewable and Sustainable Energy Reviews*, 13 (2), p. 318-345.

SCHOELLER TEXTILES AG, Sevelen, Switzerland (2012) 'Power of innovation', [Online], Available: http://www.schoeller-textiles.com/en.html [Accessed Nov, 10 2012].

SOFRIGAM, Rueil-Malmaison, France (2012) 'Sofrigam', [Online], Available: http://www.sofrigam.com/ [Accessed Nov, 6 2012].

STANKOVIC, S. B. and KYRIACOU, P. A. (2012) 'The effects of thermistor linearization techniques on the T-history characterization of phase change materials', *Applied Thermal Engineering,* 44 (13), p. 78-84.

SEYF, H. R., ZHOU, Z., MA, H. B., and ZHANG, Y. (2013) 'Three dimensional numerical study of heat-transfer enhancement by nano-encapsulated phase change

material slurry in microtube heat sinks with tangential impingement', *International Journal of Heat and Mass Transfer*, 56 (1-2), p. 561-573.

SOLE, A., MIRO, L, BARRENECHE, C., MARTORELL, I., and CABEZA, L. F. (2013) 'Review of the T-history method to determine thermophysical properties of phase change materials (PCM)', *Renewable and Sustainable Energy Reviews*, 26 (10), p. 425-436.

STANKOVIC, S. B. and KYRIACOU, P. A. (2013) 'Improved measurement technique for the characterization of organic and inorganic phase change materials using the T-history method', *Applied Energy,* 109 (9), p. 433-430.

TSAI, C. F., LI, L. T., LI, C. H., and YOUNG, M. S. (2009) 'Implementation of thermistor linearization using LabVIEW' in 5th International Conference on Intelligent Information Hiding and Multimedia Signal Processing, Kyoto, Japan, September 12-14, 2009, Kyoto, Japan, p.530-533.

TEAP PCM, Mumbai, India (2012) 'Phase Change Material PCM Manufacturers for Air Conditioning, Electronics Cooling ...', [Online], Available: http://www.teappcm.com/ [Accessed Nov, 6 2012].

TCP RELIABLE, Edison, New Jersey (2012) 'A New Tier Packaging Solutions Provider', [Online], Avalaible: http://www.tcpreliable.com/cold-chain-packaging/ [Accessed Nov, 6 2012]

VERMA, P., VARUN, and SINGAL, S. K. (2008) 'Review of mathematical modeling on latent heat thermal energy storage systems using phase change materials', *Renewable and Sustainable Energy Reviews,* 12 (4), p. 999-1031.

VA-Q-TEC AG, Wuerzburg, Germany (2012) 'Creating Energy Efficiency', [Online], Available: http://www.va-q-tec.com/ [Accessed Nov, 6 2012].

WEINLÄDER, H., BECK, A., and FRICKE, J. (2005) 'PCM-façade-panel for daylighting and room heating', *Solar Energy*, 78(2), p. 177-186.

WANG, X. C. and NIU, J. L. (2009) 'Performance of cooled-ceiling operating with MPCM slurry', *Energy Conversion and Management,* 50 (3), p. 583-591.

WHIFFEN, T. R. and RIFFAT, S. B. (2012) 'A review of PCM technology for thermal energy storage in the built environment: Part I', *International Journal of Low-Carbon Technologies,* [Online], Available: http://ijlct.oxfordjournals.org/content/early/2012/05/30/ijlct.cts021.full.pdf+html [Accessed May, 10, 2013].

XIAO, X., ZHANG, P., and LI, M. (2013) 'Preparation and thermal characterization of paraffin/metal foam composite phase change material', *Applied Energy*, [Online], Available: http://dx.doi.org/10.1016/j.apenergy.2013.04.050 [Accessed, May, 9 2013].

YAMAHA, M. and MISAKI, S. (2006) 'The evaluation of peak shaving by a thermal storage system using phase-change materials in air distribution systems', *HVAC & R Research*, 12 (3c), p. 861-869.

ZHANG Y., JIANG Y., and JIANG, Y. (1999) 'A simple method, the T-history method, of determining the heat of fusion, specific heat and thermal conductivity of phase change materials', *Measurement Science and Technology*, 10 (3), p. 201–205.

ZALBA, B., MARIN, J. M., CABEZA, L. F., and MEHLING, H. (2003) 'Review on thermal energy storage with phase change: materials, heat transfer analysis and application', *Applied Thermal Engineering,* 23 (3), p. 251-283.

ZALBA, B, MARIN, J. M., CABEZA, L. F., and MEHLING, H. (2004) 'Free cooling of buildings with phase change materials', *International Journal of Refrigeration*, 27 (8), p. 839-849.

ZALBA, B., SANCHEZ-VALVERDE, B., and MARIN, J. M. (2005) 'An experimental study of thermal energy storage with phase change materials by design of experiments', *Journal of Applied Statistics*, 32 (4), p. 321-332.

ZHANG, Y. P., LIN, K. P., YANG, R., DI, H. F., and JIANG, Y. (2006a) 'Preparation, thermal performance and application of shape-stabilized PCM in energy efficient buildings', *Energy and Buildings*, 38 (10), p. 1262-1269.

ZHANG, Y. P., LIN, K. P., ZHANG, Q. L., and DI, H. F. (2006b) 'Preparation, thermal performance and application of shape-stabilized PCM in energy efficient buildings', *Energy and Buildings*, 38 (10), p. 1262-1269.

ZHANG, Y., ZHOU, G., LIN, K., ZHANG, Q., and DI, H. (2007) 'Application of latent heat thermal energy storage in buildings: state-of the-art and outlook', *Builiding and Environment*, 42 (6), p. 2197-2209.

ZENG, R., WANG, X., CHEN, B., ZHANG, Y., NIU, J., WANG, X., and DI, H. (2009) 'Heat transfer characteristics of microencapsulated phase change material slurry in laminar flow under constant heat flux', *Applied Energy,* 86 (12), p. 2661-2670.

ZHU, N., MA, Z., and WANG, S. (2009) 'Dynamic characteristics and energy performance of buildings using phase change materials: A review', *Energy Conversion and Management,* 50 (12), p. 3169-3181.

ZHOU, D. and ZHAO, C. Y. (2011) 'Experimental investigations on heat transfer in phase change materials (PCMs) embedded in porous materials', *Applied Thermal Engineering*, 31 (5), p. 970-977.

ZHOU, D., ZHAO, C.Y., and TIAN, Y. (2012) 'Review on thermal energy storage with phase change materials (PCMs) in building applications', *Applied Energy*, 92 (4), p 593-605.

ZAE Bayern, Garching, Germany 'The ZAE Bayern', [Online], Available: http://www.zae-bayern.de/en/the-zae-bayern.html [Accessed June, 7 2013].